Esta investigação foi financiada pela Fundação para a Ciência e Tecnologia através da concessão de uma bolsa de doutoramento (SFRH/BD/71396/2010), no âmbito do Quadro de Referência Estratégico Nacional (QREN), Programa Operacional Potencial Humano (POPH) – Formação Avançada, comparticipado pelo Fundo Social Europeu.

FCT
Fundação para a Ciência e a Tecnologia
MINISTÉRIO DA EDUCAÇÃO E CIÊNCIA

QUADRO DE REFERÊNCIA ESTRATÉGICO NACIONAL
PORTUGAL 2007.2013

POPH
PROGRAMA OPERACIONAL POTENCIAL HUMANO

UNIÃO EUROPEIA
Fundo Europeu de Desenvolvimento Regional

High-throughput combinatorial analysis of three-dimensional biomaterials behavior using superhydrophobic patterned platforms
Mariana Braga de Oliveira
UMinho | 2014

Universidade do Minho
Escola de Engenharia

Mariana Braga de Oliveira

High-throughput combinatorial analysis of three-dimensional biomaterials behavior using superhydrophobic patterned platforms

outubro de 2014

Universidade do Minho
Escola de Engenharia

Mariana Braga de Oliveira

High-throughput combinatorial analysis of three-dimensional biomaterials behavior using superhydrophobic patterned platforms

Tese de Doutoramento em Engenharia Biomédica

Trabalho realizado sob a orientação do
Professor Doutor João Filipe Colardelle da Luz Mano

outubro de 2014

DECLARAÇÃO

Nome: Mariana Braga de Oliveira

Endereço electrónico: mariana.oliveira@dep.uminho.pt

Número do Bilhete de Identidade: 13175224

Título da Tese: High-throughput combinatorial analysis of three-dimensional biomaterials behavior using superhydrophobic patterned platforms

Orientador: Professor Doutor João Filipe Colardelle da Luz Mano

Ano de conclusão: 2014

Designação do Doutoramento: Doutoramento em Engenharia Biomédica

É AUTORIZADA A REPRODUÇÃO PARCIAL DESTA TESE, APENAS PARA EFEITOS DE INVESTIGAÇÃO, MEDIANTE DECLARAÇÃO ESCRITA DO INTERESSADO, QUE A TAL SE COMPROMETE;

Universidade do Minho, ___/___/_____

_____

(Mariana Braga de Oliveira)

É AUTORIZADA A REPRODUÇÃO PARCIAL DESTA TESE APENAS PARA EFEITOS DE INVESTIGAÇÃO, MEDIANTE DECLARAÇÃO ESCRITA DO INTERESSADO, QUE A TAL SE COMPROMETE.

Universidade do Minho, ____/____/_____

_____

(Mariana Braga de Oliveira)

STATEMENT OF INTEGRITY

I hereby declare having conducted my thesis with integrity. I confirm that I have not used plagiarism or any form of falsification of results in the process of the thesis elaboration.

I further declare that I have fully acknowledged the Code of Ethical Conduct of the University of Minho.

University of Minho, _____

_____

(Mariana Braga de Oliveira)

In memory of my grandfather

ACKNOWLEDGMENTS

In the end of four years in which I had the opportunity of evolving as a researcher and as an individual, it is gratifying to be able to thank those who were important during this journey.

I would like to first acknowledge my supervisor, Prof. João Mano. I am heartly grateful for his acceptance to have me as a PhD student and it is to him that I attribute my scientific growth. His pursuit for innovative work, challenging ideas and encouragement are inspiring to me.

I would also like to acknowledge the 3B's Research Group and its director, Prof. Rui Reis, for the possibility of developing my PhD work in such well-equiped facilities and highly reputed institution. I would also like to acknowledge the 3B's Research Group for the opportunity to attend several national and international conferences in order to present my work to the scientific community.

I would like to acknowledge Prof. Nuno Neves who, as a representative of the Doctoral Program in Biomedical Engineering, helped me through the academic process related to the University of Minho.

I thank the whole team of Prof. João Mano for the productive meetings with fruitful discussion. My special thanks are directed to Christiane Salgado, Clara Correia, Gisela Luz, Isabel Neto and Wenlong Song, who directly contributed with their specific expertise to the work presented in this thesis.

I have met many amazing people in the 3B's Research Group, so I would like to show my appreciation for several colleagues that helped me professionally and personally. As this is a risky task, since there are so many important people and I may forget someone important, I will address some people in particular. I thank Sofia Caridade for the patience while teaching me to use the DMA equipment. It was not easy (is it ever easy?), so I thank you for your support during the times of despair, even by Skype! I thank you for the times you came to me while writing this thesis offering support and help. I thank my "lunch group" – Albino, Álvaro (for listening to me, even when I have a temper), Nuno (for your good advice) and Rui (for being such a helpful guy) - for being supportive in the times of need and also to make my days a little lighter and so much funnier. I also thank Sara Oliveira and Ana Catarina, my PhD journey companions. I also thank Nelson, Yan and Simone.

I would like to leave a word of appreciation to Prof. Ilídio Correia. I acknowledge him for the fruitful collaboration work at Universidade da Beira Interior, where he was always readily available. I also

acknowledge his students Maximiano Ribeiro and Sónia Miguel (both of them showed total availability; it was truly easy to work with them), as well as Prof. Paula Coutinho, from Instituto Politécnico da Guarda.

I thank Prof. Dror Seliktar for giving me the opportunity to work in his lab in Technion – Israel Institute of Technology – and for his availability. I thank all his team, especially Michal for taking care of all burochratic logistics, Olga for introducing me to the lab and helping me with my work, and Revital for the friendliness and hospitatly.

João Pedro. For being cold when I need rationality. For bringing warmth when I am cold and demanding to the point of exhaustion. For the perfect balance. For showing me the beauty of silence while holding my cold hands. For staying with me, even miles and miles away and showing me I can stay with you, even miles and miles away. For being my compass, and how I've been lost before I met you... Because every day you stumble in my footsteps and keep the same appointments I keep. For this I was given name.

I dedicate this thesis to my parents for being the beginning and the end. For helping me out during all the so called in-between. For teaching me how to be independent, and still feel so loved. For allowing me to think freely. For supporting all my steps and, although unconventional but not less important, for your amazing sense of humor. For being the best and my favorite role models. Your support and values made me who I am today.

I acknowledge financial support from Fundação para a Ciência e Tecnologia (FCT) - PhD Grant SFRH/71396/2010 -, Programa Operacional Potencial Humano (POPH) and Quadro de Referência Estratégica Nacional (QREN), and Fundo Social Europeu (FSE).

ABSTRACT

One of the still unaccomplished struggles in the maintenance of population life quality is related to the current need for effective biomaterials. The optimization of tissue engineering (TE) strategies by combining biomaterials, cells and soluble factors usually relies on time-consuming iterative processes. Rapid and low-cost high-throughput testing is needed to accelerate the discovery of ideal TE systems. The main hypothesis of this thesis was that superhydrophobic surfaces patterned with wettable spots were amenable to be used as platforms for high-throughput complete testing of 3D biomaterials. Indeed, such platforms allowed taking advantage of wettability contrast to pattern biomaterials with precise shape and pre-determined height, by controlling the volume dispensed in each spot.

The superhydrophobic chips were first used to pattern ionic alginate-based cell-laden hydrogels in the wettable spots. The chemical composition of each biomaterial was evaluated by FTIR and the cellular response of fibroblast and osteoblast-like cell lines was assessed on-chip by image-based analysis. Image-based non-destructive assessment was validated by comparison with conventional biochemical colorimetric tests. Superhydrophobic chips were later used to produce and study miniaturized porous scaffolds. The size of the spots in the milimetric range allowed having porous biomaterial structures with significant pore size for cell migration and growth. Chitosan/alginate scaffolds were processed by polyelectrolyte complexation and freeze-drying, followed by fibronectin adsorption. Cell number and viability were assessed using two cell lines. DMA and μCT techniques were adapted to be used on-chip, in dry conditions, to characterize the scaffolds mechanically and morphologically. The on-chip DMA method was upgraded to be performed under physiological-like conditions using chitosan/bioactive glass nanoparticles hydrogels. The selective adhesion and proliferation of a pre-osteoblast cell line allowed hit-spotting favorable *in vitro* biomaterial formulations.

After demonstrating their adequacy for *in vitro* cell-3D biomaterials interactions assessment, superhydrophobic chips containing 36 biomaterials were implanted in single Wistar rats, allowing the high-throughput *in vivo* study of inflammatory response caused by biomaterials.

An important aspect in TE is the dependency of tissue regeneration on prolonged action of bioactive agents. Superhydrophobic chips were imprinted with ring-shaped spots with concentric superhydrophobic regions where polymeric protein-loaded spheres were deposited. The acquisition of sequential images of each spot over time using microscopy methods allowed monitoring protein release. Finally, cell suspension droplets were fixed in the wettable regions of the chips to produce cell spheroids/microtissues for drug screening by the hanging drop methodology in a robot-free automated manner.

In conclusion, the superhydrophobic platforms patterned with wettable spots used in this thesis proved to be compatible with a complete study of 3D biomaterials-cells interactions, comprising a wide set of factors as biomaterials characterization, *in vitro* testing, innovative *in vivo* assessment and bioactive molecules-related tests.

RESUMO

Um dos desafios correntes para a manutenção da qualidade de vida das populações prende-se com a falta de biomateriais eficazes. A otimização de estratégias em engenharia de tecidos (ET) através da combinação de biomateriais, células e fatores solúveis requer, em geral, processos iterativos. Testes expeditos e de baixo custo são necessários para acelerar a descoberta de sistemas de ET ideiais. A hipótese desta tese consiste na possibilidade do uso de superfícies superhidrofóbicas padronizadas com regiões hidrofílicas como plataformas para a análise expedita e completa de biomateriais 3D. As plataformas permitiram usar o contraste de molhabilidade para depositar biomateriais com forma e altura precisas, controlando o volume colocado em cada região hidrofílica.

As plataformas foram usadas para dispensar hidrogéis de alginato com células encapsuladas nas regiões molháveis. A composição química de cada biomaterial foi avaliada por FTIR, e a resposta celular foi testada através de análises de imagem, efetuadas no *chip*. As análises não destrutivas baseadas em imagem foram validadas por comparação com teses bioquímicos colorimétricos. As plataformas foram depois adaptadas para a produção e caracterização de estruturas porosas miniaturizadas. A dimensão milimétrica das regiões molháveis permitiu processar estruturas com poros de tamanho representativo para migração e crescimento celulares. As estruturas porosas de quitosano/alginato foram preparadas por complexação de polielectrólitos/liofilização, seguidas de adsorção de fibronectina. O número e viabilidade celulares foram estudados. As técnicas de DMA e μCT foram adaptadas para uso nos *chips*, em condições secas, para caracterização mecânica e morfológica. O método de DMA realizado no *chip* foi melhorado de forma a permitir uma análise em condições semelhantes às fisiológicas, usando hidrogéis de quitosano/nanopartículas de vidro bioactivo. A adesão selectiva e proliferação de uma linha celular de pré-osteoblastos permitiu selecionar as formulações de biomateriais mais favoráveis. Após demonstrar a sua adequabilidade para testes *in vitro*, implantaram-se plataformas superhidrofóbicas contendo 36 biomateriais em ratos Wistar, mostrando a sua utilidade para testes expeditos executados *in vivo*,para estudo da resposta inflamatória causada por biomateriais.

Outro aspeto importante em ET é a dependência da regeneração de tecidos na ação prolongada de agentes bioactivos. Regiões molháveis com uma região superhidrofóbica concêntrica foram usadas para depositar esferas poliméricas contendo proteína. A aquisição sequencial de imagens por microscopia permitiu monitorizar a libertação de proteína. Finalmente, fixaram-se gotas de suspensão celular nas regiões hidrofílicas para produzir esferóides celulares para a análise de fármacos pelo método da gota suspensa.

Em conclusão, as superficies superhidrofóbicas padronizadas com regiões molháveis usadas nesta tese provaram ser compatíveis com um estudo completo de interações entre células e biomateriais 3D, compreendendo um vasto conjunto de fatores, como caracterização dos biomateriais, testes *in vitro* e *in vivo,* e testes relacionados com moléculas bioactivas.

TABLE OF CONTENTS

List of Abbreviations and Acronyms

α-CD - alpha-cyclodextrin

β-GP – beta-glycerophosphate

ι-Carr – iota carrageenan

μCT – microcomputed tomography

2D – two-dimensional

3D – three-dimensional

A

A - area

ADA - 4,4'-azodibenzoic acid

AFM – atomic force microscopy

Alg - alginate

ANOVA – analysis of variance

ATR – attenuated total reflectance

B

BG-NP – bioactive glass nanoparticles

BMP – bone morphogenic protein

BSA – bovine serum albumin

BSA-FITC - bovine serum albumin-fluorescein isothiocyanate

C

CA – contact angle

CD – cluster of differentiation

Chi - chitosan

Coll - collagen

D

DAPI - 4',6-diamidino-2-phenylindole

DMAA - *N,N*-dimethylacrylamide

DMEM - Dubelcco's Modified Eagle Medium

DOE – design of experiments

DOPA - L-3,4-dihydroxyphenylalanine

Dox - doxorubicin

dsDNA – double stranded DNA

E

E' – storage modulus

E'' – loss modulus

ECM – extracelular matrix

ELP – elastina–like polymer

ePTFE – expanded poly(tetrafluoroethylene)

Er – reduced modulus

ESC – embryonic stem cell

F

FBS – fetal bovine serum

Fn – fibronectin

FTIR – Fourier transform infrared

G

GAG - glycosaminoglycan

GF – growth factor

GG – α-L-guluronate dimer

GTR – guided tissue regeneration

H

h - height

H – high (Chapter 8)

H&E – hematoxilin and eosin

HA – hyaluronic acid

HCA – hydroxycarbonate apatite

HEMA-MMA - poly(hydroxyethyl methacrylate-co-methyl methacrylate)

HEMAPC - hydroxyethylmethacrylate phosphatidylcholine

HEPES - 4-(2-hydroxyethyl)-1-piperazineethanesulfonic acid

HPLC - high performance liquid chromatography

HTS – high-throughput systems

I

IFN-γ - interferon gamma

IPN – interpenetrated network

ITO - indium tin oxide

K

k-Carr – kappa-carrageenan

L

L – low (Chapter 8)

LbL – layer-by-layer

LCST – low critical solution temperature

Lymph. - lymphocytes

M

M – medium (Chapter 8)

Macro. - macrophages

MAP – mussel adhesive proteins

MSC – mesenchymal stem cells

Mw – molecular weight

O

OD – optical density

P

(p(AA/C12)) – (C12)-modified poly-(acrylic acid)

PAH - poly(allylamine hydrochloride)

PAPA - *N*-4-phenylazophenyl acrylamide

PBS – phosphate buffered saline

PCL – poly(ε-caprolactone)

PCU - Poly(carbonate urethane)

PDMS – polydimethylsiloxane

PEG – poly(ethylene glycol)

PEO – poly(ethylene oxide)

PET – poly(ethylene terephthalate)

PHA - Polyhydroxyalkanoate

PHB - poly(3-hydroxybutyrate)

PHBHHx - poly(3-hydroxybutyrate-co-3-hydroxyhexanoate)

PI – propidium iodide

PLGA – poly(lactic-*co*-glycolic acid)

PMN - polymorphonuclear

PNIPAAM - poly(*N*-isopropylacrylamide)

PS - polystyrene

R

RGD – arginylglycylaspartic acid

S

S.D. – standard deviation

S.E.M. – standard error mean

SC - silyl chitosan

SEM – scanning electron microscopy

SHS – superhydrophobic surfaces

SPCL – starch with poly(ε-caprolactone)

SPLA – starch with poly(lactic acid)

T

TBPB - tetrabromophenol blue

TE – tissue engineering

TERM – tissue engineering and regenerative medicine

TGF-β - tranforming growth factor-beta

TNF-α - tumor necrosis factor alpha

Tt – transition temperature

U

UCST – upper critical solution temperature

V

VEGF – vascular endothelial growth factor

X

XG – xanthan gum

LIST OF FIGURES

conditions. Blue lines indicate significant differences between spheroids prepared using cell suspensions with distinct cell densities, but exposed to the same Dox concentration. Statistically differences were considered for $p<0.05$. 299

LIST OF TABLES

LIST OF PUBLICATIONS AND COMMUNICATIONS

The work performed under the scope of this PhD thesis resulted in the publications listed below:

Scientific papers in peer-reviewed journals

1. Salgado CL*, **Oliveira MB***, Mano JF. Combinatorial cell-3D biomaterials cytocompatibility screening for tissue engineering using bioinspired superhydrophobic substrates. Integr Biol-Uk. 2012;4:318-27 (*the authors contributed equally to this work).
2. **Oliveira MB**, Salgado CL, Song WL, Mano JF. Combinatorial On-Chip Study of Miniaturized 3D Porous Scaffolds Using a Patterned Superhydrophobic Platform. Small. 2013;9:768-78.
3. **Oliveira MB**, Luz GM, Mano JF. A combinatorial study of nanocomposite hydrogels: on-chip mechanical/viscoelastic and pre-osteoblast interaction characterization. J Mater Chem B. 2014;2:5627-38.
4. **Oliveira MB**, Ribeiro MP, Miguel SP, Neto AI, Coutinho P, Correia IJ, et al. In Vivo High-Content Evaluation of Three-Dimensional Scaffolds Biocompatibility. Tissue Eng Part C Methods. 2014 (in press), doi: 10.1089/ten.tec.2013.0738.
5. **Oliveira MB**, Mano JF. On-Chip Assessment of the Protein-Release Profile from 3D Hydrogel Arrays. Analytical Chem. 2013;85:2391-6.
6. **Oliveira MB**, Neto AI, Correia CR, Rial-Hermida MI, Alvarez-Lorenzo C, Mano JF. Superhydrophobic Chips for Cell Spheroids High-Throughput Generation and Drug Screening. Acs Appl Mater Inter. 2014;6:9488-95.
7. **Oliveira MB**, Mano JF, High-Throughput Screening for Integrative Biomaterials Design: Exploring Advances and New Trends. Trends in Biotechnology. (in press), doi: 10.1016/j.tibtech.2014.09.009.

Book Chapters

1. **Oliveira MB**, Mano JF. Chapter 7: Natural-Based and Stimuli-Responsive Polymers for Tissue Engineering and Regenerative Medicine. In Pradas MP, Vicent MJ (eds.) Polymers in Regenerative Medicine: Biomedical Applications from Nano- to Macro-Structures, John Wiley & Sons, Inc. Germany, ISBN 978-0-470-59638-8.
2. **Oliveira MB**, Mano JF. Chapter 2: Biomimetic superhydrophobic surfaces. In Jabbari E, Kim D-K, Lee LP, Ghaem-Maghami A, Khademhosseini A (eds.) Handbook of Biomimetics and Bioinspiration, pp. 153-180, World Scientific, Singapore, 2014, doi: 10.1142/9789814354936.

Conference abstracts published in international scientific journals

1. Salgado CL, **Oliveira MB**, Mano JF, "Combinatorial Cell-Porous Scaffolds Interactions Study And Scaffold Physicochemical Characterization In An Innovative Bioinspired High-Throughput Platform", Int J Artif Organs, vol. 34, issue SI, pp. 685-6, 2011.
2. Salgado CL, **Oliveira MB**, Mano JF, "Innovative three-dimensional platform for combinatorial analysis of cell/biomaterials interaction", Histology and Histopathology, vol. 26, issue supplement1, pp. 28, 2011.
3. **Oliveira MB**, Salgado CL, Mano JF, "Patterned superhydrophobic surfaces for the combinatorial assessment of 3D biomaterials-cells interactions", J Tissue Eng Reg Med, vol. 6, issue SI, pp. 230-230, 2012.
4. **Oliveira MB**, Salgado CL, Mano JF, "Superhydrophobic platforms for the combinatorial analysis of biomaterials-cells interactions using arrays of 3D scaffolds with distinct mechanical and morphological properties", J Tissue Eng Reg Med, vol. 6, pp. 240-240, 2012.
5. **Oliveira MB**, Salgado CL, Song W, Mano JF, "Superhydrophobic patterned chips for the combinatorial and rapid study of 3D biomaterials-cells interactions and protein delivery systems", J Tissue Eng Reg Med, vol. 6, issue S2, pp. 25-25, 2012.

Invited oral communications

1. **Oliveira MB**, Mano JF, Combinatorial analysis of biomaterials for Tissue Engineering. 3rd 3B's Symposium on Biomaterials and Stem Cells in Regenerative Medicine. Taipas, Guimarães, Portugal, 2013.

Oral communications

1. Salgado CL, **Oliveira MB** and Mano JF, Innovative three-dimensional platform for combinatorial analysis of cell/biomaterials interactions, TERMIS-EU 2011, Granada, Spain, June 2011.
2. **Oliveira MB**, Salgado CL, Mano JF, "Superhydrophobic platforms for the combinatorial analysis of biomaterials-cells interactions using arrays of 3D scaffolds with distinct mechanical and morphological properties", 3rd TERMIS World Congress 2012, Vienna, Austria, 2012.
3. **Oliveira MB**, Salgado CL, Mano JF, "High-throughput physicochemical characterization anc

biological assessment of 3D porous scaffolds using a patterned superhydrophobic platform", 9th World Biomaterials Congress, Chengdu, China, 2012.

4. **Oliveira MB**, Mano JF, High-throughput analysis of cells-3D biomaterials interactions using superhydrophobic patterned surfaces as chips, Society for Biomaterials, 2014 Annual Meeting and Exposition, Denver, USA, 2014.

5. **Oliveira MB**, Neto AI, Correia CR, Rial-Hermida MI, Alvarez-Lorenzo C, Mano JF. Superhydrophobic patterned Chips As Platforms for High-content Drug Screening in 3D Tissues Produced in vitro. Society for Biomaterials, 2014 Annual Meeting and Exposition, Denver, USA, 2014.

Poster communications

1. Salgado CL, **Oliveira MB**, Mano JF, , Combinatorial cell-porous scaffolds interactions study and scaffold physicochemical characterization in an innovative bioinspired high-throughput platform, 4th Joint ESAO-IFAO Congress, 2011.

2. **Oliveira MB**, Salgado CL, Mano JF, "Superhydrophobic platforms for the combinatorial analysis of biomaterials-cells interactions using arrays of 3D scaffolds with distinct mechanical and morphological properties", 3rd TERMIS World Congress 2012.

3. **Oliveira MB**, Luz GM, Mano JF, On-chip High-throughput Analysis of Biomaterials Viscoelastic Properties using Patterned Suprhydrophobic Surfaces, Society for Biomaterials 2014 Annual Meeting and Exposition, Denver, USA, 2014.

Awards

1. Young Investigator Travel Award. 3rd TERMIS World Congress 2012. TERMIS SYIS, TERMIS-EU.

INTRODUCTION TO THE STRUCTURE OF THE THESIS

This thesis is organized in 4 sections, in a total of 11 chapters. The first section provides a general introduction to the thesis. It is based on two book chapters and one review paper already accepted for publication. The second section comprises a single chapter addressing the materials and methods performed to accomplish the experimental work giving rise to this thesis. The third section is based on a set of 6 research articles accepted for publication in international peer-reviewed journals. The forth section summarizes the main outcomes of this thesis and explores future perspectives on the research field. The identification of the original publications regarding submitted/accepted articles can be found in the presenting page of each chapter.

Section I – General Introduction

Chapter 1 – Natural-based and Stimuli-responsive Polymers for Tissue Engineering and Regenerative Medicine. Natural polymers used in the tissue engineering field are reviewed. The use of such polymers in the design of stimuli-responsive devices is also addressed.

Chapter 2 – Biomimetic Superhydrophobic Surfaces. The methods used to process superhydrophobic surfaces are reported and analyzed. The applications of superhydrophobic surfaces in the biotechnology and biomaterials fields are explored.

Chapter 3 – High-Throughput Screening for Integrative Biomaterials Design: Exploring Advances and New Trends. A critical exposition of the evolution of the methods used for high-throughput analysis of biomaterials is presented. Main emphasis is given to recent trends, such as *in vivo* high-throughput analysis of biomaterials and single cell encapsulation techniques.

Section II – Experimental Section

Chapter 4 – Materials and Methods. The experimental setups used to produce the materials used in this thesis are presented. The techniques performed for biomaterials physicochemical, morphological and cellular interaction analysis are also addressed.

Section III – Superhydrophobic Surfaces Patterned with Wettable Spots as Chips to Perform High-throughput Tissue Engineering Studies

Chapter 5 – Combinatorial Cell-3D Biomaterials Cytocompatibility Screening for Tissue Engineering using Bioinspired Superhydrophobic Substrates. Viability and cell number of two distinct cell lines were tested in miniaturized combinatorial alginate-based semi-interpenetrated networks. Image-based methods for cell response analysis were developed and validated against conventional biochemical methods.

Chapter 6 – Combinatorial On-Chip Study of Miniaturized 3D Porous Scaffolds Using a Patterned Superhydrophobic Platform. Combinatorial miniaturized porous scaffolds were processed on-chip by a complexation technique, followed by freeze-drying. Their mechanical and morphological analysis under dry conditions was performed on-chip and validated against samples with sizes frequently used in conventional TE studies. The viability and proliferation of two distinct cell lines was evaluated in-situ by assessing each spot of the chip by image-based techniques. Such methodologies were validated against conventional biochemical methods.

Chapter 7 – Combinatorial study of nanocomposite hydrogels: on-chip mechanical/viscoelastic and pre-osteoblasts interactions characterization. Hydrogels with combinatorial formulations containing bioactive glass nanoparticles targeting bone tissue engineering were processed on-chip. The miniaturized biomaterials were analyzed on-chip for mechanical and viscoelastic properties, similarly to what was performed on Chapter 6, but this time under physiological-like conditions. The selective attachment, proliferation and morphological evolution of a pre-osteoblast cell line were assessed on-chip and analyzed by image-based methodologies.

Chapter 8 – In vivo high-content evaluation of three-dimensional scaffolds biocompatibility. Superhydrophobic patterned chips used in Chapters 5 to 7 for *in vitro* assessment of cell-biomaterials interactions were implanted in an animal model to assess the inflammatory response of 36 biomaterials with combinatorial compositions *in vivo*.

Chapter 9 – On-chip assessment of the protein-release profile from 3D hydrogel arrays. In TE strategies, an adequate response of biomaterials is not only determined by their direct interactions with cells. The formation of an healthy tissue is often dependent on the controlled delivery of bioactive molecules. In an effort to assess on a high-throughput strategy this aspect of effective TE design, the superhydrophobic chips were patterned with alternative circular shapes with superhydrophobic central regions in order to process and fix drug-loaded polymeric spheres and study the release profile of a growth factor model on-chip, by image analysis.

Chapter 10 – Superhydrophobic Chips for Cell Spheroids High-Throughput Generation and Drug Screening. Superhydrophobic chips with wettable spots were used to pattern cellular suspensions by pipetting and also by an automated robot-free protocol. The chips were turned 180° and cell spheroids/microtissues were formed using two distinct cell lines in a hanging-drop system. The effect of on-chip administration of doxorubicin was assessed using image-based analysis.

Section IV – Concluding Remarks and Future Perspectives

Chapter 11 Conclusions and Future Perspectives. This chapter finalizes the thesis by comprising its major conclusions and exploring future perspectives and needs in the field.

SECTION I. GENERAL INTRODUCTION

CHAPTER 1. NATURAL-BASED AND STIMULI-RESPONSIVE POLYMERS FOR TISSUE ENGINEERING AND REGENERATIVE MEDICINE[1]

1.1. INTRODUCTION

Problems and costs related to primordial permanent substitution approaches for tissue defects – i.e. the use of prosthetics - led to the development of biomaterials that aim for synchronized degradability with tissue formation. The development of tissue engineering and regenerative medicine (TERM) approaches which combine biodegradable materials, cells and stimulating factors working as an orchestra for rapid and correct tissue regeneration has immerged as a recent and promising approach for defect regeneration [1,2]. Biomaterials and respective degradation products used in TERM must be non-cytotoxic and promote favorable cellular interactions and tissue development, as well as show adequate mechanical properties and kinetics degradation according to the required application. Ease of sterilization, processing freedom and, ideally, the possibility of incorporation of bioactive molecules are also important aspects that dictate the biocompatibility of a biomaterial [3].

Biodegradable polymeric materials can be obtained synthetically or extracted from natural resources. Nature-derived materials have been proposed for TERM purposes since in general they are similar to macromolecules present in the biological environment and produce degradation products which are recognizable and metabolically processed by the body [4,5]. These characteristics allow for low inflammatory response and toxicity, often associated to synthetic polymers. Different sources for the extraction of natural polymers have been reported. The majority of these polymers are obtained from animal, plant and algae sources. However, microbial sources and enzymatic processes have allowed for the extraction of alternative biopolymers [6]. Besides their origin, natural polymers are usually classified according to their chemical composition in three groups: (i)polysaccharides, which are polymeric carbohydrate structures, formed by repeating units joined together by glycosidic bonds, (ii)proteins, which consist of organic compounds made of amino acids arranged in a linear chain and folded into a globular or fibrillar forms, joined together by peptide bonds and (iii)polyesters, which contain the ester functional group in their main chain.

[1]This chapter was based on the publication: Oliveira MB, Mano JF. Natural-Based and Stimuli-Responsive Polymers for Tissue Engineering and Regenerative Medicine. In Pradas MP, Vicent MJ (eds.) Polymers in Regenerative Medicine: Biomedical Applications from Nano- to Macro-Structures, Germany, John Wiley & Sons, Inc. ISBN 978-0-470-59638-8.

The control of degradation kinetics according to tissue formation is one of the most challenging aspects in the design of a TERM device. The phenomena occurring during the acute inflammatory response obtained after the implantation of a foreign material can be used to modulate the degradation of biomaterials, either by physical, chemical or enzymatic means, by controlling the decrease of pH values and secretion of hydrolytic enzymes by inflammatory cells. Both intrinsic (e.g. molecular weight, crystallinity, hydrophilicity balance, existence of hydrolizable bonds and surface area) and extrinsic factors (e.g. applied stress, biological environment) affect polymers' degradation. Under physiological conditions, natural polymers are usually degraded by hydrolysis (which can be enzyme-catalysed or may occur simply by the contact of the polymer with water, depending on the structure of the polymer), followed by oxidation (promoted by enzymes with oxidative activity and by the release of peroxide and other oxidative agents by inflammatory cells) [7]. Modification of biomaterials' processing parameters and properties such as polymeric chain size, use of different crosslinking agents or inclusion of hydrophobic domains in its structure in order to delay hydrolysis are possible approaches to control degradation kinetics.

Natural polymers have been processed in different structures, obtained by a wide range of techniques, attempting to overcome the tissue regeneration paradigm. Scaffolds, for example, consist of interconnected porous structures in which cells are able to migrate, proliferate and produce ECM. Their main advantage is the control of mechanical properties, which are important not only on load-bearing defects but also on mechanisms of mechanotransduction which affect cell response in aspects such as adhesion and proliferation, as well as differentiation of stem cells [8-10]. The interconnected porous structure is of high importance: it allows for cells to be seeded in an adequate number, followed by migration and colonization of the whole scaffold. Also, it allows for exchanges of nutrients, gases and wastes to be easily managed in the scaffold structure.

Hydrogels have also been proposed for TERM purposes, consisting of hydrophilic polymers usually in a crosslinked form [11]. Several interesting application have been suggested for these structures such as their use as injectable materials for *in situ* hardening by ionic crosslinking, temperature or photopolymerization, allowing for mild cell encapsulation and delivery [12-14]. Hydrogels have also shown to be adequate for drugs and growth factors (GFs) encapsulation, as well as for their sustained release. Microengineered hydrogels have been designed in order to obtain gradients of bioactive molecules and self-assembly of microgels in controlled manner relying in physical interactions has been used in organ printing strategies [15,16].

The use of materials in particulate form offers several advantages such as injectability and enhanced surface area for cell proliferation [17]. The production of particles has been proposed by the use of superhydrophobic surfaces, allowing for high encapsulation rates of bioactive factors [18] that may be further used as implants and tissue growth platforms [19]. In TERM field, microparticles have been proposed not only for delivery of bioactive agents, but also to form injectable *in situ* forming scaffolds after their aggregation by cells and extracellular matrix (ECM) [20], or as cell carriers for enhanced cell expansion in stirring bioreactors due to high surface area compared to conventional two-dimensional cell expansion systems (tissue flasks) [21,22].

According to specific tissue needs, the processing of natural polymers has been adapted. For example, membranes have been developed for several applications, being the most remarkable skin regeneration [23] and guided tissue regeneration (GTR) - generally used for periodontal regeneration [24-26]. Drug permeability of membranes has also been studied [27] as well as ability of mineralization [28] aiming for successful osteogenic tissue regeneration.

Although bulk properties of biomaterials can influence important aspects for tissue regeneration such as mechanical properties of the implantable device, cell interactions with biomaterials are mostly influenced by surface characteristics. Therefore, chemical and physical surface modifications have been widely carried out. A particular case is the creation of coating using the layer-by-layer (LbL) technique. Considering charged polymers as electrolytes, this technique allows for the obtaining of electrostatically adsorbed coatings, which may be a single layer or a set of oppositely charged layers. Natural-derived polymers are often charged and thus can be used in LbL build-up. These complexes may be used as diffusion reservoirs/barriers for active agent delivery [29-34]. However, the use of LbL technique is not restricted to two-dimensional structures: capsules obtained by free-standing LbL techniques using natural polymers have been proposed in the design of porous 3D structures [35] and as cell carrying systems [36].

Regarding response at-will, the inherent responsiveness of some natural polymers has been used in TERM field. Also, combinations and modifications of natural polymers with synthetic polymers characterized by response to external stimuli have been widely proposed [37].

Several natural polymers used for TERM applications will be presented herein, as well as examples of their application and clinical use. Moreover, emphasis will be given to the responsive nature of these polymers or to their modification in order to obtain responsive biomaterial systems for tissue engineering.

1.2. NATURAL POLYMERS AND THEIR APPLICATION IN TERM

1.2.1. Polyssacharides

1.2.1.1. Marine origin

Chitin and Chitosan

Chitin is the second most abundant natural polymer in nature and can be found in the shell of crustaceans, cuticles of insects, and cell walls of fungi [38-40]. Its structure is composed of β(1→4)-linked *N*-acetyl-D-glucosamine units [40] and its applications have been limited due to its insolubility in water and in most of the common organic solvents. An improvement in the biocompatibility of chitin has been achieved by associating chitin with other polysaccharides or proteins [41], or by creating chitin derivatives (e.g. water-soluble chitin, dibutyl chitin) [42-44].

Chitosan is a natural polysaccharide obtained from the deacetylation of chitin, and it is arguably the most widely used biopolymer for biomedical applications. It has structural similarity to glycosaminoglycans (GAGs), making it a potential candidate for connective tissue engineering. Free amine and hydroxyl groups on its molecular chain make physically or chemically modification possible. Chitosan has unique biological properties which include non-cytotoxicity, biodegradability to harmless products, physiological inertness, remarkable affinity to proteins, haemostatic, antitumoral and anticholesteremic properties [40].

In a study regarding *in vitro* and *in vivo* degradations of chitin and desacetylated chitin (in different percentages) films, the *in vitro* degradation was carried out by immersing the films in buffered aqueous solution at pH 7 containing lysozyme at 37°C, while the *in vivo* degradation was studied by subcutaneously implanting the films in the back of rats. It was found that the rate of *in vivo* biodegradation was very high for chitin and that the films which were more than 73.3 mol% deacetylated (including chitosan) showed slower biodegradation [44].

The cationic nature of chitosan allows for pH-dependent electrostatic interactions with anionic GAGs, proteoglycans and proteins (including DNA) widely distributed throughout the body. This property is one of the important elements for tissue engineering applications because numbers of cytokines/GFs are known to be bound and modulated by GAGs such as hyaluronic acid [45,46] and chondroitin sulfate [47], remarkable in cartilage repair.

Chitosan-based complexes have an excellent ability to be processed into sponges, for example with collagen [48], alginate [49], silk [50] or starch [51]. Interactions between chitosan and other proteins besides gelatin [52-54] have been studied as matrices with suitable mechanical properties, biodegradability, and good biocompatibility. Aiming for the improvement of mechanical properties of scaffolds and modulation of their degradability, chitosan has been blended with synthetic polymers, such as poly(lactic-*co*-glycolic acid) (PLGA) [55,56], polyethylene oxide (PEO) [57], carbon nanotubes [58] and different polyesters such as poly(ε-caprolactone) (PCL) [59].

Regarding bone tissue engineering, in efforts to improve mineralization, chitosan has been blended with ceramics such as calcium phosphates, hydroxyapatite, glasses or silicates, which enhance its mechanical properties and provide osteoconductive properties to the devices [60-70].

Multilayer systems containing chitosan have also been proposed. For example, a chitosan/silk fibroin multilayer system was studied in order to assess the aligning of the fibers formed in parallel to the dipping direction. Monodirectional and bidirectional alignments were varied simply by rotating the substrate towards the dipping solution. These surface characteristics, added to the inherent biocompatibility of both constituting materials of the multilayer system and respective enhanced mechanical properties (especially from silk fibroin) make this system an interesting possibility for the coating of implantable biomaterials or to be used as biotemplates for cell orientated growth [71]. Also, polyssacharide multilayers containing chitosan enhanced the response of mesenchymal stem cells (MSCs) to GFs [33]. LbL processing can be also performed aiming for the production of membranes, instead of direct coating of implantable devices: free standing and detachable chitosan/hyaluronic acid multilayers were fabricated by depositing the layers in a hydrophobic substrate and by light crosslinking before detachment [72].

Regarding examples of injectable hydrogels and *in situ* forming scaffolds which application avoids complex surgery procedures, a chitosan and hyaluronic acid blend was proposed for cartilage repair by the encapsulation of chondrocyes [45] and chemically crosslinked chitosan particles were proposed as injectable microparticles for injection and further gathering by cells [20].

In the clinical practice, the high swelling properties of chitosan have been used for the development of wound dressing such as ChitoSkin (approved by European Comission) and HidroKi®.

Alginate

Alginate is one of the most studied and applied polysaccharidic polymers in tissue engineering. Commercial alginates are extracted from three species of brown algae*: Laminaria hyperborean,*

Ascophyllum nodosum and *Macrocystis pyrifera*. Alginate exists as a mixed salt of various cations found in the seawater such as Mg^{2+}, Sr^{2+}, Ba^{2+}, and Na^{+} [6,73]. Although more rare, bacterial alginates have also been isolated [74]. This water-soluble linear polysaccharide extracted from brown seaweed is composed of alternating blocks of (1→4) linked α-L-guluronic and β-D-mannuronic acid residues, which are sequentially assembled in either repeating or alternating blocks. The composition and extent of the sequences and the molecular weight determine the physical properties of the alginates [73].

Although alginate is an attractive material due to its biocompatibility and ability to form hydrogels, its slow and uncontrollable degradation can be an undesirable feature. For example, in a study aiming for cartilage regeneration, although histologic evaluation revealed the architecture of the newly formed tissue to be similar to that of native cartilage, there was little sign of alginate degradation after 12 weeks [75]. Mooney and co-workers characterized gels formed using a combination of partial oxidation of polymer chains and a bimodal molecular weight distribution of polymer. The rate of degradation could be controlled by both the oxidation and the ratio of high to low MW alginates [76]. Considering ionically crosslinked alginate hydrogels, they usually undergo slow dissolution mainly due to the sensitivity of the gels towards divalent ions (usually calcium) chelating compounds (e.g. phosphate, citrate and lactate) or gradual exchange with monovalent cations [7].

The gelation of alginate can be carried out under an extremely mild environment and uses non-toxic reactants. The most important property of alginates is their ability to form gels by reaction with divalent cations [6,77]. The obtained gels are similar to solids in retaining their shape and resisting to stress. Depending on the amount of calcium present in the system, inter-chain associations can be either temporary or permanent [78]. The chemical structure, molecular size, gel forming kinetics and the crosslink cation have significant impact on functional properties including porosity, swelling, stability, gel strength and the gel's immunological characteristics and biocompatibility [73].

Due to its gelation in the presence of calcium ions, alginate is an appealing polymer to use as *in situ* forming hydrogel, counting on the hardening of the solution after injection [12,79]. For this reason and due to the unique properties of alginate, combined with its relatively low cost, is an important polymer in medical applications. Alginates are approved by several regulatory authorities, such as the FDA, for human use as wound dressing. Alginate hydrogels are used extensively in cell encapsulation, cell transplantation and tissue engineering applications [12,49,66,77,80-90]. Recently, a new method for cell encapsulation in alginate particles was proposed by Song *et al*[18] based on the dropping of an alginate solution in superhydrophobic surfaces.

This polymer has been widely used as a model polymer to prove concepts for TE purposes. For example, a system composed of a perforated electrospun mesh and bone morphogenic protein (BMP)-modified alginate was efficient in regenerating a challenging femur defect in a mouse model [83]. Hollow interconnected capsules resulting in scaffold-like structures obtained by LbL technology [86] and the production of cell-laden hollow fibers by microfluidic chips using the "on-the-fly" method aiming for the development of biomimetic structures have been concepts based on the use of alginate [85].

A mixture of alginate and gelatin has been used to cryopreservate cell/hydrogel constructs by incorporation of cryoprotectants in the predesigned structures that were then subjected by a freeze/thaw process. This method may be useful for the preservation of new fabricated organs [91].

Carrageenans

Carrageenans are a family of sulfated polysaccharides extracted from red marine algae, widely utilized in the industry because they can form reasonably stiff and thermoreversible gels in the presence of gel-promoting salts at room temperature [92]. These linear polymers consist of chains of (1→3)-linked β-D-galactose and (1→4)-linked α-D-galactose units which are variously substituted and modified to the 3,6-anhydro derivative, depending on the source and extraction conditions [81]. According to their patterns of sulfate esterification, the three major types of carrageenan are: κ (kappa), ι (iota), and λ (lambda), which are all flexible molecules and at higher concentrations wind around each other to form double-helical structures. These polymers are thixotropic [93], i.e., they thin under shear stress and recover their viscosity once the stress is removed.

In TERM field, carrageenans have been used to produce hydrogels for controlled delivery of GFs for bone tissue regeneration [94] and injectable systems for cartilage repair, in combination with other natural polymers [95]. Also regarding cell encapsulation, it has been used to form membranes and microcapsules, combined with sodium alginate, providing an effective support for cell proliferation with appealing diffusion and mechanical properties [96].

A blend of carrageenan/gelatin obtained by freeze drying and further chemical crosslinking was tested in Wistar rats, showing to be safe and as a promising system to be used in tissue engineering [97] Moreover, blends with calcium phosphates have been successfully obtained, improving hydroxyapatite formation [98].

Ulvan

Among the three main divisions of macroalgae, green algae remain largely unexploited. In the past decade, marine eutrophication has promoted the proliferation of algal biomasses, namely, of Ulva.

Ulvan is designated in order to denote polysaccharides from members of the Ulvales, namely, Ulva. This polymer is mostly composed of rhamnose, glucuronic acid, iduronic acid, xylose and sulfate [99-101]. Ulvan has been proposed as a biomaterial after functionalization (methacrylation), which allowed for the obtaining of a photopolymerizable hydrogel [102]. However, developments on tissue regeneration area still lack to prove the potential applications of this abundant natural polymer.

Galactans

- **Agarose**

Agarose is a typical naturally occurring polysaccharide which is biocompatible, shows soft tissue-like mechanical properties, transparency (allowing for photochemical modification) and mechanical tunnability by varying its weight concentration. It gels in water at reduced temperatures and is considered to be non-adhesive to cells, non-adsorptive to proteins and resistant to swelling, thereby providing a blank canvas on which specific biological molecules can be immobilized. The use of agarose for *in vivo* applications does not induce specific immunological response, so it has been used as a carrier to deliver cell secreting factors via encapsulation. Several cell types such as hamster islet cells were encapsulated in agarose beads, exhibiting prolonged viability. Also, intraperitoneally injected mouse fibroblasts co-encapsulated with poly(hydroxyethyl methacrylate-co-methyl methacrylate) (HEMA-MMA) and agarose prevented aggregation of cells, which also happened in the encapsulation of human and mouse ESCs. Functionalization with vascular endothelial growth factor (VEGF) for use in guide pluripotent stem cell aggregares toward blood progenitor cells was carried out [103]. Aiming for bone regeneration, quick-forming hydroxyapatite/agarose gel composites induced *in vitro* bone regeneration [104] were further implanted in rat cranial defects [105]. Cryogels composed of agarose and gelatin with elastic and macroporous features, with isotropic and anisotropic porosity were also proposed for general TE [106].

1.2.1.2. Vegetal Origin

Starch

Starch is the predominant energy-storing compound in many plants. It can be found in storage organs such as roots and tubers in a granular form. The structure and composition of native starches vary with the botanical sources, but all granules consist of two types of α-glucan polymers, that is, amylose and amylopectin. Amylose, the minor constituent, is defined as a relative long and linear polymer consisting mainly of α(1→4) linked D-glucopyranosyl units. Amylopectin, the major component, is a branched

polysaccharide composed of hundreds of short (1→4)-α-glucan chains, which are interlinked by (1→6)-α-linkages [107].

The human body can degrade starch by using specific enzymes including α-amylase present in saliva and also in the blood plasma. Starch degradation products are oligosaccharides that can be metabolized to produce energy. Other enzymes involved in starch degradation are β-amylase, α-glucosidases, and other debranching enzymes [61,108].

Starch-based materials possess a wide range of properties that support their potential for biomedical applications, such as their biodegradability [109] and the processing freedom into diverse shapes: 3D porous scaffolds obtained by freeze-drying [110], rapid prototyping [111] or supercritical precipitation [112], microparticles [107], fillers [113], smart hydrogels [51] or electrospun fibers [114]. Starch has been studied for several biomedical applications, such as scaffolds for bone engineering [61,107,111,115] or spinal cord injury treatment [116] and hydrogel for cartilage regeneration [51]. 3D porous scaffolds based on starch-based materials have been shown to be biocompatible and to possess interesting *in vivo* behavior [117].

Due to the thermoplastic behavior of the starch-based blends and composites, it is possible to produce 3D porous scaffolds using traditional melt-based technologies, such as compression molding combined with particulate leaching [118], melt-fiber depositions [119] and injection molding [120] or extrusion with blowing agents [121]. This processing routine offers the unique advantage of avoiding the use of solvents, which sometimes are detrimental in the biomedical field. SPCL-(starch with PCL) and SPLA-(starch with PLA) based scaffolds were prepared by a fiber-bonding process using fibers obtained by melt-spinning [122].

Cellulose

Cellulose is the most abundant natural polymer in the world having, as a consequence, a low cost. In nature, it is the primary structural component of plant cell walls. It is a linear polysaccharide of D-glucose units linked by β(1→4) glycosidic bonds where every other glucose residue is rotated approximately 180° [78]. The glucan chains in cellulose are parallel to each other and are packed side by side to form microfibrils, which stabilizes the structure, minimizing its flexibility [78]. This highly cohesive, hydrogen-bonded structure, gives cellulose fibers exceptional strength and makes them water insoluble despite their hydrophilicity [123].

Several works have investigated the use of cellulose for cartilage [124], bone [125] and cardiac [126] applications. Cellulose has also been electrospun to form high protein affinity membranes [127].

Hydroxypropylcellulose is non-ionic water-soluble cellulose ether with a remarkable combination of properties. It combines organic-solvent solubility, thermoplasticity and surface activity. A commercially available hydroxyethylcellulose named Natrosol® 250HX is distributed by Hercules in United States and has a degree of substitution of 1.5 (three hydroxyls substituted/two units). Genialab in Germany trades geniaBeads® MC which are hydrogel beads made from modified cellulose [78].

Pectin

Pectins are polysaccharides enriched in galacturonic acid and galacturonic acid methyl ester units. They form the chemically and physically stable skeletal tissues of plants, when combined with proteins and other polysaccharides. These polymers have high molecular weight and polyanionic nature, and react to their environments, ranging from dense gels to dilute solutions. These properties enable pectin polymers to carry signal molecules and support various biologically active substances [128].

Regarding regenerative medicine approaches, dry particles of pectin and calcium chloride have been blended with PLGA, forming a porous matrix in which the presence of the synthetic polymer – PLGA – reinforced the mechanical properties of the structure, while the presence of the natural polymer – pectin – allowed for enhanced cell behavior of preosteoblastic cell line cells [69]. Aiming a biomimetic approach for bone tissue engineering, *in situ* polymer matrix-mediated synthesis of hydroxyapatite was achieved using a natural polymer polyelectrolyte chitosan-pectin/hydroxyapatite composite network. Hydroxyapatite nucleation could be modulated varying the pH value of the medium since it begins with the formation of the complex among calcium/phosphate ions on amino/ carboxyl groups of the molecular chain of chitosan and pectin. This allowed for the modulation of the size of the nanohydroxyapatite particles formation in the prepared 3D scaffold [129].

1.2.1.3. Microbial Origin

Gellan Gum

Gellan gum is a linear anionic polysaccharide composed of tetrasaccharide (1,3-β-D-glucose, 1,4-β-D-glucuronic acid, 1,4-β-D-glucose, 1,4-α-L-rhamnose) repeating units, containing one carboxyl side group. This polymer is manufactured by microbial fermentation of *Sphingomonas paucimobilis* and is water soluble. When heated and mixed with mono or divalent cations, gellan gum gellifies upon lowering the temperature under mild conditions [130]. Due to easy processing into transparent gels resistant to heat and acid stress, lack of toxicity, processing under mild conditions, ability to be used as an injectable system in a minimally invasive manner, and the structural similarity with native cartilage GAGs, this

polymer has been widely used in biomedical field [130]. The polymer exists in two forms - acetylated and deacetylated being the deacetylated the most common and commercially available form. Thermoreversible gels formed by both types vary in their mechanical properties from soft and elastic for the acetylated form to hard and brittle for the fully deacetylated polysaccharide.

In regenerative strategies, this polymer has been proposed for spinal cord injury repair [116] and cartilage repair [131] in the form of hydrogels. Also, membranes for GTR were suggested [132] Gellan gum methacrylation allowed for its crosslinking by exposure to UV light, permitting easy cell encapsulation [133]. The gelation temperature of this polymer has been tailored to physiological values and conductive properties have been achieved by the incorporation of carbon nanotubes aiming for cell electrical stimulation [134].

Dextran

Dextran is a biodegradable and biocompatible branched high molecular weight polymer produced by different bacterial strains from sucrose via the action of dextransucrase enzyme. It consists of α(1→6)-linked D-glucose residues with some degree of branching via α(1→3) linkages [135]. It is widely used as plasma expander and blood substitute, since it binds to erythrocytes, platelets and vascular endothelium by reducing their aggregation and adhesiveness [78].

Chemically crosslinked dextran hydrogels can be obtained by reaction with bifunctional reagents like diisocyanates and epichlorohydrine or by derivatization with, e.g. polymerizable methacrylate groups, which can be polymerized by UV light after the addition of an initiator system [136].

Dextran has been processed in the form of nanofibers by electrospinning and combined with PCL for general tissue engineering purposes [137]. It was also blended with PLGA to study the effect in fibroblast/macrophages co-culture [138] and used in the fabrication of interpenetrated networks with gelatin for vascular regeneration [139]. The immobilization of RGD peptide domains in dextran has allowed for enhanced cell attachment [140] while, on the other hand, the immobilization of dextran in polyethylene terephtalate (PET) limited cell adhesion and spreading [141]. Dextran membranes have also been used as absorbents in wound healing [142].

Pullulan

Pullulan is a neutral, linear and nonimmunogenic polysaccharide produced from starch fermentation by *Aureobasidium pullulan*. It consists of glucose units linked through α(1→6) and α(1→4) glycosidic bonds [143]. It has been widely used in food, pharmaceutical, and cosmetic industries for its functional properties that include adhesiveness, film formability, and enzymatically-mediated degradability [110]. It

is considered an attractive polymer for biomaterial development because of its good mechanical properties and biocompatibility, as well as lack of mutagenic, carcinogenic, and toxicological activities [143].

In regenerative medicine, its applications have covered wound healing in the form of nanohydrogels combined with prostaglandin E1 [144], vascular tissue regeneration [145,146] as well as for bone tissue engineering using scaffolds which porosity was controlled by simply varying freeze-drying conditions [110]. Bae *et al* [147] have produced methacylated pullulan photocrosslinkable cell laden hydrogels that promoted cell proliferation and formation of clusters.

Xanthan Gum

Xanthan gum (XG) is an extracellular polysaccharide secreted by the microorganism *Xanthomonas campestris*. It consists of a primary chain of β-D-(1→4)-glucose backbone, which has a branching trisaccharide side chain composed of β-D-(1→2)-mannose, attached to β-D-(1→4)-glucuronic acid, which terminates in a final β-D-mannose [148].

Due to its anionic character, inertness and non-cytotoxicity, XG offers a potential utility as a drug carrier. However, applications of this polymer in regenerative medicine are still rare. In 2009, a novel super-porous hydrogel was synthesized through chemical crosslinking by graft copolymerization of 2-hydroxyethyl methacrylate and acrylic acid on to XG. The hydrogel seemed to be suitable for various biomedical applications due to its high water absorption capability, swelling and biodegradability [148].

Glycosaminoglycans

- **Hyaluronic Acid**

Hyaluronic Acid (HA) is a linear, unbranched polymer composed of repeating disaccharide units: glucuronic acid, β(1→3) and β(1→4) linked *N*-acetyl-glucosamine [149]. HA is a major component of the ECM and of the synovial fluid. It is implicated in joint lubrication, water homeostasis of tissues, cell motility and inflammation[150]. It is also a highly conserved GAG that functions in matrix stabilization, cell signaling, adhesion, migration, proliferation and differentiation [45].

As a biomaterial, HA has been proposed for adipose [151], vascular [152], general soft tissue [153], skin [154], neural [155], bone [156], osteochondral [150], cardiac [157] and, mainly, cartilage tissue regeneration [135-137]. In formulations with other materials, it has shown induction of chondral differentiation [158] and direction of chondrocyte phenotype [159]. It has been used alone or in mixtures with other polymers such as chitosan [46], fibrin [160], dextran [161] and gelatin [159], and processed in different manners, in order to mainly obtain hydrogels, as well as also scaffolds and membranes (e.g.

in the form of multilayers [155]). Regarding its degradation, the metabolic degradation of HA is mainly intracellular, and it is presumed that the presence of hyaluronidase is a prerequisite for its metabolic degradation [7].

HA modified by methacrylation has been used to produce hydrogels with gradients of mechanical properties by varying the exposure time of the gels to UV light, which allowed to spatially control the morphology and proliferation of human MSCs [162]. An extrudable gel obtained from the photocrosslinking of methacrylated HA with partially photocroslinked methacrylated gelatin allowed for the bioprinting of tubular systems using drops of the polymeric mixture with encapsulated cells.[159] Also, the use of centrifuge forces (centrifugal casting) has been used for the preparation of tubular constructs and flat geometrical forms with desired cell compositions and precise cell distribution from an *in situ* crosslinkable HA with encapsulated cells [152].

Injectable hydrogels containing human articular chondrocytes were proposed by Pereira *et al* [95] for cartilage regeneration, showing appealing results in *in vivo* tests in bovine knee defects.

The biocompatibility of neural cells has been improved using HA-based multilayers [155], which were constituted of HA/poly(allylamine hydrochloride) (PAH), HA/collagen (the ending layer was always the second polymer). Results suggested that the hippocampal neurons prefer HA/PAH films, while HA/collagen films attract cortical neurons.

In efforts to develop a new bone tissue engineering material, Antunes *et al.* [164] modified PLLA with glutaraldehyde-crosslinked HA. Cells were kept viable in such structures and mechanical properties were dictated basically by the ones of the PLLA construct.

- **Chondroitin Sulfate**

Chondroitin sulfates are heparin-like GAGs composed of alternate sequences of differently sulfated residues of uronic acid (β-D-glucuronic) and α-D-*N*-acetyl-galactosamine linked by β(1→3) bonds. These sulfated proteoglycans are widely found in the ECM of various tissues, at the surface of many cell types and in intracellular secretory granules [165,166].

This proteoglycan has been used mainly in the regeneration of chondral tissue [46-48,161,167-170] since it is one of the major components of cartilage, and showed ability to induce chondrogenic differentiation of MSCs [171]. On the other hand, it has shown to be an important inhibitor of neural cells regeneration [172,173]. It has been often blended with other polymers such as chitosan [46,67,167]. The stabilization and release of important GFs for tissue regeneration in matrices containing this polymer has also been performed [167,174].

1.2.2. Protein-Based Polymers

Silk

Silks are generally defined as protein polymers that are spun into fibers by some *Lepidoptera larvae* such as silkworms, spiders, scorpions, mites and flies. These proteins are usually produced within specialized glands after biosynthesis in epithelial cells, followed by secretion into the lumen of these glands where the proteins are stored prior to spinning into fibers. Silks differ widely in composition structure and properties depending on the specific source. The most extensively characterized silks are from the domesticated silkworm, *Bombyx mori*, and from spiders [175,176].

Silks are characterized by a highly repetitive primary sequence that leads to significant homogeneity in secondary structure: β-sheets. Their relative environmental stability, in combination with their biocompatibility, unique mechanical properties, and options for genetic control to tailor their sequence [177] provide an important basis to exploit these natural proteins for biomedical applications. Their thermal stability up to 250°C allow for their processing over a wide range of temperatures [175].

Structures such as hydrogels, fibers and sponges aiming for different tissues regeneration such as cartilage [50, 178], soft tissue [23], bone [179,180], breast [181], corneal [182] and tendon [183] have been proposed using this polymer. Microcarriers for BMPs release were processed [184] and cell encapsulation in silk hydrogels was successfully performed [185].

Silk obtained from *Bombyx mori* has been widely used by Kaplan and co-workers [186]. In the case of corneal regeneration, RGD-functionalized-silk was studied with corneal human fibroblasts in order to mimic the structural hierarchy of human corneal stroma within thin stacks of lamellae-like tissues. RGD surface modification enhanced cell attachment, proliferation, alignment and expression of collagens type I and V and proteoglycans (decorin and biglycan), being a useful strategy for engineering human corneal [182].

Regarding the production of fiber scaffolds, silk has been processed by electrospinning, usually in blends with other polymers in order to improve the processability of the solutions. Polyethelene oxide (PEO) has been processed with silk fibroin in order to obtain aligned fibers and porous scaffolds, joining electrospinning technique - hampered by final low porosity - with salt-leaching technique, previously applied to simple 3D freeze-dried silk fibroin scaffolds, aiming for spatially distributed porosity in a single scaffold [187].

In clinical practice, silk sutures such as DemeTech® and Perma-Hand® are commonly used in clinical practice as non-degradable sutures, since the time they take to degrade is higher than the FDA standard for biodegradable materials (2 months).

Collagen

Collagen is a naturally occurring protein and the major component of ECM, providing support to connective tissues [188,189]. In tissues, it transduces signals for the regulation of cell anchorage, migration, proliferation, differentiation and survival [190]. Twenty-seven types of collagens have been identified, but collagen type I is the most abundant and the most investigated for biomedical applications [191]. Fibril-forming collagen molecules consist of three polypeptide chains of glycine-X-Y amino acid repeats twined around one another to form triple helices [192]. High mechanical strength, good biocompatibility, low antigenicity and ability of being crosslinked, and tailored for its mechanical, degradation and water-uptake are properties of this polymer. It is mainly isolated from animal tissues, leading to safety concerns based on the potential for viral and prion contamination. Usually, collagen is a hard to process polymer and the extent and rate of degradability is difficult to control, requiring crosslinking procedures. Moreover, sterilization of collagen usually incurs in some degree of alteration of the polymer structure [193]. Collagen gels belong to a special kind of injectable hydrogels, called shear-thinning, which solidify due to changes in shear stresses [6].

Le-Ping *et al* proposed a blend of chitosan with collagen crosslinked with genipin for articular cartilage regeneration [170]. Polylactide microspheres covered with collagen were proposed as chondrocyte carriers [194] and particles of this biomaterial were used as building blocks for organ printing [195]. Surface modification by grafting of collagen has shown to improve cell adhesion and cell viability of bone marrow stromal cells in chitosan/poly(lactic acid) scaffolds, which biodegradation was also improved [196].

The pluripotency of bone marrow stem cells could be maintained in collagen scaffolds, and neural differentiation occurred while the cells were exposed to differentiating agents. Blends of collagen with other natural polymers such as GAGs [174] have been used for tranforming growth factor-β (TGF-β) release and collagen scaffolds loaded with this GF have been successful in the regeneration of full-thickness abdominal defects in rats [197].

Recently, a broad range of tissue engineering products based on collagen scaffolds has been developed and commercialized, especially for skin in the form of skin grafts (for example FDA-approved Integra® Dermal Regeneration Template, which showed good results in full-thickness burns treatment [198]),

bone regeneration (in the form of sponges and composites with hydroxyapatite [61]) and GTR, widely used in dentistry (for example, resorbable double-layered Bio-Gide® membranes). For example, a Collagen Bone Healing Protective Sheet (Collagen Matrix, Inc.), derived from type I collagen was approved by FDA for orthopaedic applications. Other examples of commercial collagen sponges are CollaPlug® and Ultrafoam®.

Gelatin

Gelatin is a protein obtained by the controlled hydrolysis of collagen. It has been widely applied in clinic for its nonantigenicity, favorable absorbability, and cost efficiency. It has also been proven to accelerate wound healing and tissue regeneration [199]. The biodegradation of gelatin can be tailored by controlling the crosslinking density using a wide variety of chemical and physical crosslinking techniques [200].

Different forms of this polymer have been processed: membranes have been obtained by electrospinning to be used in GTR [201] and blends with PLGA have also been electrospun [202], Hydrogels of interpenetrated networks with dextran were proposed for vascular tissue engineering [139], as well as blends with hyaluronic acid [152]. These blends were also proposed for chondrogenic differentiation [158] and for the obtaining of a photocrosslinkable hydrogel [159]. Other blends with natural polymers include its mixture with chitosan for liver tissue engineering [52,53]. Resorbable sponges have been prepared for cartilage repair [203], and a composite with hydroxyapatite has been proposed for bone regeneration [204]. Hydrogels of gelatin have also been used for cell delivery [205] and as carriers for cell sheets [206]. Microcarriers of this polymer have been widely used for GFs delivery [207}, for example in the treatment of osteoarthritis in rabbit knees [208] or aiming for chondrogenic differentiation of stem cells [209]. A clinical study aiming for GTR of healthy dermis was carried out by Huss *et al* [210].

Elastin

Elastin is an ECM protein that is known for providing elasticity to tissues and organs. Tropoelastin, the precursor protein of elastin synthesized as a 72 kDa peptide by a variety of cells including smooth muscle cells, endothelial cells, fibroblasts and chondrocytes, and elastin-like peptides have the potential to self-assemble under physiological conditions [211].

Incorporation of elastin in biomaterials is especially indicated when elasticity or its biological effects are required. However, problems such as calcification, usually detected in cardiac grafts and valves [211], may occur.

Purified elastin allows the construction of highly defined scaffolds, e.g composed of elastin and collagen [212], membranes for wound healing [213] and tubular structures to be used as vascular grafts [214]. In some cases GFs were incorporated with this polymer, and the mixture has been electrospun [215,216].

Repeated elastin-like sequences can be produced by synthetic or recombinant means. Using protein engineering, many different parameters of elastin-like molecules can be controlled: including amino acid sequence, peptide length, and — in the case of block copolymers — the length and number of the blocks. Another advantage is the opportunity to incorporate specific sequences that have cell biological effects [217]. Recombinant expression systems result in highly homogeneous protein preparations. The thermally responsive behavior of ELPs may also be exploited in biomaterials (soluble below transition temperature Tt, but aggregated above Tt), for example as injectable biomaterials. Urry and co-workers showed that physical properties of ELPs are highly dependent on the amino acid composition of the peptide repeat. One particular property of these polypeptides is the transition temperature Tt. The Tt of polymers based on (Val-Pro-Gly-Xaa-Gly)n could be extensively manipulated by the amino acid at the Xaa position and resulted in a dependency on e.g. temperature, pH, and electrochemical potential [218]. Urry and co-workers proposed various elastin-like materials, first by chemical synthesis and later by recombinant expression systems. Several bioelastic materials have been tested in animal models for soft-tissue restoration, e.g. in intervertebral-disc restoration in a rabbit model [147]. Also, ELPs have been used for the production of injectable particles for *in situ* scaffold formation by cell-induced particle agglomeration, as well as for the modification of surfaces by LbL methodology allowing for multi-stimuli response [219,220].

Fibrin

Fibrin is one of the natural ECM proteins which effectively has wide applications in reconstructive surgery and bioengineering. Fibrin glue has been successfully tested to seal severed nerve ends in experimental animals and in surgical trials for primary nerve repair in humans [221]. This polymer has been used as matrix for cartilage repair, either as a cell carrier [77], or mixed with synthetic [222] and natural polymers [162]. Also, in the form of suture [223] and tubular conduit [224], it has been helpful in nervous regeneration. Wound healing is also a major field of application of fibrin [225] and heart tissue has also been regenerated using this polymer [226].

Fibrin glue is used in medical practice to promote wound healing and skin grafting. Commercially prepared fibrin sealants, Tisseel (Immuno, Vienna, Austria), Beriplast (Behringwerke AG, Marburg/Lahn, FRG), and Biocol (CRTS, Lille, France) have been used extensively in Europe for almost 15 years.

Fibronectin

Fibronectin (Fn) is an ECM protein known to promote cell attachment and spreading. The mechanism is thought to involve attachment of $\alpha 5\beta 1$ transmembrane integrin receptors to Fn's cell binding site, located on the 10th type-III repeat module and containing the specific amino acid sequence RGD, as well as to synergy sites located on the 8th and 9th type-III repeats [6, 227].

The coating of biomaterials with Fn allowed for a variety of cell-contacting applications, where cell adhesion is enhanced. This concept has been proven adsorbing Fn on the surface of starch-based scaffolds, leading to enhanced endothelization [228], and also in alginate hydrogels [229]. In films obtained by layer-by-layer technique, in which Fn was adsorbed in the outermost layer cell adhesion and morphology were also improved [31,230,231].

Keratin

Keratins are a family of structural proteins that can be isolated from a variety of tissues. ''Soft'' keratins are cytoskeletal elements found in epithelial tissues while protective tissues such as nails, hooves, and hair are composed of ''hard'' keratins. Numerous methods exist for denaturing these proteins which are characterized by a high sulfur content and extensive disulfide bonding, under either oxidative or reductive conditions [231]. Kerateines or keratoses (oxidatively or reductively derived, respectively), alone or in combination with other biomaterials, have been tested in a small number of systems to demonstrate feasibility for medical applications such as wound healing [232], bone regeneration (in a blend with hydroxyapatite) [233], olfactory ensheathing cells proliferation (blended with PLGA) [234] and peripheral nerve repair [235]. Electrospun nanofibers of a blend of keratin with poly(L-lactic acid) were also tested for bone tissue regeneration [236] These investigations have shown generally good compatibility with cells and tissues.

Resilin

Resilin belongs to the family of a unique extracellular matrix ECM protein with outstanding elasticity and long fatigue life due to its role in nature, where it is adapted for the jumping mechanism of fleas, the vibrating membrane of cicadas and the flight system in the wings of dragonflies [237]. Regenerative medicine applications of resilin include the use of its recombinant analogs [238]. By the adsorption of a

resilin-like polymer obtained by recombinant technology, pH responsive coatings have been fabricated [239].

Mussel-based adhesive polymers

Marine and freshwater mussels secrete proteinaceous adhesive materials for adherence to the substrates upon which they reside. The protein adhesives, called mussel adhesive proteins (MAPs), are capable of mediating the firm attachment of the organisms onto substrates with highly hydrated conditions. One of the defining characteristics of MAPs is the presence of L-3,4-dihydroxyphenylalanine (DOPA), an amino acid that is formed by posttranslational modification of tyrosine and is responsible for their adhesive behavior [240,241].

When DOPA and its derivatives are chemically coupled to synthetic polymers, these synthetic mimics demonstrate strong moisture-resistant adhesive properties to various substrates, including titanium, soft tissue, and bone [242].

Mixtures of DOPA with poly(ethylene glycol) (PEG) and PCL were processed as films for soft tissue repair [243], as well as DOPA-functionalized PCL nanofiber meshes were used for endothelial cells culture, showing improved performance compared to gelatin-coated fibers [244]. Surface modification of gold and titanium has been performed by adsorption of DOPA and MAPs analogues conjugated with DOPA to monomethoxy-terminated PEGs. The ability of the surfaces to resist cell attachment was examined by culturing 3T3 fibroblasts on the surfaces, and results showed inhibition of cell attachment for up to 14 days, which can be interesting in the development of biomaterials to which certain cell types attachment must be avoided such as vascular tissue engineering [245].

1.2.3. Polyesters

1.2.3.1. Microbial Origin

Polyhydroxyalkanoates

Polyhydroxyalkanoates (PHAs) are a family of biopolyesters produced by some bacteria as intracellular carbon and energy compound. This production occurs under unfavorable growth conditions such as limitation of nitrogen, phosphorus, oxygen or magnesium in the presence of excess supply of carbon source. These polymers are considered attractive for tissue engineering due to their bioabsorbability and non-cytotoxicity [246]. The properties of these polymers can range from hard and brittle to soft and

elastomeric. In general, degradation occurs by enzymes (depolymerases) and by hydrolysis [247], and *in vivo* it is catalyzed by lipases, esterases and proteases.

Poly(3-hydroxybutyrate) (PHB) is the most thoroughly investigated member of the PHA family and has shown good biocompatibility with several cell types. However, its high brittleness and low degradation have limited its application [248]. Poly(3-hydroxybutyrate-co-3-hydroxyhexanoate) (PHBHHx) is a new member of PHA family and has been reported to have much better elastomeric mechanical properties than PHB and PHBV [249].

This class of polymers has already been used for bone [250-252], cartilage [253-254], skin [247], heart [255] and ligament/tendon [245] tissue regeneration and has been processed by techniques such as electrospinning [246]. TephaFlex® are commercial resorbable sutures made of a recombinant PHA.

1.3. NATURAL POLYMERS IN STIMULI-RESPONSIVE SYSTEMS

Stimuli-sensitive or "smart" polymeric systems are polymers that undergo strong physical or chemical property changes responding to small changes in the environmental conditions. The change may be dependent on the magnitude of the signal and different stimuli have been reported as modulators of polymeric systems. Stimuli may be physical (e.g. temperature, light, mechanical stress or electric field) or chemical (e.g. pH or ionic strength) and their application changes the interaction between polymeric chains or between the polymer and a solvent (see Figure 1.1).

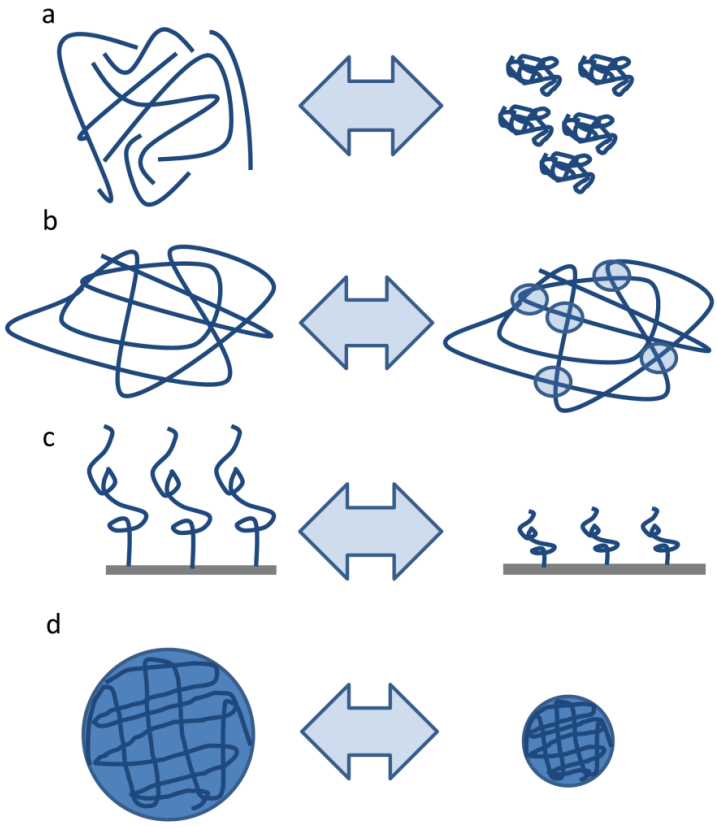

Figure 1.1 – Several types of response of polymeric chains to different stimuli. (a) Response to stimuli of polymeric solutions, from random dispersion of the polymeric chains (left) to coiled state (right). Examples of this type of response are natural polymers modified with PNIPAAm, ELPs with temperature, pH or ionic strength shifts, and natural polymers with sol-gel transition with temperature (*e.g.* gelatin) or pH (*e.g.* alginate). Also, responsive systems in which the configuration of molecules or polymeric chains is different according to the stimuli can be taken as examples in this type of response. An example is the azobenzene-cyclodextrin conjugates, in which the isomeric form of the azobenzene is changed from *trans* to *cis* form according to the exposure to visible or UV light. The *trans* form is known to bind strongly in cyclodextrins hydrophobic cavities, while the *cis* form binding is considered unstable. This results in a sol-gel transition. (b) Crosslinking of the polymeric chains according to the application of a stimulus (e.g. crosslinking of chitosan by hydrogen bonding with β-GP according to the temperature). (c) Stimulus-responsive surface. Examples of this type of system are PNIPAAm-grafted chitosan surfaces; the PNIPAAm chains are extended or coiled according to the temperature which allows for selective cell sheet detachment (d) Response of an hydrogel structure to some stimuli, such as temperature (in the case of a gelatin hydrogel, or a natural polymer blended with PNIPAAm or Pluronics) or pH (in the case of an alginate or chitosan hydrogel). [Figure adapted from Hoffman *et al.*[256]].

Considering the case of natural polymers, a responsive system can be composed of the natural polymer itself or by the mixture of a natural polymer with other polymer in order to conjugate the advantages of using a natural polymer with the advantages of the use of a responsive polymer (usually synthetic and thermoresponsive). The responsive polymer can be conjugated with the natural polymer in an interpenetrated network (IPN), grafted to the polymer, by polyelectrolyte assembly, among others.

Some natural polymers' response has been tailored by chemical modification, usually resulting in non-reversible transitions, such as crosslinking by UV light after methacrylation or mineralization by the incorporation of ceramics (such as hydroxyapatite) or glasses. However, in this section, only reversible/switchable response will be considered.

The most common intrinsic responses of natural polymers are to pH and/or ionic strength shifts, which can be seen in alginate, chitosan and other electrolyte polymers. To obtain a responsive behavior to other stimuli, such as temperature, which is probably the most seek and practically used stimuli, these polymers have been blended with other responsive polymers such as the well-known PNIPAAm. The possibly obtained dual (e.g. to pH and temperature) or multiple responses system may be useful in TERM applications, in order to engineer *in situ* sequential release of bioactive agents or cells.

In Table 1.1 examples of responsive systems for TERM totally or partially constituted of natural polymers are presented, and aspects such as the shapes in which they have been processed, responsive polymer and aim to which the system was design for are resumed.

A brief description of the principles behind the responsiveness of natural polymers and polymers often blended with them in order to obtain responsive biomaterial systems are presented in the next sub-sections.

1.3.1. pH-sensitive natural polymers

pH-sensitive polymers are polyelectrolytes that bear in their structure weak acidic or basic groups that either accept or release protons in response to changes in environmental pH. The generation of charge along polymeric backbone results in an increase in the hydrodynamic volume of the polymer. The transition from collapsed state to expanded state has been explained by changes in the osmotic pressure exerted by mobile counterions neutralizing the network charges. Examples of natural polymers with this behavior are chitosan (a polybase) and alginate (a polyacid). Polyacidic polymers unswell at low pH, since the acidic groups are protonated and unionized. The opposite behaviour is found in polybasic polymers, since the ionization of the basic groups will increase when decreasing the pH [281]. The pH range that a reversible phase transition occurs can be generally modulated by selecting the ionizable

moiety with a pKa matching the desired pH range or by incorporating hydrophobic moieties into the polymer backbone and controlling their nature, amount and distribution.

1.3.2. Temperature sensitive natural polymers

Sol-gel polymers

Gellan gum, gelatin and agarose are some of the biopolymers that exhibit temperature sensitivity by different gelation mechanisms that lead to the formation of helix conformations by physical crosslinks. These polymers are *sol* at high temperatures and become *gel* at lower by formation of aggregation of double helices that act as crosslinking knots. The polysaccharide gellan gum attains these conformations by hydrogen bonding in aqueous media. In the case of gelatin, gels are formed in aqueous solution when lowering the temperature that promotes the formation of gel networks due to the change from random to triple helix conformation. The low stability of gelatines under physiological conditions has promoted their conjugation with other polymers such as chitosan being stable at temperatures

1.3.3. Natural polymers modified to show thermoresponsive behavior - Modifying responsive polymers and agents

Temperature-responding synthetic polymers present a fine hydrophobic-hydrophilic balance in their structure, and small temperature changes around the critical temperature, make the chains to collapse or to expand responding to the new adjustments of the hydrophobic and hydrophilic interactions between the polymeric chains and the aqueous media.

Some temperature-responsive polymers, usually mixed with other polymers, have a unique property: a critical solution temperature, which is the temperature at which the phase of polymer and solution is discontinuously changed according to their composition. This can be a lower critical solution temperature (LCST) - which is the most common - if the polymer is phase-separate from the solvent above this temperature, or a upper critical solution temperature (UCST) in the reverse case. For example, PNIPAAm has a LCST, at which it undergoes a reversible volume phase transition caused by the coil-to-globule transition. Intramolecular collapse occurs before intermolecular aggregation through LCST and the collapse of individual polymer chains increases the scattering of light in solution (cloud point). Intermolecular interactions in water medium may also create hydrogel shrinkage, micelle aggregation or the physical cross-links [282,283].

Table 1.1. – Some exemples of responsive systems using natural polymers.

Main polymer	Type of Response	Responsive agent	Type of structure	Application	Reference
Chitosan	Temperature pH	PNIPAAm	IPN membranes	-	262
	Temperature	Chitosan modification to hydroxylbutyl chitosan	Sol-gel hydrogel	MSC and intervertebral disk cells encapsulation	263
		β-GP	*In situ* forming hydrogel	Encapsulation and *in vivo* delivery of rat bone marrow MSC	264
		PNIPAAm	Membrane	Cell sheet engineering	265
		Pluronics	Hydrogel	EGF delivery; wound adhesive and photo-crosslinkable properties	266
		PNIPAAm	Hydrogel (grafting)	Cultivation of chondrocytes and meniscus cells	267
	Temperature (Mineralization)	β -GP ELP (with hydroxyapatite)	Hydrogel	Bone regeneration	268
Alginate	Temperature pH	PNIPAAm Alginate	Beads	-	269
			Semi-IPN and comb-type graft hydrogels	-	270
			Semi-IPN	-	271
			Aqueous core capsules	Diffusion of molecules (potential bioactive factor release)	272
		Hydroxypropylcellulose Alginate	Hydrogel	-	273
	pH	Modification of alginate into tetra-functional acetal-linked network polymer (SNAP) with carboxylate moieties	Hydrogel	Absorptive encapsulation and controlled release of protein therapeuthics for oral drug delivery	274

Alginate and hydroxylapatite (HAp)		Alginate	Hydrogel	Bone regeneration	275
Gelatin	Temperature	PNIPAAm	Hydrogel	Cartilage repair	276
		Gelatin	Sol-gel hydrogel	Fabrication of particles by template dissolution method	277
ELP		PNIPAAm	Hydrogel	Modulation of cell response according to mechanical stimuli	278
Collagen		PNIPAAm (grafted)	Hydrogel	*In situ* retinal pigment epithelial cell delivery	279
Hyaluronic Acid	Temperature	PNIPAAm	SemiIPN hydrogel	-	280
		PNIPAAm	Aminated hyaluronic acid-g-poly(N-isopropylacrylamide) (AHA-g-PNIPAAm) copolymer hydrogel	Adipose tissue regeneration	281
		Pluronics	Photocrosslinkable hydrogel	Delivery of chondrocytes "at will"	282
hyaluronic acid + silk fibroin	pH Electric tension	-	LbL film	Drug delivery	283
Silk fibroin	Temperature	PNIPAAm	Sponges (IPN)	Bioactive agents release/general tissue regeneration	284
Carrageenan	Temperature pH	PNIPAAm	IPN hydrogels	Potential application in bioactive factors delivery at will	285
Starch	Temperature	β-GP	Hydrogel	Encapsulation of adipose tissue derived stem cells	51

Other class of thermoresponsive polymers is the ones based on amphiphilic balance, the so-called Poloxamers (Pluronics, as commercial name). These are nonionic triblock copolymers composed of a central hydrophobic chain (e.g. poly(propylene oxide) (PPO)) flanked by two hydrophilic chains (e.g. poly(ethylene oxide) (PEO)). Several amphiphilic block copolymers were reported to have temperature responsive micellization behavior and to form hydrogels above a critical gelation temperature. They have *sol–gel* phase transition under body temperature and *gel-sol* phase transition around 50°C in a relatively high concentration range [283].

Beta-glycerophosphate (β-GP) - a weak base - has also been used to obtain responsive behavior in chitosan hydrogels. Highly deacetylated semi-diluted CS solutions can be used to formulate homogenous heat-induced hydrogels by neutralizing the solution with this weak base.

The addition of disodium β-GP into chitosan solution increases the pH, thereby reducing the electrostatic repulsion between chitosan chains. This reaction, in turn, induces an increase in chitosan interchain hydrogen bonding. In addition, raising the temperature releases hydrogen bonds between water molecules and chitosan chains, which allow increased hydrophobic interactions between chitosan chains. However, in order to achieve a physiologically acceptable pH range and form the gel network at body temperature, it is necessary to include high concentration of β-GP, which can lead to potential toxicity. To improve biocompatibility of this system, several researches have used low concentration of inorganic phosphate salts or added crosslinkers such as glyoxal and hydroxyethyl cellulose, which are responsible for the solidification of chitosan based hydrogels with low concentrations of β-GP [283].

1.3.4. Light-sensitive polymers - Potential use of Azobenzene/α-Cyclodextrin inclusion complexes

The use of photoresponsive materials represents a rapid and clean way of having low invasive smart response. For example, in the case of cell-sheet engineering applications, the exposure to irradiations of different non-harmful ranges would probably be less toxic to cells than the prolonged exposure to low temperatures. Also, the manipulation of new molecules for the seeking of new systems that could be responsive in milder irradiation ranges than UV - which may impair cell encapsulation if used for long periods of time - would be an interesting and useful challenge.

Azobenzene and its derivatives have a unique *trans-cis* isomeration depending on the irradiating units exposed to light [284]. Systems of azobenzene-containing polymers with cyclodextrins have been engineered, allowing for a controlled *sol-gel* response. In the specific case of alpha-Cyclodextrins (α-CD), these are oligosaccharides consisting of six glucose units which present a toroidal form with a

hydrophobic inner cavity and a hydrophilic outer side. This property is in favor of forming inclusion compounds with a large variety of organic molecules, namely benzenes, that have suitable size, shape, and polarity [285]. When the azobenzene units are in the *trans* form, these are included inside the hydrophobic cavity of the cyclodextrins, and in the case of a polymeric solution, this corresponds to a *gel* phase. On the other hand, when the azobenzene units are photochemically converted to its *cis* configuration - in the presence of UV irradiation -, the azobenzene units dissociate from the cyclodextrin cavity, and in the case of a polymer in solution, the system can be (re)converted to the *sol* phase [284].

Two examples of the use of alpha-cyclodextrin to tailor the response of synthetic hydrogels are described in the next paragraphs. However, to our knowledge, reversible photomodification of natural polymers with azobenzenes has never been reported, which would be a challenging and certainly useful path to obtain interesting TERM systems.

A photoresponsive polymer with azobenzene pendant group (PDMAA-co-PAPA) was synthesized by radical polymerization of *N,N*-dimethylacrylamide (DMAA) and *N*-4-phenylazophenyl acrylamide (PAPA) [286]. The solubility of PDMAA-co-PAPA and α-CD inclusion complexes in aqueous solution showed tunable properties that could be triggered by alternating UV–visible light irradiation at a certain temperature due to the effect of molecular recognition of α-CD with azobenzene moiety in the polymer.

Also using molecular recognition of α-cyclodextrin (α-CD), a photoresponsive hydrogel system was obtained by combination of α-CD, dodecyl (C12)-modified poly-(acrylic acid) (p(AA/C12)), and a photoresponsive competitive guest, 4,4'-azodibenzoic acid (ADA). An aqueous solution of p(AA/C12) exhibited a gel-like behavior because polymer chains form a network structure via hydrophobic associations of C12 side chains. When α-CD was added to the gel-like aqueous solution, the gel was converted to a *sol* mixture because hydrophobic interactions of C12 side chains were dissociated by the formation of inclusion complexes of α-CD with C12 side chains. Upon addition of ADA to a binary sol mixture of p(AA/C12) and α-CD, α-CD interacted predominantly with ADA, and then hydrophobic associations of C12 side chains were restored, resulting in a *sol-gel* transition. When a ternary gel mixture of p(AA/C12), α-CD, and ADA was irradiated with UV light, ADA was isomerized from *trans* to *cis*, and the mixture underwent a *gel-sol* transition because α-CD formed inclusion complexes more favorably with C12 side chains than with *cis*-ADA. When the ternary *sol* mixture was irradiated with visible light, ADA was isomerized from *cis* to *trans* and the mixture underwent a *sol-gel* transition [285].

1.4. CONCLUSIONS

Polymers derived from natural sources have been widely used in the production of biomaterials. Their origin varies from marine-origin crustacean and algae, as well as mammalians, plants and microorganism processed products. These polymers have been processed in different shapes and structures aiming for the regeneration of lost or damaged tissues relying in their biodegradability, usual low inflammatory response and reduced cytotoxicity.

Among natural polymers, response to several external stimuli, such as pH and ionic strength, are commonly observed. Moreover, these polymers have been often combined with responsive synthetic polymers in order to obtain smart characteristics alloyed to the similarity of natural polymers to GAGs existing in the body, degradability and low cytotoxicity. These stimuli-responsive systems have proven to be a step ahead for clinical treatment of damaged tissue, for example in the case of cell-sheet engineering. Moreover, responsive systems may avoid complex surgery procedures by *in situ* crosslinking/gelling and may allow controlled delivery and targeting of several therapeutic agents.

Despite the number of polymers available in nature and their effective use in the clinic field, there is still much work to be done in terms of extending their chemical modification, improve processability and optimization of their response *in vitro* and *in vivo*, considering their applicability in real therapeutics.

1.5. REFERENCES

[1] Langer R, Vacanti JP. Tissue engineering. Science 1993;260:920–926.

[2] van Blitterswijk C, editor. Tissue Engineering. 1st ed. London: Elsevier; 2008.

[3] Donaruma LG. Definitions in biomaterials, D. F. Williams, Ed., Elsevier, Amsterdam, 1987. J Polym Sci C Polym Lett 1988;26:414.

[4] Rincones J, Zeidler AF, Grassi MCB, Carazzolle MF, Pereira GAG. The Golden Bridge for nature: the new biology applied to bioplastics. Polym Rev 2009;49:85–106.

[5] Tabata Y. Biomaterial technology for tissue engineering applications. J R Soc Interface 2009;6:S311–S324.

[6] Mano JF, Silva GA, Azevedo HS, Malafaya PB, Sousa RA, Silva SS, Boesel LF, Oliveira JM, Santos TC, Marques AP, Neves NM, Reis RL. Natural origin biodegradable systems in tissue engineering and regenerative medicine: present status and some moving trends. J R Soc Interface 2007;4:999–1030.

[7] Reis RL, Neves NM, Mano JF, Gomes ME, Marques AP, Azevedo HS, editors. Controlling Degradation of Natural Polymers for Biomedical Applications in Natural-Based Polymers for Biomedical Applications. Cambridge: Woodhead Publishing Limited; 2008.

[8] Moroni L, de Wijn JR, van Blitterswijk CA. 3D fiber-deposited scaffolds for tissue engineering: Influence of pores geometry and architecture on dynamic mechanical properties. Biomaterials 2006;27:974–985.

[9] Tran TT, Kulis C, Long SM, Bryant D, Adams P, Smythe ML. Defining scaffold geometries for interacting with proteins: geometrical classification of secondary structure linking regions. J Comput Aided Mol Des 2010;24:917–934.

[10] Sikavitsas VI, Temenoff JS, Mikos AG. Biomaterials and bone mechanotransduction. Biomaterials 2001;22:2581–2593.

[11] Peppas NA, Hilt JZ, Khademhosseini A, Langer R. Hydrogels in biology and medicine: from molecular principles to bionanotechnology. Adv Mater 2006;18:1345–1360.

[12] Balakrishnan B, Jayakrishnan A. Self-cross-linking biopolymers as injectable in situ forming biodegradable scaffolds. Biomaterials 2005;26:3941–3951.

[13] Slaughter BV, Khurshid SS, Fisher OZ, Khademhosseini A, Peppas NA. Hydrogels in regenerative medicine. Adv Mater 2009;21:3307–3329.

[14] Tan H, Marra KG. Biodegradable hydrogels for tissue engineering applications. Mater Lett 2010;3:1746–1767.

[15] Khademhosseini A, Langer R, Borenstein J, Vacanti JP. Microscale technologies for tissue engineering and biology. Proc Natl Acad Sci U S A 2006;103:2480–2487.

[16] Khademhosseini A, Langer R. Microengineered hydrogels for tissue engineering. Biomaterials 2007;28:5087–5092.

[17] Oliveira MB, Mano JF. Polymer-based microparticles in tissue engineering and regenerative medicine. Biotechnol Prog 2011;27 (4):897–912.

[18] Song W, Lima AC, Mano JF. Bioinspired methodology to fabricate hydrogel spheres for multi-applications using superhydrophobic substrates. Soft Matter 2010;6:5868–5871.

[19] Silva GA, Ducheyne P, Reis RL. Materials in particulate form for tissue engineering. 1. Basic concepts. J Tissue Eng Regen Med 2007;1:4–24.

[20] Cruz DMG, Ivirico JLE, Gomes MM, Ribelles JLG, Sánchez MS, Reis RL, Mano JF. Chitosan microparticles as injectable scaffolds for tissue engineering. J Tissue Eng Regen Med 2008;2:378–380.

[21] Malda J, van Blitterswijk CA, Grojec M, Martens DE, Tramper J, Riesle J. Expansion of bovine chondrocytes on microcarriers enhances redifferentiation. Tissue Eng 2003;9: 939–948.

[22] Malda J, Frondoza CG. Microcarriers in the engineering of cartilage and bone. Trends Biotechnol 2006;24:299–304.

[23] Kumbar SG, James R, Nukavarapu SP, Laurencin CT. Electrospun nanofiber scaffolds: engineering soft tissues. Biomed Mater 2008;3:034002.

[24] Hughes FJ, Ghuman M, Talal A. Periodontal regeneration: a challenge for the tissue engineer? Proc Inst Mech Eng Part H-J Eng Med 2010;224:1345–1358.

[25] Liao S, Wang W, Uo M, Ohkawa S, Akasaka T, Tamura K, Cui FZ, Watari F. A threelayered nano-carbonated hydroxyapatite/collagen/PLGA composite membrane for guided tissue regeneration. Biomaterials 2005;26:7564–7571.

[26] Knecht S, Erggelet C, Endres M, Sittinger M, Kaps C, Stussi E. Mechanical testing of fixation techniques for scaffold-based tissue-engineered grafts. J Biomed Mater Res Part B Appl Biomater 2007;83B:50–57.

[27] Caridade SG, da Silva RMP, Reis RL, Mano JF. Effect of solvent-dependent viscoelastic properties of chitosan membranes on the permeation of 2-phenylethanol. Carbohydr Polym 2009;75:651–659.

[28] Zhang K, Wang YB, Hillmyer MA, Francis LF. Processing and properties of porous poly(l-lactide)/bioactive glass composites. Biomaterials 2004;25:2489–2500.

[29] Berg MC, Yang SY, Hammond PT, Rubner MF. Controlling mammalian cell interactions on patterned polyelectrolyte multilayer surfaces. Langmuir 2004;20:1362–1368.

[30] Tang ZY, Wang Y, Podsiadlo P, Kotov NA. Biomedical applications of layer-bylayer assembly: from biomimetics to tissue engineering. Adv Mater 2006;18:3203–3224.

[31] Ting JHY, Haas MR, Valenzuela SM, Martin DK. Terminating polyelectrolyte in multilayer films influences growth and morphology of adhering cells. IET Nanobiotechnol 2010;4:77–90.

[32] Boudou T, Crouzier T, Ren KF, Blin G, Picart C. Multiple functionalities of polyelectrolyte multilayer films: new biomedical applications. Adv Mater 2010;22:441–467.

[33] Almodovar J, Bacon S, Gogolski J, Kisiday JD, Kipper MJ. Polysaccharide-based polyelectrolyte multi layer surface coatings can enhance mesenchymal stem cell response to adsorbed growth factors. Biomacromolecules 2010;11:2629–2639.

[34] Zhang J, Senger B, Vautier D, Picart C, Schaaf P, Voegel JC, Lavalle P. Natural polyelectrolyte films based on layer-by layer deposition of collagen and hyaluronic acid. Biomaterials 2005;26:3353–3361.

[35] Sher P, Custodio CA, Mano JF. Layer-by-layer technique for producing porous nanostructured 3D constructs using moldable freeform assembly of spherical templates. Small 2010;6:2644–2648.

[36] Stadler B, Price AD, Zelikin AN. A critical look at multilayered polymer capsules in biomedicine: drug carriers, artificial organelles, and cell mimics. Adv Funct Mater 2011;21:14–28.

[37] Mano JF. Stimuli-responsive polymeric systems for biomedical applications. Adv Eng Mater 2008;10:515–527.

[38] Muzzarelli RAA. Chitins and chitosans for the repair of wounded skin, nerve, cartilage and bone. Carbohydr Polym 2009;76:167–182.

[39] Ravi Kumar MNV, Muzzarelli RAA, Muzzarelli C, Sashiwa H, Domb AJ. Chitosan chemistry and pharmaceutical perspectives. Chem Rev 2004;104:6017–6084.

[40] Ravi Kumar MNV. A review of chitin and chitosan applications. React Funct Polym 2000;46:1–27.

[41] Lee JE, Kim KE, Kwon IC, Ahn HJ, Lee S-H, Cho H, Kim HJ, Seong SC, Lee MC. Effects of the controlled-released TGF-[beta]1 from chitosan microspheres on chondrocytes cultured in a collagen/chitosan/glycosaminoglycan scaffold. Biomaterials 2004; 25:4163–4173.

[42] Muzzarelli RAA, Guerrieri M, Goteri G, Muzzarelli C, Armeni T, Ghiselli R, Cornelissen M. The biocompatibility of dibutyryl chitin in the context of wound dressings. Biomaterials 2005;26:5844–5854.

[43] Cho Y-W, Cho Y-N, Chung S-H, Yoo G, Ko S-W. Water-soluble chitin as a wound healing accelerator. Biomaterials 1999;20:2139–2145.

[44] Tomihata K, Ikada Y. In vitro and in vivo degradation of films of chitin and its deacetylated derivatives. Biomaterials 1997;18:567–575.

[45] Tan HP, Chu CR, Payne KA, Marra KG. Injectable in situ forming biodegradable chitosan-hyaluronic acid based hydrogels for cartilage tissue engineering. Biomaterials 2009;30:2499–2506.

[46] Yamane S, Iwasaki N, Majima T, Funakoshi T, Masuko T, Harada K, Minami A, Monde K, Nishimura S. Feasibility of chitosan-based hyaluronic acid hybrid biomaterial for a novel scaffold in cartilage tissue engineering. Biomaterials 2005;26:611–619.

[47] Chen YL, Lee HP, Chan HY, Sung LY, Chen HC, Hu YC. Composite chondroitin-6-sulfate/ dermatan sulfate/chitosan scaffolds for cartilage tissue engineering. Biomaterials 2007;28:2294–2305.

[48] Yan JH, Qi NM, Zhang QQ. Rabbit articular chondrocytes seeded on collagen-chitosan- GAG scaffold for cartilage tissue engineering in vivo. Artif Cells Blood Sub Biotechnol 2007;35:333–344.

[49] Li ZS, Ramay HR, Hauch KD, Xiao DM, Zhang MQ. Chitosan-alginate hybrid scaffolds for bone tissue engineering. Biomaterials 2005;26:3919–3928.

[50] Silva SS, Motta A, Rodrigues MT, Pinheiro AFM, Gomes ME, Mano JF, Reis RL, Migliaresi C. Novel genipin-cross-linked chitosan/silk fibroin sponges for cartilage engineering strategies. Biomacromolecules 2008;9:2764–2774.

[51] Sa-Lima H, Caridade SG, Mano JF, Reis RL. Stimuli-responsive chitosan-starch injectable hydrogels combined with encapsulated adipose-derived stromal cells for articular cartilage regeneration. Soft Matter 2010;6:5184–5195.

[52] Kathuria N, Tripathi A, Kar KK, Kumar A. Synthesis and characterization of elastic and macroporous chitosan-gelatin cryogels for tissue engineering. Acta Biomater 2009;5:406–418.

[53] Wang XH, Yu X, Yan YN, Zhang RJ. Liver tissue responses to gelatin and gelatin/chitosan gels. J Biomed Mater Res A 2008;87A:62–68.

[54] Huang Y, Onyeri S, Siewe M, Moshfeghian A, Madihally SV. In vitro characterization of chitosan-gelatin scaffolds for tissue engineering. Biomaterials 2005;26:7616–7627.

[55] Shim IK, Lee SY, Park YJ, Lee MC, Lee SH, Lee JY, Lee SJ. Homogeneous chitosan-PLGA composite fibrous scaffolds for tissue regeneration. J Biomed Mater Res A 2008;84A:247–255.

[56] Jiang T, Abdel-Fattah WI, Laurencin CT. In vitro evaluation of chitosan/poly(lactic acidglycolic acid) sintered microsphere scaffolds for bone tissue engineering. Biomaterials 2006;27:4894–4903.

[57] Kuo YC, Hsu YR. Tissue-engineered polyethylene oxide/chitosan scaffolds as potential substitutes for articular cartilage. J Biomed Mater Res A 2009;91A:277–287.

[58] Sahithi K, Swetha M, Ramasamy K, Srinivasan N, Selvamurugan N. Polymeric composites containing carbon nanotubes for bone tissue engineering. Int J Biol Macromol 2010;46:281–283.

[59] Neves SC, Moreira Teixeira LS, Moroni L, Reis RL, Van Blitterswijk CA, Alves NM, Karperien M, Mano JF. Chitosan/poly(-caprolactone) blend scaffolds for cartilage repair. Biomaterials 2011;32:1068–1079.

[60] Rochet N, Balaguer T, Boukhechba F, Laugier JP, Quincey D, Goncalves S, Carle GF. Differentiation and activity of human preosteoclasts on chitosan enriched calcium phosphate cement. Biomaterials 2009;30:4260–4267.

[61] Martins AM, Pham QP, Malafaya PB, Raphael RM, Kasper FK, Reis RL, Mikos AG. Natural stimulus responsive scaffolds/cells for bone tissue engineering: influence of lysozyme upon scaffold degradation and osteogenic differentiation of cultured marrow stromal cells induced by CaP coatings. Tissue Eng A 2009;15:1953–1963.

[62] Lee EJ, Shin DS, Kim HE, Kim HW, Koh YH, Jang JH. Membrane of hybrid chitosansilica xerogel for guided bone regeneration. Biomaterials 2009;30:743–750.

[63] Di Martino A, Sittinger M, Risbud MV. Chitosan: a versatile biopolymer for orthopaedic tissue-engineering. Biomaterials 2005;26:5983–5990.

[64] Park YJ, Lee YM, Park SN, Sheen SY, Chung CP, Lee SJ. Platelet derived growth factor releasing chitosan sponge for periodontal bone regeneration. Biomaterials 2000;21: 153–159.

[65] Lahiji A, Sohrabi A, Hungerford DS, Frondoza CG. Chitosan supports the expression of extracellular matrix proteins in human osteoblasts and chondrocytes. J Biomed Mater Res 2000;51:586–595.

[66] Xu HHK, Zhao L, Weir MD. Stem cell-calcium phosphate constructs for bone engineering. J Dent Res 2010;89:1482–1488.

[67] Venkatesan J, Kim SK. Chitosan composites for bone tissue engineering—an overview. Mar Drugs 2010;8:2252–2266.

[68] Swetha M, Sahithi K, Moorthi A, Srinivasan N, Ramasamy K, Selvamurugan N. Biocomposites containing natural polymers and hydroxyapatite for bone tissue engineering. Int J Biol Macromol 2010;47:1–4.

[69] Li JJ, Zhu DW, Yin JW, Liu YX, Yao FL, Yao KD. Formation of nano-hydroxyapatite crystal in situ in chitosan-pectin polyelectrolyte complex network. Mater Sci Eng C Mater Biol Appl 2010;30:795–803.

[70] Chang CH, Tsao CT, Chang KY, Wang JL, Young TH, Han JL, Hsieh KH. Chitosan membrane with surface-bonded growth factor in guided tissue regeneration applications. J Bioact Compat Polym 2010;25:465–482.

[71] Nogueira GM, Swiston AJ, Beppu MM, Rubner MF. Layer-by-layer deposited chitosan/ silk fibroin thin films with anisotropic nanofiber alignment. Langmuir 2010;26:8953–8958.

[72] Larkin AL, Davis RM, Rajagopalan P. Biocompatible, detachable, and free-standing polyelectrolyte multilayer films. Biomacromolecules 2010;11:2788–2796.

[73] George M, Abraham TE. Polyionic hydrocolloids for the intestinal delivery of protein drugs: alginate and chitosan—a review. J Control Release 2006;114:1–14.

[74] Skjgk-Bræk G, Grasdalen H, Larsen B. Monomer sequence and acetylation pattern in some bacterial alginates. Carbohydr Res 1986;154:239–250.

[75] Johnson PC. De novo cartilage generation using calcium alginate-chondrocyte constructs. Plast Reconstr Surg 1996;97:179,180.

[76] Boontheekul T, Kong H-J, Mooney DJ. Controlling alginate gel degradation utilizing partial oxidation and bimodal molecular weight distribution. Biomaterials 2005;26:2455–2465.

[77] Scotti C, Mangiavini L, Boschetti F, Vitari F, Domeneghini C, Fraschini G, Peretti GM. Effect of in vitro culture on a chondrocyte-fibrin glue hydrogel for cartilage repair. Knee Surg Sports Traumatol Arthrosc 2010;18:1400–1406.

[78] Malafaya PB, Silva GA, Reis RL. Natural-origin polymers as carriers and scaffolds for biomolecules and cell delivery in tissue engineering applications. Adv Drug Deliv Rev 2007;59:207–233.

[79] Drury JL, Dennis RG, Mooney DJ. The tensile properties of alginate hydrogels. Biomaterials 2004;25:3187–3199.

[80] Augst AD, Kong HJ, Mooney DJ. Alginate hydrogels as biomaterials. Macromol Biosci 2006;6:623–633.

[81] Moyer HR, Kinney RC, Singh KA, Williams JK, Schwartz Z, Boyan BD. Alginate microencapsulation technology for the percutaneous delivery of adipose-derived stem cells. Ann Plast Surg 2010;65:497–503.

[82] Liang Y, Liu WS, Han BQ, Yang CZ, Ma Q, Song FL, Bi QQ. An in situ formed biodegradable hydrogel for reconstruction of the corneal endothelium. Colloid Surf B Biointerfaces 2010;82:1–7.

[83] Kolambkar YM, Dupont KM, Boerckel JD, Huebsch N, Mooney DJ, Hutmacher DW, Guldberg RE. An alginate-based hybrid system for growth factor delivery in the functional repair of large bone defects. Biomaterials 2010;32:65–74.84.

[84] Hwang CM, Sant S, Masaeli M, Kachouie NN, Zamanian B, Lee SH, Khademhosseini A. Fabrication of three-dimensional porous cell-laden hydrogel for tissue engineering. Biofabrication 2010;2:035003.

[85] Lee KH, Shin SJ, Park Y, Lee SH. Synthesis of cell-laden alginate hollow fibers using microfluidic chips and microvascularized tissue-engineering applications. Small 2009;5:1264–1268.

[86] Dang TT, Xu QB, Bratlie KM, O'Sullivan ES, Chen XY, Langer R, Anderson DG. Microfabrication of homogenous, asymmetric cell-laden hydrogel capsules. Biomaterials 2009;30:6896–6902.

[87] Awad HA, Wickham MQ, Leddy HA, Gimble JM, Guilak F. Chondrogenic differentiation of adipose-derived adult stem cells in agarose, alginate, and gelatin scaffolds. Biomaterials 2004;25:3211–3222.

[88] Uludag H, De Vos P, Tresco PA. Technology of mammalian cell encapsulation. Adv Drug Deliv Rev 2000;42:29–64.

[89] Temenoff JS, Mikos AG. Injectable biodegradable materials for orthopedic tissue engineering. Biomaterials 2000;21:2405–2412.

[90] Rowley JA, Madlambayan G, Mooney DJ. Alginate hydrogels as synthetic extracellular matrix materials. Biomaterials 1999;20:45–53.

[91] Wang XH, Paloheimo KS, Xu HR, Liu C. Cryopreservation of cell/hydrogel constructs based on a new cell-assembling technique. J Bioact Compat Polym 2010;25:634–653.

[92] Mangione MR, Giacomazza D, Bulone D, Martorana V, Cavallaro G, San Biagio PL. K+ and Na+ effects on the gelation properties of [kappa]-Carrageenan. Biophys Chem 2005;113:129–135.

[93] Bartkowiak A, Hunkeler D. Carrageenan-oligochitosan microcapsules: optimization of the formation process. Colloids Surf B Biointerfaces 2001;21:285–298.

[94] Espírito Santo V, Frias AM, Carida M, Cancedda R, Gomes ME, Mano JF, Reis RL. Carrageenan-based hydrogels for the controlled delivery of PDGF-BB in bone tissue engineering applications. Biomacromolecules 2009;10:1392–1401.

[95] Pereira RC, Scaranari M, Castagnola P, Grandizio M, Azevedo HS, Reis RL, Cancedda R, Gentili C. Novel injectable gel (system) as a vehicle for human articular chondrocytes in cartilage tissue regeneration. J Tissue Eng Regen Med 2009;3:97–106.

[96] Luna SM, Gomes ME, Mano JF, Reis RL. Development of a novel cell encapsulation system based on natural origin polymers for tissue engineering applications. J Bioact Compat Polym 2010;25:341–359.

[97] Lim Y-M, Gwon H-J, Choi J-H, Shin J, Nho Y-C, Jeong S, Chong M, Lee Y-M, Kwon I, Kim S. Preparation and biocompatibility study of gelatin/kappa-carrageenan scaffolds. Macromol Res 2010;18:29–34.

[98] Daniel-da-Silva A, Lopes A, Gil A, Correia R. Synthesis and characterization of porous κ-carrageenan/calcium phosphate nanocomposite scaffolds. J Mater Sci 2007;42: 8581–8591.

[99] Alves A, Caridade SG, Mano JF, Sousa RA, Reis RL. Extraction and physico-chemical characterization of a versatile biodegradable polysaccharide obtained from green algae. Carbohydr Res 2010;345:2194–2200.

[100] Robic A, Gaillard C, Sassi JF, Lerat Y, Lahaye M. Ultrastructure of ulvan: a polysaccharide from green seaweeds. Biopolymers 2009;91:652–664.

[101] Paradossi G, Cavalieri F, Chiessi E. A conformational study on the algal polysaccharide ulvan. Macromolecules 2002;35:6404–6411.

[102] Morelli A, Chiellini F. Ulvan as a new type of biomaterial from renewable resources: functionalization and hydrogel preparation. Macromol Chem Phys 2010;211:821–832.

[103] Rahman N, Purpura KA, Wylie RG, Zandstra PW, Shoichet MS. The use of vascular endothelial growth factor functionalized agarose to guide pluripotent stem cell aggregates toward blood progenitor cells. Biomaterials 2010;31:8262–8270.

[104] Watanabe J, Kashii M, Hirao M, Oka K, Sugamoto K, Yoshikawa H, Akashi M. Quickforming hydroxyapatite/agarose gel composites induce bone regeneration. J Biomed Mater Res A 2007;83A:845–852.

[105] Suzawa Y, Funaki T, Watanabe J, Iwai S, Yura Y, Nakano T, Umakoshi Y, Akashi M. Regenerative behavior of biomineral/agarose composite gels as bone grafting materials in rat cranial defects. J Biomed Mater Res A 2010;93A:965–975.

[106] Tripathi A, Kathuria N, Kumar A. Elastic and macroporous agarose-gelatin cryogels with isotropic and anisotropic porosity for tissue engineering. J Biomed Mater Res A 2009;90A:680–694.

[107] Silva GA, Coutinho OP, Ducheyne P, Shapiro IM, Reis RL. The effect of starch and starch-bioactive glass composite microparticles on the adhesion and expression of the osteoblastic phenotype of a bone cell line. Biomaterials 2007;28:326–334.

[108] Duarte ARC, Mano JF, Reis RL. Enzymatic degradation of 3D scaffolds of starch-poly-(epsilon-caprolactone) prepared by supercritical fluid technology. Polym Degrad Stabil 2010;95:2110–2117.

[109] Santos MI, Pashkuleva I, Alves CM, Gomes ME, Fuchs S, Unger RE, Reis RL, Kirkpatrick CJ. Surface-modified 3D starch-based scaffold for improved endothelialization for bone tissue engineering. J Mater Chem 2009;19:4091–4101.

[110] Autissier A, Le Visage C, Pouzet C, Chaubet F, Letourneur D. Fabrication of porous polysaccharide-based scaffolds using a combined freeze-drying/cross-linking process. Acta Biomater 2010;6:3640–3648.

[111] Martins A, Chung S, Pedro AJ, Sousa RA, Marques AP, Reis RL, Neves NM. Hierarchical starch-based fibrous scaffold for bone tissue engineering applications. J Tissue Eng Regen Med 2009;3:37–42.

[112] Duarte ARC, Mano JF, Reis RL. Preparation of starch-based scaffolds for tissue engineering by supercritical immersion precipitation. J Supercrit Fluids 2009;49:279–285.

[113] Chan ES, Wong SL, Lee PP, Lee JS, Ti TB, Zhang ZB, Poncelet D, Ravindra P, Phan SH, Yim ZH. Effects of starch filler on the physical properties of lyophilized calciumalginate beads and the viability of encapsulated cells. Carbohydr Polym 2010;83:225–232.

[114] Lee KY, Jeong L, Kang YO, Lee SJ, Park WH. Electrospinning of polysaccharides for regenerative medicine. Adv Drug Deliv Rev 2009;61:1020–1032.

[115] Puppi D, Chiellini F, Piras AM, Chiellini E. Polymeric materials for bone and cartilage repair. Prog Polym Sci 2010;35:403–440.

[116] Silva NA, Salgado AJ, Sousa RA, Oliveira JT, Pedro AJ, Leite-Almeida H, Cerqueira R, Almeida A, Mastronardi F, Mano JF, Neves NM, Sousa N, Reis RL. Development and characterization of a novel hybrid tissue engineering-based scaffold for spinal cord injury repair. Tissue Eng Part A 2010;16:45–54.

[117] Santos TC, Marques AP, Horing B, Martins AR, Tuzlakoglu K, Castro AG, van Griensven M, Reis RL. In vivo short-term and long-term host reaction to starch-based scaffolds. Acta Biomater 2010;6:4314–4326.

[118] Gomes ME, Godinho JS, Tchalamov D, Cunha AM, Reis RL. Alternative tissue engineering scaffolds based on starch: processing methodologies, morphology, degradation and mechanical properties. Mater Sci Eng C Biomimetic Supramol Syst 2002;20:19–26.

[119] Sobral JM, Caridade SG, Sousa RA, Mano JF, Reis RL. Three-dimensional plotted scaffolds with controlled pore size gradients: Effect of scaffold geometry on mechanical performance and cell seeding efficiency. Acta Biomater 2011;7:1009–1018.

[120] Gomes ME, Ribeiro AS, Malafaya PB, Reis RL, Cunha AM. A new approach based on injection moulding to produce biodegradable starch-based polymeric scaffolds: morphology, mechanical and degradation behaviour. Biomaterials 2001;22:883–889.

[121] Salgado AJ, Coutinho OP, Reis RL. Novel starch-based scaffolds for bone tissue engineering: cytotoxicity, cell culture, and protein expression. Tissue Eng 2004;10:465–474.

[122] Gomes ME, Azevedo HS, Moreira AR, Ella V, Kellomaki M, Reis RL. Starchpoly(epsilon-caprolactone) and starch-poly(lactic acid) fibre-mesh scaffolds for bone tissue engineering applications:

structure, mechanical properties and degradation behaviour. J Tissue Eng Regen Med 2008;2:243–252.

[123] Somerville C. Cellulose synthesis in higher plants. Annu Rev Cell Dev Biol 2006;22:53–78.

[124] Müller FA, Müller L, Hofmann I, Greil P, Wenzel MM, Staudenmaier R. Cellulosebased scaffold materials for cartilage tissue engineering. Biomaterials 2006;27:3955–3963.

[125] Märtson M, Viljanto J, Hurme T, Saukko P. Biocompatibility of cellulose sponge with bone. Eur Surg Res 1998;30:426–432.

[126] Entcheva E, Bien H, Yin L, Chung CYC-Y, Farrell M, Kostov Y. Functional cardiac cell constructs on cellulose-based scaffolding. Biomaterials 2004;25:5753–5762.

[127] Ma ZW, Kotaki M, Ramakrishna S. Electrospun cellulose nanofiber as affinity membrane. J Membr Sci 2005;265:115–123.

[128] Schols HA, Voragen AGJ, Visser J, Voragen AGJ. Progress in Biotechnology Pectins and Pectinases. Volume 14, Amsterdam: Elsevier; 1996. p 3–19.

[129] Liu LS, Won YJ, Cooke PH, Coffin DR, Fishman ML, Hicks KB, Ma PX. Pectin/ poly(lactide-co-glycolide) composite matrices for biomedical applications. Biomaterials 2004;25:3201–3210.

[130] Oliveira JT, Martins L, Picciochi R, Malafaya IB, Sousa RA, Neves NM, Mano JF, Reis RL. Gellan gum: a new biomaterial for cartilage tissue engineering applications. J Biomed Mater Res Part A 2010;93A:852–863.

[131] Oliveira JT, Gardel LS, Rada T, Martins L, Gomes ME, Reis RL. Injectable gellan gum hydrogels with autologous cells for the treatment of rabbit articular cartilage defects. J Orthop Res 2010;28:1193–1199.

[132] Chang SJ, Kuo SM, Liu WT, Niu CCG, Lee MW, Wu CS. Gellan gum films for effective guided bone regeneration. J Med Biol Eng 2010;30:99–103.

[133] Coutinho DF, Sant SV, Shin H, Oliveira JT, Gomes ME, Neves NM, Khademhosseini A, Reis RL. Modified Gellan Gum hydrogels with tunable physical and mechanical properties. Biomaterials 2010;31:7494–7502.

[134] Ferris CJ, Panhuis MIH. Conducting bio-materials based on gellan gum hydrogels. Soft Matter 2009;5:3430–3437.

[135] Naessens M, Cerdobbel A, Soetaert W, Vandamme EJ. Leuconostoc dextransucrase and dextran: production, properties and applications. J Chem Technol Biotechnol 2005;80:845–860.

[136] Liu H, Szunerits S, Xu W, Boukherroub R. Preparation of superhydrophobic coatings on zinc as effective corrosion barriers. ACS Appl Mater Interfaces 2009;1:1150–1153.

[137] Bajgai MP, Aryal S, Bhattarai SR, Bahadur KCR, Kim KW, Kim HY. Poly(epsiloncaprolactone) grafted dextran biodegradable electrospun matrix: a novel scaffold for tissue engineering. J Appl Polym Sci 2008;108:1447–1454.

[138] Pan H, Jiang HL, Chen WL. The biodegradability of electrospun dextran/PLGA scaffold in a fibroblast/macrophage co-culture. Biomaterials 2008;29:1583–1592.

[139] Liu YX, Chan-Park MB. Hydrogel based on interpenetrating polymer networks of dextran and gelatin for vascular tissue engineering. Biomaterials 2009;30:196–207.

[140] Massia SP, Stark J. Immobilized RGD peptides on surface-grafted dextran promote biospecific cell attachment. J Biomed Mater Res 2001;56:390–399.

[141] Massia SP, Stark J, Letbetter DS. Surface-immobilized dextran limits cell adhesion and spreading. Biomaterials 2000;21:2253–2261.

[142] Chakravarthy D, Smith DJ. Preparation of a dextran-based degradable absorbent suitable for wound healing applications. J Bioact Compat Polym 1995;10:313–326.

[143] Shingel KI. Current knowledge on biosynthesis, biological activity, and chemical modification of the exopolysaccharide, pullulan. Carbohydr Res 2004;339:447–460.

[144] Kobayashi H, Katakura O, Morimoto N, Akiyoshi K, Kasugai S. Effects of cholesterolbearing pullulan (CHP)-nanogels in combination with prostaglandin E1 on wound healing. J Biomed Mater Res Part B 2009;91B:55–60.

[145] Na K, Shin D, Yun K, Park KH, Lee KC. Conjugation of heparin into carboxylated pullulan derivatives as an extracellular matrix for endothelial cell culture. Biotechnol Lett 2003;25:381–385.

[146] Autissier A, Letourneur D, Le Visage C. Pullulan-based hydrogel for smooth muscle cell culture. J Biomed Mater Res Part A 2007;82A:336–342.

[147] Bae H, Ahari AF, Shin H, Nichol JW, Hutson CB, Masaeli M, Kim S-H, Aubin H, Yamanlar S, Khademhosseini A. Cell-laden microengineered pullulan methacrylate hydrogels promote cell proliferation and 3D cluster formation. Soft Matter 2011;7:1903–1911.

[148] Gils PS, Ray D, Sahoo PK. Characteristics of xanthan gum-based biodegradable superporous hydrogel. Int J Biol Macromol 2009;45:364–371.

[149] Laurent T, Fraser J. Hyaluronan. FASEB J 1992;6:2397–2404.

[150] Solchaga LA, Yoo JU, Lundberg M, Dennis JE, Huibregtse BA, Goldberg VM, Caplan AI. Hyaluronan-based polymers in the treatment of osteochondral defects. J Orthop Res 2000;18:773–780.

[151] Flynn L, Prestwich GD, Semple JL, Woodhouse KA. Adipose tissue engineering in vivo with adipose-derived stem cells on naturally derived scaffolds. J Biomed Mater Res Part A 2009;89A:929–941.

[152] Mironov V, Kasyanov V, Shu XZ, Eisenberg C, Eisenberg L, Gonda S, Trusk T, Markwald RR, Prestwich GD. Fabrication of tubular tissue constructs by centrifugal casting of cells suspended in an in situ crosslinkable hyaluronan-gelatin hydrogel. Biomaterials 2005;26:7628–7635.

[153] Hemmrich K, von Heimburg D, Rendchen R, Di Bartolo C, Milella E, Pallua N. Implantation of preadipocyte-loaded hyaluronic acid-based scaffolds into nude mice to evaluate potential for soft tissue engineering. Biomaterials 2005;26:7025–7037.

[154] Huang L, Gu H, Burd A. A reappraisal of the biological effects of hyaluronan on human dermal fibroblast. J Biomed Mater Res Part A 2009;90A:1177–1185.

[155] Wu Z-R, Ma J, Liu B-F, Xu Q-Y, Cui F-Z. Layer-by-layer assembly of polyelectrolyte films improving cytocompatibility to neural cells. J Biomed Mater Res Part A 2007;81A:355–362.

[156] Bergman K, Engstrand T, Hilborn J, Ossipov D, Piskounova S, Bowden T. Injectable cell-free template for bone-tissue formation. J Biomed Mater Res Part A 2009;91A:1111–1118.

[157] Ifkovits JL, Tous E, Minakawa M, Morita M, Robb JD, Koomalsingh KJ, Gorman JH, Gorman RC, Burdick JA. Injectable hydrogel properties influence infarct expansion and extent of postinfarction left ventricular remodeling in an ovine model. Proc Natl Acad Sci U S A 2010;107:11507–11512.

[158] Angele P, Muller R, Schumann D, Englert C, Zellner J, Johnstone B, Yoo J, Hammer J, Fierlbeck J, Angele MK, Nerlich M, Kujat R. Characterization of esterified hyaluronan- gelatin polymer composites suitable for chondrogenic differentiation of mesenchymal stem cells. J Biomed Mater Res Part A 2009;91A:416–427.

[159] Skardal A, Zhang JX, McCoard L, Xu XY, Oottamasathien S, Prestwich GD. Photocrosslinkable hyaluronan-gelatin hydrogels for two-step bioprinting. Tissue Eng Part A 2010;16:2675–2685.

[160] Hegewald AA, Ringe J, Bartel J, Kruger I, Notter M, Barnewitz D, Kaps C, Sittinger M. Hyaluronic acid and autologous synovial fluid induce chondrogenic differentiation of equine mesenchymal stem cells: a preliminary study. Tissue Cell 2004;36:431–438.

[161] Nguyen LH, Kudva AK, Guckert NL, Linse KD, Roy K. Unique biomaterial compositions direct bone marrow stem cells into specific chondrocytic phenotypes corresponding to the various zones of articular cartilage. Biomaterials 2010;32:1327–1338.

[162] Rampichova M, Filova E, Varga F, Lytvynets A, Prosecka E, Kolacna L, Motlik J, Necas A, Vajner L, Uhlik J, Amler E. Fibrin/hyaluronic acid composite hydrogels as appropriate scaffolds for in vivo artificial cartilage implantation. Asaio J 2010;56:563–568.

[163] Luo Y, Kobler JB, Heaton JT, Jia XQ, Zeitels SM, Langer R. Injectable hyaluronic aciddextran hydrogels and effects of implantation in ferret vocal fold. J Biomed Mater Res Part B 2010;93B:386–393.

[164] Marklein RA, Burdick JA. Spatially controlled hydrogel mechanics to modulate stem cell interactions. Soft Matter 2010;6:136–143.

[165] Antunes JC, Oliveira JM, Reis RL, Soria JM, Gómez-Ribelles JL, Mano JF. Novel poly(L-lactic acid)/hyaluronic acid macroporous hybrid scaffolds: characterization and assessment of cytotoxicity. J Biomed Mater Res Part A 2010;94A:856–869.

[166] Hardingham TE, Fosang AJ. Proteoglycans—many forms and many functions. FASEB J 1992;6:861–870.

[167] Mi FL, Shyu SS, Peng CK, Wu YB, Sung HW, Wang PS, Huang CC. Fabrication of chondroitin sulfate-chitosan composite artificial extracellular matrix for stabilization of fibroblast growth factor. J Biomed Mater Res Part A 2006;76A:1–15.

[168] Abe M, Takahashi M, Tokura S, Tamura H, Nagano A. Cartilage-scaffold composites produced by bioresorbable beta-chitin sponge with cultured rabbit chondrocytes. Tissue Eng 2004;10:585–594.

[169] Sechriest VF, Miao YJ, Niyibizi C, Westerhausen-Larson A, Matthew HW, Evans CH, Fu FH, Suh JK. GAG-augmented polysaccharide hydrogel: A novel biocompatible and biodegradable material to support chondrogenesis. J Biomed Mater Res 2000;49:534–541.

[170] Yan L-P, Wang Y-J, Ren L, Wu G, Caridade SG, Fan J-B, Wang L-Y, Ji P-H, Oliveira JM, Oliveira JT, Mano JF, Reis RL. Genipin-cross-linked collagen/chitosan biomimetic scaffolds for articular cartilage tissue engineering applications. J Biomed Mater Res Part A 2010;95A:465–475.

[171] Wang TW, Wu HC, Wang HY, Lin FH, Sun JS. Regulation of adult human mesenchymal stem cells into osteogenic and chondrogenic lineages by different bioreactor systems. J Biomed Mater Res Part A 2009;88A:935–946.

[172] Han QQ, Jin W, Xiao ZF, Ni HB, Wang JH, Kong J, Wu J, Liang WB, Chen L, Zhao YN, Chen B, Dai JW. The promotion of neural regeneration in an extreme rat spinal cord injury model using a collagen scaffold containing a collagen binding neuroprotective protein and an EGFR neutralizing antibody. Biomaterials 2010;31:9212–9220.

[173] Silver J, Miller JH. Regeneration beyond the glial scar. Nat Rev Neurosci 2004;5:146–156.

[174] Mullen LM, Best SM, Brooks RA, Ghose S, Gwynne JH, Wardale J, Rushton N, Cameron RE. Binding and release characteristics of insulin-like growth factor-1 from a collagen-glycosaminoglycan scaffold. Tissue Eng Part C Meth 2010;16:1439–1448.

[175] Altman GH, Diaz F, Jakuba C, Calabro T, Horan RL, Chen JS, Lu H, Richmond J, Kaplan DL. Silk based biomaterials. Biomaterials 2003;24:401–416.

[176] Hardy JG, Scheibel TR. Composite materials based on silk proteins. Prog Polym Sci 2010;35:1093–1115.

[177] Widhe M, Bysell H, Nystedt S, Schenning I, Malmsten M, Johansson J, Rising A, Hedhammar M. Recombinant spider silk as matrices for cell culture. Biomaterials 2010;31:9575–9585.

[178] Wang Y, Bella E, Lee CSD, Migliaresi C, Pelcastre L, Schwartz Z, Boyan BD, Motta A. The synergistic effects of 3-D porous silk fibroin matrix scaffold properties and hydrodynamic environment in cartilage tissue regeneration. Biomaterials 2010;31:4672–4681.

[179] Park SH, Gil ES, Shi H, Kim HJ, Lee K, Kaplan DL. Relationships between degradability of silk scaffolds and osteogenesis. Biomaterials 2010;31:6162–6172.

[180] Mieszawska AJ, Fourligas N, Georgakoudi I, Ouhib NM, Belton DJ, Perry CC, Kaplan DL. Osteoinductive silk-silica composite biomaterials for bone regeneration. Biomaterials 2010;31:8902–8910.

[181] Wang XL, Sun L, Maffini MV, Soto A, Sonnenschein C, Kaplan DL. A complex 3D human tissue culture system based on mammary stromal cells and silk scaffolds for modeling breast morphogenesis and function. Biomaterials 2010;31:3920–3929.

[182] Gil ES, Mandal BB, Park S-H, Marchant JK, Omenetto FG, Kaplan DL. Helicoidal multi-lamellar features of RGD-functionalized silk biomaterials for corneal tissue engineering. Biomaterials 2010;31:8953–8963.

[183] Chen JL, Yin Z, Shen WL, Chen X, Heng BC, Zou XH, Ouyang HW. Efficacy of hESCMSCs in knitted silk-collagen scaffold for tendon tissue engineering and their roles. Biomaterials 2010;31:9438–9451.

[184] Bessa PC, Balmayor ER, Azevedo HS, Nurnberger S, Casal M, van Griensven M, Reis RL, Redl H. Silk fibroin microparticles as carriers for delivery of human recombinant BMPs. J Tissue Eng Regen Med 2010;4:349–355.

[185] Wang XQ, Kluge JA, Leisk GG, Kaplan DL. Sonication-induced gelation of silk fibroin for cell encapsulation. Biomaterials 2008;29:1054–1064.

[186] Vepari C, Kaplan DL. Silk as a biomaterial. Prog Polym Sci 2007;32:991–1007.

[187] Jin H-J, Chen J, Karageorgiou V, Altman GH, Kaplan DL. Human bone marrow stromal cell responses on electrospun silk fibroin mats. Biomaterials 2004;25:1039–1047.

[188] Chevallay B, Herbage D. Collagen-based biomaterials as 3D scaffold for cell cultures: applications for tissue engineering and gene therapy. Med Biol Eng Comput 2000;38:211–218.

[189] Lee CH, Singla A, Lee Y. Biomedical applications of collagen. Int J Pharm 2001;221:1–22.

[190] Yang C, Hillas PJ, Báez JA, Nokelainen M, Balan J, Tang J, Spiro R, Polarek JW. The application of recombinant human collagen in tissue engineering. BioDrugs 2004;18:103–119.

[191] Kivirikko KI. Collagen biosynthesis: a mini-review cluster. Matrix Biol 1998;16:355–356.

[192] Berisio R, Vitagliano L, Mazarella L, Zagari A. Recent progress on collagen triple helix structure, stability and assembly. Protein Pept Lett 2002;9:107–116.

[193] Friess W. Collagen—biomaterial for drug delivery. Eur J Pharm Biopharm 1998;45:113–136.

[194] Hong Y, Gao C, Xie Y, Gong Y, Shen J. Collagen-coated polylactide microspheres as chondrocyte microcarriers. Biomaterials 2005;26:6305–6313.

[195] Roth EA, Xu T, Das M, Gregory C, Hickman JJ, Boland T. Inkjet printing for highthroughput cell patterning. Biomaterials 2004;25:3707–3715.

[196] Kuo Y-C, Yeh C-F. Effect of surface-modified collagen on the adhesion, biocompatibility and differentiation of bone marrow stromal cells in poly(lactide-co-glycolide)/chitosan scaffolds. Colloids Surf B Biointerfaces 2011;82:624–631.

[197] Shi C, Chen W, Zhao Y, Chen B, Xiao Z, Wei Z, Hou X, Tang J, Wang Z, Dai J. Regeneration of full-thickness abdominal wall defects in rats using collagen scaffolds loaded with collagen-binding basic fibroblast growth factor. Biomaterials 2010;32:753–759.

[198] Ryan CM, Schoenfeld DA, Malloy M, Schulz JTI, Sheridan RL, Tompkins RG. Use of integra(R) artificial skin is associated with decreased length of stay for severely injured adult burn survivors. J Burn Care Res 2002;23:311–317.

[199] Zhang YZ, Ouyang HW, Lim CT, Ramakrishna S, Huang ZM. Electrospinning of gelatin fibers and gelatin/PCL composite fibrous scaffolds. J Biomed Mater Res Part B 2005;72B:156–165.

[200] Ozeki M, Tabata Y. In vivo degradability of hydrogels prepared from different gelatins by various cross-linking methods. J Biomater Sci Polym Ed 2005;16:549–561.

[201] Zhang S, Huang YQ, Yang XP, Mei F, Ma Q, Chen GQ, Ryu S, Deng XL. Gelatin nanofibrous membrane fabricated by electrospinning of aqueous gelatin solution for guided tissue regeneration. J Biomed Mater Res Part A 2009;90A:671–679.

[202] Meng ZX, Wang YS, Ma C, Zheng W, Li L, Zheng YF. Electrospinning of PLGA/gelatin randomly-oriented and aligned nanofibers as potential scaffold in tissue engineering. Mater Sci Eng C Mater Biol Appl 2010;30:1204–1210.

[203] Ponticiello MS, Schinagl RM, Kadiyala S, Barry FP. Gelatin-based resorbable sponge as a carrier matrix for human mesenchymal stem cells in cartilage regeneration therapy. J Biomed Mater Res 2000;52:246–255.

[204] Leeuwenburgh SCG, Jo J, Wang HA, Yamamoto M, Jansen JA, Tabata Y. Mineralization, biodegradation, and drug release behavior of gelatin/apatite composite microspheres for bone regeneration. Biomacromolecules 2010;11:2653–2659.

[205] Lau TT, Wang CM, Wang DA. Cell delivery with genipin crosslinked gelatin microspheres in hydrogel/microcarrier composite. Compos Sci Technol 2010;70:1909–1914.

[206] Lai JY, Li YT. Functional assessment of cross-linked porous gelatin hydrogels for bioengineered cell sheet carriers. Biomacromolecules 2010;11:1387–1397.

[207] Patel ZS, Yamamoto M, Ueda H, Tabata Y, Mikos AG. Biodegradable gelatin microparticles as delivery systems for the controlled release of bone morphogenetic protein-2. Acta Biomater 2008;4:1126–1138.

[208] Inoue A, Takahashi KA, Arai Y, Tonomura H, Sakao K, Saito M, Fujioka M, Fujiwara H, Tabata Y, Kubo T. The therapeutic effects of basic fibroblast growth factor contained in gelatin hydrogel microspheres on experimental osteoarthritis in the rabbit knee. Arthritis Rheum 2006;54:264–270.

[209] Ogawa T, Akazawa T, Tabata Y. In vitro proliferation and chondrogenic differentiation of rat bone marrow stem cells cultured with gelatin hydrogel microspheres for TGF-1 release. J Biomater Sci Polym Ed 2010;21:609–621.

[210] Huss FRM, Nyman E, Bolin JSC, Kratz G. Use of macroporous gelatine spheres as a biodegradable scaffolds for guided tissue regeneration of healthy dermis in humans: an in vivo study. J Plast Reconstr Aesthet Surg 2010;63:848–857.

[211] Daamen WF, Veerkamp JH, van Hest JCM, van Kuppevelt TH. Elastin as a biomaterial for tissue engineering. Biomaterials 2007;28:4378–4398.

[212] Lu QJ, Ganesan K, Simionescu DT, Vyavahare NR. Novel porous aortic elastin and collagen scaffolds for tissue engineering. Biomaterials 2004;25:5227–5237.

[213] Lamme EN, de Vries HJC, van Veen H, Gabbiani G, Westerhof W, Middelkoop E. Extracellular matrix characterization during healing of full-thickness wounds treated with a collagen/elastin dermal substitute shows improved skin regeneration in pigs. J Histochem Cytochem 1996;44:1311–1322.

[214] Koens MJW, Faraj KA, Wismans RG, van der Vliet JA, Krasznai AG, Cuijpers V, Jansen JA, Daamen WF, van Kuppevelt TH. Controlled fabrication of triple layered and molecularly defined collagen/elastin vascular grafts resembling the native blood vessel. Acta Biomater 2010;6:4666–4674.

[215] Choi JY, Jung KY, Lee JS, Cho SK, Jheon SH, Lim JO. Fabrication and in vivo evaluation of the electrospun small diameter vascular grafts composed of elastin/PLGA/PCL and heparin-VEGF. Tissue Eng Regen Med 2010;7:149–154.

[216] Sell SA, McClure MJ, Barnes CP, Knapp DC, Walpoth BH, Simpson DG, Bowlin GL. Electrospun polydioxanone-elastin blends: potential for bioresorbable vascular grafts. Biomed Mater 2006;1:72–80.

[217] Girotti A, Reguera J, Rodríguez-Cabello J, Arias F, Alonso M, Testera A. Design and bioproduction of a recombinant multi(bio)functional elastin-like protein polymer containing cell adhesion sequences for tissue engineering purposes. J Mater Sci Mater Med 2004;15:479–484.

[218] Rodríguez-Cabello JC, Reguera J, Girotti A, Alonso M, Testera AM. Developing functionality in elastin-like polymers by increasing their molecular complexity: the power of the genetic engineering approach. Prog Polym Sci 2005;30:1119–1145.

[219] Oliveira MB, Song W, Martín L, Oliveira SM, Caridade SG, Alonso M, Rodríguez JC. Development of an injectable system based on elastin-like recombinamer particles for tissue engineering applications. Soft Matter 2011;7:6426–6434.

[220] Costa RR, Custódio CA, Testera AM, Arias FJ, Rodríguez-Cabello JC, Alves NM, Mano JF. Stimuli-responsive thin coatings using elastin-like polymers for biomedical applications. Adv Funct Mater 2009;19:3210–3218.

[221] Pettersson J, Kalbermatten D, McGrath A, Novikova LN. Biodegradable fibrin conduit promotes long-term regeneration after peripheral nerve injury in adult rats. J Plast Reconstr Aesthet Surg 2009;63:1893–1899.

[222] Wang W, Li B, Yang JZ, Xin L, Li YL, Yin HP, Qi YY, Jiang YZ, Ouyang HW, Gao CY. The restoration of full-thickness cartilage defects with BMSCs and TGF-beta 1 loaded PLGA/fibrin gel constructs. Biomaterials 2010;31:8964–8973.

[223] Young JZ, Medawar PB. Fibrin suture of peripheral nerves—measurement of the rate of regeneration. Lancet 1940;2:126–128.

[224] Huang S, Fu XB. Naturally derived materials-based cell and drug delivery systems in skin regeneration. J Control Release 2010;142:149–159.

[225] Conradi L, Hansen A, Eder A, Hirt M, Schaaf S, Reinsch A, Reichenspurner H, Eschenhagen T. Fibrin-based engineered heart tissue (fbeht): a potential future strategy towards cardiac regeneration? Transpl Int 2010;23:0154.

[226] Pankov R, Yamada KM. Fibronectin at a glance. J Cell Sci 2002;115:3861–3863.

[227] Shachar M, Tsur-Gang O, Dvir T, Leor J, Cohen S. The effect of immobilized RGD peptide in alginate scaffolds on cardiac tissue engineering. Acta Biomater 2010;7:152–162.

[228] Wittmer CR, Phelps JA, Saltzman WM, Van Tassel PR. Fibronectin terminated multilayer films: Protein adsorption and cell attachment studies. Biomaterials 2007;28:851–860.

[229] Olenych SG, Moussallem MD, Salloum DS, Schlenoff JB, Keller TCS. Fibronectin and cell attachment to cell and protein resistant polyelectrolyte surfaces. Biomacromolecules 2005;6:3252–3258.

[230] Hill P, Brantley H, Van Dyke M. Some properties of keratin biomaterials: kerateines. Biomaterials 2010;31:585–593.

[231] Martin P. Wound healing—aiming for perfect skin regeneration. Science 1997;276:75–81.

[232] Tachibana A, Kaneko S, Tanabe T, Yamauchi K. Rapid fabrication of keratin-hydroxyapatite hybrid sponges toward osteoblast cultivation and differentiation. Biomaterials 2005;26:297–302.

[233] Jeon NR, Jo EH, Park HJ, Choi JS, Lee SJ, Van Dyke M, Lee JJ, Lee D, Rhee JM, Khang G. Effects of keratin/PLGA scaffolds on proliferation and phenotype of olfactory ensheathing cells. Tissue Eng Regen Med 2009;6:819–824.

[234] Sierpinski P, Garrett J, Ma J, Apel P, Klorig D, Smith T, Koman LA, Atala A, Van Dyke M. The use of keratin biomaterials derived from human hair for the promotion of rapid regeneration of peripheral nerves. Biomaterials 2008;29:118–128.

[235] Li JS, Li Y, Li L, Mak AFT, Ko F, Qin L. Preparation and biodegradation of electrospun PLLA/keratin nonwoven fibrous membrane. Polym Degrad Stabil 2009;94:1800–1807.

[236] Weis-Fogh T. A rubber-like protein in insect cuticle. J Exp Biol 1960;37:889–907.

[237] Elvin CM, Carr AG, Huson MG, Maxwell JM, Pearson RD, Vuocolo T, Liyou NE, Wong DCC, Merritt DJ, Dixon NE. Synthesis and properties of crosslinked recombinant pro-resilin. Nature 2005;437:999–1002.

[238] Truong MY, Dutta NK, Choudhury NR, Kim M, Elvin CM, Hill AJ, Thierry B, Vasilev K. A pH-responsive interface derived from resilin-mimetic protein Rec1-resilin. Biomaterials 2010;31:4434–4446.

[239] Lee BP, Dalsin JL, Messersmith PB. Synthesis and gelation of DOPA-modified poly(ethylene glycol) hydrogels. Biomacromolecules 2002;3:1038–1047.

[240] Lee H, Dellatore SM, Miller WM, Messersmith PB. Mussel-inspired surface chemistry for multifunctional coatings. Science 2007;318:426–430.

[241] Lee H, Lee BP, Messersmith PB. A reversible wet/dry adhesive inspired by mussels and geckos. Nature 2007;448:338–341.

[242] Murphy JL, Vollenweider L, Xu FM, Lee BP. Adhesive performance of biomimetic adhesive-coated biologic scaffolds. Biomacromolecules 2010;11:2976–2984.

[243] Ku SH, Park CB. Human endothelial cell growth on mussel-inspired nanofiber scaffold for vascular tissue engineering. Biomaterials 2010;31:9431–9437.

[244] Dalsin JL, Hu BH, Lee BP, Messersmith PB. Mussel adhesive protein mimetic polymers for the preparation of nonfouling surfaces. J Am Chem Soc 2003;125:4253–4258.

[245] Ying TH, Ishii D, Mahara A, Murakami S, Yamaoka T, Sudesh K, Samian R, Fujita M, Maeda M, Iwata T. Scaffolds from electrospun polyhydroxyalkanoate copolymers: fabrication, characterization, bioabsorption and tissue response. Biomaterials 2008;29:1307–1317.

[246] Rathbone S, Furrer P, Lubben J, Zinn M, Cartmell S. Biocompatibility of polyhydroxyalkanoate as a potential material for ligament and tendon scaffold material. J Biomed Mater Res Part A 2010;93A:1391–1403.

[247] Ye C, Hu P, Ma M-X, Xiang Y, Liu R-G, Shang X-W. PHB/PHBHHx scaffolds and human adipose-derived stem cells for cartilage tissue engineering. Biomaterials 2009;30:4401–4406.

[248] Chen G-Q, Wu Q. The application of polyhydroxyalkanoates as tissue engineering materials. Biomaterials 2005;26:6565–6578.

[249] Wu CKA, Pettit AR, Toulson S, Grondahl L, Mackie EJ, Cassady AI. Responses in vivo to purified poly(3-hydroxybutyrate-co-3-hydroxyvalerate) implanted in a murine tibial defect model. J Biomed Mater Res Part A 2009;91A:845–854.

[250] Cool SM, Kenny B, Wu A, Nurcombe V, Trau M, Cassady AI, Grondahl L. Poly(3-hydroxybutyrate-co-3-hydroxyvalerate) composite biomaterials for bone tissue regeneration: in vitro performance assessed by osteoblast proliferation, osteoclast adhesion and resorption, and macrophage proinflammatory response. J Biomed Mater Res Part A 2007;82A:599–610.

[251] Misra SK, Valappil SP, Roy I, Boccaccini AR. Polyhydroxyalkanoate (PHA)/inorganic phase composites for tissue engineering applications. Biomacromolecules 2006;7:2249–2258.

[252] Zheng Z, Bei FF, Tian HL, Chen GQ. Effects of crystallization of polyhydroxyalkanoate blend on surface physicochemical properties and interactions with rabbit articular cartilage chondrocytes. Biomaterials 2005;26:3537–3548.

[253] Deng Y, Zhao K, Zhang XF, Hu P, Chen GQ. Study on the three-dimensional proliferation of rabbit articular cartilage-derived chondrocytes on polyhydroxyalkanoate scaffolds. Biomaterials 2002;23:4049–4056.

[254] Sodian R, Hoerstrup SP, Sperling JS, Daebritz SH, Martin DP, Schoen FJ, Vacanti JP, Mayer JE. Tissue engineering of heart valves: in vitro experiences. Ann Thorac Surg 2000;70:140–144.

[255] Aguilar MR, Elvira C, Gallardo A, Vásquez B, Román JS. Smart polymers and their applications as biomaterials in topics in tissue engineering. In: Ashammakhi N, Reis RL, Chiellini E, editors. Topics in Tissue Engineering. Volume 3, Oulu: University of Oulu; 2007.

[256] Hoffman AS, Stayton PS. Bioconjugates of smart polymers and proteins: synthesis and applications. Macromol Symp 2004;207:139–152.

[257] Peniche C, Arguelles-Monal W, Davidenko N, Sastre R, Gallardo A, San Roman J. Selfcuring membranes of chitosan/PAA IPNs obtained by radical polymerization: preparation, characterization and interpolymer complexation. Biomaterials 1999;20:1869–1878.

[258] Zhu B, Wei CZ, Hou CL, Gu QS, Chen DJ. Preparation and characterization of hydroxybutyl chitosan. e-Polymers 2010;10:883–892.

[259] Cho MH, Kim KS, Ahn HH, Kim MS, Kim SH, Khang G, Lee B, Lee HB. Chitosan gel as an in situ-forming scaffold for rat bone marrow mesenchymal stem cells in vivo. Tissue Eng Part A 2008;14:1099–1108.

[260] da Silva RMP, Lopez-Perez PM, Elvira C, Mano JF, Roman JS, Reis RL. Poly(Nisopropylacrylamide) surface-grafted chitosan membranes as a new substrate for cell sheet engineering and manipulation. Biotechnol Bioeng 2008;101:1321–1331.

[261] Choi JS, Yoo HS. Pluronic/chitosan hydrogels containing epidermal growth factor with wound-adhesive and photo-crosslinkable properties. J Biomed Mater Res Part A 2010;95A:564–573.

[262] Chen J-P, Cheng T-H. Thermo-responsive chitosan-graft-poly(N-isopropylacrylamide) injectable hydrogel for cultivation of chondrocytes and meniscus cells. Macromol Biosci 2006;6:1026–1039.

[263] Barbosa JS, Ribeiro A, Testera AM, Alonso M, Arias FJ, Rodríguez-Cabello JC, Mano JF. Development of biomimetic chitosan-based hydrogels using an elastin-like polymer. Adv Eng Mater 2010;12:B37–B44.

[264] Shi J, Alves NM, Mano JF. Chitosan coated alginate beads containing poly(Nisopropylacrylamide) for dual-stimuli-responsive drug release. J Biomed Mater Res Part B 2008;84B:595–603.

[265] Ju HK, Kim SY, Lee YM. pH/temperature-responsive behaviors of semi-IPN and combtype graft hydrogels composed of alginate and poly(N-isopropylacrylamide). Polymer 2001;42:6851–6857.

[266] Ju HK, Kim SY, Kim SJ, Lee YM. pH/temperature-responsive semi-IPM hydrogels composed of alginate and poly(N-isopropylacrylamide). J Appl Polym Sci 2002;83:1128–1139.

[267] Wang JY, Jin Y, Xie R, Liu JY, Ju XJ, Meng T, Chu LY. Novel calcium-alginate capsules with aqueous core and thermo-responsive membrane. J Colloid Interface Sci 2011;353:61–68.

[268] Li H, Gong GL. Synthesis and characterization of temperature/pH-sensitive hydroxypropylcellulose/ sodium alginate hydrogel. e-Polymers 2010;2:252–264.

[269] Chan AW, Neufeld RJ. Modeling the controllable pH-responsive swelling and pore size of networked alginate based biomaterials. Biomaterials 2009;30:6119–6129.

[270] Suárez-González D, Barnhart K, Saito E, Vanderby R, Hollister SJ, Murphy WL. Controlled nucleation of hydroxyapatite on alginate scaffolds for stem cell-based bone tissue engineering. J Biomed Mater Res Part A 2010;95A:222–234.

[271] Ibusuki S, Iwamoto Y, Matsuda T. System-engineered cartilage using poly(Nisopropylacrylamide)-grafted gelatin as in situ-formable scaffold: In vivo performance. Tissue Eng 2003;9:1133–1142.

[272] Acharya G, Shin CS, McDermott M, Mishra H, Park H, Kwon IC, Park K. The hydrogel template method for fabrication of homogeneous nano/microparticles. J Control Release 2010;141:314–319.

[273] Ozturk N, Girotti A, Kose GT, Rodriguez-Cabello JC, Hasirci V. Dynamic cell culturing and its application to micropatterned, elastin-like protein-modified poly(N-isopropylacrylamide) scaffolds. Biomaterials 2009;30:5417–5426.

[274] Fitzpatrick SD, Mazumder MAJ, Lasowski F, Fitzpatrick LE, Sheardown H. PNIPAAmgrafted-collagen as an injectable, in situ gelling, bioactive cell delivery scaffold. Biomacromolecules 2010;11:2261–2267.

[275] Santos JR, Alves NM, Mano JF. New thermo-responsive hydrogels based on poly (N-isopropylacrylamide)/hyaluronic acid semi-interpenetrated polymer networks: swelling properties and drug release studies. J Bioact Compat Polym 2010;25:169–184.

[276] Tan HP, Ramirez CM, Miljkovic N, Li H, Rubin JP, Marra KG. Thermosensitive injectable hyaluronic acid hydrogel for adipose tissue engineering. Biomaterials 2009;30:6844–6853.

[277] Lee H, Park TG. Photo-crosslinkable, biomimetic, and thermo-sensitive pluronic grafted hyaluronic acid copolymers for injectable delivery of chondrocytes. J Biomed Mater Res Part A 2009;88A:797–806.

[278] Malay Ö, Batlgün A, Bayraktar O. pH- and electro-responsive characteristics of silk fibroin-hyaluronic acid polyelectrolyte complex membranes. Int J Pharm 2009;380:120–126.

[279] Gil ES, Park SH, Tien LW, Trimmer B, Hudson SM, Kaplan DL. Mechanically robust, rapidly actuating, and biologically functionalized macroporous poly(N-isopropylacrylamide)/ silk hybrid hydrogels. Langmuir 2010;26:15614–15624.

[280] Chen J, Liu M, Chen S. Synthesis and characterization of thermo- and pH-sensitive kappa-carrageenan-g-poly(methacrylic acid)/poly(N,N-diethylacrylamide) semi-IPN hydrogel. Mater Chem Phys 2009;115:339–346.

[281] Schild HG. Poly(N-isopropylacrylamide): experiment, theory and application. Prog Polym Sci 1992;17:163–249.

[282] Gil ES, Hudson SM. Stimuli-responsive polymers and their bioconjugates. Prog Polym Sci 2004;29:1173–1222.

[283] Molinaro G, Leroux JC, Damas J, Adam A. Biocompatibility of thermosensitive chitosan- based hydrogels: an in vivo experimental approach to injectable biomaterials. Biomaterials 2002;23:2717–2722.

[284] Luo C, Zuo F, Ding X, Zheng Z, Cheng X, Peng Y. Light-triggered reversible solubility of α-cyclodextrin and azobenzene moiety complexes in PDMAA-co-PAPA via molecular recognition. J Appl Polym Sci 2008;107:2118–2125.

[285] Tomatsu I, Hashidzume A, Harada A. Photoresponsive hydrogel system using molecular recognition of alpha-cyclodextrin. Macromolecules 2005;38:5223–5227.

[286] Bortolus P, Monti S. cis trans photoisomerization of azobenzene-cyclodextrin inclusion complexes. J Phys Chem 1987;91:5046–5050.

CHAPTER 2. BIOMIMETIC SUPERHYDROPHOBIC SURFACES[2]

2.1. ABSTRACT

Inspiration from nature has been widely used in the development of new materials and in the improvement of their properties. Superhydrophobic surfaces inspired in species present in nature with highly water repellent self-cleaning properties - such as the well-known lotus leaf - are interesting examples of the biomimetic approach for the development of new materials and devices. The discovery of new applications from these materials in the biotechnology and biomedical fields was in wide expansion during the last years. As recent examples of application of surfaces highly repellent to water, applications as implantable biomaterials with anti-adherent properties for vascular grafts or with bactericidal properties were proposed. By patterning these surfaces with wettable regions, microfluidic devices and sensors for the simple and economical diagnosis/monitoring of diseases and cell studies were developed. Another relevant approach regarding patterned superhydrophobic surfaces is their use as chips for high-throughput combinatorial studies in tissue engineering and regenerative medicine. The use of these platforms allowed circumventing several limitations associated with state-of-the-art techniques. Considering the recent innovative approaches and the wide possibilities for future work using these surfaces, we consider that the development of biomimetic superhydrophobic surfaces and their application as innovative and affordable devices is a promising research area.

[2] **Oliveira MB**, Mano JF. Biomimetic superhydrophobic surfaces. In Jabbari E, Kim D-K, Lee LP, Ghaem-Maghami A, Khademhosseini A (eds.) Handbook of Biomimetics and Bioinspiration, pp. 153-180, Singapore, World Scientific, 2014, doi: 10.1142/9789814354936.

2.2. SUPERHYDROPHOBIC SURFACES

The development of new devices for microfluidics, electronics, biosensors, environmental and biomedical applications often requires substrates exhibiting low adhesion and non-wetting properties [1]. Evolution and species selection led to several beneficial wetting phenomena that can be observed in nature. Many surfaces found in nature exhibit highly hydrophobic and self-cleaning properties, including the leaves of plants such as lotus, the wings of cicada and butterflies or the water strider's leg. It is generally accepted that superhydrophobic surfaces – surfaces with water contact angle, higher than 150◦ - must combine two essential properties: (i) surface roughness, especially hierarchically roughness at the micro (and sometimes nano) scale levels and (ii) low surface energy [2]. Inspired by natural biological surfaces, synthetic biomimetic superhydrophobic substrates have been produced by a variety of methodologies, from chemical modifications treatments that lower the surface energy (normally adding fluorides compounds to the surface) to the introduction of double-scaled roughness features, resembling the lotus leaves or other natural models' topography [1-5].

Surface wetting is characterized by how a liquid makes contact with a solid surface and, as referred, depends upon the combined effects of surface chemistry and morphology. Again regarding examples observed in nature, certain plant surfaces have specialized structural and chemical characteristics to manage surface wetting. In this way, a super-hydrophobic surface of a lotus leave enables self-cleaning, whereas a super-hydrophilic surface of a water plant enables water absorption and spreading to achieve a sustained wet state [6,7]. Also, some parts of animals, such as butterfly wings, moth eyes, and desert beetles, exhibit distinct wettability properties enabling adoption of surroundings and promoting animal survival.

2.3. PRINCIPLES EXPLAINING SUPERHYDROPHOBICITY

Young's equation defines the wetting model in a totally rigid, homogeneous, inert, smooth and flat surface. The drop contacts its substrate on a circle where the three phases of the system coexist, and a three phase contact line is formed. The liquid joins the solid at a contact angle θ. Each interface draws the contact line in order to minimize the corresponding surface area, balancing the surface tensions on the direction of potential motion so that there will yield the following relation:

$$\cos\theta = (\gamma SV - \gamma SL)/\gamma LV$$

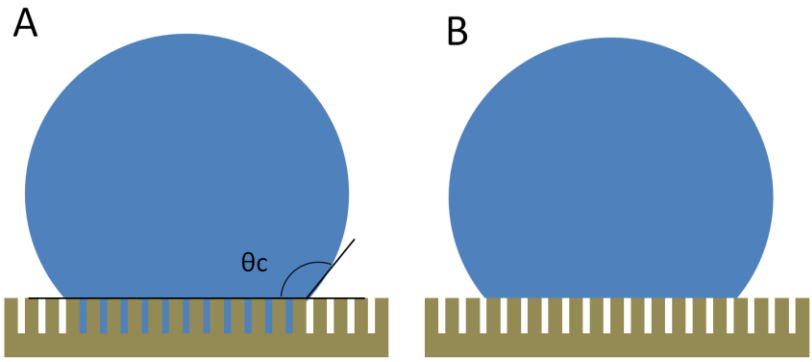

Figure 2.1. - Schematic representation of wetting behavior on solid substrates following: (A) the Wenzel model and (B) the Cassie model.

where γ is the surface tension that indicates the energy per unit surface area of the interface (*S*, *L*, *V* as solid, liquid and vapor, respectively). Real surfaces, though, usually do not fulfill all the requirements of homogeneity, inertness, and absence of roughness, so they cannot be analyzed by the Young's model. A model relating surface roughness and surface energies was proposed by Wenzel (Figure 2.1A) [8]. *r* corresponds to the "roughness factor" – defined as the ratio of the actual area of a rough surface to the geometric projected area and θ^W is the apparent Wenzel contact angle. It can be written as:

$$\cos\theta W = r\cos\theta$$

In the Wenzel state, liquids penetrate surface asperities, or surface irregularities. In Cassie-Baxter state (Figure 2.1B), liquids only contact the top of surface asperities, thereby trapping air pockets underneath the liquid [9]. As a result of the suspension of the water droplet on the asperities, the apparent contact angle is the sum of all the contributions of the different phases:

$$\cos\theta^c = f1\cos\theta_1 + f2\cos\theta_1$$

where θ^c is the apparent contact angle; *f1* and *f2* are the surface fraction of phase 1 and 2, respectively; and $\theta 1$ and $\theta 2$ on the contact angles of phase 1 and phase 2, respectively. Considering rough surfaces with one type of aspirities, and the contact angle of the air 180°, the equation can be re-written as:

$$\cos\theta^c = f(1+\cos\theta^c)-1$$

The combined model (or intermediate state between Wenzel and Cassie states) is also employed to describe the wetting state where the liquid partially fills the open voids on a rough surface in some situations. The transition between Wenzel and Cassie states is observed as well under conditions of droplet press and impact [10].

2.4. SUPERHYDROPHOBIC SURFACES IN NATURE: A BRIEF CORRELATION ANALYSIS BETWEEN TOPOGRAPHY/CHEMICAL FEATURES AND SURFACE PROPERTIES

2.4.1. Lotus leaf

Lotus leaf (*N. nucifera*) is probably the most well-know of surfaces in nature with highly water repellent characteristics (Figure 2.2 A1), and the model that led to the fabrication of the highest number of biomimetic synthetic surfaces. The cause of self-cleaning properties of these surfaces is the hydrophobic water-repellent double structure of the surface: this hierarchical double structure is formed of a characteristic epidermis (including the cuticle, Figure 2.2 A2) and the covering wax crystalloids (nanostructures, Figure 2.2 A3). The epidermis of the lotus plant possesses papillae with 10 to 20 μm in height and 10 to 15 μm in width on which the epicuticular waxes are imposed. These superimposed waxes are hydrophobic and form the second layer of the double structure [2,11]. Barthlot *et al.* [11] reported for the first time the impressive self cleaning properties of these structures by contaminating the leaves' surfaces with particles and subjecting them to artificial rinsing. The authors also compared those results with the ones corresponding to the same procedure performed in naturally smooth leaves, in which the higher presence of particles after rinsing was observed.

2.4.2. Bird Wings

The water repellency of birds' feathers was also studied, and the reasons for their superhydrophobic behavior were compared with the ones of the well-known lotus leaves. It was demonstrated that physical mechanisms of superhydrophobicity of birds' feathers and lotus leaves are very different. While lotus leaves topography is truly hierarchical, birds' feathers show pseudohierarchical relief (Figure 2.2 B1, B2), where various scales do not interact [12]. The pronounced stability of the Cassie state observed on birds' feathers is due to the high value of critical pressure necessary for their total wetting, which is on the order of magnitude of 100 kPa. This high value allows feathers to withstand large dynamical pressure of rain droplets and remain dry under the rain. The energy barrier separating the Cassie state

from the complete wetting situation calculated for a feather is also very high, allowing the increased stability of superhydrophobicity [12].

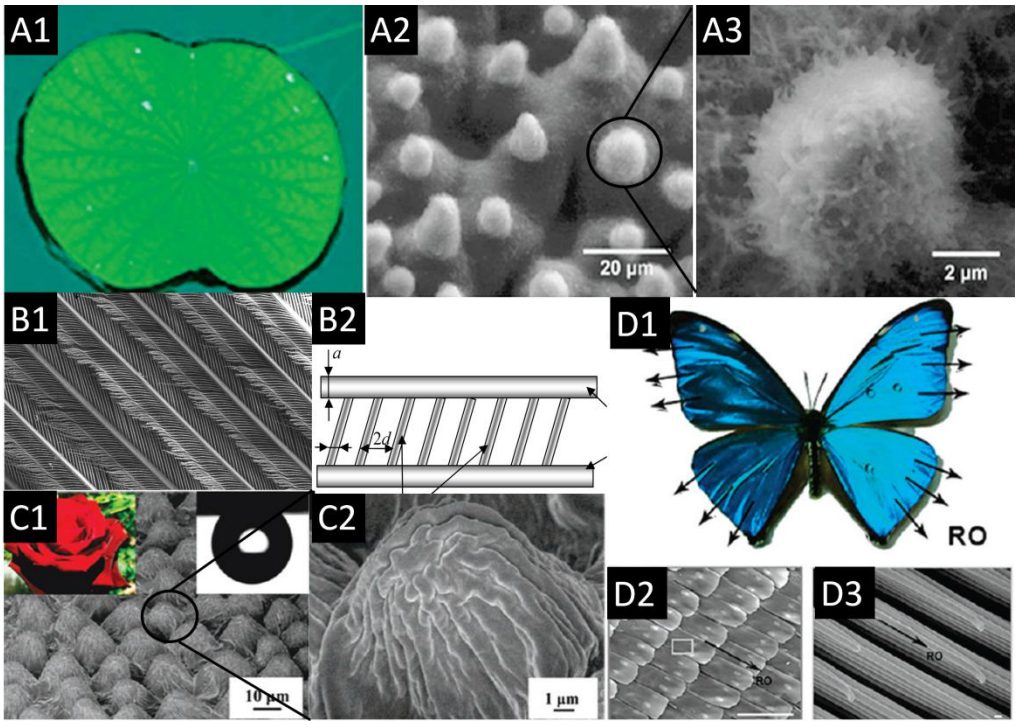

Figure 2.2. – Some examples of superhydrophobic surfaces found in nature. (A1) Lotus leaf, (A2) lotus leaf microstructure with micropapillae and (A3) magnification of one micropapillae, nanostructured wax crystalloids. (B1) Surface microstructure of a pigeon feather and (B2) a schematic representation of its pseudohierarchical structure. (C1) Surface microstructure of a rose petal and (C2) magnification of one micropapillae, in which its nanostructure is visible. (D1) Butterfly wings as example of anisotropic wetting surface. Surface images of the butterfly wings in (D2) microscale and (D3) nanoscale. [Figures (B1), (B2) reprinted with permission from Bormashenko *et al.*, Langmuir 28, 14992 (2012). Copyright 2012. American Chemical Society. All other figures reprinted with permission from Liu *et al.* Accounts on Chemical Research 43, 368 (2010). Copyright 2010. American Chemical Society].

2.4.3. Rose Petal

As well as in Lotus leaves, hierarchical micropapillae (Figure 2.2 C1) and nanofolds (Figure 2.2 C2) are known to exist on the petals' surfaces of red roses [13]. However, differently from the Lotus leaf, these micro- and nanostructures not only provide a sufficient roughness for superhydrophobicity, but at the same time a high adhesive force with water. A water droplet on the surface of the petal appears spherical in shape; however, it cannot roll off even when the petal is turned upside down. This phenomenon is usually defined as the "petal effect" as compared with the popular "lotus effect".

Artificial fabrication of biomimic polymer films by the well-defined nanoembossing of duplicating of the petal's surface indicated that the superhydrophobic surface and the adhesive petal are in Cassie impregnating wetting state [14].

2.4.4. Spider Web

Spider silk was reported to be capable of efficiently collecting water from air. This water-collecting ability of the capture silk of the cribellate spider (*Uloborus walckenaerius)* is the result of a unique fiber structure that forms after wetting. The fibers characterized by periodic spindle-knots made of random nanofibrils and separated by joints made of aligned nanofibrils [15]. Those structural features result in a surface energy gradient between the spindle-knots and the joints and also in a difference in Laplace pressure, with both factors acting together to achieve continuous condensation and directional collection of water drops around spindle-knots. Submillimeter-sized liquid drops have been driven by surface energy gradients or a difference in Laplace pressure. However, neither force by itself was effective on overcoming the larger hysteresis effects that make the movement of micrometer-sized drops more difficult. By conjugating both forces, spider silk achieves this task.

2.4.5. Anisotropic Surfaces in Nature

Anisotropic wetting involves the non-homogeneous distribution of liquid and accompanying wetting properties upon a surface. Physical origin of anisotropic wetting is attributed to liquid contact line encountering physical discontinuity and chemical heterogeneity present on solid surfaces [16,17]. Both natural and synthetic surfaces exhibit anisotropic wetting behavior originating from dissimilarities in chemical or physical surface properties. Anisotropic wetting phenomena include both dynamic properties (e.g., different sliding angles in different directions) and static properties (different static contact angles in different directions). The design of surfaces with anisotropic wetting that support movement of liquid in a single direction can be useful for guiding liquid flow in, for example, microfluidic applications.

In nature, anisotropic wetting is observed on biological surfaces including certain plant leaves, butterfly wings (Figure 2.2 D1, D2, D3) flower petals and bird feathers. For example, rice leaves possess anisotropic hierarchical structures with ordered arrangements of micropapillae and nanoprotrusions [18]. They present a quasi-1D ordering of micropapillae parallel to leaf edges. Superhydrophobicity and

anisotropic wetting of leaf surfaces encourage water droplet movement along the direction parallel to the leaf edge while hindering movement in the direction perpendicular to the leaf edge.

2.5. Preparation of Synthetic Superhydrophobic Surfaces

According to Dorrer and Ruhe [19], in the design of superhydrophobic surfaces two approaches have been exploited: surfaces with controlled design and surfaces with random structures. In the first class, the roughness features are precisely defined using techniques such as lithography or micromachining. The other approach is to obtain materials in which the wettability is random distributed in the surface, i.e. in which the roughness features are statistical. Low surface energy modifications of rough surfaces are also usually used in order to increase the water contact angle of the surfaces. Examples of such kind of chemical and physical modifications are etching of fluoropolymer layers [20,21], solidification, carbon tubes deposition [22], phase separation [23], crystal growth [24,25], aggregation of particles [26], lithography [27,28], vapor deposition [29], electrospinning [30}, layer-by-layer techniques [31] and plasma treatments [32]. Regarding the second class of techniques based on the modification of already rough surfaces, the self-assembly of monolayers of alkanethiols [33], organic silanes [34] and fatty acids [35] have been proposed [36].

In this section, the development of superhydrophobic surfaces inspired by nature will be addressed. This issue will be preceded by a discussion on the need of multiscale roughness (as observed in nature) in order to obtain highly water-repellent substrates.

2.6. Effect of multiscale/hierachical roughness on superhydrophobic surfaces

Pictures of the most well-know superhydrophobic natural surface – the Lotus leaf - show protrusions that resemble paraboloids, which are covered by hairy structures smaller by at least 1 order of magnitude than the main protrusions (Figure 2.2 A1, A2) [11]. However, nonwettable surfaces have been produced by photolithography, without necessarily employing multiscale roughness [37]. Therefore, the need of multiscale roughness to produce high-quality, useful, nonwettable surfaces has been questioned by some authors. This question was partially answered by various thermodynamics analyses that have been published during the past few years [38,39]. It was shown, by using various simple model surfaces, that multiplicity of roughness scales increases the resistance to water penetration into the roughness grooves and reduces the solid– liquid contact area, thus improving

nonwettability. It was also suggested that a combination of mechanical stability and nonwettability properties can be achieved by at least two levels of roughness [40].

The role of multiscale (hierarchical) roughness in optimizing the structure of nonwettable solid surfaces was theoretically studied on three different types of surface topographies with up to four roughness scales: sinusoidal, flat-top pillars, and triadic Koch curves [39]. Theoretical understanding of the effect of multiscale roughness on nonwettability of solid surfaces was sought, so studies of the Gibbs energy maps of wetting systems were made, representing the three very different surface-roughness geometries, and multiscale levels. As the number of roughness scales increased, the authors concluded that: for sinusoidal surfaces the transition contact between Cassie and Wenzel state angle slightly increases, the wetted area slightly decreases, but the height of the roughness feature significantly decreases. For flattop pillars, the changes are not monotonous: the minimal wetted area comes with the maximal contact angle, but also with the maximal roughness feature height. For Triadic-Koch curve roughness the feature height is constant by definition, and the Cassie state becomes stable only when there are four roughness scales. By comparing the distinct topographies, it was then concluded that multiple roughness scales are beneficial, but in a way and to an extent that strongly depend on the basic geometry of the roughness. In the same study, the authors also concluded that it cannot be taken for granted that multiscale roughness is always meaningfully beneficial. In another approach [37], superhydrophobic polypropylene surfaces were produced with hierarchical micro–microstructuring and without chemical surface modification. Polymer substrates were prepared by injection molding, having static water contact angles above 150° and low sliding angles. The authors claim that, besides being easier to produce, durability and robustness of the produced hierarchical structures are higher than the ones of micro-nanostructured surfaces, since virtually the fragile nanolevel structure show very poor resistance to pressure and wear.

2.7. DEVELOPMENT OF SUPERHYDROPHOBIC SURFACES: SOME EXAMPLES

Superhydrophobic surfaces can be produced either by one-step methods or two-step methods [7]. There are methods that allow for a direct processing of the superhydrophobic surface, avoiding the need for further surface modifications: the one-step methods. In those, roughness is produced on/with low surface energy materials. Two-step methods are considered when it is necessary to introduce both low energy and roughness on the surface, so roughness and chemical treatments have to be performed.

2.7.1. One-step processing superhydrophobic surfaces

A common one-step processing method for the increase of surface roughness in the micro- and nano-scale is the solvent/non-solvent method. This method was applied to poly-(L-lactic acid) dissolved in dioxane. The solution was poured onto Petri dishes and gelation took place after evaporation. The films were then immersed in ethanol and the resulting films were totally dried [23,41]. Polystyrene was also treated by a phase-inversion method, using the solvent/non-solvent technique. Polystyrene was dissolved in tetrahydrofuran and the film obtained after pouring the solution in PS commercial available plates was immersed in ethanol (a non-solvent for polystyrene), forcing the polymer precipitation. The polystyrene precipitation on the surface led to formation of a rough surface due to the following mechanism: the mixture of a solvent and a nonsolvent of polystyrene forms both poor and rich polystyrene phases. In the poor PS phase, polymer nuclei are formed by precipitation. The rich polystyrene phase aggregates around these nuclei in order to decrease surface tension. During polymer precipitation within the rich polystyrene phase, a continuous deposition of spheres on the surface takes place [42]. Silyl chitosan (SC) - 3,6-O-di-tertbutyldimethyl silyl chitosan - a chitosan derivative, was synthesized and used to prepare extreme water-repellent films in the whole pH range of 1–14 using a phase separation method that exhibit topography with a three-level hierarchical roughness organization. The SC solution in dichloromethane was dropped on the glass slide first, and the ensemble was immersed in ethanol [43]. The polymer also allows posterior chemical modification specifically through the amine group, permitting to control the surface chemistry and wettability.

Fabrication, namely microfabrication, techniques are also used often to prepare controlled topographies in surfaces. For example, microfiber adhesives were fabricated starting with a high-density polyethylene film and a polycarbonate template with holes of 0.3 μm. The film was placed on the template and heated rollers at 145°C were pressed in the film, leading it to enter in the template holes. As such, the polyethylene film melted into the holes in the template and fibers were generated on the polyethylene surface. Adjusting the roller speed, the fill depth of the molten film - the length of the microfibers - was adjusted [44]. Microfabrication also allowed solving the problem of the poor mechanical robustness of the majority of the superhydrophobic surfaces, which limits their practical applications. Polypropylene surface structuring was done using injection molding, where the microstructured molds were made with a microworking robot [37].

Electrospinning has attracted great deal of attention associated with producing superhydrophobic and self-cleaning surfaces due to small fiber diameters, simple implementation, and to the wide range of

polymers and additives that can be used [30]. Microsphere/nanofiber composite films exhibiting the self-cleaning properties of the lotus leaf were formed by carefully controlling the concentration of the polystyrene solution during electrospinning [45]. Porous microspheres contributed to the superhydrophobicity by increasing the surface roughness, while nanofibers interweave to form a stable multilayer 3D network and reinforce the composite film that is structurally similar to a lotus leaf. In addition to electrospinning, some authors used multistep procedures to induce hydrophobicity of the surface. For example, in the case of polymers with fluorinated compounds, annealing was used to reorient the perfluorinated groups to a fiber surface [46].

Advances have also been observed in the wettability control of self-assembled structures. For example, aligned carbon nanotubes have been used to produce superhydrophobic surfaces. Carbon nanotubes are inherently somewhat hydrophilic, with a water contact angle of less than 86 degrees. When they are arranged in a textured manner on substrates having different surface topographies, different wettabilities are obtained [22]. The surfaces ranged from hydrophilic to hydrophobic, and even superhydrophobic, and with isotropic to anisotropic contact angle hysteresis.

2.7.2. Two-step processing superhydrophobic surfaces

Shark skin was used to develop a method using polydimethylsiloxane (PDMS) containing nano-silica as a substrate for producing a dual-biomimetic surface structure comprising both the shark-skin surface morphology and the lotus leaf-like hierarchical micro/nano-structures. The “shark skin effect” is defined as a mechanism of wall friction reduction of a fluid resulted from a riblet structured surface similar to that of shark skin. Micron-sized grooved scales growing on shark skin - called dermal denticles - are interlocked to form a natural non-smooth surface. The grooves between adjacent riblets on the scales are directed almost parallel to the longitudinal body axis of the shark. The grooved scales can reduce vortice formation or lift the vortice off the surface, resulting in water moving easily over the skin. The shark skin allowed patterning a micro-sized structure, while the subsequent flame treatment made it possess hierarchical micro/nano-structures without damaging the shark skin pattern structure, thereby constructing the dual-biomimetic superhydrophobic surface [47].

Regarding surfaces inspired by the rose petal, the effect of the surface energy of materials on the contact angle values, as well as wear resistance have been poorly studied. Surfaces of varying microstructure pitch and nanostructure density were fabricated by depositing ZnO nanoparticles onto micropatterned substrates [13]. The prepared surfaces were then modified with octadecylphosphonic

acid in order to hydrophobize the ZnO nanoparticles. To study wear resistance for industrial applications, a wear experiment was performed using an atomic force microscope. Rose petal-like surfaces resistant to wear were obtained using both modified and non-modified ZnO nanoparticles, depending on the amount deposited in the surface.

A simple way to make robust, transparent, superamphiphobic coatings was described, inspired by the morphology of candle soot [48]. A technique to coat the soot layer with a silica shell was developed, making use of chemical vapor deposition of tetraethoxysilane catalyzed by ammonia. The porous deposit of candle soot was coated with a 25-nanometer-thick silica shell, and after silanization the final surface showed superamphipilic – i.e. both superhydrophobic and superoleophobic - properties.

The self-assembly of particles has been used in the two-step fabrication of superhydrophobic surfaces [49]. Ordered macroporous ceramic particles were produced by the emulsion templating process: large polystyrene beads and small silica nanoparticles were assembled simultaneously inside an emulsion, which formed composite structured particles during the evaporation of droplets. By burning out polystyrene beads, macroporous ceramic particle films were produced on substrate. The size of ordered macroporous particles could be controlled by adjusting the emulsification condition for confining emulsions. The surface of the ordered macroporous particle films was coated with fluorinated molecules, and showed superhydrophobic properties due to multi-scale roughness.

2.8. Application of Superhydrophobic Surfaces in the Biomedical field

2.8.1. Applications as Biomaterials

2.8.1.1. Cell-superhydrophobic surfaces interactions

Interactions of eukaryotic cells with implantable biomaterials

The response of different cell types to distinct types of superhydrophobic surfaces has been studied. Oliveira *et al.* [50] studied the effect of the surface topography in three distinct cell types seeded onto polystyerene superhydrophobic surfaces prepared by phase separation, and in their analogues treated chemically (with UV/Ozone), that showed decreasing contact angle values. Compared to standard tissue culture polystyrene, it was found that ATDC5 (derived from cartilage tissue) and SaOs-2 (derived from an osteosarcoma, and considered to be similar to osteoblasts) cell lines were not able to proliferate on superhydrophobic surfaces and the cell morphology was affected. L929 cells (fibroblasts) could proliferate. The attachment, morphology and proliferation of SaOs-2 were studied on rough and smooth

PS surfaces with wettability controlled by UV/Ozone irradiation, ranging from superhydrophobic to superhydrophilic. After 4 hours in culture, the attachment of SaOs-2 was higher on the surfaces treated during 18 minutes, namely on rough superhydrophilic and highly hydrophilic smooth PS surfaces. Lourenço *et al.* [51] studied cell adhesion and proliferation ability of primary chondrocytes and MC3T3-E1 osteoblast cell line in superhydrophobic polystyrene and poly(L-lactic acid) surfaces, prepared by phase-separation methodology. The study allowed concluding about the predominant effects of surface topography or polymer type in the cells response in these surfaces, since both types of surfaces show distinct types of micro/nanotopographies but the same wettability properties. The presence of roughness in both surfaces led to a decrease in total protein adsorption, compared to the one observed in smooth (non-treated) wettable surfaces. The superhydrophobic surfaces allowed cells to adhere but inhibited their proliferation, and it was concluded that surface wettability, rather than polymer type or the topography of the superhydrophobic surfaces, was the critical factor in determining cell behavior. In another study, the fibronectin adsorption and cellular behavior of MC3T3-E1 cells was studied in the same polystyrene superhydrophobic surfaces, and compared to controls of smooth polystyrene and glass [52]. The fibronectin surface density was lower on the superhydrophobic surfaces than on non-modified polystyrene, and the adsorbed protein showed altered conformation of cell adhesion domains. Cell adhesion occurred on the superhydrophobic polystyrene without the formation of mature focal adhesions, as assessed by immunofluorescence for vinculin, talin and paxillin. The development of the actin cytoskeleton was delayed and without the presence of defined F-actin fibers and FAK phosphorylation was reduced on superhydrophobic polystyrene. Also, cell contractility was diminished on the superhydrophobic polystyrene as revealed by phosphorylation of myosin light chain. Again, it could be concluded that osteoblasts proliferation was significantly lower in superhydrophobic polystyrene as compared with polystyrene up to 21 days of culture.

The effect of surface roughness and surface chemistry in the osteointegration was studied in titanium implants [53]. Titanium was sandblasted/acid-etched in order to introduce roughness in its surface. The obtained superhydrophobic surfaces were then exposed to oxygen plasma treatment, to increase the reactive oxygen density on the surface. All surfaces were then coated with chitosan, and this process showed that surfaces with different wettabilities, but unchanged microroughness, could be obtained. The cell number, alkaline phosphatase activity and gene expression were studied for all conditions. Surface wettability as a primary regulator enhanced osteoblast differentiation, but integrin expression and silencing beta 1 results indicated that surface wettability regulates osteoblast through differential

integrin expression profiles than microtexture does. The results showed that both microtexture and wettability with a specific chemistry have important regulatory effects on osteointegration.

Interactions with bacteria

Besides the response of eukaryotic cells to superhydrophobic surfaces, some authors have also studied the effect of these surfaces in bacterial response, aiming to develop, for example, bactericidal surfaces. Cicada wing nanopillars showed to be extremely effective at killing *Pseudomonas aeruginosa* cells within approximately 3 minutes [54]. This bactericidal ability of the wing surface is primarily a physico-mechanical effect, as it is retained when the surface chemistry is substantially altered. It was also shown that this effect had no direct relation with the superhydrophobicity of the surfaces: i.e. it was not an antibiofouling effect. However the net result was somewhat similar in that the bacteria are prevented from proliferating on the surface. Imaging experiments demonstrated that the nanopillars began to perforate the cells immediately upon cell attachment.

A study involving superhydrophobic poly(L-lactic acid) surfaces obtained by phase separation and their effect with the same bacteria species - *Pseudomonas aeruginosa* – and also with *S. aureus* showed a contrary effect [55]. In fact, both bacteria types proliferated more effectively in the superhydrophobic surfaces than in the smooth controls, opening a new application for superhydrophobic surfaces as bacterial colonization platforms. It seems then that the reaction of bacteria do superhydrophobic surfaces can show opposite tendencies that could be highly dependent on the topography of the surfaces.

Interactions with blood: as vascular grafts

Superhydrophobic surfaces have also been widely proposed as ideal materials for vascular grafts, since some studies reported a significant decrease of the adhesion of platelets. Nonetheless, depending on the type of surfaces used, their suitability for this purpose varies.

To determine whether superhydrophobic modification of small diameter expanded poly(tetrafluoroethylene) (ePTFE) vascular grafts improves the performance of these grafts, control and superhydrophobic vascular grafts were implanted in the carotid arteries of rabbits and pigs [56]. Furthermore, standard and superhydrophobic vascular patches were implanted in the carotid arteries of seven pigs for 4 weeks. All superhydrophobic and standard ePTFE vascular grafts occluded 15 minutes to 1 hour after implantation in both rabbit and pig carotid arteries. All implanted patches remained patent and were completely covered by endothelium. In this case, superhydrophobic modification of

ePTFE vascular grafts did not lead to less neointima formation and resulted in significantly more platelet deposition than did standard ePTFE vascular grafts.

Poly(carbonate urethane)s (PCUs) used to develop superhydrophobic surfaces showed opposite characteristics [57]. Fluorinated alkyl side chains were used to lower the surface energy of the polymer, and aligned carbon nanotubes films were used as the nanostructured templates. These materials showed largely improved blood compatibility and very low platelet adhesion, contradicting the usual consideration that smooth surfaces are propitious to good blood compatibility. The authors also tested other kinds of medical polymers, such as a PCU without fluorinated side chains and medical polyurethane, and the same effects were achieved.

Surfaces of PDMS irradiated by a CO_2-pulsed laser and further grafted with hydroxyethylmethacrylate phosphatidylcholine (HEMAPC) in order to show superhydrophobic characericsts were studied for platelet adhesion. Results from *in vitro* testing indicated that chemical structures, such as negative-charge polar groups and wettability, were important factors in blood compatibility of these surfaces and the superhydrophilic (the most wettable) and the superhydrophobic (the most unwettable) of modified PDMS surfaces have excellent blood compatibility compared to the unmodified PDMS [58].

2.8.2. Superhydrophobic surfaces as platforms for the fabrication of biomaterials spheres

Inspired by water rolling on the lotus leaf a fabrication process for hydrogel and polymeric spheres was developed [59]. The technique involves basically liquid-air interfaces, in which liquid droplets - that acquire a spherical shape when suspended over a superhydrophobic substrate - harden into a hydrogel form without being in contact with any other liquid media. During the solidification step, the drop is basically involved by the atmospheric environment and the contact with the solid substrate will cover a negligible area. This could enable the creation of a novel platform for processing spherical shape hydrogels may be directly applied in different areas such as the biotechnological and biomedical fields. Potential advantages of this method include the easy operation for preparing hydrogel spheres, high encapsulation efficiency and high encapsulation loading of cells, proteins or soluble therapeutic molecules, low production costs and scale-up possibility using an environmentally friendly technology and, by using adequate devices for dispensing liquid droplets, one can prepare non agglomerated particles with narrow size distribution.

In principle, almost all kinds of superhydrophobic substrates can be employed in this novel method for processing hydrogel spheres. Polystyrene superhydrophobic surfaces prepared by phase inversion

method were used to produce protein and drug-loaded hydrogel spheres for release studies [60], to encapsulate cells in a biocompatible environment [59], and to produce scaffold particles to produce aggregates formed by spheres linked by cells and extracellular matrix [61].

2.8.3. Exploiting the wettability contrast for the design of microfluidic sensors and reactors

Relying in a wettability contrast concept between hydrophobic and hydropholic regions, Whitesides and co-workers proposed a patterned paper device for the detection of several clinically relevant molecules [62]. Chromatography paper was patterned with a photoresist hardened by UV irradition, becoming hydrophobic in the patterned regions, while paper hydrophilic regions were kept by using a protective mask during the UV treatment [62]. As such, well-defined, millimeter-sized channels, comprising hydrophilic paper bounded by hydrophobic polymer could be generated. The design of the chip consisted in a central wettable channel capable of absorbing the sample to be tested by capillary action and the pattern directs the sample into three separate test areas. This represented a breakthrough in the development of low-cost, portable, and technically simple multiplexed bioassays, using equipment that is small, disposable, easy to use (and carry), requiring no external equipment, reagents, or power sources. A method for the simultaneous detection of glucose and protein in low a volume of urine using those chips was developed. The glucose assay was based on the enzymatic oxidation of iodide to iodine, in which a color change from clear to brown is associated with the presence of glucose. The protein assay was based on the color change of tetrabromophenol blue (TBPB) when it ionizes and binds to proteins; a positive result in this case is indicated by a color change from yellow to blue. In 18 minutes assay of this type, two analytes in 20 different samples could be measured.

A paper device consisting in wettable spots surrounded by hydrophobic cured photoresist was also used in the detection of two important markers of liver function: alkaline phosphatase and aspartate aminotransferase, as well as total serum protein [63]. The device consists of a top plastic sheet, a filter membrane, a patterned paper chip containing the reagents necessary for analysis, and a bottom plastic sheet. The device was capable of performing sample preparation using blood from a fingerstick (separating blood plasma from erythrocytes) and the assays. The data obtained from the paper-microfluidic devices showed standard deviations in calibration runs and “spiked” standards that are acceptable for routine clinical use. The chip can be burned after the assays to dispose of biohazard components. The microfluidic paper-based analytical device described in the previous examples was also used in the design of an electrochemical system for flow-injection analysis. When the device is

dipped into a fluid – e.g. urine -, capillary wicking transports the fluid through the paper by gravity-driven flow [64]. In this work, the authors combined this device with electrochemical sensing using amperometry for the detection of the concentration of glucose in urine by a non-invasive test. This can be useful for diagnosis and monitoring of diabetes. The method avoided the use of disposable test stripes with enzymes or electrodes. Such kind of lab-on-a-paper platforms could find other potentialities if superhydrophobic substrates could be used as stating materials. A simple method was proposed to provide superhydrophobic properties to paper [65]. It was shown that plasma treatment could be used to control the wettability in certain regions, opening the possibility to use such substrates to produce non-expensive open-microfluidics on lab-on-a-chip devices.

Using glass slides coated with hydrophobic molecules with a hydrophilic pattern generated by protecting a region of the glass slide with tape during the treatment, Hancock *et al.* [66] proposed a simple method to generate centimeters-long gradients of molecules and particles using a micropipette. A drop of solution was pipetted onto a fluid stripe held in place on a glass slide by a hydrophobic boundary. The resulting difference in curvature pressure drove the flow and created a concentration gradient by convection. The method was compatible with microwell arrays, allowing soluble gradients to be applied to cells in shear-protected microwells. The shapes of micro- and nanodrops were also controlled by patterning those glass surfaces with special hydrophilic regions surrounded by hydrophobic boundaries. Finite element method simulations link the shape of the hydrophilic regions to that of the droplets. Shaped droplets were used to controllably pattern planar surfaces and microwell arrays with microparticles and cells at the micro- and macroscales. Droplets containing suspended sedimenting particles, initially at uniform concentration, deposit more particles under deeper regions than under shallow regions. The resulting surface concentration is thus proportional to the local fluid depth and agrees well with the measured and simulated droplet profiles. Shaped droplets of prepolymer solution were also generated and further crosslinked to synthesize microgels with tailored 3D geometry [67].

Regarding the use of superhydrophobic surfaces and their wettability contrast with patterned channels, Oliveira *et al.* [42] suggested the use of biomimetic superhydrophobic polystyrene surfaces patterned with hydrophilic channels for open microfluidics studies. In comparison with hydrophobic surfaces, superhydrophobicity offers higher wetting contrast and more precise control on the triple line and interfacial elasticity for microfluidics. Open microfluidics (also called surface microfluidics), when compared to its closed counterpart shows advantages such as simple monolithic construction, direct environmental accessibility, no cavitation/interfacial obstruction, clear optical path, and compatibility

with biological experiments. The wettability of the 2D channels could be precisely controlled between the superhydrophobic and superhydrophilic states by changing the exposure time to UV/ozone irradiation. The ability of superhydrophilic paths to drive liquid flows in a horizontal position was found to be significantly higher than for the case of hydrophilic paths patterned onto smooth surfaces.

A similar concept was used to study droplet-based transport phenomena driven by surface using a comprehensive theoretical and experimental investigation of unconventional droplet-based motions [68]. The surfaces were monolithically fabricated using a facile two-step laser micromachining technique on regular PDMS chemistry. Unlike the traditional droplet-driven pumps built on an enclosed microfluidic network, this network pins the liquid–solid interface of droplets to the lithographically defined wetting boundary and establishes a direct linkage between the volumetric and hydraulic measures. Multi-stage programmable bidirectional pumping has been implemented on the platform, according to the newly established droplet manipulation principle, to illustrate its potential use for automated biomicrofluidic and point-of-care diagnostic applications.

2.8.4. Superhydrophobic Surfaces as Devices for High-Throughput Analysis in the Tissue Engineering and Regenerative Medicine field

High-throughput analysis techniques to be used in Tissue Engineering and Regenerative Medicine approaches

One of the main challenges in tissue engineering is to obtain optimized products, combining biomaterials, cells and soluble factors able to stimulate tissue regeneration. Multiple combinations may be considered by changing the conditions among these three factors. The unpredictable response of each combination requires time-consuming tests. High-throughput methodologies have been proposed to master such complex analysis in tissue engineering. Usually, these tests are performed using cells cultured into two-dimensional biomaterials or by dispensing arrays of cell loaded hydrogels [69,70]. However, since it is well reported that cell culture in 3D environments allows for a higher mimicry of the native extracellular matrix, in the last years efforts were made to adapt and create new techniques for high-throughput analysis of cells-3D biomaterials interactions. In this section, we revise the main techniques developed for cell studies in 2D and 3D environments.

Surface patterning techniques which allow for arrays fabrication can be divided in direct writing techniques and other techniques. A sum-up of the current and potential techniques for the study of

combinatorial biomaterials for tissue engineering purposes will be presented, along with the examples of their applications in this field.

In direct writing techniques the use of a mask or pre-templates is not necessary. These techniques can be divided in (i) contact printing, (ii) non-contact printing and (iii) beam-based techniques. In contact printing, a tip (usually metallic) is used to apply a material or energy into a surface; for this reason, this technique is also called scanning-probe lithography, since the tips used for this purpose are usually probes from some microscopic equipment, such as atomic force microscopy. In constructive contact printing, the tip is immersed in the solution and the deposition of a material in a surface occurs by, for example, electrostatic assembly of the deposited material and the surface. When a pattern is not made by the direct deposition of material, but by the application of a mechanical force - which may be compressive or in the form of shear stress - the technique is considered destructive, since the substrate is destructed in the spot that the tip touches. Contact printing against an agarose-coated silane surfaces has been performed aiming for the development of strategies for cell manipulation and skeletal tissue engineering using high-throughput polymer blend formulation, aiming for bone tissue regeneration [71].

Mei *et al.* have used contact printing in epoxy monolayer-coated glass slides to map the interactions among biomaterials, adsorbed proteins, and human embryonic stem cells (hESC) [72]. Monomers were deposited in each spot and the polymerization was performed via 10 second exposure to long-wave UV light. Combining high throughput polymer synthesis and rapid quantification of material/protein/cell interactions, the authors have shown that it is possible to quickly map out the interactions among hESC cell attachment, Fn adsorption, and the chemical structures of the substrates. A similar approach for the obtaining of polymeric nanoliter-scale arrays was developed by Tweedi *et al.* [73], who in few days analyzed the mechanical properties (namely, stiffness) of over 1700 combinations of photopolymerizable polymers by nanoindentation.

Non-contact printing, also known as inkjet printing, is performed by ejecting nanolitre volumes of the desired solution from a microcapillary onto specified positions on a surface. Inkjet printing has been adapted for high-throughput cell patterning [74,75] using glass microscope cover slips as an optically transparent substrate material. To prevent the unhindered attachment of cells across the substrate, the cover slips were dip coated with an autoclaved solution of type II agarose. This work enabled the rapid identification of 'smart' hydrogels for the binding and mild thermal release (from 37°C to 20°C) of all the evaluated cell lines, allowing for example the identification of novel polymers for stem cell binding

and proliferation with subtle temperature mediated release. Polymer synthesis was achieved by depositing the redox initiator followed by combinations of the 18 monomers on a drop-by-drop basis.

High-throughput laser printing of cells and biomaterials for tissue engineering has been proposed by Guillemot *et al*[76]. This work presents results of high-throughput laser printing of a biopolymer (sodium alginate), other biomaterial (nano-sized hydroxyapatite synthesized by wet precipitation) and human endothelial cells. To design an efficient biological laser printer, various pulsed lasers were first considered to determine their suitability for working with living cells and biomaterials as well as for rapid prototyping applications. This technique is complex due to its major requirements, which include: (a) wavelength, which should not induce alteration of the biological materials used, leading to a preference for near-IR lasers, in spite of UV lasers, capable of DNA denaturation; (b) pulse duration and frequency; (c) beam quality, in order to ensure the reproducibility, the stability and the high resolution of the system. A sophisticated five-axe positioning system was integrated into the workstation with the purpose of printing multi-color patterns and building 3D biostructures. Droplet generation was performed by driving the laser beam by means of a high speed scanning system composed of two galvanometric mirrors.

Considering indirect writing techniques - which require the use of masks – photolithography is a technique in which a substrate is irradiated with high energy (such as UV radiation) through a photo-mask. The surface alterations can include the ablation of a photoresist layer, initialization of polymerization, among others. A method in which photolithography was used to produce the masters to produce microfluid channels was presented by Yuan *et al*[77]. This method allowed for the patterning of different types of cells on several types of flat substrates, for instance: glass, PDMS, polystyrene, indium tin oxide (ITO), and even substrates with micro- and nanometer-scale topographic cues like microgrooves. After culturing cells on microfluidic channels (whose separation barrier was PDMS membranes), the membranes separating the channels were removed, and cells were free to migrate under the influence of each other and the substrate, and eventually directly contact each other. As such, migration and co-culture studies could be performed.

Photolithography was used to imprint topographical cues designed by algorithm-based methods, using combinations of simple geometric shapes in a suface of poly(lactic acid). Having in mind that material surface topography is able to evoke specific cellular responses, endowing materials with instructive properties that were formerly reserved for growth factors, the cells behavior was tested in these chips, and “hit” spots for ALP expression could be detected, as morphology could also be studied. The authors

could observe that some surface topography is capable of enhancing osteogenic differentiation of hMSCs [78].

Techniques that involve the use of hard molds to produce patterns are imprint lithography and soft lithography. In imprint lithography, a thermoplastic film covers a heat-resistant substrate. When the temperature is raised about the glass transition temperature of the thermoplastic, a stiff mold previously prepared by photolithography or electron beam lithography is applied and compressed against the thermoplastic. After the cooling of the thermoplastic, the rigid mold is removed, and patterns are obtained. In soft lithography, the same type of rigid templates is used. However, instead of the use of a thermoplastic, usually an elastomer (e.g. PDMS) is applied in the master and further crosslinked, i.e. its mechanical properties and stability is increased by the strengthening of chemical or physical bounds. After crosslinking, the master is removed, and the elastomer possesses a pattern correspondent to the negative of the mold. A microfabricated platform was developed to perform high-throughput unconfined compression of biomaterials in micropatterned arrays. A micropatterned platform was obtained by soft-lithography by Moraes *et al.* [79] It was capable of applying a range of cyclic, compressive mechanical forces to cells encapsulated in an array of micropatterned biomaterials. Nuclear and cellular deformation in response to applied compression was assessed in mouse mesenchymal stem cells encapsulated PEG hydrogels.

To study arrays of isolated materials, commercially available well-plates are also commonly used. They allow for a simple and inexpensive generation of arrays of 3D structures. Combinatorial screening of osteoblast response to 3D calcium phosphate/poly(ε-caprolactone) (PCL) scaffolds using gradients and arrays was performed by Chaterjee *et al* [80]. The effect of the incorporation of nanoamorphous calcium phosphate (nACP) particles on osteoblast response was evaluated. Increasing nACP content in PCL scaffolds promoted osteoblast adhesion and proliferation. Libraries of scaffolds were fabricated in two formats: gradients in well-plates and arrays. A gradient approach for systematic screening of cell response to 3D scaffold composition has been presented using a salt-leached gradient scaffold. Comparison of gradients and arrays suggests that gradients were more sensitive for detecting effects of scaffold composition on cell adhesion whereas arrays were more sensitive at detecting effects on cell proliferation. Combinatorial extracellular matrices for human embryonic stem cell differentiation in 3D were also prepared using well-plates [81]. Advances in understanding cell-ECM interactions and signaling can provide valuable insights in guiding the design of biomimetic materials to regulate stem cell fate for various tissue regeneration applications.

All previous examples consist usually of isolated spots in a substrate. However, an array of conditions may be obtained by generating gradients of crosslinking [82] or loading of some bioactive agent in the structure of a unique biomaterial. The effect of the modulus of 3D scaffolds on osteoblasts differentiation and mineralization was studied by combinatorial screening using gradients [83]. Prepolymeric solutions were polymerized by UV irradiation in different regions, so a simple and inexpensive combinatorial platform was developed to rapidly screen 3D tissue scaffolds. A similar approach was developed to rapidly generate biologically relevant hydrogels containing chemical gradients, using a microfluidic channel [84]. Cellular response to gradients of microgrooves was addressed using an assay format comprising orthogonal gradients of continuously varied groove pitch and depth. The attachment and morphological response of distinct cell types to the variation in topographical cues was studied [85]. Gradients of polyelectrolyte coating obtained by layer-by-layer technology were also fabricated so the interaction between the films and cells could be studied [86].

Superhydrophobic surfaces in High-Throughput Analysis strategies applicable in Tissue Engineering and Regenerative Medicine

Many of the previously reported strategies to study combinatorial cell-materials interactions represented an advance in the development of devices for high-throughput screening. However, some needs for the tissue engineering field remained still to accomplish. With the use of polystyrene superhydrophobic surfaces patterned with wettable regions, Mano and co-workers proposed a series of works in which a method that does not involve complicated processing or expensive equipments or materials is proposed to perform combinatorial studies. In these platforms, protein-cells interactions could be studied in independent spots, avoiding the contamination of neighboring spots with factors released from the cells or materials present in other patterned regions [87]. Also, hydrogels with encapsulated cells could were studied, showing the total cytocompatibility of the platforms [88]. Miniaturized studies of cell-porous scaffolds interactions could be performed for the first time in a platform compatible with the minimum size required for a scaffold with a representative number of pores [89]. These platforms also allow for the direct access to the biomaterials constructs, since these are not confined by walls. This feature allowed performing on-chip porosity assessment and unconfined dynamic mechanical analysis of the structures using in-situ and non-destructive techniques.

Levkin and co-workers propose a superhydrophilic surface patterned with superhydrophobic borders for high-density cell arrays and generation of arrays of cell arrays avoiding the need of pipetting solutions in single individual spots [90].

In this section both approaches and their applications will be revised and their advantages will be discussed.

- **For 2D strategies**

Polystyrene superhydrophobic surfaces patterned with hydrophilic spots have been proposed as devices to be used for high-throughput analysis of cell-biomaterials interactions. These platforms present several advantages for the multiplexed study of biomaterials-cells interaction. Firstly, the superhydrophobic surface that is used in this approach consists of pure polystyrene, which is a non-cytotoxic material, used as a gold-standard for cell culture studies, and a non-expensive material. The patterning of the surfaces with wettable spots was achieved by the exposition of the surface to UV/ozone irradiation through a photomask. As such, this showed to be a simple, rapid and low-cost method for the preparation of the platforms. The chips are totally flat and robust, which eases their manipulation and storage. The biomaterials can be dispensed in each wettable spot and are kept separated from each other due to the highly repellent character of the surrounding area (Figure 2.3). The volumes of solutions dispensed in the spots can be easily varied, as well as the size of the spots. These platforms allow for the sloping and transportation of the whole platform without the mixture of the individual volumes dispensed in each hydrophilic spot.

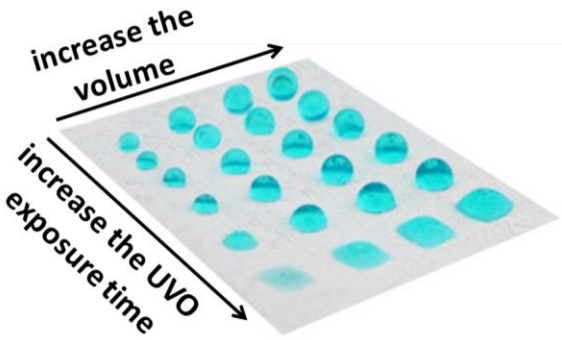

Figure 2.3. – Device for high-throughput analysis: droplets of different volumes from 2 to 8 µl confined in wettable regions produced by different UV/Ozone irradiation times from 1 to 12 minutes in polystyrene superhydrophobic surfaces produced by phase-separation method. Neto *et al.* Soft Matter 7, 4147 (2011) – Reproduced with permission of The Royal Society of Chemistry.

Regarding studies in two-dimensional environment, these platforms allowed screening the biological performance of independent combinations of proteins adsorbed in the wettable patterned regions and cells (Figure 2.4) [87]. In the proof of concept, human fibronectin and albumin were adsorbed in the wettable spots, either separately or together. The amount of adsorbed proteins and their competing

adsorption could be observed by image analysis of the fluorescent-tagged molecules. Cell adhesion studies were performed directly in the wettable spots containing combinatorial dispositions of protein amounts, and cell count was performed by using image-based techniques. Similar chips of poly(L-lactic acid) patterned by the same method as the previously described chips were used to study the mineralization of distinct bioglass nanoparticles formulations, processed by sol-gel technology [91], by performing SEM and EDS analysis in each individual spot.

Levkin and co-workers developed superhydrophobic-superhydrophilic micropatterned chips. A superhydrophilic nanoporous HEMA-EDMA film was firstly prepared by photopolymerization. A grid-like superhydrophobic pattern was then created in the film, by modifying HEMA-EDMA surface with brushes of poly(2,2,3,3,3-pentafluoropropyl methacrylate-co-ethylene dimethacrylate) (PFPMA-EDMA) by photografting using UV irradiation. These chips were used as high-density cell microarrays [90]. The microspots absorb water solutions, while the barriers prevent cross-contamination, thus allowing the spots to be used as reservoirs for transfection mixtures and preventing cell proliferation and cell migration between the microspots. These chips were also used for the generation of isolated microdroplets and 3D cell-encapsulated hydrogels for cell studies; these works will be addressed in the next section regarding high-throughput studies in 3D environments. The same authors also described a simple method for creating superhydrophilic micropatterns on superhydrophobic surfaces [92]. The method was based on printing an “ink”, an ethanol solution of a phospholipid, onto a porous superhydrophobic surface, which is compatible with a variety of commonly available printing techniques.

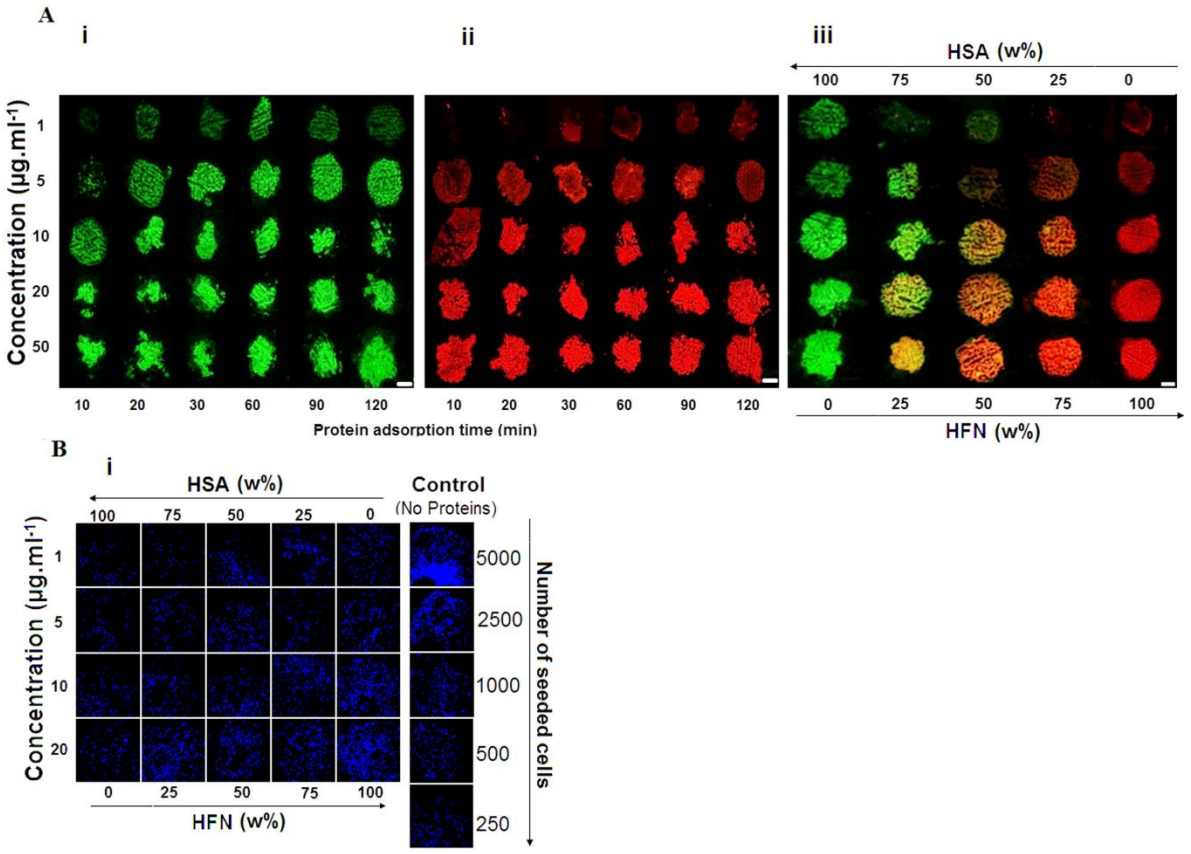

Figure 2.4. – Fluorescence microscopy images of substrates where wettable spots were incubated with protein solutions for 2 hours of (i) albumin (green) and (ii) fibronectin (red) with different concentrations (vertical axis) and during different adsorption times (horizontal axis). (iii) Albumin and fibronectin fluorescent fingerprints in patterned surfaces after different relative amounts and protein concentrations were deposited in the hydrophilic spots. Lower image: confocal microscope pictures of osteoblast-like cells cultured for 4 hours on the micropatterned array pre-adsorbed with different protein quantities (equivalent to the array in (iii)). Scale bars, 500 µm. Neto *et al.* Soft Matter 7, 4147 (2011) – Reproduced with permission of The Royal Society of Chemistry.

- **For 3D strategies**

The array-based screening flat platform described above, consisting of superhydrophobic polystyrene patterned with wettable millimetric spots also showed potential to be used as a high-throughput device for combinatorial cell/3D biomaterials screening assays in the context of tissue engineering (Figure 2.5A,B) [88]. The biological performance of encapsulated cells in hydrogels could be tested in an *in vitro* 3D environment assuming that each site was isolated from the others due to the high contrast of wettability between the patterned spots and the superhydrophobic surroundings. Three different

polymers – chitosan, collagen and hyaluronic acid - were combined with alginate in different proportions in order to obtain combinatorial binary alginate-based polymeric arrays. The effect of the addition of gelatin to the binary structures was also tested. The gels were chemically analyzed on-chip by FTIR microscopic mapping. The observed cell culture results varied according to the hydrogel composition and encapsulated cell types: L929 fibroblast cells and MC3T3-E1 pre-osteoblast cells. Cell viability and number were assessed by conventional chip-destructive methods, in which the samples were removrd from the chip and analyzed individually. MTS reduction test and dsDNA quantification were the selected tests. Non-destructive image analysis was performed on-chip using cytoskeleton and nuclei staining agents (Figure 2.5). The results between both types of tests were coherent. Briefly, L929 cells showed both higher number and viability for higher alginate and collagen-containing hydrogels, while MC3T3-E1 showed higher cell viability and cell number in lower alginate-content and chitosan containing hydrogels. The addition of gelatin did not influence significantly cell metabolic activity or cell number in any of the encapsulated cell types.

Using the same type of high-throughput analysis platforms, the on-chip combinatorial study of 3D miniaturized porous scaffolds was proposed. Arrays of biomaterials were dispensed and processed in-situ as porous scaffolds with distinct composition, surface characteristics, porosity/pore size and mechanical properties (Figure 2.6 A) [89]. On-chip porosity, pore size and mechanical properties of scaffolds based on chitosan and alginate were assessed by adapting microcomputed tomography equipment and a dynamic mechanical analyzer - and cell response after 24 hours. The interactions between cell types of two distinct origins – osteoblast-like and fibroblasts - and the scaffolds modified with fibronectin are studied by image-based methods (Figure 2.6 B,C) and validated by comparison with conventional destructive methods (dsDNA quantification and MTS tests). Physical and biological on-chip analyses were coherent with the conventional measures, and conclusions about the most favorable conditions for each cell type were taken.

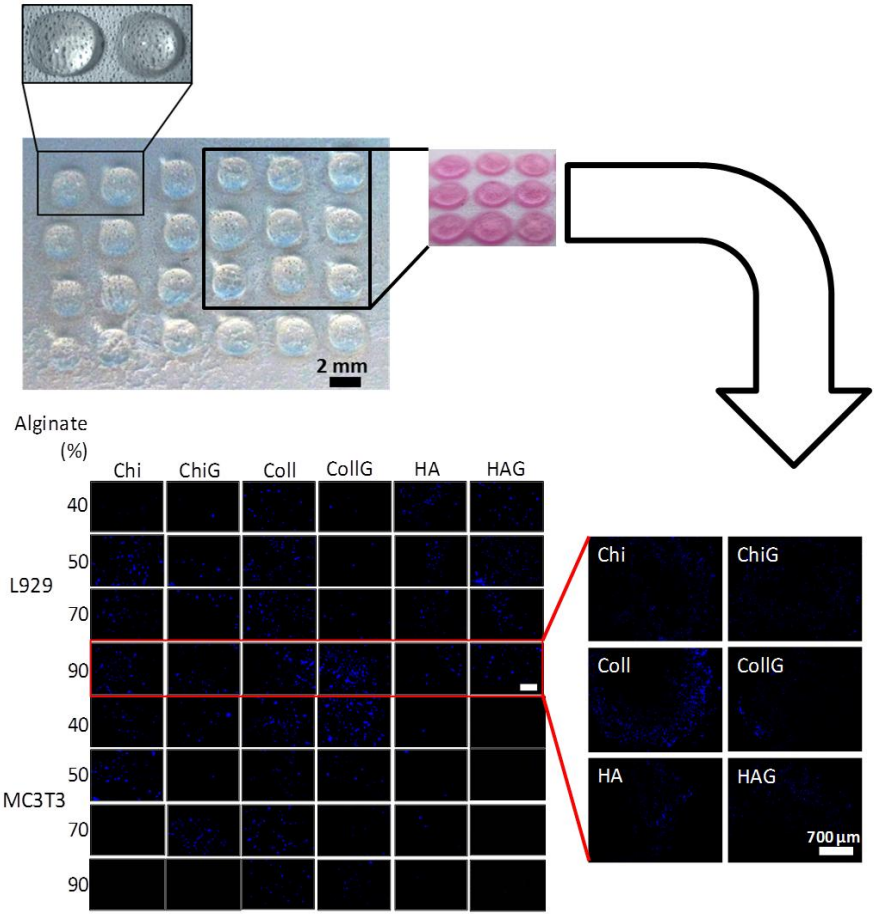

Figure 2.5. – In the upper image: a superhydrophobic chip with hydrogels (left) after preparation by ionic crosslinking and (right) after immersion in medium. Bottom image: the acquisition of microscopy images allowed to study the cell number (by nuclei staining) in each hydrogel by non-destructive means. Salgado *et al.* Integrative Biology 4, 318 (2012) – Reproduced with permission of The Royal Society of Chemistry.

Using the nanoporous superhydrophilic surfaces patterned with superhydrophobic spots described above [93], a one-step method for creating thousands of isolated pico- to microliter-sized droplets with defined geometry and volume was proposed. Arrays of droplets were formed as liquid moves along a superhydrophilic–superhydrophobic patterned surface. Isolated microdroplets with defined geometry and volume could be generated by a technology referred by the authors as a Droplet Microarray. The extreme wettability contrast of superhydrophilic spots on a superhydrophobic background allowed for the spontaneous separation of an aqueous solution, leading to the formation of high-density arrays of completely separated microdroplets, avoiding manual pipetting or a liquid handling device. High-density arrays of hydrogel micropads encapsulating live cells were also prepared in this device, with potential to be used for high-throughput screening of cells in 3D microenvironments.

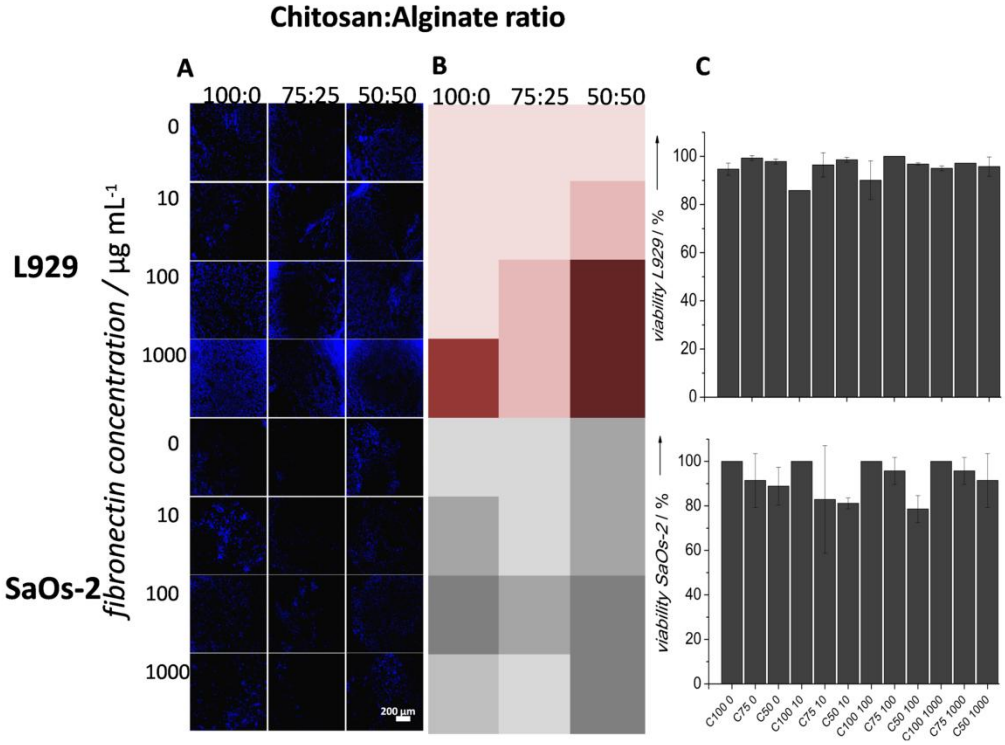

Figure 2.6. – (A) Fluorecence microscopy images of on-chip produced scaffolds with L929 and SaOs-2 cell nuclei stained with DAPI. (B) Intensity maps of image-based quantification of cell nuclei. (C) On-chip calculated cell viability on each scaffold with gradients of adsorbed fibronectin obtained by the image-based quantification of dead cells. Oliveira *et al.* Small– Reproduced by permission of John Wiley and Sons.

2.9. CONCLUSIONS

The understanding and development of superhydrophobic surfaces has been in wide expansion during the last decades. One of the main areas of application for these highly water repellent surfaces is biomedical engineering, biotechnology and development of biomaterials. Recently, these materials were proposed for applications as implantable biomaterials with anti-adherent properties for vascular grafts or with bactericidal properties. In their simple form, these surfaces were used as devices for the simple, biocompatible and economically viable production of biomaterials loaded with drug, cells or other active agents. Moreover, the patterning of such surfaces with wettable channels or spots has allowed developing devices for microfluidics studies and high-throughput combinatorial studies, allowing circumventing problems associated with previous state-of-the-art techniques. Regarding this information, we consider that the development of biomimetic superhydrophobic surfaces and their discovery as innovative, affordable and versatile devices is a promising research area, with a broad set of future perspectives.

2.10. REFERENCES

[1] Shahsavan H, Arunbabu D, Zhao BX. Biomimetic Modification of Polymeric Surfaces: A Promising Pathway for Tuning of Wetting and Adhesion. Macromol Mater Eng. 2012;297:743-60.

[2] Feng L, Li SH, Li YS, Li HJ, Zhang LJ, Zhai J, et al. Super-hydrophobic surfaces: From natural to artificial. Adv Mater. 2002;14:1857-60.

[3] Bhushan B. Biomimetics: lessons from nature - an overview. Philos T R Soc A. 2009;367:1445-86.

[4] Yan YY, Gao N, Barthlott W. Mimicking natural superhydrophobic surfaces and grasping the wetting process: A review on recent progress in preparing superhydrophobic surfaces. Adv Colloid Interfac. 2011;169:80-105.

[5] Webb HK, Hasan J, Truong VK, Crawford RJ, Ivanova EP. Nature Inspired Structured Surfaces for Biomedical Applications. Curr Med Chem. 2011;18:3367-75.

[6] Xia F, Jiang L. Bio-inspired, smart, multiscale interfacial materials. Adv Mater. 2008;20:2842-58.

[7] Oliveira SM, Alves NM, Mano JF. Cell interactions with superhydrophilic and superhydrophobic surfaces. Journal of Adhesion Science and Technology. 2012:1-21.

[8] Wenzel RN. Ind Eng Chem. 1936;28:988–94.

[9] Lafuma A, Quere D. Superhydrophobic states. Nat Mater. 2003;2:457-60.

[10] Luo C, Xiang M, Heng X. A Stable Intermediate Wetting State after a Water Drop Contacts the Bottom of a Microchannel or Is Placed on a Single Corner. Langmuir. 2012;28:9554-61.

[11] Barthlott W, Neinhuis C. Purity of the sacred lotus, or escape from contamination in biological surfaces. Planta. 1997;202:1-8.

[12] Bormashenko E, Gendelman O, Whyman G. Superhydrophobicity of Lotus Leaves versus Birds Wings: Different Physical Mechanisms Leading to Similar Phenomena. Langmuir. 2012;28:14992-7.

[13] Ebert D, Bhushan B. Wear-resistant rose petal-effect surfaces with superhydrophobicity and high droplet adhesion using hydrophobic and hydrophilic nanoparticles. J Colloid Interf Sci. 2012;384:182-8.

[14] Feng L, Zhang YA, Xi JM, Zhu Y, Wang N, Xia F, et al. Petal effect: A superhydrophobic state with high adhesive force. Langmuir. 2008;24:4114-9.

[15] Zheng Y, Bai H, Huang Z, Tian X, Nie F-Q, Zhao Y, et al. Directional water collection on wetted spider silk. Nature. 2010;463:640-3.

[16] Xia DY, Johnson LM, Lopez GP. Anisotropic Wetting Surfaces with One-Dimesional and Directional Structures: Fabrication Approaches, Wetting Properties and Potential Applications. Adv Mater. 2012;24:1287-302.

[17] Neuhaus S, Spencer ND, Padeste C. Anisotropic Wetting of Microstructured Surfaces as a Function of Surface Chemistry. Acs Appl Mater Inter. 2012;4:123-30.

[18] Zhu D, Li X, Zhang G, Zhang X, Zhang X, Wang T, et al. Mimicking the Rice Leaf—From Ordered Binary Structures to Anisotropic Wettability. Langmuir. 2010;26:14276-83.

[19] Dorrer C, Ruhe J. Some thoughts on superhydrophobic wetting. Soft Matter. 2009;5:51-61.

[20] Busscher HJ, Stokroos I, Golverdingen JG, Schakenraad JM. Adhesion and Spreading of Human Fibroblasts on Superhydrophobic Fep-Teflon. Cell Mater. 1991;1:243-9.

[21] Busscher HJ, Stokroos I, Vandermei HC, Rouxhet PG, Schakenraad JM. Preparation and Characterization of Superhydrophobic Fep-Teflon Surfaces. Journal of Adhesion Science and Technology. 1992;6:347-56.

[22] Liu H, Zhai J, Jiang L. Wetting and anti-wetting on aligned carbon nanotube films. Soft Matter. 2006;2:811-21.

[23] Shi J, Alves NM, Mano JF. Towards bioinspired superhydrophobic poly(L-lactic acid) surfaces using phase inversion-based methods. Bioinspir Biomim. 2008;3.

[24] Shibuichi S, Onda T, Satoh N, Tsujii K. Super water-repellent surfaces resulting from fractal structure. J Phys Chem-Us. 1996;100:19512-7.

[25] Mohammadi R, Wassink J, Amirfazli A. Effect of Surfactants on wetting of super-hydrophobic surfaces. Langmuir. 2004;20:9657-62.

[26] Tsai PS, Yang YM, Lee YL. Fabrication of hydrophobic surfaces by coupling of Langmuir-Blodgett deposition and a self-assembled monolayer. Langmuir. 2006;22:5660-5.

[27] Dorrer C, Ruhe J. Advancing and receding motion of droplets on ultrahydrophobic post surfaces. Langmuir. 2006;22:7652-7.

[28] Shirtcliffe NJ, McHale G, Newton MI, Perry CC. Wetting and wetting transitions on copper-based super-hydrophobic surfaces. Langmuir. 2005;21:937-43.

[29] Liu H, Feng L, Zhai J, Jiang L, Zhu DB. Reversible wettability of a chemical vapor deposition prepared ZnO film between superhydrophobicity and superhydrophilicity. Langmuir. 2004;20:5659-61.

[30] Sas I, Gorga RE, Joines JA, Thoney KA. Literature review on superhydrophobic self-cleaning surfaces produced by electrospinning. J Polym Sci Pol Phys. 2012;50:824-45.

[31] Liao K-S, Wan A, Batteas JD, Bergbreiter DE. Superhydrophobic Surfaces Formed Using Layer-by-Layer Self-Assembly with Aminated Multiwall Carbon Nanotubes. Langmuir. 2008;24:4245-53.

[32] Fernández-Blázquez JP, Fell D, Bonaccurso E, Campo Ad. Superhydrophilic and superhydrophobic nanostructured surfaces via plasma treatment. J Colloid Interf Sci. 2011;357:234-8.

[33] Guix M, Orozco J, García M, Gao W, Sattayasamitsathit S, Merkoçi A, et al. Superhydrophobic Alkanethiol-Coated Microsubmarines for Effective Removal of Oil. ACS Nano. 2012;6:4445-51.

[34] Song X, Zhai J, Wang Y, Jiang L. Fabrication of Superhydrophobic Surfaces by Self-Assembly and Their Water-Adhesion Properties. The Journal of Physical Chemistry B. 2005;109:4048-52.

[35] Hu Z, Deng Y. Superhydrophobic Surface Fabricated from Fatty Acid-Modified Precipitated Calcium Carbonate. Industrial & Engineering Chemistry Research. 2010;49:5625-30.

[36] Roach P, Shirtcliffe NJ, Newton MI. Progess in superhydrophobic surface development. Soft Matter. 2008;4:224-40.

[37] Huovinen E, Hirvi J, Suvanto M, Pakkanen TA. Micro–Micro Hierarchy Replacing Micro–Nano Hierarchy: A Precisely Controlled Way To Produce Wear-Resistant Superhydrophobic Polymer Surfaces. Langmuir. 2012;28:14747-55.

[38] Li X-M, Reinhoudt D, Crego-Calama M. What do we need for a superhydrophobic surface? A review on the recent progress in the preparation of superhydrophobic surfaces. Chemical Society Reviews. 2007;36:1350-68.

[39] Bittoun E, Marmur A. The Role of Multiscale Roughness in the Lotus Effect: Is It Essential for Super-Hydrophobicity? Langmuir. 2012;28:13933-42.

[40] Callies M, Quere D. On water repellency. Soft Matter. 2005;1:55-61.

[41] Alves NM, Shi J, Oramas E, Santos JL, Tomas H, Mano JF. Bioinspired superhydrophobic poly(L-lactic acid) surfaces control bone marrow derived cells adhesion and proliferation. J Biomed Mater Res A. 2009;91A:480-8.

[42] Oliveira NM, Neto AI, Song WL, Mano JF. Two-Dimensional Open Microfluidic Devices by Tuning the Wettability on Patterned Superhydrophobic Polymeric Surface. Appl Phys Express. 2010;3:085205.

[43] Song WL, Gaware VS, Runarsson OV, Masson M, Mano JF. Functionalized superhydrophobic biomimetic chitosan-based films. Carbohyd Polym. 2010;81:140-4.

[44] Lee J, Fearing RS. Wet Self-Cleaning of Superhydrophobic Microfiber Adhesives Formed from High Density Polyethylene. Langmuir. 2012;28:15372-7.

[45] Wang XF, Ding B, Yu JY, Wang MR. Engineering biomimetic superhydrophobic surfaces of electrospun nanomaterials. Nano Today. 2011;6:510-30.

[46] Acatay K, Simsek E, Ow-Yang C, Menceloglu YZ. Tunable, superhydrophobically stable polymeric surfaces by electrospinning. Angew Chem Int Edit. 2004;43:5210-3.

[47] Liu Y, Li G. A new method for producing "Lotus Effect" on a biomimetic shark skin. J Colloid Interf Sci. 2012;388:235-42.

[48] Deng X, Mammen L, Butt HJ, Vollmer D. Candle Soot as a Template for a Transparent Robust Superamphiphobic Coating. Science. 2012;335:67-70.

[49] Cho Y-S, Choi S-Y, Kim Y-K, Yi G-R. Bulk synthesis of ordered macroporous silica particles for superhydrophobic coatings. J Colloid Interf Sci. 2012;386:88-98.

[50] Oliveira SM, Song WL, Alves NM, Mano JF. Chemical modification of bioinspired superhydrophobic polystyrene surfaces to control cell attachment/proliferation. Soft Matter. 2011;7:8932-41.

[51] Lourenco BN, Marchioli G, Song WL, Reis RL, van Blitterswijk CA, Karperien M, et al. Wettability Influences Cell Behavior on Superhydrophobic Surfaces with Different Topographies. Biointerphases. 2012;7:46-50.

[52] Ballester-Beltran J, Rico P, Moratal D, Song WL, Mano JF, Salmeron-Sanchez M. Role of superhydrophobicity in the biological activity of fibronectin at the cell-material interface. Soft Matter. 2011;7:10803-11.

[53] Park JH, Wasilewski CE, Almodovar N, Olivares-Navarrete R, Boyan BD, Tannenbaum R, et al. The responses to surface wettability gradients induced by chitosan nanofilms on microtextured titanium mediated by specific integrin receptors. Biomaterials. 2012;33:7386-93.

[54] Ivanova EP, Hasan J, Webb HK, Truong VK, Watson GS, Watson JA, et al. Natural Bactericidal Surfaces: Mechanical Rupture of Pseudomonas aeruginosa Cells by Cicada Wings. Small. 2012;8:2489-94.

[55] Sousa C, Rodrigues D, Oliveira R, Song W, Mano JF, Azeredo J. Superhydrophobic poly(L-lactic acid) surface as potential bacterial colonization substrate. AMB Express. 2011;1:1-9.

[56] Toes GJ, van Muiswinkel KW, van Oeveren W, Suurmeijer AJH, Timens W, Stokroos I, et al. Superhydrophobic modification fails to improve the performance of small diameter expanded polytetrafluoroethylene vascular grafts. Biomaterials. 2002;23:255-62.

[57] Sun TL, Tan H, Han D, Fu Q, Jiang L. No platelet can adhere - Largely improved blood compatibility on nanostructured superhydrophobic surfaces. Small. 2005;1:959-63.

[58] Khorasani MT, Mirzadeh H. In vitro blood compatibility of modified PDMS surfaces as superhydrophobic and superhydrophilic materials. J Appl Polym Sci. 2004;91:2042-7.

[59] Song WL, Lima AC, Mano JF. Bioinspired methodology to fabricate hydrogel spheres for multi-applications using superhydrophobic substrates. Soft Matter. 2010;6:5868-71.

[60] Lima AC, Song WL, Blanco-Fernandez B, Alvarez-Lorenzo C, Mano JF. Synthesis of Temperature-Responsive Dextran-MA/PNIPAAm Particles for Controlled Drug Delivery Using Superhydrophobic Surfaces. Pharm Res-Dordr. 2011;28:1294-305.

[61] Oliveira MB, Song WL, Martin L, Oliveira SM, Caridade SG, Alonso M, et al. Development of an injectable system based on elastin-like recombinamer particles for tissue engineering applications. Soft Matter. 2011;7:6426-34.

[62] Martinez AW, Phillips ST, Butte MJ, Whitesides GM. Patterned paper as a platform for inexpensive, low-volume, portable bioassays. Angew Chem Int Edit. 2007;46:1318-20.

[63] Vella SJ, Beattie P, Cademartiri R, Laromaine A, Martinez AW, Phillips ST, et al. Measuring Markers of Liver Function Using a Micropatterned Paper Device Designed for Blood from a Fingerstick. Anal Chem. 2012;84:2883-91.

[64] Lankelma J, Nie ZH, Carrilho E, Whitesides GM. Paper-Based Analytical Device for Electrochemical Flow-Injection Analysis of Glucose in Urine. Anal Chem. 2012;84:4147-52.

[65] Obeso CG, Sousa MP, Song W, Rodriguez-Pérez MA, Bhushan B, Mano JF. Modification of paper using polyhydroxybutyrate to obtain biomimetic superhydrophobic substrates. Colloids and Surfaces A: Physicochemical and Engineering Aspects. 2013;416:51-5.

[66] Hancock MJ, He JK, Mano JF, Khademhosseini A. Surface-Tension-Driven Gradient Generation in a Fluid Stripe for Bench-Top and Microwell Applications. Small. 2011;7:892-901.

[67] Hancock MJ, Yanagawa F, Jang YH, He JK, Kachouie NN, Kaji H, et al. Designer Hydrophilic Regions Regulate Droplet Shape for Controlled Surface Patterning and 3D Microgel Synthesis. Small. 2012;8:393-403.

[68] Xing SY, Harake RS, Pan TR. Droplet-driven transports on superhydrophobic-patterned surface microfluidics. Lab Chip. 2011;11:3642-8.

[69] Mei Y. Microarrayed materials for stem cells. Mater Today. 2012;15:444-52.

[70] Potyrailo R, Rajan K, Stoewe K, Takeuchi I, Chisholm B, Lam H. Combinatorial and High-Throughput Screening of Materials Libraries: Review of State of the Art. ACS Comb Sci. 2011;13:579-633.

[71] Khan F, Tare RS, Kanczler JM, Oreffo ROC, Bradley M. Strategies for cell manipulation and skeletal tissue engineering using high-throughput polymer blend formulation and microarray techniques. Biomaterials. 2010;31:2216-28.

[72] Mei Y, Gerecht S, Taylor M, Urquhart AJ, Bogatyrev SR, Cho S-W, et al. Mapping the Interactions among Biomaterials, Adsorbed Proteins, and Human Embryonic Stem Cells. Advanced Materials. 2009;21:2781-6.

[73] Tweedie CA, Anderson DG, Langer R, Van Vliet KJ. Combinatorial Material Mechanics: High-Throughput Polymer Synthesis and Nanomechanical Screening. Advanced Materials. 2005;17:2599-604.

[74] Roth EA, Xu T, Das M, Gregory C, Hickman JJ, Boland T. Inkjet printing for high-throughput cell patterning. Biomaterials. 2004;25:3707-15.

[75] Zhu XC, Zheng Q, Yang H, Cai J, Huang L, Duan YW, et al. Recent advances in inkjet dispensing technologies: applications in drug discovery. Expert Opin Drug Discov. 2012;7:761-70.

[76] Guillemot F, Souquet A, Catros S, Guillotin B, Lopez J, Faucon M, et al. High-throughput laser printing of cells and biomaterials for tissue engineering. Acta Biomaterialia. 2010;6:2494-500.

[77] Yuan B, Li Y, Wang D, Xie Y, Liu Y, Cui L, et al. A General Approach for Patterning Multiple Types of Cells Using Holey PDMS Membranes and Microfluidic Channels. Advanced Functional Materials. 2010;20:3715-20.

[78] Unadkat HV, Hulsman M, Cornelissen K, Papenburg BJ, Truckenmuller RK, Post GF, et al. An algorithm-based topographical biomaterials library to instruct cell fate. Proc Natl Acad Sci U S A. 2011;108:16565-70.

[79] Moraes C, Wang G, Sun Y, Simmons CA. A microfabricated platform for high-throughput unconfined compression of micropatterned biomaterial arrays. Biomaterials. 2010;31:577-84.

[80] Chatterjee K, Sun L, Chow LC, Young MF, Simon Jr CG. Combinatorial screening of osteoblast response to 3D calcium phosphate/poly([epsilon]-caprolactone) scaffolds using gradients and arrays. Biomaterials. 2011;32:1361-9.

[81] Yang F, Cho S-W, Son SM, Hudson SP, Bogatyrev S, Keung L, et al. Combinatorial Extracellular Matrices for Human Embryonic Stem Cell Differentiation in 3D. Biomacromolecules. 2010;11:1909-14.

[82] Burdick JA, Khademhosseini A, Langer R. Fabrication of gradient hydrogels using a microfluidics/photopolymerization process. Langmuir. 2004;20:5153-6.

[83] Chatterjee K, Lin-Gibson S, Wallace WE, Parekh SH, Lee YJ, Cicerone MT, et al. The effect of 3D hydrogel scaffold modulus on osteoblast differentiation and mineralization revealed by combinatorial screening. Biomaterials. 2010;31:5051-62.

[84] He J, Du Y, Villa-Uribe JL, Hwang C, Li D, Khademhosseini A. Rapid Generation of Biologically Relevant Hydrogels Containing Long-Range Chemical Gradients. Advanced Functional Materials. 2010;20:131-7.

[85] Reynolds PM, Pedersen RH, Riehle MO, Gadegaard N. A Dual Gradient Assay for the Parametric Analysis of Cell-Surface Interactions. Small. 2012;8:2541-7.

[86] Sailer M, Sun KLW, Mermut O, Kennedy TE, Barrett CJ. High-throughput cellular screening of engineered ECM based on combinatorial polyelectrolyte multilayer films. Biomaterials. 2012;33:5841-7.

[87] Neto AI, Custodio CA, Song WL, Mano JF. High-throughput evaluation of interactions between biomaterials, proteins and cells using patterned superhydrophobic substrates. Soft Matter. 2011;7:4147-51.

[88] Luz GM, Leite AJ, Neto AI, Song WL, Mano JF. Wettable arrays onto superhydrophobic surfaces for bioactivity testing of inorganic nanoparticles. Mater Lett. 2011;65:296-9.

[89] Geyer FL, Ueda E, Liebel U, Grau N, Levkin PA. Superhydrophobic-Superhydrophilic Micropatterning: Towards Genome-on-a-Chip Cell Microarrays. Angew Chem Int Edit. 2011;50:8424-7.

[90] Salgado CL, Oliveira MB, Mano JF. Combinatorial cell-3D biomaterials cytocompatibility screening for tissue engineering using bioinspired superhydrophobic substrates. Integr Biol-Uk. 2012;4:318-27.

[91] Oliveira MB, Salgado CL, Song W, Mano JF. Combinatorial On-Chip Study of Miniaturized 3D Porous Scaffolds Using a Patterned Superhydrophobic Platform. Small. 2012;(accepted for publication).

[92] Ueda E, Geyer FL, Nedashkivska V, Levkin PA. DropletMicroarray: facile formation of arrays of microdroplets and hydrogel micropads for cell screening applications. Lab Chip. 2012;12:5218-24.

[93] Li JSS, Ueda E, Nallapaneni A, Li LXX, Levkin PA. Printable Superhydrophilic-Superhydrophobic Micropatterns Based on Supported Lipid Layers. Langmuir. 2012;28:8286-91.

CHAPTER 3. HIGH-THROUGHPUT SCREENING FOR INTEGRATIVE BIOMATERIALS DESIGN: EXPLORING ADVANCES AND NEW TRENDS[3]

3.1. ABSTRACT

With the increasing need for biomaterials and tissue engineering alternatives, more accurate, rapid and cost-saving methods and models to study biomaterials-cells interactions must be developed. We review the evolution of microarray platforms used for such studies in order to meet the criteria of the complex tissue engineering biological environments. Particular aspects regarding biomaterials processing, data acquisition and treatment are addressed. Besides *in vitro* array-based strategies we also address the emerging *in vivo* high-throughput approaches and its associated trends, such as the role of inflammation in regeneration. The up-scaling of high-throughput methods using single cell encapsulation systems is also explored. Possible limitations related to the use of such methods, such as spot-to-spot crosstalk, are also discussed.

[3] This chapter was based on the publication: Oliveira MB, Mano JF. High-Throughput Screening for Integrative Biomaterials Design: Exploring Advances and New Trends. Trends in Biotechnology. (in press). DOI: 10.1016/j.tibtech.2014.09.009

3.2. HIGH-THROUGHPUT ANALYSIS FOR BIOMATERIALS DEVELOPMENT

The challenges associated with life quality maintenance in ageing populations require better biomaterials, particularly in the field of tissue engineering. However, the development of new materials designed to address specific biological problems is hampered by multiple complex factors associated with their application, including materials chemistry, topography, cell-protein interactions, cell types and physiological state (Box 1). Rapid cost-saving testing of biomaterials-cells interactions is needed to understand the complexity affecting this area [1, 2]. Moreover, efforts to design more truthful biomimetic cell niches are needed [3-6] as conditions used *in vitro* are still fairly distant from mimicking the body environment, in particular at the cellular level.

In this review, we focus on the advances in the design of biomaterials' arrays compatible with cell/drug encapsulation, miniaturization of porous scaffolds and adaptation with mini/micro-bioreactors (Table 3.1). The dependence of automated equipment for the patterning of biomaterials/cells in the platforms used for high-throughput screening (HTS) will be compared with techniques that allow for bench-top dispensing of biomaterials [7-9]. A recent trend consisting of the implantation of biomaterials arrays in animal models will also be explored (Figure 3.1) [10]. Single cell encapsulation in biomaterial microparticles will also be addressed, as it rises as an easily up-scalable method for the study of biomaterials [11].

BOX 1

Complexity of biomaterials development for tissue regeneration or substitution strategies

Tissue regeneration is mediated by cellular response, affected by the environment created by biomaterials, delivered molecules and stimulation of the whole tissue by, e.g. mechanical means. The complex choice of a biomaterial for organ substitution or regeneration is decided after evaluating the type of damage and its dimension. The final goal is having a biomaterial that, alone or in combination with other factors such as bioactive molecules and with specific cells, modulates cells and tissue response to achieve full regeneration.

According to the defect, materials in the form of coatings/membranes (isotropic or with gradients), three-dimensional scaffolds or cell laden hydrogels must be chosen. One may process biomaterials from several types: metallic, polymeric, ceramic, composite, self assembled low molecular weight molecules, among others. A wide range of techniques is available to process such materials, e.g. solvent casting, layer-by-layer, photopolymerization, ionic gelation and rapid prototyping. Materials origin, composition and processing will determine biomaterials physicochemical characteristics such as topography, wettability, protein adsorption profile, mechanical properties, viscoelasticity, soluble factors uptake/release and degradability. Some of these factors will

vary in time after implantation with mechanical and chemical stimuli (e.g. by mechanisms of degradation), that may occur by action of cells.

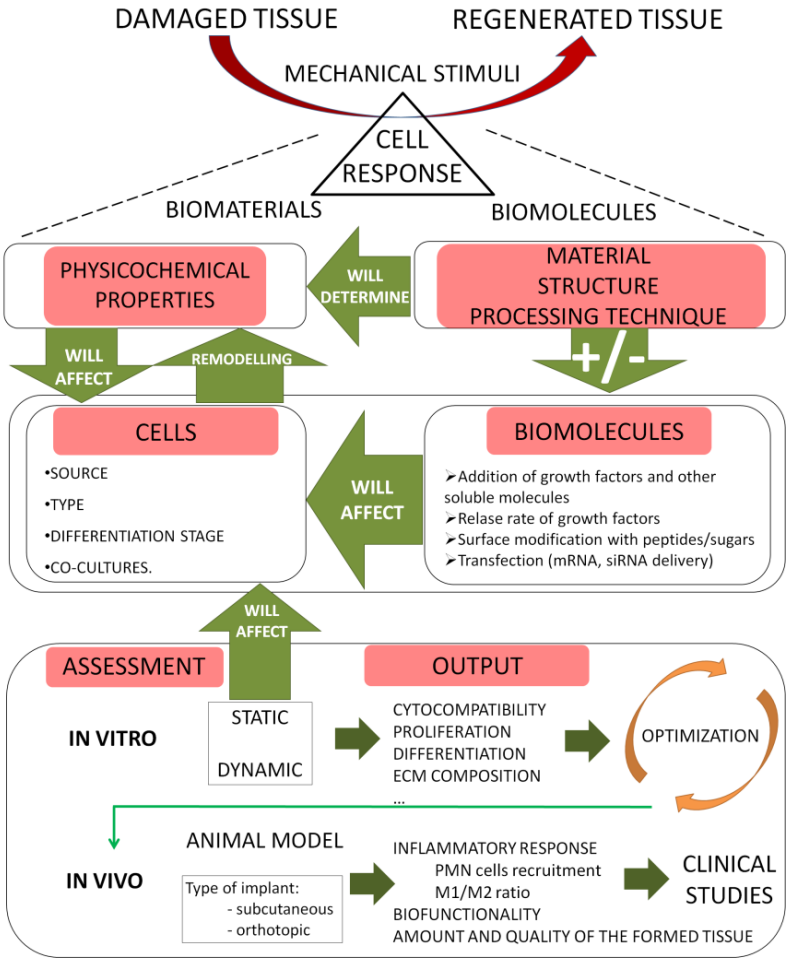

Figure 3I. (Box 1) – Schematic representation of the main interactions affecting the design, testing and performance of biomaterials.

The implanted biomaterials may contain seeded or encapsulated cells - from autologous or allogenic origin - and bioactive molecules. Such cells may be of primary lineage or stem cells derived from different origins (e.g. adipose tissue, bone marrow), or induced pluripotent stem cells. Stem cells may be implanted in a native post-retrieval state or with different times of pre-differentiation *in vitro*. It is well also known that in some biological tissues – such as the osteochondral tissue, where there is an interaction between chondrocytes and osteoblasts – the presence of co-cultures may be important to promote natural-occurring interactions.

For biomaterials loaded with bioactive molecules, their release must be controlled so they induce the desired response in cells. Such molecules may consist of growth factors to promote cells differentiation, molecules for surface modification of biomaterials or genetic material to be delivered intracellularly to tailor cells fate.

The study of cell response must be studied *in vitro* – either with mechanical stimuli that mimic the organism action, or in static environment. This process must be optimized until promising results are achieved. Selected conditions must be implanted in animal models, firstly for initial response studies (e.g. inflammatory response) and later for tissue regeneration.

3.3. EVOLUTION OF HIGH-THROUGHPUT SYSTEMS FOR BIOMATERIALS SCREENING: FINDING INSPIRATION TO SOLVE CURRENT NEEDS

The perspective of a rapid, efficient and industry-paced discovery of adequate materials for implantation was implemented with the development of miniaturized biomaterials arrays [12,13]. Such systems have seen significant development during the last decade to meet specific needs of the evolving biomaterials field, where the importance of reproducing biological niche-like three-dimensional environments [14] and the effect of several external parameters affecting biological response were reported [15-18]. In this section we present a critical report on the developments of biomaterials HTS systems.

3.3.1. Direct writing techniques

The first biomaterials microarray was suggested in 2004 by Anderson *et al* [13]. It consisted of over 1700 contact-printed and polymerized monomers onto which embryonic stem cells (ESCs) were seeded. Relevant and unexpected effects of materials on cells proliferation and differentiation were identified on chips with the size of a microscopy glass slide. Contact printing uses pins to dispense a material volume, whose deposition occurs after the direct contact with the surface, previously treated to prevent cell adhesion. Materials size and shape is determined by the pin size [19]. Such technique allowed the rapid mapping of interactions between biodegradable polymeric biomaterials, proteins and stem cells [20,21]. The stiffness of more than 1700 biodegradable biomaterials was also characterized by nanoindentation in a few days [22]. Hook *et al.* identified biomaterials formulations that reduced the attachment of pathogenic bacteria and validated such results by implanting "hit" biomaterials-coated silicone in mice [23]. Contact printing was recently used to print photopolymerizable hydrogels containing encapsulated cells, followed by analyzes of their osteogenic potential totally on-chip [24].

Inkjet printing rose as a non-contact direct writing printing technique (Table 3.2). It was used to pattern hydrogels, proteins and cells in the form of miniaturized arrays [25-28]. It is performed by ejecting nanoliter volumes of solutions from a microcapillary onto specified surface positions. Piezoelectric stimuli or heat may be applied in order to separate the liquid from the tip of the nozzle; the use of heating strategy allowed cell encapsulation with viability in the range of 90% [29]. Alternatively, laser

printing (Table 3.2), as firstly suggested by Guillemot *et al.* [30], was used to print microarrays of cells - avoiding DNA fragmentation [31,32] - ceramic/polymeric biomaterials and proteins [33].

3.3.2. Indirect writing techniques

Indirect writing techniques require the pre-production of a template to pattern biomaterials and mixtures thereof [34]. In photolithography (Table 3.2) a substrate is irradiated with high energy through a photo-mask. Surface alterations can include the ablation of a photoresist layer, initialization of polymerization or surface modification. Yuan *et al.* [35] developed a method for patterning and studying the migration of different types of cells on substrates composed by different materials with flat features or with grooves. Poly(ethylene glycol)-diacrylate (PEG-DA) microwells produced by photolithography [36] were used as reservoirs to study biomaterials-stem cells interactions after depositing biomaterials in the microwells by contact printing [37].

In soft lithography an elastomer - usually polydimethylsiloxane (PDMS) - is applied in a pre-designed mold and further crosslinked, possessing a pattern correspondent to the negative of the template. Moraes *et al.* produced a microfabricated platform for unconfined compression of biomaterial arrays by soft-lithography (Table 3.1) to study its effect on encapsulated mesenchymal stem cells [38].

The particular case of wettability contrast-based arrays

Superhydrophobic surfaces patterned with wettable regions are a particular case of indirect writing platforms used for biomaterials studies. It is generally accepted that superhydrophobic surfaces show water contact angles higher than 150◦ and low surface energy, effectively repelling water adhesion [40]. In such surfaces biomaterials remain restricted to the wettable spots due to the wettability constrast between them and the superhydrophobic surrounding [7, 41, 42]. This approach allows patterning water-based biomaterials with distinct shapes and heights, depending on the shape and area of the wettable spot, as well as on the volume dispensed (Figure 3.1a). It was shown that cell attachment or proliferation is avoided in the superhydrophobic parts of the chips [43-45].

Protein-cells interactions were studied in independent spots of polystyrene chips, avoiding the contamination or cross-talk of neighboring spots with factors released from the cells or materials present in neighboring spots [42]. Using polystyrene chips, biomaterials were dispensed in the wettable spots by pipetting [46-48]. Nonetheless, the total flatness of the platforms makes them compatible with any automated printing strategy. Hydrogels with encapsulated cells were also patterned and analyzed by image-based techniques (Table 3.2) [46]. Porous scaffolds were also processed in the form of miniaturized arrays (Figure 3.1a) for the first time in a platform compatible with the minimum size

required for a scaffold with a representative number of pores [47]. These platforms also allow for the direct access to the biomaterials constructs, since these are not confined by walls. This feature allowed performing on-chip porosity assessment and unconfined dynamic mechanical analysis of the structures using *in situ* and non-destructive techniques [47, 48].

Levkin and co-workers suggested a superhydrophilic surface patterned with superhydrophobic borders composed of HEMA-EDMA photopatterned with PFPMA through a photo-mask. High-density hydrogel/cell arrays were patterned in the wettable spots avoiding pipetting or handling solutions in single individual spots [8, 9], as arrays of droplets were formed by dragging the cell-laden polymer solution along the surface.

In biomaterials development, besides direct cells-biomaterials contact, the presence of bioactive molecules, such as growth factors or genetic material [49], may also determine cell fate and therapeutic effects (Box 1). Upon implantation, the delivery rate of such molecules is of utmost importance to promote a desired response [50]. Our group developed polystyrene superhydrophobic surfaces patterned with a ring-shaped wettable region to study the release of growth factors from hydrogels by image analysis (Table 3.1) [51].

Polystyrene chips based on wettability contrast containing miniaturized biomaterials were also implanted in Wistar rats for the assessment of localized early inflammatory response in a high-throughput context (Figure 3.1) [10].

3.3.3. Direct and indirect writing techniques: a critical comparison

In direct writing techniques biomaterials are deposited in uniform surfaces and the size of such unconfined biomaterials is not limited by the definition of the surface patterns. Techniques such as contact, inkjet and laser printing allowed patterning biomaterials and biomaterials/cells mixtures with diameters ranging from 50 μm to 500 μm [13,26-33] attaining, mainly in the case of cell-laden hydrogels, lower values than indirect writing techniques (Table 3.2). However, the spreading of the biomaterials in such platforms is dependent on their chemical/physical interactions with the surface. For such reason, materials with different chemical compositions may generate heterogeneous spots with distinct diameters/shapes and their printing requires optimization.

The wide range of patterns used in indirect writing printing strategies provides several advantages regarding biomaterials homogenous geometry and volume control, mainly with the use of platforms temporary masks [35] and patterns of wettability contrast [46-48]. The use of microwells has been evidenced as beneficial to avoid crosstalk and contamination between biomaterials [39].

Table 3.1. – Examples of high-throughput screening platforms adapted to be compatible with relevant topics for efficient biomaterials.

Use of the chips	Relevant topic studied for tissue engineering/biomaterials development	Disposition of the biomaterials on space	Examples of interactions/characteristics assessed on-chip	Refs.
In vitro	Cell-biomaterials direct contact interactions	2D array	2D interactions protein-materials-cells	[21,42]
			2D interactions biomaterial films/hydrogel-cells/bacteria	[13, 20, 23, 27, 28, 35, 37, 53, 60-63]
			Topographical cues-cells interaction	[4, 54]
			Cell-laden hydrogels	[24, 26, 30, 31, 39, 46, 52]
			Porous scaffolds-cells interaction	[47, 59, 69]
		3D "array" (microparticles in a 3D environment)	Cell-laden hydrogels	[76, 79, 80]
	Effect of externally applied stimuli (bioreactors on-chip)	2D array	Cyclic mechanical stimuli (compression) on cells encapsulated on hydrogels	[38]
		3D "array" (particles inside a coiled tube)	Shear stress on cells seeded on the surface of microparticles	[93]
	Physical-chemical characterization of biomaterials	2D array	Mechanical and viscoelastic properties (nanoindentation, DMA)	[22, 48]
			Surface wettability (WCA)	
			Surface chemistry (TOF-SIMS, Raman Spectroscopy, XPS, FTIR)	[46]; reviewed in [91]
	Drug/growth factor release from biomaterials	2D array	BSA-FITC release from alginate hydrogels; fully on-chip image-based technique	[51]
In vivo	Assessment of the *in vivo* response to individual biomaterials implanted as arrays on-chip on animal models	2D array	Inflammatory response for each biomaterials on the arrays upon subcutaneous implantation in Wistar rats	[10]

However, the presence of walls may impair easy on-chip mechanical characterization of the samples. Lithographic methods are particularly advantageous when complex designs for integration of bioreactors on-chip are required [38]. Superhydrophobic patterned chips offer the advantage of having totally flat surfaces and unconfined samples. It is also compatible with the design of complex devices for, e.g. drug release assessment [51].

3.3.4. Gradients

Biomaterials libraries and combinations in the form of an array are, so far, the most common method to perform time and resource-saving studies in the field. Nonetheless, materials gradients also gained momentum to study the effect of continuous variations of biomaterials' stiffness [52], surface chemistry [53] and other chemical features [54-56], topography or presence of bioactive agents [57] on cell response (Table 3.2).

Although gradients sizes may achieve the scale of centimeters, the variation of properties of the biomaterials is continuous in the whole range of the gradient (Table 3.2). In a comparative study on the use of gradients versus discrete spots of biomaterials with RGD gradients, authors concluded that an individual cell is unlikely to feel nano-alterations along the gradients. However, diffusional length was sufficiently small so adjacent cells had significant influence in neighboring counterparts by paracrine effects [58].

Besides microfluidic-generated linear gradients of 3D hydrogels stiffness and cell adhesion ligand molecules [59,60], non-linear concentration gradients in biomaterials were also prepared [61]. The non-orthogonal patterning of two bone morphogenic proteins (BMP-2 and BMP-7) gave insights on their individual and combined effects on C2C12 cells fate [62]. Using capillary flow to produce gradients, Hammond and co-workers patterned isolated spots of a microfluidic chip with layer-by-layer thin film constructs with different compositions [63]. Biomaterials gradients were also designed to promote cell migration using chemotaxis mechanisms [64].

3.4. THE NEED FOR NEW SYSTEMS TO IMPROVE THE STUDY OF COMPLEX BIOMATERIALS SYSTEMS

One of the most evident difficulties of generating usable high-throughput systems for the patterning of biomaterials is the need of automated equipment to deposit samples on the chips. Levkin and co-workers patterned hydrogel micropads in the form of a microarray, using superhydrophobic/superhydrophilic contrast by dragging a hydrogel solution along the wettable regions [9]. The hydrogels, however, were not automatically dispensed in with combinatorial

Table 3.2. – Listing and characterization of techniques used to study biomaterials-cells in a high-throughput manner.

	Technique characterization by platform type	HTS technique	Platform material	Dispensing of biomaterials	Size of biomaterials spots	Cell-biomaterials interactions	3D biomaterial-cells interactions: type of structure	Refs.
Arrays	Direct	**Contact printing**	Glass coated with agarose/epoxy/ 3-(trimethoxysilyl) propyl methacrylate	Contact (robot)	100 µm – 1 mm	2D	-	[13, 20,23]
						3D	Hydrogels for cell encapsulation	[24]
		Inkjet printing	Glass coated with collagen/polystyrene PET	Non-contact (commercially available printers)	100 µm – 1mm	2D	-	[26-29]
						3D	Hydrogels for cell encapsulation	
		Laser printing	Quartz		10 µm – 100 µm	3D	Hydrogels for cell encapsulation	[30]
	Indirect	**Microwells**	PEG-DA	Microcontact printing using PDMS stamps	50 µm- 100 µm	2D	-	[6]
		Photolithography	PDMS	Polymer selective crosslinking by action of UV irradiation through a mask	1 mm – 10 mm	3D	Hydrogels for cell encapsulation	[38]
		Arrays of topography	PLA PMMA	Topography induced by hot embossing	290 µm (pattern units in the range of 10 µm-28 µm²)	2D	-	[4, 54]
		Commercially available well plates	Polystyrene	Pipetting	1 mm – 10 mm	3D	Hydrogels for cell encapsulation Porous scaffolds	[52, 59]
		Superhydrophobic Surfaces patterned with wettable spots	Polystyrene HEMA-EDMA photopatterned with PFPMA	Pipetting on the wettable spots Dragging of the solution in the patterned platform	500 µm – 5 mm	2D	-	[46]
						3D	Hydrogels for cell encapsulation Porous scaffolds (miniaturized)	[10, 42, 47, 48]
Others	-	**Gradients**	Glass	Microfluidics	... nm – 10 mm	2D	-	[54 – 63]
		Single cell encapsulation	-		1 µm – 10 µm	3D	Hydrogel particles for cell encapsulation	[11, 76, 79]

formulations. Nonetheless, this approach opened an interesting possibility of patterning different biomaterials in each wettable spot by dragging dynamic mixtures of polymers and cells, easily obtained using a multi-inlet pump with programmable variable speeds. Cells were also cultured in arrays using magnetic forces [65]. This may also open a possibility to increase the throughput of cell-laden hydrogels in a robot-independent strategy. Recently, a technique named as "partipippeting" – consisting of wiping hydrogels that are randomly pipetted on the top of a microwell array in order to force each individual hydrogel to enter a single microwell - was suggested in order to rapidly pipette distinct hydrogels, in parallel and in the absence of manual or sophisticated pipetting systems [66].

The scale factor is also an important aspect to take in consideration while studying biomaterials. In a straightforward approach, the concept of high-throughput would ideally rely in the maximum miniaturization of each individual unit to be studied. However, due to the micrometric size of cells, biomaterials must have a representative size, allowing their encapsulation or seeding of cell suspensions. Although cell-laden hydrogels are the most common way of performing combinatorial studies of cells-biomaterials interactions in a 3D environment, some biomaterials are not amenable to be processed in the mild conditions that allow cell encapsulation. Moreover, modulation of porous scaffolds' porosity, pore size and degree of interconnectivity not only influences cell seeding efficiency and migration, but were also reported to influence cells response [67-68]. While cell-laden hydrogels with diameters of 500 μm show compatibility with long-term high-throughput studies, preparing a miniaturized porous scaffold with a representative number of pores and a truly interconnected structure required a minimum spot size of 1-2 mm [47]. Importantly, arrays of dried porous scaffolds may be an interesting way of commercializing biomaterials sets in ready-to-use, off-the-shelf platforms for cell-biomaterials tests [69].

Surface topography of biomaterials is known to affect cell response, namely stem cells differentiation [70, 71]. In prosthesis, the achievement of an adequate surface topography also determines their successful integration. Unadkat *et al.* designed a poly(lactic acid) (PLA) chip whose spots contained non-biased topographies generated randomly by machine learning algorithms. Such chips were used to discover materials topographies that promote mesenchymal stem cells proliferation and commitment in the osteogenic lineage [4]. Orthogonal topography gradients in combination with chemical cues were also suggested to study cell response – namely morphology - in poly(methyl methacrylate) (PMMA) surfaces (Table 3.1) [54].

A critical aspect in high-throughput engineering of biomaterials relies on the effects of eventual crosstalk between spots immersed under the same cell culture medium. In most of microarray-based high-

throughput tests platforms are treated to avoid cell adhesion and crossover from spot to spot. However, it is well described that cells express soluble factors that are responsible for cell interactions in indirect co-cultures [72]. Methods to assess the reliability of on-chip results have been suggested: the comparison of spot-to-spot results in chips with biomaterials organized in an "ordered" configuration, as well as in a "scrambled" configuration were studied [24]. Flow dynamics simulations were performed in modular chips, where each unit is under dynamic flow conditions, in order to prove absence of cross-talk between spots [73]. On-chip results were also compared to the ones of conventional-sized materials for physical-chemical characterization [47, 48] and *in vivo* studies [10]. The concern of cross-contamination does not only apply to the factors expressed by cells. It also may limit the study of materials in what could be considered a 4th dimension, i.e. using biomaterials whose properties vary with time, namely the ones that show biodegradability. In this case, debris of each biomaterial could possibly contaminate the surrounding conditions. The loading of biomaterials with biomolecules to be released in a controlled manner has also been widely impaired due to the usual lack of independence between the spots of the arrays. We suggested a system where the release solution is miniaturized and individualized [51].

A recent trend on the high-throughput analysis of biomaterials is the implantation of chips containing distinct combinations of biomaterials in *in vivo* models. Conventional biomaterials implantation often requires the use of high numbers of animals. As such, implanting a high number of biomaterials in a single animal and concluding about its performance is a major ethical breakthrough in the area of biomaterials development. Furthermore, it is known that *in vitro* assays fail to mimic the whole complexity of biological environment. For example, in the majority of cells-biomaterials studies performed *in vitro*, the role of inflammatory cells and factors recruited to the biomaterials site is often neglected. However, immunomodulation is determinant for biomaterials integration on the tissue and it actively intervenes in aspects as angiogenesis [74]. Our group recently reported the subcutaneous implantation of polystyrene superhydrophobic patterned chips with 36 biomaterials in Wistar rats [10]. The recruitment of lymphocytes and macrophages to each individual spot of the chip was assessed.

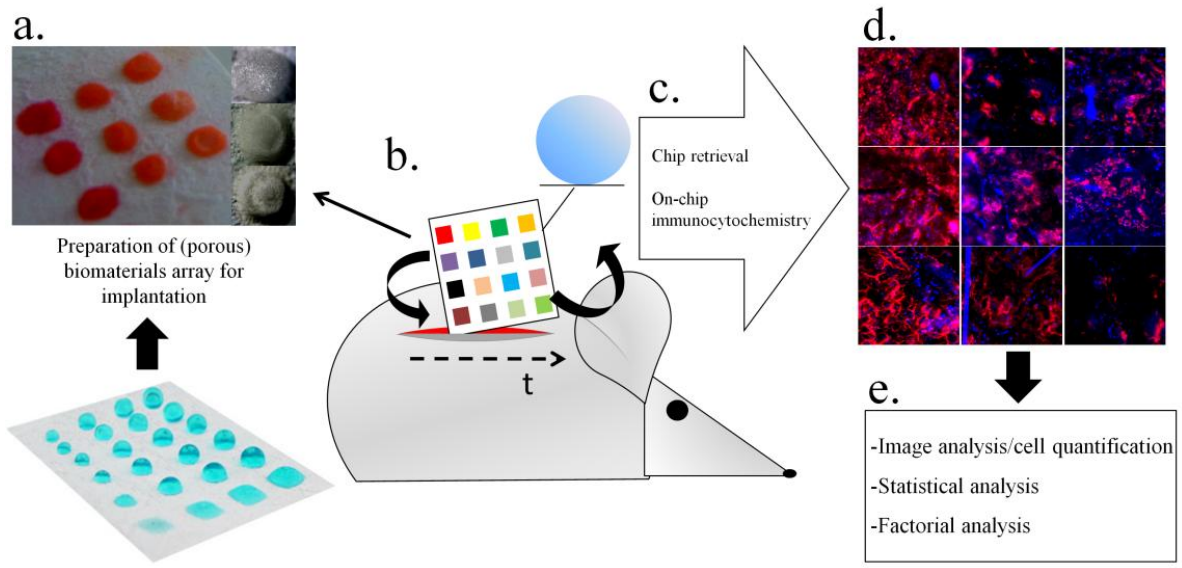

Figure 3.1. – Conceptual diagram showing the steps required to perform the evaluation of *in vivo* inflammatory response to biomaterials in a high-throughput manner using superhydrophobic surfaces patterned with wettable regions as chips. a. Preparation of superhydrophobic surfaces with arrays of wettable regions, where droplets of aqueous solutions can be dispensed with different volumes in spots with different shapes and sizes. Such solutions may be polymeric and were amenable to be freeze-dried on-chip [10,47], generating arrays of miniaturized porous scaffolds, widely used in the tissue engineering field. B. The chips with arrays of combinatorial biomaterials were implanted subcutaneously in a Wistar rat model [10]. After a determined time of implantation ("t", in the figure), the chip is retrieved from the animal and the scaffolds on the chip are analyzed by immunocytochemistry. D. Immunocytochemistry and cell staining images are then collected by microscopy techniques and analyzed, preferentially by automated processes using softwares as ImageJ (NIH, USA). E. Results must be analyzed for statistical significance and with factorial analysis, so main and combined effects of biomaterials design and processing can be associated to occurring biological phenomena.

Such results were validated using chips in which biomaterials were randomly disposed. Hydrogels with conventional dimensions were also implanted individually as controls. The control over biomaterials degradation and respective debris' migration in long term studies may be one of the main challenges of this approach. Furthermore, while starting the study of new sets of biomaterials preliminary studies guaranteeing the independence of responses between array spots must be performed, as most biological phenomena involve paracrine signaling. Despite such concerns, this approach opens the possibility of making combinatorial high-throughput studies for tissue regeneration in the complex *in vivo* environment considering important phenomena as immunomodulation and *in vivo* clearance conditions. Using larger animal models the number of spots and the sizes of the implanted chips may be increased.

Besides microarrays, new methods are gaining relevance with the aim of scaling up HTS of biomaterials-cells interactions, in space-saving and high yield approaches. Confinement of single cells to small, picoliter-sized droplets within a continuous phase of oil provides chemical isolation of each cell, creating individual micro-reactors where undetectable cellular signals can be concentrated to measurable levels [11, 75-80].

3.5. HIGH-CONTENT DATA COLLECTION AND ANALYSIS

The development of platforms to produce diverse combinations of biomaterials in a high-throughput manner must be followed by the development of high-content methods for data collection to assess cells-biomaterials interactions/therapeutic effects. For single-cell encapsulation, data can be obtained by particle flow cytometry followed by sorting. However, systems based in arrays disposed two-dimensionally require the development of image acquisition methods compatible with the integrity of the chip. This avoids sample destruction, allowing the reuse of samples for further analysis [81]. Another important feature is the ability to monitor reactions and quantify, on-chip, the products of such reactions. For example, Neto *et al.* quantified the degree of crosslinking of chitosan hydrogels reacted with genipin by analysis of images acquired from a droplet-on-indentation system prepared using superhydrophobic chips [82].

Schonbrun *et al.* stated, in 2009, that there was a lack of optical integrated systems for rapid and accurate image acquisition in microarrays [83]. The existing methods were not capable of the large field-of-view and detection sensitivity required to collect fluorescence from parallel arrays of microfluidic devices. The authors presented a method for the parallel image detection from microarrays capable of reading 184 000 drops/second. A laser scanning cytometry approach was developed to be used as a bench-top microarray scanner to automatically acquire fluorescence of each single cell, improving the sensitivity by two orders of magnitude as compared to epifluorescence microscopy [84]. Computational microscopy tools were also developed, as they offer accessible optical imaging platforms, as compared to conventional microscopes, by replacing costly and complex optical hardware with image reconstruction algorithms. Lens-free on-chip imaging platforms form an important example of this research theme, by providing field-portability and compatibility with microfluidic devices by enabling wide field-of-view in lab-on-a-chip devices [85-87].

After acquisition, data must be analyzed in a totally automated manner. Algorithms must be developed to analyze the images acquired in the arrays both for single cell morphometric and proteomic parameters. Yu *et al.* reviewed the type of functional and morphometric parameters studied by image

analysis [88]. Unadkat *et al.* developed a model to correlate morphometric features in cells with underlying genetic expression [89]. Cell response obtained on-chip is usually correlated with materials properties using partial least square regressions [21, 23]. Moreover, multifactorial analysis has been used to identify important factors and combination thereof in biological systems [10, 37, 48]. Hook *et al.* proved that the collection of data regarding interactions between bacteria and polymeric libraries allowed predicting, *in silico*, polymers' effects on bacterial adhesion, up to second generation polymers [23]. More prediction models included using *in silico* models to predict protein adhesion to materials [90].

BOX 2

Optimization of reverse engineered results as a path to unravel Nature

Results in the area of biomaterials development, namely in the area of tissue regeneration, have shown to be affected by a wide range of factors that act not only individually but, very often, in a combined manner. Due to non-independent interactions between factors in distinct scales is not a straightforward task finding the most adequate conditions to promote tissue development in order to construct biologically relevant niches [2].

Two starting points can be taken when designing arrays of biomaterials: biomimetism or reverse engineering. The aim of biomimetism is to replicate native niches conditions. In biomimetic approaches a limited number of parameters are usually studied individually. Topography, mechanical properties or concentration of extracellular matrix proteins are examples of parameters previously attempted to be reproduced *in vitro*. However, it is difficult - if not impossible - to replicate the complexity of native tissues, as living tissues are organized in a high number of features, ranging from the pico- to the macro-scale, that interact in a complex manner.

Reverse engineering - where a wide range of close-to-native and outlier formulations are studied - may bring unexpected positive results for the tissue regeneration field. Besides being hard to predict, the challenge of discovering the most favorable condition for tissue development or integration often lies in disclosing optimization peaks. This process must consist of iterative studies of arrays. The most promising conditions must be then studied as sub-arrays, where the step between conditions is narrowed, until an ideal condition is found.

Furthermore, it is also a challenging task to know which factors must be studied individually, or where interactions between factors will be relevant. Studying the field in a reductionist approach – which usually happens *in vitro* - may induce errors when considering the whole biological system affecting the implanted material performance. Studying biomaterials science in a reverse engineering perspective would allow performing fine iterative processes of selection of materials where individual and combined effects would be carefully studied. After discovering the most promising combinations of materials/externally applied stimuli/soluble factors, the final test would consist of the *in vivo* implantation of the system (or several systems) using appropriate models, as a key to test its efficiency.

3.6. CONCLUDING REMARKS AND FUTURE PERSPECTIVES

For an effective development of biomaterials for tissue substitution or regeneration efforts must be made to study the highest number of possible combinations. Such effort may be developed using biomimetic strategies, where the 3D niches of the microarrays or other high-throughput analysis strategies aim to mimic the *in vivo* milieu, or reverse engineering strategies can be chosen to randomly generate biomaterials, eliminating uninteresting formulations in a step-by-step strategy (Box 2).

High-throughput analysis must be accompanied by a multiplexed analysis, resulting from a complete characterization of the whole system. Biomaterials must be characterized for their physicochemical characteristics [91], combination with drugs/soluble factors and respective release rate. Their interactions must be studied not only with the cells of the tissue but also with other factors possibly affecting cells, in efforts to mimic the *in vivo* circumstances. Evolution from static systems to bioreactors for cells mechanical stimulation in the biomaterials is needed using, for example, microfluidics to apply shear stress to the cells [92, 93]. Issues such as recruitment of inflammatory cells to the implant site as well as coagulation effects after injury must not be forgotten; they are early determinants of the success of biomaterials implantation and full functional performance; they are involved, for example, in angiogenesis and neural regeneration [74, 94].

The use of concepts such as patterning of hydrogels in three-dimensional manner [95, 96], as proposed for other applications, may be an elegant way to study biomaterials allowing or avoiding the crosstalk of soluble factors between distinct patterned biomaterials by varying the distance between each patterned spot and the density of the polymeric matrix separating each spot. The heterogeneity and compartmentalization observed in natural cellular microenvironments should also be addressed in the future by localizing, in each spot, different materials with controlled relative positioning, resembling Janus particles [97]. Furthermore we believe that devices compatible with the study of cell response to drugs released in a controlled/sequential manner are also one of the needs in the field of high-throughput devices. This would not only be important for the discovery of biomaterials for tissue regeneration strategies, but also in the optimization of drug formulations and complex release strategies [97, 98] for diseases studies [99].

3.7. ACKNOWLEDGEMENTS

Mariana B. Oliveira acknowledges the Fundação para a Ciência e a Tecnologia (FCT) for the PhD grant SFRH/BD/71396/2010. FEDER through the Competitive Factors Operation Program – COMPETE and by National funds through FCT in the scope of the project PTDC/CTM-BIO/1814/2012.

3.8. REFERENCES

[1] Simon CG, Lin-Gibson S. Combinatorial and High-Throughput Screening of Biomaterials. Adv Mater. 2011;23:369-87.

[2] Cranford SW, de Boer J, van Blitterswijk C, Buehler MJ. Materiomics: An -omics Approach to Biomaterials Research. Adv Mater. 2013;25:802-24.

[3] Schurgers E, Kelchtermans H, Mitera T, Geboes L, Matthys P. Discrepancy between the in vitro and in vivo effects of murine mesenchymal stem cells on T-cell proliferation and collagen-induced arthritis. Arthritis Research & Therapy. 2010;12:R31.

[4] Unadkat HV, Hulsman M, Cornelissen K, Papenburg BJ, Truckenmüller RK, Post GF, et al. An algorithm-based topographical biomaterials library to instruct cell fate. Proceedings of the National Academy of Sciences. 2011.

[5] Sala A, Hanseler P, Ranga A, Lutolf MP, Voros J, Ehrbar M, et al. Engineering 3D cell instructive microenvironments by rational assembly of artificial extracellular matrices and cell patterning. Integr Biol (Camb). 2011;3:1102-11.

[6] Gobaa S, Hoehnel S, Roccio M, Negro A, Kobel S, Lutolf MP. Artificial niche microarrays for probing single stem cell fate in high throughput. Nat Methods. 2011;8:949-55.

[7] Ueda E, Levkin PA. Emerging Applications of Superhydrophilic-Superhydrophobic Micropatterns. Adv Mater. 2013;25:1234-47.

[8] Geyer FL, Ueda E, Liebel U, Grau N, Levkin PA. Superhydrophobic-superhydrophilic micropatterning: towards genome-on-a-chip cell microarrays. Angew Chem Int Ed Engl. 2011;50:8424-7.

[9] Ueda E, Geyer FL, Nedashkivska V, Levkin PA. DropletMicroarray: facile formation of arrays of microdroplets and hydrogel micropads for cell screening applications. Lab Chip. 2012;12:5218-24.

[10] Oliveira M, Ribeiro M, Miguel S, Neto A, Coutinho P, Correia I, et al. In Vivo High-Content Evaluation of Three-Dimensional Scaffolds Biocompatibility. Tissue Engineering Part C - Methods. 2014;(in press) doi: 10.1089/ten.tec.2013.0738.

[11] Brouzes E, Medkova M, Savenelli N, Marran D, Twardowski M, Hutchison JB, et al. Droplet microfluidic technology for single-cell high-throughput screening. Proceedings of the National Academy of Sciences of the United States of America. 2009;106:14195-200.

[12] Schena M, Shalon D, Davis RW, Brown PO. Quantitative monitoring of gene expression patterns with a complementary DNA microarray. Science. 1995;270:467-70.

[13] Anderson DG, Levenberg S, Langer R. Nanoliter-scale synthesis of arrayed biomaterials and application to human embryonic stem cells. Nat Biotechnol. 2004;22:863-6.

[14] Santos E, Hernandez RM, Pedraz JL, Orive G. Novel advances in the design of three-dimensional bio-scaffolds to control cell fate: translation from 2D to 3D. Trends Biotechnol. 2012;30:331-41.

[15] Discher DE, Janmey P, Wang YL. Tissue cells feel and respond to the stiffness of their substrate. Science. 2005;310:1139-43.

[16] Kim KM, Choi YJ, Hwang JH, Kim AR, Cho HJ, Hwang ES, et al. Shear Stress Induced by an Interstitial Level of Slow Flow Increases the Osteogenic Differentiation of Mesenchymal Stem Cells through TAZ Activation. Plos One. 2014;9.

[17] Stewart MP, Helenius J, Toyoda Y, Ramanathan SP, Muller DJ, Hyman AA. Hydrostatic pressure and the actomyosin cortex drive mitotic cell rounding. Nature. 2011;469:226-30.

[18] Wei J, Han J, Zhao Y, Cui Y, Wang B, Xiao Z, et al. The importance of three-dimensional scaffold structure on stemness maintenance of mouse embryonic stem cells. Biomaterials. 2014;35:7724-33.

[19] Hull R, Chraska T, Liu Y, Longo D. Microcontact printing: new mastering and transfer techniques for high throughput, resolution and depth of focus. Mat Sci Eng C-Bio S. 2002;19:383-92.

[20] Khan F, Tare RS, Kanczler JM, Oreffo ROC, Bradley M. Strategies for cell manipulation and skeletal tissue engineering using high-throughput polymer blend formulation and microarray techniques. Biomaterials. 2010;31:2216-28.

[21] Mei Y, Gerecht S, Taylor M, Urquhart A, Bogatyrev SR, Cho SW, et al. Mapping the Interactions among Biomaterials, Adsorbed Proteins, and Human Embryonic Stem Cells. Adv Mater. 2009;21:2781-86.

[22] Tweedie CA, Anderson DG, Langer R, Van Vliet KJ. Combinatorial Material Mechanics: High-Throughput Polymer Synthesis and Nanomechanical Screening. Advanced Materials. 2005;17:2599-604.

[23] Hook AL, Chang CY, Yang J, Luckett J, Cockayne A, Atkinson S, et al. Combinatorial discovery of polymers resistant to bacterial attachment. Nat Biotechnol. 2012;30:868-75.

[24] Dolatshahi-Pirouz A, Nikkhah M, Gaharwar AK, Hashmi B, Guermani E, Aliabadi H, et al. A combinatorial cell-laden gel microarray for inducing osteogenic differentiation of human mesenchymal stem cells. Sci Rep-Uk. 2014;4.

[25] Akagi T, Fujiwara T, Akashi M. Inkjet Printing of Layer-by-Layer Assembled Poly(lactide) Stereocomplex with Encapsulated Proteins. Langmuir. 2014;30:1669-76.

[26] Moon S, Hasan SK, Song YS, Xu F, Keles HO, Manzur F, et al. Layer by Layer Three-Dimensional Tissue Epitaxy by Cell-Laden Hydrogel Droplets. Tissue Eng Part C-Me. 2010;16:157-66.

[27] Zhang R, Liberski A, Sanchez-Martin R, Bradley M. Microarrays of over 2000 hydrogels - Identification of substrates for cellular trapping and thermally triggered release. Biomaterials. 2009;30:6193-201.

[28] Suntivich R, Drachuk I, Calabrese R, Kaplan DL, Tsukruk VV. Inkjet printing of silk nest arrays for cell hosting. Biomacromolecules. 2014;15:1428-35.

[29] Cui X, Boland T, D'Lima DD, Lotz MK. Thermal inkjet printing in tissue engineering and regenerative medicine. Recent Pat Drug Deliv Formul. 2012;6:149-55.

[30] Guillemot F, Souquet A, Catros S, Guillotin B, Lopez J, Faucon M, et al. High-throughput laser printing of cells and biomaterials for tissue engineering. Acta Biomaterialia. 2010;6:2494-500.

[31] Ringeisen BR, Kim H, Barron JA, Krizman DB, Chrisey DB, Jackman S, et al. Laser printing of pluripotent embryonal carcinoma cells. Tissue Eng. 2004;10:483-91.

[32] Koch L, Kuhn S, Sorg H, Gruene M, Schlie S, Gaebel R, et al. Laser printing of skin cells and human stem cells. Tissue Eng Part C Methods. 2010;16:847-54.

[33] Okano K, Matsui A, Maezawa Y, Hee PY, Matsubara M, Yamamoto H, et al. In situ laser micropatterning of proteins for dynamically arranging living cells. Lab Chip. 2013;13:4078-86.

[34] Ankam S, Teo BKK, Kukumberg M, Yim EKF. High throughput screening to investigate the interaction of stem cells with their extracellular microenvironment. Organogenesis. 2013;9:128-42.

[35] Yuan B, Li Y, Wang D, Xie Y, Liu Y, Cui L, et al. A General Approach for Patterning Multiple Types of Cells Using Holey PDMS Membranes and Microfluidic Channels. Advanced Functional Materials. 2010;20:3715-20.

[36] Kang LF, Hancock MJ, Brigham MD, Khademhosseini A. Cell confinement in patterned nanoliter droplets in a microwell array by wiping. Journal of Biomedical Materials Research Part A. 2010;93A:547-57.

[37] Charnley M, Textor M, Khademhosseini A, Lutolf MP. Integration column: microwell arrays for mammalian cell culture. Integr Biol (Camb). 2009;1:625-34.

[38] Moraes C, Wang GH, Sun Y, Simmons CA. A microfabricated platform for high-throughput unconfined compression of micropatterned biomaterial arrays. Biomaterials. 2010;31:577-84.

[39] Yao X, Song YL, Jiang L. Applications of Bio-Inspired Special Wettable Surfaces. Adv Mater. 2011;23:719-34.

[40] Lima AC, Mano JF. Micro/nano structured superhydrophobic surfaces in the biomedical field. Part 2: applications overview. Nanomedicine http://dx.doi.org/10.2217/NNM.14.175.

[41] Neto AI, Custodio CA, Song WL, Mano JF. High-throughput evaluation of interactions between biomaterials, proteins and cells using patterned superhydrophobic substrates. Soft Matter. 2011;7:4147-51.

[42] Oliveira SM, Song WL, Alves NM, Mano JF. Chemical modification of bioinspired superhydrophobic polystyrene surfaces to control cell attachment/proliferation. Soft Matter. 2011;7:8932-41.

[43] Ballester-Beltran J, Rico P, Moratal D, Song WL, Mano JF, Salmeron-Sanchez M. Role of superhydrophobicity in the biological activity of fibronectin at the cell-material interface. Soft Matter. 2011;7:10803-11.

[44] Lourenco BN, Marchioli G, Song WL, Reis RL, van Blitterswijk CA, Karperien M, et al. Wettability Influences Cell Behavior on Superhydrophobic Surfaces with Different Topographies. Biointerphases. 2012;7.

[45] Salgado CL, Oliveira MB, Mano JF. Combinatorial cell-3D biomaterials cytocompatibility screening for tissue engineering using bioinspired superhydrophobic substrates. Integr Biol-Uk. 2012;4:318-27.

[46] Oliveira MB, Salgado CL, Song WL, Mano JF. Combinatorial On-Chip Study of Miniaturized 3D Porous Scaffolds Using a Patterned Superhydrophobic Platform. Small. 2013;9:768-78.

[47] Oliveira MB, Luz GM, Mano JF. A combinatorial study of nanocomposite hydrogels: on-chip mechanical/viscoelastic and pre-osteoblast interaction characterization. J Mater Chem B. 2014;2:5627-38.

[48] Lu CH, Chang YH, Lin SY, Li KC, Hu YC. Recent progresses in gene delivery-based bone tissue engineering. Biotechnol Adv. 2013;31:1695-706.

[49] Lima AC, Custodio CA, Alvarez-Lorenzo C, Mano JF. Biomimetic Methodology to Produce Polymeric Multilayered Particles for Biotechnological and Biomedical Applications. Small. 2013;9:2487-92.

[50] Oliveira MB, Mano JF. On-Chip Assessment of the Protein-Release Profile from 3D Hydrogel Arrays. Anal Chem. 2013;85:2391-6.

[51] Ranga A, Gobaa S, Okawa Y, Mosiewicz K, Negro A, Lutolf MP. 3D niche microarrays for systems-level analyses of cell fate. Nat Commun. 2014;5:4324.

[52] Chatterjee K, Lin-Gibson S, Wallace WE, Parekh SH, Lee YJ, Cicerone MT, et al. The effect of 3D hydrogel scaffold modulus on osteoblast differentiation and mineralization revealed by combinatorial screening. Biomaterials. 2010;31:5051-62.

[53] Zonca MR, Jr., Yune PS, Heldt CL, Belfort G, Xie Y. High-throughput screening of substrate chemistry for embryonic stem cell attachment, expansion, and maintaining pluripotency. Macromol Biosci. 2013;13:177-90.

[54] Yang J, Rose FRAJ, Gadegaard N, Alexander MR. A High-Throughput Assay of Cell-Surface Interactions using Topographical and Chemical Gradients. Adv Mater. 2009;21:300-4.

[55] He JK, Du YA, Guo YQ, Hancock MJ, Wang B, Shin H, et al. Microfluidic Synthesis of Composite Cross-Gradient Materials for Investigating Cell-Biomaterial Interactions. Biotechnol Bioeng. 2011;108:175-85.

[56] Hancock MJ, He JK, Mano JF, Khademhosseini A. Surface-Tension-Driven Gradient Generation in a Fluid Stripe for Bench-Top and Microwell Applications. Small. 2011;7:892-901.

[57] Allazetta S, Cosson S, Lutolf MP. Programmable microfluidic patterning of protein gradients on hydrogels. Chem Commun. 2011;47:191-3.

[58] Smith Callahan LA, Policastro GM, Bernard SL, Childers EP, Boettcher R, Becker ML. Influence of discrete and continuous culture conditions on human mesenchymal stem cell lineage choice in RGD concentration gradient hydrogels. Biomacromolecules. 2013;14:3047-54.

[59] Chatterjee K, Young MF, Simon CG. Fabricating Gradient Hydrogel Scaffolds for 3D Cell Culture. Comb Chem High T Scr. 2011;14:227-36.

[60] He J, Du Y, Villa-Uribe JL, Hwang C, Li D, Khademhosseini A. Rapid Generation of Biologically Relevant Hydrogels Containing Long-Range Chemical Gradients. Advanced Functional Materials. 2010;20:131-7.

[61] Selimovic S, Sim WY, Kirn SB, Jang YH, Lee WG, Khabiry M, et al. Generating Nonlinear Concentration Gradients in Microfluidic Devices for Cell Studies. Anal Chem. 2011;83:2020-8.

[62] Almodovar J, Guillot R, Monge C, Vollaire J, Selimovic S, Coll JL, et al. Spatial patterning of BMP-2 and BMP-7 on biopolymeric films and the guidance of muscle cell fate. Biomaterials. 2014;35:3975-85.

[63] Castleberry SA, Li W, Deng D, Mayner S, Hammond PT. Capillary Flow Layer-by-Layer: A Microfluidic Platform for the High-Throughput Assembly and Screening of Nanolayered Film Libraries. ACS Nano. 2014.

[64] Andreas K, Sittinger M, Ringe J. Toward in situ tissue engineering: chemokine-guided stem cell recruitment. Trends Biotechnol. 2014.

[65] Ino K, Okochi M, Konishi N, Nakatochi M, Imai R, Shikida M, et al. Cell culture arrays using magnetic force-based cell patterning for dynamic single cell analysis. Lab on a Chip. 2008;8:134-42.

[66] Chung SE, Kim J, Oh DY, Song Y, Lee SH, Min S, et al. One-step pipetting and assembly of encoded chemical-laden microparticles for high-throughput multiplexed bioassays. Nat Commun. 2014;5.

[67] Leferink AM, Hendrikson WJ, Rouwkema J, Karperien M, van Blitterswijk CA, Moroni L. Increased cell seeding efficiency in bioplotted three-dimensional PEOT/PBT scaffolds. J Tissue Eng Regen Med. 2013;9:1864:75.

[68] Sobral JM, Caridade SG, Sousa RA, Mano JF, Reis RL. Three-dimensional plotted scaffolds with controlled pore size gradients: Effect of scaffold geometry on mechanical performance and cell seeding efficiency. Acta Biomaterialia. 2011;7:1009-18.

[69] Zhao S, Zhao H, Zhang XY, Li YQ, Du YA. Off-the-shelf microsponge arrays for facile and efficient construction of miniaturized 3D cellular microenvironments for versatile cell-based assays. Lab on a Chip. 2013;13:2350-8.

[70] Bettinger CJ, Langer R, Borenstein JT. Engineering Substrate Topography at the Micro- and Nanoscale to Control Cell Function. Angew Chem Int Edit. 2009;48:5406-15.

[71] Nandakumar A, Truckenmuller R, Ahmed M, Damanik F, Santos DR, Auffermann N, et al. A Fast Process for Imprinting Micro and Nano Patterns on Electrospun Fiber Meshes at Physiological Temperatures. Small. 2013;9:3405-9.

[72] Levorson EJ, Santoro M, Kasper FK, Mikos AG. Direct and indirect co-culture of chondrocytes and mesenchymal stem cells for the generation of polymer/extracellular matrix hybrid constructs. Acta Biomaterialia. 2014;10:1824-35.

[73] Unadkat HV, Rewagad RR, Hulsman M, Hulshof GF, Truckenmuller RK, Stamatialis DF, et al. A modular versatile chip carrier for high-throughput screening of cell-biomaterial interactions. J R Soc Interface. 2013;10:20120753.

[74] Spiller KL, Anfang RR, Spiller KJ, Ng J, Nakazawa KR, Daulton JW, et al. The role of macrophage phenotype in vascularization of tissue engineering scaffolds. Biomaterials. 2014;35:4477-88.

[75] Lagus TP, Edd JF. A review of the theory, methods and recent applications of high-throughput single-cell droplet microfluidics. J Phys D Appl Phys. 2013;46.

[76] Mazutis L, Gilbert J, Ung WL, Weitz DA, Griffiths AD, Heyman JA. Single-cell analysis and sorting using droplet-based microfluidics. Nat Protoc. 2013;8:870-91.

[77] Dendukuri D, Pregibon DC, Collins J, Hatton TA, Doyle PS. Continuous-flow lithography for high-throughput microparticle synthesis. Nat Mater. 2006;5:365-9.

[78] Lutolf MP, Gilbert PM, Blau HM. Designing materials to direct stem-cell fate. Nature. 2009;462:433-41.

[79] Tumarkin E, Tzadu L, Csaszar E, Seo M, Zhang H, Lee A, et al. High-throughput combinatorial cell co-culture using microfluidics. Integr Biol. 2011;3:653-62.

[80] Velasco D, Tumarkin E, Kumacheva E. Microfluidic Encapsulation of Cells in Polymer Microgels. Small. 2012;8:1633-42.

[81] Gorocs Z, Ozcan A. On-chip biomedical imaging. IEEE Rev Biomed Eng. 2013;6:29-46.

[82] Neto AI, Correia CR, Custódio CA, Mano JF. Biomimetic Miniaturized Platform Able to Sustain Arrays of Liquid Droplets for High-Throughput Combinatorial Tests. Advanced Functional Materials. 2014;24:5096-103.

[83] Schonbrun E, Abate AR, Steinvurzel PE, Weitz DA, Crozier KB. High-throughput fluorescence detection using an integrated zone-plate array. Lab on a Chip. 2010;10:852-6.

[84] Zhou J, Wu Y, Lee SK, Fan R. High-content single-cell analysis on-chip using a laser microarray scanner. Lab on a Chip. 2012;12:5025-33.

[85] Su TW, Xue L, Ozcan A. High-throughput lensfree 3D tracking of human sperms reveals rare statistics of helical trajectories. Proceedings of the National Academy of Sciences of the United States of America. 2012;109:16018-22.

[86] Coskun AF, Sencan I, Su TW, Ozcan A. Lensfree Fluorescent On-Chip Imaging of Transgenic Caenorhabditis elegans Over an Ultra-Wide Field-of-View. Plos One. 2011;6.

[87] Wei QS, McLeod E, Qi HF, Wan Z, Sun R, Ozcan A. On-Chip Cytometry using Plasmonic Nanoparticle Enhanced Lensfree Holography. Sci Rep-Uk. 2013;3.

[88] Yu HY, Lim KP, Xiong SJ, Tan LP, Shim W. Functional Morphometric Analysis in Cellular Behaviors: Shape and Size Matter. Advanced Healthcare Materials. 2013;2:1188-97.

[89] Unadkat HV, Groen N, Doorn J, Fischer B, Barradas AMC, Hulsman M, et al. High content imaging in the screening of biomaterial-induced MSC behavior. Biomaterials. 2013;34:1498-505.

[90] Smith JR, Kholodovych V, Knight D, Kohn J, Welsh WJ. Predicting fibrinogen adsorption to polymeric surfaces in silico: a combined method approach. Polymer. 2005;46:4296-306.

[91] Hook AL, Anderson DG, Langer R, Williams P, Davies MC, Alexander MR. High throughput methods applied in biomaterial development and discovery. Biomaterials. 2010;31:187-98.

[92] Oliveira NM, Neto AI, Song WL, Mano JF. Two-Dimensional Open Microfluidic Devices by Tuning the Wettability on Patterned Superhydrophobic Polymeric Surface. Appl Phys Express. 2010;3:085205.

[93] Song WL, Oliveira MB, Sher P, Gil S, Noobrega JM, Mano JF. Bioinspired methodology for preparing magnetic responsive chitosan beads to be integrated in a tubular bioreactor for biomedical applications. Biomed Mater. 2013;8.

[94] Kyritsis N, Kizil C, Zocher S, Kroehne V, Kaslin J, Freudenreich D, et al. Acute inflammation initiates the regenerative response in the adult zebrafish brain. Science. 2012;338:1353-6.

[95] Ruder WC, Pratt ED, Bakhru S, Sitti M, Zappe S, Cheng CM, et al. Three-dimensional microfiber devices that mimic physiological environments to probe cell mechanics and signaling. Lab on a Chip. 2012;12:1775-9.

[96] Khetan S, Burdick JA. Patterning hydrogels in three dimensions towards controlling cellular interactions. Soft Matter. 2011;7:830-8.

[97] Walther A, Muller AHE. Janus Particles: Synthesis, Self-Assembly, Physical Properties, and Applications. Chem Rev. 2013;113:5194-261.

[98] Lima AC, Batista P, Valente TAM, Silva AS, Correia IJ, Mano JF. Novel Methodology Based on Biomimetic Superhydrophobic Substrates to Immobilize Cells and Proteins in Hydrogel Spheres for Applications in Bone Regeneration. Tissue Eng Pt A. 2013;19:1175-87.

[99] Oliveira MB, Neto AI, Correia CR, Rial-Hermida MI, Alvarez-Lorenzo C, Mano JF. Superhydrophobic chips for cell spheroids high-throughput generation and drug screening. ACS Appl Mater Interfaces. 2014;6:9488-95.

SECTION II. EXPERIMENTAL SECTION

CHAPTER 4. MATERIALS AND METHODS

This chapter aims at explaining in more detail and adding relevant information that is not present in the practical chapters (5 to 10) of this thesis regarding materials and methods used during the development of such works.

4.1. SUPERHYDROPHOBIC SURFACES

Polystyrene sheets (Goodfellow, UK; ref. ST311190) or flakes cut from tissue culture plates (Corning, USA) were treated by two methods in order to induce superhydrophobicity on its surface: phase inversion and treatment with a commercially-available superhydrophobic spray (WX2100™; Cytonix, USA). In Chapters 8 and 10 the use of thin polystyrene sheets allowed easily cutting the surfaces to the needed shape and size. Both surface modification techniques to induce superhydrophobicity on polystyrene platforms are described in the following sub-sections.

4.1.1. Phase inversion

To induce superhydrophobicity on polystyrene surfaces we followed the phase separation protocol described by Oliveira *et al.* [1]. Commercial grade polystyrene (injection molding grade, Styrolution 158 k, UL Ides, Portugal) was dissolved in anhydrous tetrahydrofuran (THF) containing 250 ppm butylated hydroxytoluene as inhibitor, ≥99.9% (Sigma, USA), in a concentration of 70 mg/mL for 24 hours under stirring at 300 rpm. After total dissolution of the polystyrene in THF, absolute ethanol (Panreac, Spain) was added to this solution in a proportion of 2 : 1.3 (polystyrene solution : absolute ethanol), and the mixture was shaken for 1 minute. The final mixture, with a transparent aspect, was poured onto the polystyrene surfaces in an amount of about 1 mL per 4 cm^2. The mixture was removed from the surface after phase transitions started to occur, i.e., as soon as the surface started showing an opaque aspect. Polymer precipitation was then forced with the immersion of the coated surface in a non-solvent for the polymer (absolute ethanol). The treated surfaces were then dried under a gentle flow of nitrogen. The wettability of the surfaces was measured on an OCA 15+ goniometer (DataPhysics) at room temperature, where the static contact angle was measured by a sessile drop method with a 6 µL water droplet.

The polystyrene precipitation on the surface leads to formation of a rough surface explained by the following mechanism: the mixture of a solvent and a non-solvent of polystyrene forms both poor and rich polymeric phases. In the poor phase, polymer nuclei are formed by precipitation. The rich phase aggregates around these nuclei in order to decrease surface tension. During polymer precipitation within the rich polystyrene phase, a continuous deposition of spheres on the surface takes place [1].

This surface treatment was applied in polystyrene flakes cut from Petri dishes for Chapters 5, 6, 7, 9 and 10. In Chapter 8, for implantation in Wistar rats, we used thin polystyrene sheets (h=0.19 mm, according to the manufacturer), as they were more flexible. It is important to notice that, for implantation, the fact that superhydrophobic surfaces made from polystyrene sheets are amenable to be cut, allowed the vertexes of the surfaces to be smoothed, avoiding inflammatory response on such sites due to harsh physical damage to the animals' muscles.

4.1.2. Use of commercially available spray

WX2100™ (Cytonix, USA) is an air-cured fluoro-urethane alkyd, as reported by the manufacturer. It was previously used for cell culture and did not show cytotoxic effect on animal cells [2]. We used the spray as recommended by the supplier. A thin coating was sprayed onto the polystyrene flaks or sheets from a distance of about 15 cm, for a period of 2 seconds/4 cm^2. The surface was then let to dry in a chemical hood for 24 hours.

4.2. METHODS FOR PATTERNING SUPERHYDROPHOBIC SURFACES WITH WETTABLE REGIONS

4.2.1. First generation of superhydrophobic patterned chips: treatment of regions with UV/Ozone using a photo-mask

The first method to pattern the superhydrophobic surfaces with wettable spots was described by Neto *et al.* [3]. It consisted of the exposure of selected regions of the superhydrophobic polystyrene surfaces to UV/ozone (UVO) irradiation through the holes of a UV-opaque polycarbonate mask. Using such treatment, it was previously shown that the wettability of the rough surfaces was amenable to be controlled in the entire superhydrophobic to superhydrophilic range. Figure 4.1, adapted from [1], shows the variation of the water contact angles of polystyrene according to the time exposed to UVO irradiation. After 20 minutes of exposure to UVO irradiation, the surfaces were totally hydrophilic, with a water contact angle close to 0°.

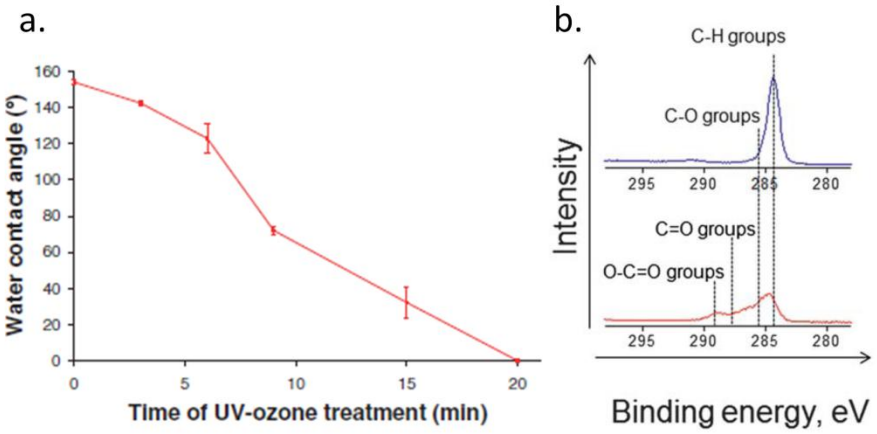

Figure 4.1. – a) Water contact angle evolution of superhydrophobic polystyrene surfaces while exposed for different periods to UVO irradiation. b) XPS spectra from superhydrophobic polystyrene surfaces before (blue line) and after (red line) exposure to UVO irradiation for 12 minutes. Figures adapted from [1].

X-Ray photoelectron spectroscopy (XPS) measurements, shown in Figure 4.1b (adapted from [3]), permitted assessing the changes in the chemical features on superhydrophobic surface upon UVO irradiation. The spectrum obtained from the untreated superhydrophobic substrate was divided into two peaks corresponding to C–H and C–O groups, centered at 285.01 and 286.30 eV, respectively. The first component clearly dominates the C1s peak, being consistent with the molecular structure of polystyrene. Upon 12 minutes of UVO irradiation, two other contributions were detected in the C1s peak, at 287.90 and 289.26 eV that attributed to C=O and O–C=O groups, respectively. The peak area corresponding to the C–H groups was substantially reduced with the effect of the UVO irradiation. The results are consistent with the photochemical modification of the $-CH_3$ groups on the superhydrophobic surface into CHO, COOH and OH groups. Neto *et al.* [3] also showed that the topography of the rough surface did not change substantially with UVO irradiation. The authors concluded that the lowering water contact angle after exposition to UVO irradiation would be the result of the increasing hydrophilicity of the material due to the introduction of oxygen-containing groups. This method for patterning of wettable regions was used in Chapters 5 and 6. A representative scheme of the steps used to obtain such surfaces can be seen on Figure 4.2.

4.2.2. Second generation of superhydrophobic patterned chips: Protection of wettable regions with stickers

Exposure to UVO irradiation allowed the fast and simple patterning of hydrophilic regions with tailored wettability in superhydrophobic polystyrene surfaces. Such patterns were compatible with fluorescence

microscopy analysis of cells attached to such regions or encapsulated/seeded in biomaterials [4, 5]. However, such method lacked transparency of the wettable spots (compatible with transmitted light microscopy). Moreover, UVO patterning were not totally permanent, as with such treatment the recovery of low water contact angles to more hydrophobic angles has been reported [6]. This limited the storage of the samples to few days.

We developed a new method that allowed patterning transparent and permanent wettable regions in the superhydrophobic surfaces. This technique was applied in Chapters 7 to 10. The fact that the stickers allow having transparent spots after their removal improved the compatibility of the superhydrophobic patterned chips with inverted transmitted light microscopy, as observed in Chapter 10. In such applications, stickers of polyvinyl chloride (PVC) (Oracal 614) were cut from an A4 sheet in a typography service using a computer numerical control laser cutting machine in the shape of the wettable spot. In Chapter 9, they had a ring shape with 5 mm of outer diameter and 2 mm of inner diameter, and were separated by 2 mm. In Chapters 7, 9 and 10, they had the shape of squares, with areas varying from 1x1 mm^2 to 3x3 mm^2, and were separated by 2 mm.

A representative scheme of the steps used to obtain superhydrophobic patterned surfaces can be seen in Figure 4.2.

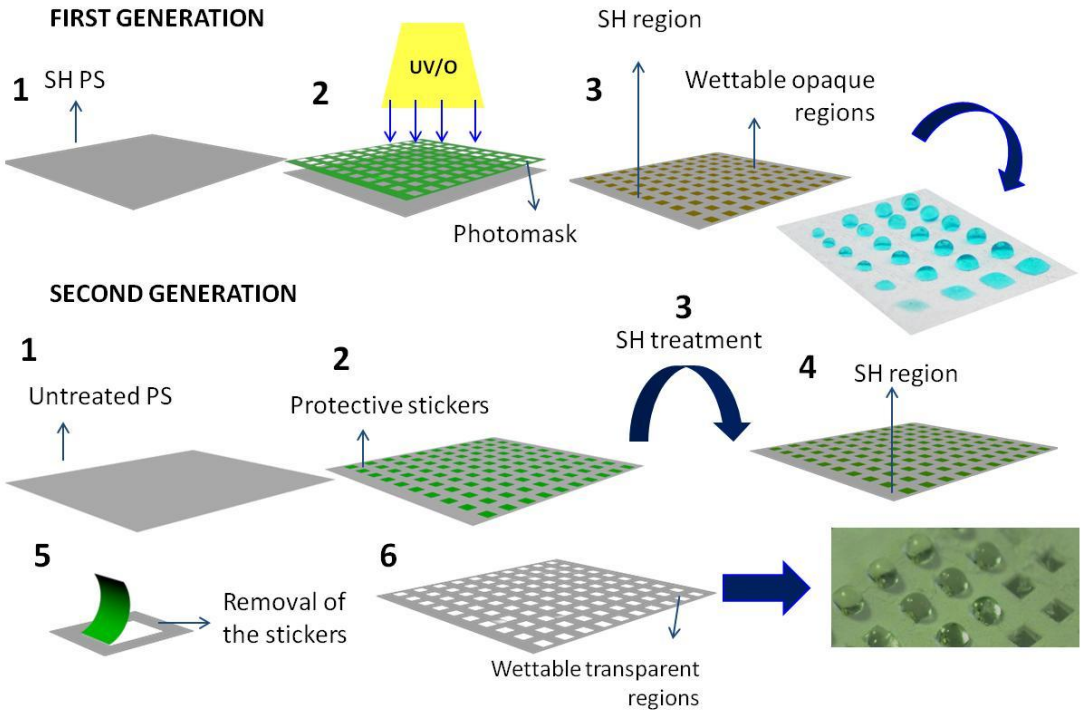

Figure 4.2. – Schematic representation of the production of wettable patterns on polystyrene (PS) superhydrophobic surfaces. The "First generation" refers to the exposure to UVO irradiation through a photomask. The "second generation" method refers to the protection of untreated polystyrene with stickers before treating the polymer with phase-separation technique.

4.3. BIOMATERIALS USED TO PRODUCE HYDROGELS AND SCAFFOLDS ON-CHIP AND RESPECTIVE PROCESSING METHODS

4.3.1. Chitosan

Chitosan is a biodegradable material whose characteristics and several applications in the biomaterials field can be found in more detail in section 2.2.1.1 of Chapter 1.

In Chapter 5, we used water soluble chitosan (with the commercial name PROTASAN UP CL 213) as received from the supplier (Novamatrix, Norway). PROTASAN UP CL 213 is based on a chitosan with 75-90% of deacetylation. It is in the form of a cationic polymer with a highly purified and well-characterized water-soluble chloride salt. Typically, the molecular weight for PROTASAN UP CL 213 is in the range of 150-400 kDa.

In Chapters 6 to 8, we used low molecular weight (LMW) chitosan (Sigma, USA; ref. 448869). According to the manufacturer, such chitosan has a degree of deacetylation ranging from 75 to 85%, and a molecular weight in the range of 50 to 190 kDa. In Chapter 6 we also used medium molecular weight (MMW) chitosan (Sigma, ref. 448877). According to the manufacturer, it has a degree of deacetylation ranging from 75 to 85%, and a molecular weight in the range of 190 to 310 kDa.

Both LMW and MMW chitosans used in Chapters 6 to 8 were purified by a re-precipitation method. A total amount of 10 g of each type of chitosan were purified separately. The batches used during the execution of all works were kept constant, in order to avoid batch-to-batch variability. The polymers were dissolved in an aqueous solution (1% w/v) with acetic acid (1% v/v; Panreac, Spain). Figure 4.3 depicts the deprotonation of chitosan occurring in the presence of acidic solutions, below its pKa: 6.3 [7]. The solution was filtered using Whatman® ashless filters, with a cutoff of 20-25 µm, so the insoluble materials remained in the filter. The filtered chitosan solution was then precipitated by adding 2M NaOH droplets under stirring conditions, until its pH reached a value of 8. The white gel that was formed after precipitation was sieved in order to remove excess of liquids and then washed with distilled water, until no changes in the pH of the washing water were detected. The chitosan gel was then washed with absolute ethanol, freeze-dried and stored in a glass container.

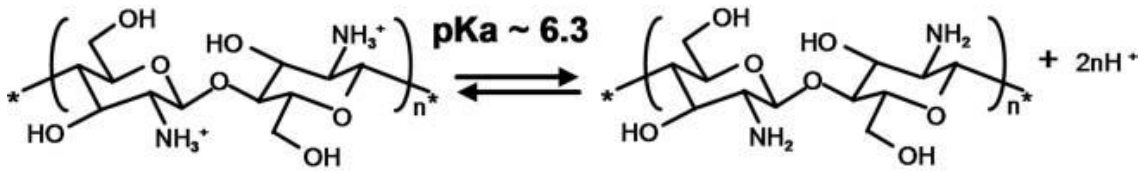

Figure 4.3. – Schematic representation of the deprotonation of chitosan molecules in acid media. Figure adapted from [7].

In Chapter 5, PROTASAN UP CL 213 chitosan was dissolved in distilled water at 1% (w/v). In order to form hydrogels in the wettable spots of the chips, it was mixed on-chip with alginate at 1% (w/v) – containing $5x10^4$ cells/spot - in proportions of 60%, 40%, 30% and 10% relatively to the alginate concentration in each polymeric mixture. The mixture of polymers, in a total of 4 µL, was then re-suspended and later crosslinked with 1 µL of 0.5 M $CaCl_2$ (Sigma, USA) in 4-(2-hydroxyethyl)-1-piperazineethanesulfonic acid (HEPES, 0.1 M, Sigma, USA), forming semi-interpenetrated networks. The solution was sterilized for 15 minutes in an autoclave cycle at 121°C, 1 atm.

In Chapter 6, both LMW and MMW chitosan were dissolved in 0.33M of acetic acid (Panreac, Spain) in concentrations of 1%, 1.5% and 2% (w/v). Such solutions were then mixed with 1% (w/v) alginate sodium salt solutions dissolved in 1M NaOH (Sigma, USA) on-chip in total volumes of 4 µL, and in proportions of alginate:chitosan of 0:100, 25:75 and 50:50. Both solutions were mixed, freeze-dried at -80°C and 0.003 bar and then rinsed thoroughly with distilled water. The chips with patterned biomaterials and the controls were sterilized with ethanol (70% v/v in water) for 2 hours, and then rinsed thoroughly with sterile distilled water.

In Chapter 7, LMW chitosan solutions were prepared in acetic acid (2% v/v) in concentrations of 2% (w/v), 3% (w/v) and 4% (w/v). Such solutions were then mixed in a combinatorial manner with bioactive glass nanoparticles and crosslinked with genipin. The experimental design to prepare such array of hydrogels can be found in Chapter 7, Figure 7.2. Briefly, parts of chitosan solutions were mixed with bioactin nanoparticles in amounts of 0%, 6.25%, 12.5%, 25% and 50% relatively to chitosan total mass in the solution. A volume of 4 µl of each solution was dropped in each hydrophilic well of the chips. Amounts of 2 µl of genipin in concentrations of either 2.5% or 12.5% (w/w of chitosan) (in a 10 ethanol/90 water mixture), relatively to the total mass of Chi in the well, were dropped on the top of each droplet of Chi/BG-NP. The crosslinking reaction occurred during 4 hours at 37°C in a humidity saturated environment. The chips were then immersed in ethanol in order to clean the genipin residues,

and afterwards in PBS at 37°C for 1 hour. More information about such nanoparticles and bioactive glasses can be found in the sub-section 4.8.

In Chapter 8, LMW chitosan solutions were dispensed in the wettable spots of the chips, in total volumes of 4 μL. Such solutions were then crosslinked on-chip, at 37°C in a water-saturated environment for 4 hours, using genipin (more detailed information about genipin properties and crosslinking mechanism can be found section 3.9). The hydrogels were then freeze-dried and a layer of ionic gelling polymers was deposited on the top of such materials. Such ionic gelling polymers were alginate, kappa (k)-carrageenan and iota (ι)-carrageenan. Such materials are described in more detail on sections 3.2, 3.6 and 3.7, respectively. More information on the processing of such biomaterials can be found in the subsection referring to these polymers, as well as in "Materials and Methods" section of Chapter 8.

4.3.2. Alginate

Alginate is a natural polysaccharide extracted from brown seaweed [8, 9]. More information on alginate properties and applications as a biomaterial can be found in Chapter 1, in section 2.2.1.1. In Chapters 5, 8 and 9, alginate was processed as an ionic hydrogel, crosslinked with calcium chloride, as indicated in the respective Chapters' "Materials and Methods" sections.

Although ionic hydrogels of alginate have been widely used, the initial binding of calcium ions by the polysaccharide chains still remains only partially explored [10]. The ability of alginate to form networks in the presence of divalent cations, namely calcium, is attributed to chelation of calcium between G units from different alginate chains via the so-called egg-box model [10-12] (represented in Figure 4.4a), adapted from [13]). The length of the G blocks is the main structural feature contributing to gel formation and gel strength.

The egg-box model for calcium–alginate was confirmed by results on X-ray scattering on G-blocks treated with excess of calcium. However, its existence in the initial step of the ion binding process has been recently questioned. Donati *et al.* [14] challenged the egg-box configuration and, in view of additional experimental data, suggested a new explanation for the initial binding of calcium by alginate chains involving a multicomplex formation. More specifically, calcium ions were explicitly considered as linkers holding two chains together by a short range attraction. This scenario comprises calcium ion-induced contact points which differ from the "classical" arrangement of the egg-box (although they are formed by four G residues) mostly because they lack physical contiguity along the chain. The authors described such conformation as tilted egg-box, schematically represented in Figure 4.4b.

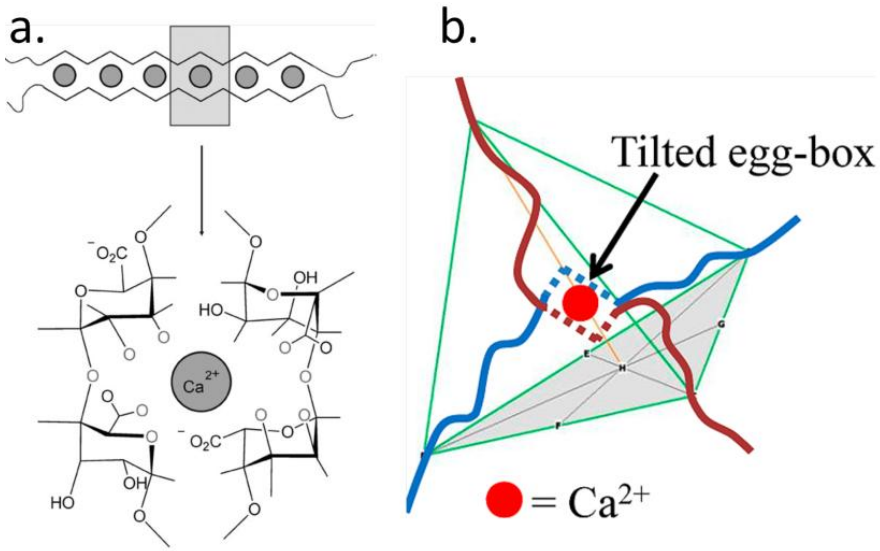

Figure 4.4. – a) Schematic representation of the egg-box model for calcium-alginate binding. Figure adapted from [13]. b) Graphical Representation of the Initial Binding of Calcium (Red Circle) by Facing GG Dimers (Dotted Bars) in the Initial Tilted Conformation, adapted from [14].

4.3.3. Hyaluronic acid

Information on hyaluronic acid structure, characteristics and applications as biomaterial can be found in Chapter 1, section 2.2.1.4. Hyaluronic acid from microbial origin (Sigma, USA; ref. 53747) was used in Chapter 5, dissolved in ultrapure water in a concentration of 1% (w/v). It was sterilized by filtering and mixed with alginate at a concentration of 1% (w/v) in PBS at different ratios, as indicated in the "Materials and Methods" section of Chapter 5. The cell-containing hydrogels were then crosslinked with $CaCl_2$ at 0.1 M, in order to form polymeric interpenetrated networks.

4.3.4. Collagen

Information on collagen structure, characteristics and applications as biomaterial can be found in Chapter 1, section 2.2.2.2. Collagen type I (Fluka, Switzerland; ref. C3867) was used in a concentration of 1% (w/v) in PBS for semi-interpenetrated alginate-based networks. The original solution provided by the manufacturer is prepared from rat tail tendons. It was sterilized by filtering. The procedure is described in more detail in the section "Materials and Methods" of Chapter 5.

4.3.5. Gelatin

Gelatin Type B (Sigma, USA; ref. C9391) was used on Chapter 5 as a ternary component to the also studied binary semi-interpenetrating networks of alginate and chitosan/collagen/hyaluronic acid. Gelatin

is produced by the partial hydrolysis of native collagen. In contrast to spherical globular proteins, collagen is composed of linear, fiber-like structures. In converting collagen to gelatin, the effects of acid or alkali as well as thermal energy create different types of collagen fragments. Two different types of gelatin can be produced depending on the method in which collagen is pretreated, prior to the extraction process. The alkaline process (giving rise to gelatin type B) targets the amide groups of asparagine and glutamine, and hydrolyses them into carboxyl groups, thus converting many of these residues to aspartate and glutamate. In contrast, acidic pre-treatment (giving rise to gelatin type A) does little to affect the amide groups present. [15]. According to the manufacturer, gelatin was extracted from bovine skin. Type B gelatin is derived from lime-cured tissue. It was sterilized for 15 minutes in an autoclave cycle at 121°C and 1 atm. The solution, prepared at 0.2% (w/v) in PBS at 40°C, was used as 50% of the volume of the other polymer added to alginate. The cell-containing hydrogels were then crosslinked with $CaCl_2$ at 0.1 M, in order to form polymeric interpenetrated networks.

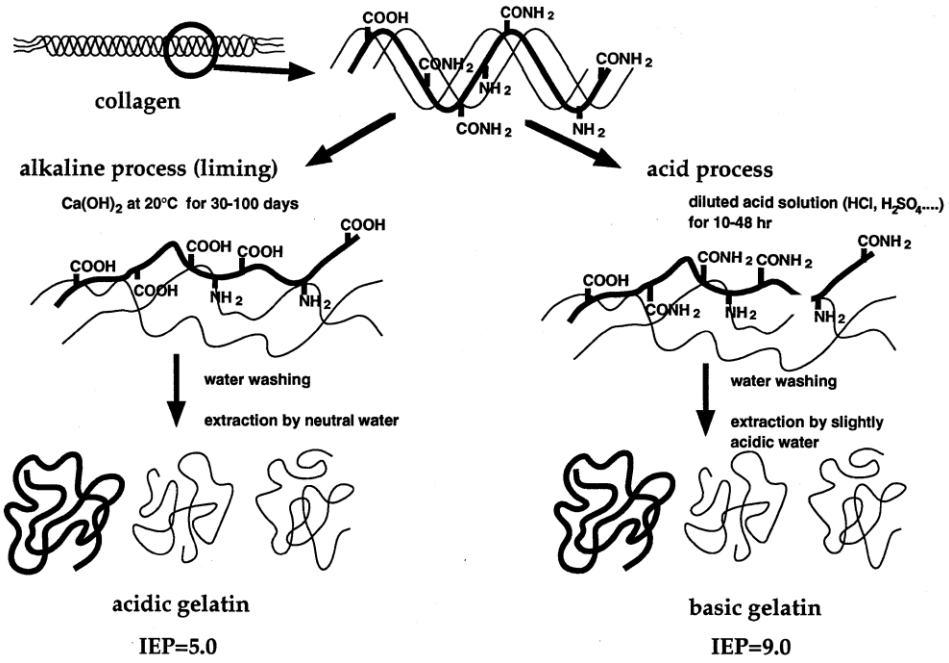

Figure 4.5 – Schematic representation of the fragmentation of collagen after hydrolysis into gelatin with respective acidic and alkali preparation processes. Adapted from [15].

4.3.6. Carrageenans

Carrageenans are water-soluble sulfated polysaccharides widely utilized in food, pharmaceutical and cosmetic industries as they can form hydrogels at body temperature in the presence of gel-promoting salts [16]. Carrageenans exists in three different forms according to the number of sulphate groups per disaccharide unit: κappa (κ) has one sulphate group, while ιota (ι) and lambda (λ) correspond with the

presence of two and three sulphate groups, respectively [16, 17]. The mechanisms for k-carrageenan gelation are, so far, the mostly well studied [16-18]. The temperature-induced gelling of k-carrageenan is reported to form the random coil conformation when the polysaccharide is in solution at a concentration below critical concentration and at a temperature above melting point. A decrease in temperature below gelling temperature leads to the formation of a helical dimer [18]. Ionically, the sulphate of anhydrous galactose of κ-carrageenan interacts with K^+ through ionic bonds [18].

According to the results obtained by Popa *et al.* [19], upon cooling and after addition of a salt, a wide variety of k- and ι-carrageenan gels can be efficiently produced due to development of double helices of polymeric chains into the building blocks of a three-dimensional network. Differences between the 2 types of carrageenans were found in terms of gelation: κ-carrageenan leading to stiff, brittle gels (crosslinked with potassium salts) and the ι-carrageenan leading to elastic gels (crosslinked with calcium salts) [19, 20].

Both ι- and k-carrageenans used in this thesis were purchased from Sigma (ref. 22048 and ref. 22045, respectively) and used without further purification. The molecular weight of commercial polymer ranges from 400 - 700 kDa. In Chapter 8, k- and ι-carrageenans were used in the form of ionic hydrogels, using $CaCl_2$ (JMGS, Portugal) 1M as a crosslinker for ι-Carr and KCl (VWR) 1M as a crosslinker for k-Carr, added in a proportion of 2 μL : 2 μL (polymer solution : crosslinker solution). The polymers were at concentrations of 2%, 1.5% and 1% (w/v of water). The reaction was left to occur at room temperature (ca. 25°C) for 1 hour.

4.3.7. Fibronectin

Fibronectin is a high-molecular weight (~440kDa) protein of the extracellular matrix that binds to membrane-spanning receptor proteins: integrins [21, 22]. Fibronectin mediates a wide variety of cellular interactions with the extracellular matrix and plays important roles in cell adhesion, migration, growth and differentiation [21, 23, 24]. It can be a ligand for a dozen members of the integrin receptor family [22], including the classic fibronectin receptor αvβ3. Extensive analyses have narrowed down the regions involved in cell adhesion along the lengthy fibronectin molecule to several minimal integrin-recognition sequences. The best known of these – RGD – is located in fibronectin repeat III10.

We used human plasma fibronectin (Sigma, USA; ref. C0895) in Chapter 6. Water-based solutions of such protein were adsorbed to porous chitosan and chitosan/alginate scaffolds for 30 minutes at 37°C, in concentrations of 10, 100 and 1000 μg/mL. Volumes of 0.5 μL were added to single miniaturized scaffolds on the chips. After adsorption, the samples were rinsed thoroughly with PBS, for three times.

More details on the preparation of such samples can be found in Chapter 6, in "Materials and Methods" section.

In order to monitor the effective adsorption of the fibronectin to the scaffolds and qualitatively monitor its relative amount in distinct types of scaffolds, we labeled fibronectin with AlexaFluor 594 (Sigma, USA), according to the protocol available from the supplier. The Alexa Fluor 594 reactive dye has a succinimidyl ester moiety that reacts efficiently with primary amines of proteins to form stable dye–protein conjugates. The qualitative monitoring of protein adsorbed to each type of scaffold was performed by quantifying the red fluorescence signal acquired in fluorescence microscopy images taken using same exposition time for all conditions. This was performed using ImageJ (NIH, USA) software. Distinct scaffolds formulations without adsorbed fibronectin (where PBS was used as a control sample) were used as control, i.e. their self-fluorescence was carefully taken in consideration during the analysis of the results.

4.3.8. Bioactive glass nanoparticles

The use of bioactive glass nanoparticles as a component of composite hydrogels and their preparation are detailed in the "Materials and Methods" section of Chapter 7. However, bioactive glass properties are not explored in detail in any chapter of this thesis. As such, its main properties and mechanisms of action are presented herein. More insights on applications as a biomaterial can be consulted in Chapter 7, in "Introduction" section.

A commonly used biodegradable glass was developed by Larry Hench, under the name of 45S5 Bioglass. It was based in the $Na_2O–CaO–SiO_2–P_2O_5$ system, high in calcium content and with a composition close to a ternary eutectic in the $Na_2O–CaO–SiO_2$ diagram [25]. The composition of Bioglass 45S5 - 46.1 mol.% SiO_2, 24.4 mol.% Na_2O, 26.9 mol.% CaO and 2.6 mol.% P_2O_5 - formed a bond with bone so strong that it could not be removed without breaking the bone [26]. After the invention of Bioglass 45S5 in the 1960s, the research field regarding bioactive glasses has seen great development. New types of bioactive glasses as well as processing methodologies to produce such materials were suggested [27].

Two processing methods can be used to produce glass: the traditional melt-quenching route and the sol–gel route. Bioglass 45S5 and other commercially available bioactive glasses are processed by melt-quenching, where oxides are melted together at high temperatures (above 1300°C) in a platinum crucible and quenched in a graphite mould (for rods or monoliths) or in water. The sol–gel route, used to produce the bioactive particles used in this thesis [28], forms and assembles nanoparticles of silica at

room temperature. It is a chemistry-based synthesis route where a solution containing the compositional precursors undergoes polymer-type reactions at room temperature to form a gel. The gel is a wet inorganic network of covalently bonded silica, which can then be dried and heated, e.g. to 600°C, to become a glass. The processing temperatures by the sol-gel route are lower than the ones used in melt-quenching, the final form of the glass products can be more easily tailored and the obtained products show a higher degree of purity [29].

The structure of bioactive glass is based on an amorphous network having SO_4^{4-} tetrahedrons as basic unit. Such tetrahedrons are usually linked by oxygen ions. The existence of non-bridging oxygen ions balanced by network modifiers (such as Na^+, K^+ or Ca^{2+}) prevents the crystalline arrangement of silica. The number of such network modifiers will determine the bioactivity of the glass, as they will dictate its instability when in contact with water. In order to be considered bioactive, the number of non-bridging ions/tetrahedron must be higher than 2.6, where 0 corresponds to a crystalline stable silica network/quartz glass, and 4 is attributed to dissolving SiO_4^{4-} [30]. A diagram with a representation of the formation of bioactive glass nanoparticles by sol-gel route is shown in Figure 4.6.

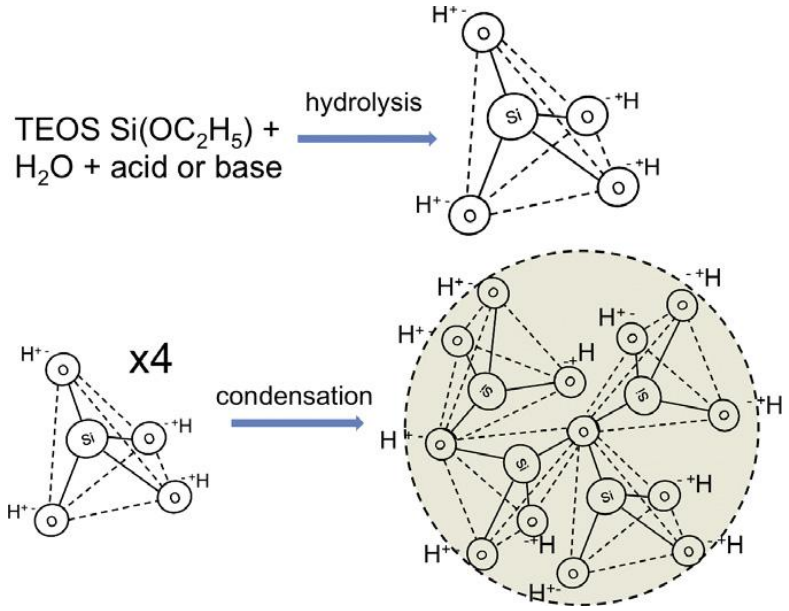

Figure 4.6. – Schematic representation of the reaction on the sol-gel process for the formation of silica tetrahedral and nanoparticles at room temperature. Adapted from [26].

The mechanisms of action of bioactive glasses are the hydroxyl-carbonate-apatite (HCA) layer formation and the ionic release to the medium. The HCA layer forms following solution-mediated dissolution of the glass with a mechanism very similar to conventional glass corrosion [31]. Accumulation of dissolution products causes both the chemical composition and the pH of the solution to change, providing surface sites and a pH conducive to HCA nucleation [32]. Once the HCA layer has formed, the next stages are

still less clear. Human osteoblasts cultured on bioactive glasses produce collagenous extracellular matrix that mineralizes to form bone nodules without the usual supplements present in the culture [33, 34], even when phosphate is not in the glass composition [35]. The culture of primary human osteoblasts with the ionic dissolution products of Bioglass 45S5 increased intracellular calcium levels [36] and upregulated the expression of seven families of genes within 48 hours [37].

4.3.9. Chemical crosslinker: genipin

Genipin was used to crosslink chitosan solutions on Chapters 7 and 8. Details on specific environmental conditions, crosslinker ratios and reaction periods can be found in Chapter 7 and Chapter 8, in the respective "Materials and Methods" sections.

Genipin is a natural chemical crosslinker. It is obtained from its parent compound, geniposide, via enzymatic hydrolysis with β-glucosidase. Geniposide is isolated from the fruits of *Genipa Americana* and *Gardenia jasminoides Ellis* [38]. It has been used in studies of tissue fixation to crosslink collagen and gelatin [39, 40] and in studies of drug delivery [41]. It proved to be much less toxic than glutaraldahyde [42]. The reaction occurring between chitosan molecules and genipin is depicted in Figure 4.7.

In Chapter 7, genipin was used as a crosslinker for LMW chitosan. It was used in proportions of 2.5% and 12.5% relatively to the mass of chitosan in the hydrogels. Those were prepared in acetic acid solutions of 2% (v/v) with concentrations of 2%, 3% or 4% (w/v).

In Chapter 8, genipin was used to crosslink MMW chitosan. A solution of crosslinker was prepared with 4% (w/v) genipin (Comercial Rafer, S.L.) in distilled water and ethanol (90:10 v/v). The chitosan scaffolds were prepared by pipetting 4 µl of Chi solutions and 2 µl of genipin in each wettable spot of the chip. Those consisted of MMW chitosan solutions of 1%, 1.5% and 2% (w/v), prepared in acetic acid (2% v/v).

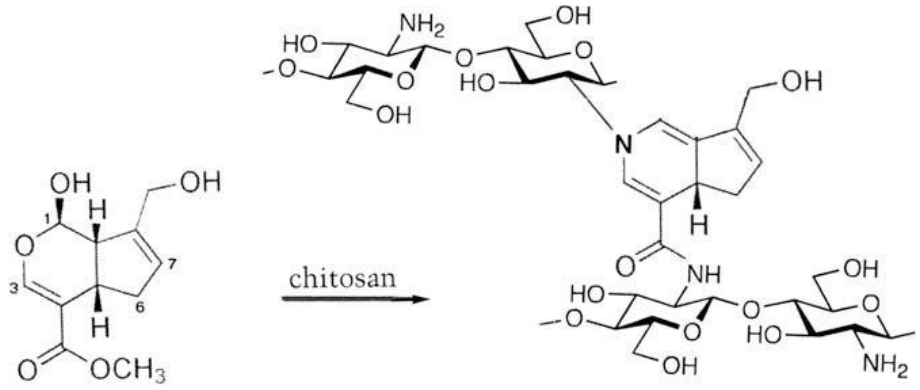

Figure 4.7. – Schematic of the crosslinking of chitosan with genipin. Adapted from [42].

4.3.10. Bioactive agents: doxorubicin

Doxorubicin is a drug used in cancer chemotherapy and derived by chemical synthesis from a bacterial species [43]. Its action occurs by interaction with DNA by intercalation and inhibition of macromolecular biosynthesis [44, 45]. This leads to the inhibition of enzyme topoisomerase II progression, which relaxes supercoils in DNA for transcription. Doxorubicin stabilizes the topoisomerase II complex after it has broken the DNA chain for replication, preventing the DNA double helix from being resealed. Thereby, it leads to the stopping of the process of replication.

We studied the effect of the addition of doxorubicin in different concentrations on the viability of two distinct cell types – L929 and SaOs-2 - cultured in the form of cellular spheroids. After 24 hours of cell culture for spheroid formation, a volume of 1 µl of doxorubicin solutions in water was added to each spot in the concentrations of 0, 0.1, 1, 10 µM (based on concentrations previously used) [46]. As live/dead images from fluorescence microscopy showed a high resistance from L929 cells to these drug concentrations, a new experiment was carried out with these cells with 0, 1, 10 and 100 µg/mL of Dox (also based on concentrations previously used) [47].

4.4. TECHNIQUES FOR PHYSICOCHEMICAL CHARACTERIZATION OF BIOMATERIALS

4.4.1. Fourier Transform Infrared Spectroscopy (FTIR)

The FTIR technique reveals information about the chemical structure of samples, as the absorption of infrared light is related to discrete energy transitions of the vibrational states of atomic and molecular units within a molecule. The fundamental requirement for infrared activity, leading to absorption of infrared radiation, is that there must be a net change in dipole moment during the vibration for the molecule or the functional group under study [48]. In transmission mode, FTIR spectra give information related to the bulk material. However, reflectance methods of measurement have gained importance. One of such methods, attenuated total reflectance (ATR), gives primarily information about the samples' surface. It is a nondestructive method, and requires only a minimum amount of sample. It is simple to handle, and its main limitation is that it provides a spectrum where the signal intensity across increases as a function of wavelength [49].

In Chapter 5, to assess the presence and distribution of the materials in each spot and to verify if the semi-IPN could maintain its integrity after 24 hours of immersion in a liquid medium, Fourier Transform Infrared (FTIR) analysis was performed for all samples. A whole chip was then placed in a Perkin-Elmer

Spectrum Spotlight 200 FTIR Microscope System and each spot was analyzed in reflectance mode. A whole chip with the polymeric mixtures—with no encapsulated cells—was immersed in PBS for 24 hours. The samples were then air-dried in order to minimize the absorption peaks of water. Spectra were collected in spot of the chip in continuous scan mode for sample areas of 100 x 100 μm^2, with a spectral resolution of 16 cm^{-1}, averaging 15 scans for each spectrum. Table 5.1 in Chapter 5 gathers the characteristic peaks and restriction bandwidths used to identify each polymer in the FTIR mapping analysis.

4.4.2. Microcomputed tomography (μCT)

μCT uses X-rays to generate cross-sections of an object that will be used to recreate a 3D model in a non-destructive way. Typical laboratory μCT scanners consist of a tungsten-anode X-ray tube with a relatively small focal spot (~10 μm), coupled to a high-resolution X-ray detector system (~50 μm pixel spacing) [50]. A small X-ray focal spot must be used with X-ray imaging systems that incorporate geometric magnification, to minimize penumbral blurring. X-ray projection views are acquired at hundreds of equally spaced angular positions around the object of interest. These views are then used to reconstruct a CT image, typically using a convolution back-projection approach [51, 52]. 3D images can be constructed either by combining contiguous single-slice images, each of which is acquired in a fan-beam configuration [52], or by using the cone-beam approach, that is favored in applications where imaging-time is important,

Scans of the scaffolds on-chip and of control samples in Chapter 6 were acquired and reconstructed using a high-resolution μCT. The X-ray source was set at 31 keV and 179 μA. Data sets were reconstructed using standardized cone-beam reconstruction software (NRecon v1.4.3, SkyScan). The output format for each sample was serial 1024 -1024 bitmap images. Representative data set of the slices was segmented into binary images with a dynamic threshold of 40–255 (grey values). The binary images were used for morphometric analysis (CT Analyser, v1.5 SkyScan) and to build the 3D models (ANT 3D creator, v2.4, SkyScan). For morphometric analysis the software was requested to calculate porosity and pore size. Three samples were tested for each condition. Due to dimension specificities, the controls produced in 96 well plates and the chips with 3 scaffolds from the same condition (MMW 1%Chi 100Chi:0Alg), with a total surface area of the chip: 3 mm x 1.2 cm^2, were acquired with a pixel size of 11.3 μm. The chips with 9 different scaffolds, with a total surface area of the chip: 1.2 x 1.2 cm^2, were acquired with a pixel size of 19.1 μm.

4.4.3. Dynamic Mechanical Analysis (DMA)

Mechanical and viscoelastic properties are important aspects to take in consideration while designing or selecting a biomaterial. This is especially relevant for implants that are required to withstand mechanical stresses in a clinical application. Moreover, native biological tissues show viscoelastic properties [53]. Such properties are conferred by tissue constituents such as cells, extracellular matrix and proteins. The correct function of the tissue is partially, but importantly, determined by such properties: tissues must be able to stand physiological load, while being capable of dissipating mechanical energy during cyclic solicitation. It was also shown that the mechanical properties of the biomaterials influence adhesion, proliferation and differentiation phenomena in cells [54, 55]. As such, it is important to design biomaterials whose mechanical and viscoelastic properties fit on those of the tissues that they will contact [56], in order to both promote tissue integration and stimulate adequate cellular response.

Among other mechanical, viscoelastic and calorimetric data, DMA permits to assess the frequency-dependent mechanical phenomena in materials, namely the evolution of complex modulus (E^*) with increasing frequencies. The storage modulus (E') corresponds to the real component of the complex modulus, and it is used as a reliable measure of samples stiffness, as represented in Equation 1.

$$E^* = E' + iE'' \quad (1)$$

The loss factor, $tan\,\delta$, gives the ratio between the amounts of mechanical energy lost (given by E'') and stored during a cycle, measuring the damping capability of the sample.

$$tan\,\delta = E''/E' \quad (2)$$

Previous studies showed that biomaterials with a high swelling capability in aqueous environments, such as chitosan, must have their mechanical/viscoelastic characterization performed in physiological-like environments [57, 58], once their mechanical behavior is significantly altered in such conditions. Therefore, in order to investigate the mechanical behavior in *in vivo*-mimicking conditions such type of characterization must be performed at physiological temperature (37°C), under immersion in saline solutions that mimic biological fluids pH (PBS).

The viscoelastic measurements of the scaffolds were performed using a TRITEC8000B DMA from Triton Technology (UK), equipped with the compressive mode. The biomaterials processed as cylindrical controls, both in Chapters 6 and 7, produced in commercially available 96 well plates were measured

using the standard protocol for the tests in compression mode. Regarding on-chip experiments, we used a steel cylindrical probe of 3.8 mm of diameter especially fabricated to perform non-destructive compression tests to the individual scaffolds. This component was inserted in the fixed upper plate of the DMA equipment and vertically aligned with the miniaturized biomaterials on the chips. The superhydrophobic platform containing the scaffolds was fixed in the down plate of the DMA equipment in a gutter previously assembled in this part of the apparatus, which allowed the platform to move two-dimensionally.

In Chapter 6, the technique involving miniaturized on-chip samples was optimized under dry conditions, at room temperature. DMA spectra were obtained during a frequency scan between 0.1 and 15 Hz. The experiments were performed under constant strain amplitude, corresponding to approximately 1% of the original height of the sample. In control samples produced in commercially available 96 well plates, the applied strain amplitude was of 50 μm, while in the on-chip samples the applied strain amplitude was of 10 μm. A small preload was applied to each sample to ensure that the entire scaffold surface was in contact with the compression plates before testing. At least three samples were used for each condition.

In Chapter 7, we adapted the technique to measure the mechanical and viscoelastic properties of miniaturized biomaterials to be used under physiological-like conditions (immersed in PBS, at 37°C). Control samples were prepared using chips with round hydrophilic spots with 8 mm width. The prepared solutions were dispensed in each well in individual volumes of 100 mL and processed in the same way of the miniaturized on-chip samples; the applied strain amplitude of the DMA equipment was of 30 μm. A small preload was applied to each sample to ensure that the entire scaffold surface was in contact with the compression plates before testing. At least three samples were used for each condition.

For on-chip hydrogels, the superhydrophobic platform containing the scaffolds was fixed in the down plate of the DMA equipment in a gutter previously assembled in this part of the apparatus. In each assay, the individual scaffolds were vertically aligned with the cylindrical steel probe. The DMA spectra were obtained during a frequency scan between 0.1 and 10 Hz. The experiments were performed under constant strain amplitude, corresponding to approximately 1% (~10 μm) of the original height of the sample. At least four samples were used for each condition.

4.4.4. Nanoindentation

The main components in a nanoindentation experiment are the material to be tested, the sensors/actuators used to apply and measure the mechanical load and indenter displacement, and the indenter tip. The latter component is conventionally made of diamond, formed into a sharp, symmetric

shape such as the three-sided Berkovich pyramid [59]. During a typical nanoindentation test, force and displacement are recorded as the indenter tip is pressed into the test material's surface with a prescribed loading and unloading profile. The response of interest is the load-displacement curve (often called the P-h curve).

In Chapter 7, nanoindentation tests were carried out at room temperature. The hydrogels on the chip were air-dried overnight. The samples were tested using a Micro Materials NanoTest equipment. A Berkovich diamond indenter was used, with a three-sided pyramid geometry with a cross-sectional area in terms of contact depth of $A(h_c)=24.5h_c^2$ was aligned with each scaffold on the chip and a loading rate of 0.01 mN/swas applied until a maximum load of 10 mN was reached. Three to five indentations were made in random locations on each side of the biomaterials.

4.5. ON-CHIP CELLULAR STUDIES

4.5.1. Cell expansion and culture conditions

In Chapters 5 to 7 and 10, we used cell lines as well known cellular models for preliminary studies. In Chapters 5, 6 and 10, we used L929 fibroblasts from murine origin (ATCC) and SaOs-2 osteoblast-like cells (ATCC), originated from a human osteosarcoma. Both cell types were expanded in basal medium consisting of Dubelcco's Modified Eagle Medium (DMEM) (Gibco, UK) supplemented with 10% heat-inactivated fetal bovine serum (BiochromAG, Germany) and 1% antibiotic/antimycotic solution (penicillin 100 units/mL and streptomycin 100 mg/mL; Gibco, UK). Cells were grown in 150 cm^2 tissue culture flasks and incubated at 37°C in a humidified air atmosphere of 5% CO_2. Every 3–4 days, fresh medium was added. At 90% of confluence, cells grown in tissue culture flasks were washed with PBS and subsequently detached by a chemical procedure with 0.05% trypsin-EDTA solution for 5 min at 37 °C in a humidified air atmosphere of 5% CO_2. To inactivate the trypsin effect, cell culture medium was added. The cells were then centrifuged at 300 g and 25 °C for 5 min and the medium was decanted. Cell suspensions with distinct densities were prepared.

In Chapter 7 we used the MC3T3-E1 cell line (ATCC), since it is widely used as a reliable pre-osteoblast model [60, 61]. Cells were expanded in basal medium consisting of alpha-MEM (Gibco, UK) supplemented with 10% heat-inactivated fetal bovine serum (BiochromAG, Germany) and 1% antibiotic/antimycotic solution (penicillin 100 units/mL and streptomycin 100 mg/mL; Gibco, UK). Cells were grown in 150 cm^2 tissue culture flasks and incubated at 37 °C in a humidified air atmosphere of 5% CO_2. Every 3–4 days, fresh medium was added. At 90% of confluence, cells grown in

tissue culture flasks were washed with PBS and subsequently detached by a chemical procedure with 0.05% trypsin-EDTA solution for 5 min at 37 °C in a humidified air atmosphere of 5% CO_2. To inactivate the trypsin effect, cell culture medium was added. The cells were then centrifuged at 300 g and 25 °C for 5 min and the medium was decanted.

4.5.2. Cell culture on biomaterials or as cell spheroids

Cell encapsulation in biomaterials

In Chapter 5 both L929 and MC3T3-E1 cells were encapsulated in hydrogels consisting of alginate combined with other polymers, under mild temperature (room temperature), pH and ionic concentration conditions (HEPES 0.1 M, crosslinking with 0.5 M $CaCl_2$). Both cell types were mixed with polymeric solutions, that were dispensed in wettable spots of the chips, in a concentration of $5x10^4$ cells/spot, where each spot contained 4 µL of material.

Cell seeding on previously prepared biomaterials

On Chapter 5 each scaffold on the chips was seeded with 0.5 µL of cell suspension. The first assays were performed with L929 cells, in a total amount of $9x10^4$ cells/spot. Another set of assays was performed by pipetting 0.5 µL of cell suspensions of L929 or SaOs-2 cell lines in each miniaturized scaffold, in order to seed $1.5x10^4$ cells/spot. The cells were left to adhere in the scaffolds for 4 hours, at 37°C and 5% CO_2. The whole chips were then placed in a 6-well plate with 5 mL of DMEM. All seeded samples and controls were incubated for 24 hours to further evaluate cells metabolic activity, viability and quantify the cell number on the different materials combinations.

On Chapter 7, a selective cell adhesion and proliferation cell study was performed by preparing a MC3T3-E1 cell suspension with a density of $1x10^6$ cells/mL. Prior to the contact with cell suspension, the chips with miniaturized hydrogels were sterilized with ethanol 70% (v/v) for 2 hours and rinsed with sterile PBS 3 times. The chips were seeded with 5 mL of cell suspension. Cells were left to adhere to distinct spots of the chips in a selective manner.

Fabrication of cell spheroids on-chip

In Chapter 10 superhydrophobic patterned chips were fixed to the lids of tissue culture plates using commercially available tape. The lower part of the plate was filled with sterile PBS, so the environment was saturated with water, in order to avoid the cell suspension droplets evaporation. A volume of 5 µl of cell suspensions of L929 or SaOs-2 cell lines of $4x10^6$ and $8x10^6$ cells/mL were dispensed by manual pipetting (method (1)) in each wettable spot of the chip. Each condition was processed in triplicate in

each chip. The spheroids were let to form during 24 hours, after turning the platforms 180°, by closing the tissue culture plate with the lid where the platform was fixed with tape.

For method (2) we used a L929 cell line cell suspension with a density of $1x10^7$ cells/mL. We dragged the cell suspension with a speed of approximately 1 wettable spot/second. To measure the average volume of cell suspension fixed in each wettable spot, we used a micropipette and removed the medium from each individual spot. The chips were turned 180°, as for Method (1), and the spheroids were let to form during 24 and 72 hours.

For method (3) L929 cell suspension was prepared with a density of $5x10^6$ cells/mL. The whole chip was dipped in the cell suspension during 5 seconds. After removing the chip, it was tilted so the remaining cell suspension was removed from the superhydrophobic part of the chip. A micropipette was used to measure the average volume of cell suspension fixed in each wettable spot. The chips were turned 180°, as in method (1), and the spheroids were let to form during 24 hours.

4.6. *IN VIVO* STUDIES: IMPLANTATION OF SUPERHYDROPHOBIC PATTERNED CHIPS IN WISTAR RATS

In Chapter 8, chips containing 36 spots with distinct combinations of biomaterials were cut in 4 parts (with 9 miniaturized scaffolds per part). Chips boarders were cut with rounded shape as close to the scaffolds as possible, and a mark was made on each chip, to identify the relative position of the biomaterials after explantation. The 4 chips were then implanted subcutaneously in the back of Wistar rats for 24 h and 7 days, one in each quadrant of the animal's back. All biomaterials faced the muscle side of the cut. A total of 27 Wistar rats (8– 10 weeks old), weighing between 150–200 g, were used. The project was conducted in accordance with the international guidelines set for animal research. The study was conducted in the animal research facility of the University of Beira Interior. Housing and animal care were provided according to procedures set for animal research. Animals were individually anesthetized with an intraperitoneal injection of ketamine (40 mg/kg) and xylazine (5 mg/kg). After the time point of results analysis, each animal was immobilized and the dorsum was shaved, washed, and disinfected with ethanol (96%).

To perform chip implantation, a 1.5- to 2-cm skin incision was done in four different sites of animal dorsum. The animals were divided in several groups (more details can be found in "Materials and Methods" section of Chapter 8):

- Group 1: animals whose 4 different implanted chips (with chitosan scaffolds in the different concentration: 1%, 1.5%, 2%, and 1.5 + %) were implanted ($n > 4$).

- Group 2: animals implanted with 4 chips with random configuration of the spotted biomaterials were implanted in rats (n = 3).
- Group 3: similar to the Group 1; however, the chip with the condition ''1.5 + %'' was substituted by a chip without any spotted biomaterials (empty chip) (n = 2).
- Group 4: Control group where one animal had two empty chips implanted, without any patterned biomaterial (n = 2).
- Group 5: Animals where one biomaterial plug (with a diameter of 5 mm) without superhydrophobic chip was implanted by animal (n = 2), to be explanted after 24 h and 7 days of implantation. For this condition, two biomaterials combinations present on-chip were implanted. More details on the composition of such biomaterials can be found in Chapter 8.

Subsequently to samples implantation, the skin flaps were sutured. During the study, animals were kept in separate cages and fed with commercial rat food and water ad libitum. Animals were sacrificed by CO_2 asphyxiation after 24 h and 7 days.

4.7. CELLULAR CHARACTERIZATION

In Chapters 5 to 8 and 10, analysis of cellular response was performed by image-based analysis. On Chapters 5 and 6 such image-based techniques were validated against biochemical standard assays performed on the same miniaturized biomaterials used for on-chip non-destructive and microscopy-based analysis. The biomaterials used for such validation tests were detached from the wettable spots of the chips and tested individually. For cell number analysis, the quantification of cell nuclei by image analysis was counterpoised with standard double-stranded DNA (dsDNA) analysis (directly proportional to the number of cells on the biomaterial samples). Cellular viability was compared with the results of metabolic activity (performed by the MTS test) normalized by the total amount of dsDNA, as it is also accepted as a fair approximation for cell viability determination. Details regarding biochemical assays and staining techniques can be found in the following sub-sections. The image-based methods used for cell quantification, identification and morphometric analysis are addressed in more detail on section sub-section 8.

4.7.1. Cell Metabolic Activity: MTS assay

The metabolic activity of cells in contact with extracts of the developed hydrogels was evaluated by the MTS assay (3-(4,5-dimethylthiazol-2-yl)-5(3-carboxymethoxyphenyl)-2(4-sulfofenyl)-2H-tetrazolium) (Cell Titer 96® Aqueous Solution Cell Proliferation Assay, Promega), in Chapters 5 and 6. MTS is bioreduced

by dehydrogenase enzymes, active in live cells, into a brown formazan product. The color intensity, measured at optical density (OD) 490 nm, is directly related to number of viable cells. The biomaterials removed from the chips were washed in PBS and incubated with MTS solution prepared in serum-free culture medium without phenol red, at 37°C for 3h. After incubation, 100 µL were transferred in triplicate into a 96-well plate for OD measurement at 490 nm. The absorbance of the resulting solution in each well was recorded using an automated Microplate Reader (Synergy™ HT, Bio-Tek Instruments).

4.7.2. Cell viability

LIVE/DEAD® Viability/Cytotoxicity Kit

The LIVE/DEAD® Viability/Cytotoxicity Kit (LifeTechnologies, USA) is a quick and easy two-color assay to determine viability of cells in a population based on plasma membrane integrity and esterase activity. Calcein AM is a cell-permeable and non-fluorescent compound. It is hydrolyzed in live cells, and the fluorescence intensity is proportional to the amount of live cells, as it becomes fluorescent after hydrolysis of AM group. Propidium iodide (PI) stains dead cells as it enters cells with damaged membrane.

Fluorescence labeling with calcein AM and PI was carried out in Chapter 5, to assess the viability of L929 and MC3T3-E1 cells encapsulated in semi-interpenetrated network hydrogels. For this assay, the chips were washed with PBS and placed in a well plate with 2 mL of PBS with 4 µL of a Calcein-AM and 2 µL of PI, and incubated for 30 minutes at 37°C in 5 % CO_2. In Chapter 6, dead cells were stained with PI, and cell death ratio was calculated by dividing such number by the total number of cells on the scaffolds (calculated as reported in section 7.4).

In Chapter 10, cell viability in cell spheroids was also calculated by image-based quantification of the ratio of live/dead cells on the spheroids. A volume of 2 µl of solution of PBS with 10% (v/v) of each reagent was added to the spheroids, after 3 µl of the culture medium (from a total volume of 5 µl) was removed from the spots. The samples were left to incubate at 37°C during 30 minutes, and then washed 3 times with 3 µl of PBS. After rinsing We observed each spot under a reflected/transmitted light microscope (Zeiss, Axiocam MRc5) – for Chapters 5 and 6 -, and in a laser confocal microscope – for Chapter 10.

4.7.3. Total cell number

Double-stranded DNA quantification

Quantitative double-stranded DNA (dsDNA) is a very accurate method to assess number of cells, since these two parameters are directly correlated. This method may be used to assess cell-seeding efficiency into biomaterials, as well as to determine cell proliferation. For Chapter 5 and 6, quantification was performed using the Quant-iT™ Pico-Green dsDNA Assay Kit (Invitrogen™, Molecular Probes™, Oregon, USA), according to the instructions of the manufacturer. Cells in each individual biomaterial were immersed in ultrapure water and frozen at -80°C after cell culture period. Before quantification, they were thawed and exposed to ultrasounds for 10 minutes. As such, cell membrane was lysed by osmotic and thermal shock. The supernatant was used for the dsDNA quantification assay. The fluorescence of the dye was measured at an excitation wavelength of 485/20 nm and at an emission wavelength of 528/20 nm, in a microplate reader (Synergie HT, Bio-Tek, USA). The dsDNA concentration for each sample was calculated using a standard curve (dsDNA concentration ranging from 0.0 to 1.5 mg/mL) relating quantity of dsDNA and fluorescence intensity.

Cell nuclei staining

Cells' nuclei were stained with 4',6-diamidino-2-phenylindole (DAPI, Sigma). DAPI is a fluorescent stain that binds strongly to A-T rich regions in DNA. When bound to dsDNA, DAPI has an absorption maximum at a wavelength of 358 nm and its emission maximum is at 461 nm (blue). In Chapters 5 to 8 and 10, the whole chips or control samples were immersed in a DAPI solution (diluted 1000x in PBS) for 15 to 30 minutes, and rinsed thoroughly 3 times with PBS, for 15 minutes prior to microscopy observation. Each spot on the chip was observed under a reflected/transmitted light microscope (Zeiss, Axiocam MRc5).

4.7.4. Cell morphology analysis

Scanning Electron Microscopy

In Chapter 7, we assessed cells morphology after 3 days of cell culture using a scanning electron microscope (SEM; NanoSEM - FEI Nova 200 (FEG/SEM); EDAX). The cells were fixed by immersion in paraformaldehyde for 2 hours and subsequent washing with PBS. SEM is a type of electron microscope that produces images of a sample by scanning it with a focused beam of electrons. The electrons interact with atoms in the sample, producing various signals that can be detected and that contain

information about the sample's surface topography and composition. When accelerated electrons enter a solid, they are scattered both elastically (by electrostatic interaction with atomic nuclei) and inelastically (by interaction with atomic electrons). Most of this interaction is "forward" scattering, which implies deflection angles of less than 90°. But a small fraction of the primaries are elastically backscattered ($\theta > 90°$) with only small fractional loss of energy. Due to their high kinetic energy, these backscattered electrons have a reasonable probability of leaving the specimen and re-entering the surrounding vacuum, in which case they can be collected as a backscattered-electron signal. Inelastic scattering involves relatively small scattering angles and so contributes little to the backscattered signal. However, it reduces the kinetic energy of the primary electrons until they are eventually brought to rest and absorbed into the solid; in a metal specimen they could become conduction electrons. The depth (below the surface) at which this occurs is called the penetration depth or the electron range [62]. SEM images were obtained from the low-energy secondary electrons emitted from each spot of the sample where the focused electron-beam impacts.

Before analysis, chips were gradually dehydrated using solutions with increasing amounts of ethanol (30%, 50%, 70% and 90%), where the chips were immersed for 10 minutes in each solution. Due to their non-conductive behavior, the whole chips were coated with a thin, electrically deposited gold palladium layer, to minimize charge accumulation using a sputter coater (JEOL JFC-1100).

F-actin staining

In Chapter 7, after fixation with paraformaldehyde, cells' F-actin filaments were stained with phalloidin-tetramethyl rhodamine isothiocyanate (Sigma, diluted 1000x). The chips were immersed in such solution for 1 hour at room temperature, and then thoroughly rinsed with PBS 3 times, during 15 minutes. Each spot on the chip was observed under a reflected/transmitted light microscope (Zeiss, Axiocam MRc5).

4.7.5. Cell type identification

Histology

Hematoxylin and eosin (H&E) staining was performed to observe general cell morphology and overall cell/matrix distribution in histological sections in Chapter 8. Hematoxylin is an alkaline dye that stains cell nuclei blue due to an affinity to nucleic acids. Eosin is an acidic dye that stains cells cytoplasm pink [63]. H&E staining was conducted in automatic staining equipment (Microm HMS 740). After hydration, sample sections were colored with Papanicolaou Harris hematoxylin (05-12011/L, Bio-optica) for 3

minutes, washed in running tap water. The sections were then stained in Eosin-Y (05-M10003, Bio-optica) for 30 seconds. Finally, slides were dehydrated through series of alcohol immersions from 30 to 100% (v/v) ethanol. The stained cells were visualized under a light microscope (Reflected/Transmitted light Microscope, Zeiss Germany) and images were taken by a digital camera (Axion MRc5, Zeiss).

For histological sections in Chapter 8, scoring was attributed to each part of the histological cuts (divided according to Figure 8.3C in Chapter 8). The following scoring scale for analysis was established, after identification of cells types in the H&E stained sections: 0—absence of inflammatory cells; 1—presence of lymphocytes and polymorphonuclear (PMN) cells; 2—higher presence of lymphocytes and PMN, and low amount of macrophages; 3—higher presence of lymphocytes; 4—high concentration of macrophages and presence of lymphocytes; 5—very high density of macrophages; 6—vascularization with very high concentration of macrophages. Images of on-chip macrophages were scored (0–6) according to the relative amount of macrophages in the scaffold, where 0 corresponded to the lowest relative amount and 6 to the highest relative amount.

Immunocytochemistry

After the explants of the 4 chips in each animal, the chips were fixed and kept in paraformaldehyde. The explanted chips were incubated with primary antibodies CD25 (AbD Serotec) (specific for IL-2 produced by lymphocytes) or CD163 (AbD Serotec) (specific for macrophages) in concentration of 1:100 overnight, at 4°C. Nonspecific binding was blocked by incubation with 3% bovine serum albumin (BSA) solution in PBS for 30 minutes, at room temperature. After 1 hour of incubation with AlexaFluor488 (Alfagene) for CD25, or AlexaFluor594 (Alfagene) for CD163, both at a concentration of 1:250, in BSA 1%, at room temperature, the cells were washed in PBS and counterstained with DAPI (Invitrogen) nuclear staining. The presence of surface markers was analyzed using an Axioplan Imager Z1 fluorescence microscope (Zeiss, Germany). Images were taken by a digital camera (Axion MR3, Zeiss, Germany). Images in a total height of 500 μm were acquired in 20 layers of 25 μm. The images used for the analysis were the ones corresponding to the final stacking of the 20 layers.

4.8. CELL IMAGE ANALYSIS

4.8.1. Cell viability and cell quantification

In Chapter 5, cells stained with Calcein AM or PI in each sample were quantified using 10 fluorescence microscopy images acquired with 200x magnification, using WCIF ImageJ software (NIH, USA). The same threshold criterions were used in all images.

In Chapter 6 and 7, cell quantification was performed by staining the cells nuclei with DAPI. In Chapter 6, cell mortality was evaluated using PI staining. In both cases, fluorescence microscopy images were used for image analyses on WCIF ImageJ software (NIH, USA), using 18 images of 200x200 pixel^2 per sample acquired with the same magnification (50x). The same threshold criterions were used in all images.

In Chapter 8, images acquired by microscopy (Axiovision, Zeiss) with a 50x magnification were cut in 4 equal images. Using ImageJ (NIH) software the background caused by the natural fluorescence of natural polymer in each image was removed or minimized. Automatic nuclei counter (ITCN, ImageJ, NIH) was used to quantify the lymphocytes. Images with the green staining were analyzed considering cells with 6 µm of diameter and a separation dependent on the density of cells, varying from 2 to 6 µm. A representative image of the steps performed for such image analysis can be found in Chapter's 8 "Supporting Information" section.

In Chapter 10, confocal microscopy images were used to determine cell viability. As such, the number of viable cells in each stack was calculated, even if the distribution of dead cells was not uniform in the spheroid. We used the particle analysis application of ImageJ software (NIH, USA) and analyzed the multiimages (multitiff) in the form of images stacks. The total number of cells in the analyzed spheroids was assumed to be the sum of cells counted in all stacks. Cell viability was determined as indicated in equation 4.3:

$$\boldsymbol{cell\ viability}\ (\%) = \frac{\sum \boldsymbol{live\ cells}}{\sum(\boldsymbol{live\ cells} + \boldsymbol{dead\ cells})} \mathbf{x\ 100}\% \quad (4.3)$$

4.8.2. Cellular area quantification

In Chapter 7, cell quantification was performed after washing the whole chips with PBS and fixing the cells with formalin, after 1 and 3 days of cell culture. Cells' nuclei were stained with DAPI and F-actin was stained with phalloidin-tetramethyl rhodamine isothiocyanate. Cell number was quantified through cell nuclei counting using particle analysis of ImageJ software (NIH, USA). Cell area was calculated by particle analysis of the F-actin staining images, using ImageJ software (NIH, USA). Each condition was analyzed in quadruplicate.

4.9. BIOACTIVE MOLECULES RELEASE STUDIES

The correct administration of bioactive agents is often dependent on tailored delivery mechanisms from hydrogel or polymeric matrices. The standard methods for the *in vitro* monitoring of molecules release

are resource spending and laborious. As a simplifying alternative to these methods we suggest the on-chip image-based determination of bioactive molecules release profile.

4.9.1. Setup preparation

Superhydrophobic biomimetic surfaces were imprinted with ring-shaped transparent spots (Figure 9.2, Chapter 9) with concentric superhydrophobic millimetric regions to be used as bioactive agents release study platforms, as referred in sub-section 9.2.

An array of combinatorial conditions for protein release was designed, aiming to control two variables: the concentration of the polymer that constitutes the hydrogel matrix and the concentration of the protein initially encapsulated in the hydrogel matrix. We used alginate sodium salt compatible with cell encapsulation (Sigma, USA) as hydrogel matrix material and BSA-FITC (Sigma, USA) as the protein model, since it is well-known as a model for proteins release studies.

Solutions of 1%, 1.5%, and 2% (w/v) of alginate were prepared using distilled water. Each of these solutions was divided in three equal parts and, to each portion, amounts of BSA-FITC in concentrations of 0.1, 0.5, and 1 mg/mL were added. A total of 9 combinatorial hydrogel precursors mixed with BSA-FITC were prepared. 2 µL of each liquid precursor was dropped in each concentric superhydrophobic spot inside the ring-shaped wettable spot. To fix the polymeric droplets, an indentation was previously made in the center of the superhydrophobic circle using a 22G needle. Each droplet was then crosslinked with 0.8 µL of 10 M $CaCl_2$ during 10 minutes in a water saturated environment. After the crosslinking reaction an amount of 40 µL of PBS was dropped in the ring-shaped hydrophilic spot, covering the particle. The maximum amount of loaded BSA-FITC – 1 mg/mL per particle – leads to a maximum proportion of 0.05 mg/mL of protein in PBS in case of total protein release to the 40 µL of medium (PBS). This value is lower than the limit solubility provided by the supplier (around 0.1 mg/mL in water).

4.9.2. On-chip image acquisition and calibration curves

Images of each spot were acquired before the addition of PBS to the wettable regions and then sequentially after the addition of the PBS to each ring-shaped wettable spot. After studying the evaporation of PBS in each spot at room temperature (20°C), we concluded that there was an average evaporation of 20% of the total volume after 30 minutes. As such, we added 2.7 µL of PBS to each spot every 10 minutes. The final images consisted of the stacking of 28 layers acquired every 25 µm on the particle z axis; those were acquired using the microscope Axiovision Rel. 4.8 program (Zeiss, Germany). The images were composed of whole particles and some surrounding area. The images were acquired

every 5 minutes until 30 minutes of protein release. After an interval of 30 minutes, images were also collected at 60 minutes after the addition of PBS to the particles.

The exposure time of the fluorescence lamp of the reflected/transmitted light microscope (Zeiss, Germany) was maintained in each experiment. Calibration curves with pre-defined concentrations from 1 mg/mL to 0.025 mg/mL of BSA-FITC were performed. Droplets of 2 µL of alginate solutions with the distinct amounts BSA-FITC and crosslinked with $CaCl_2$ were dispensed in superhydrophobic surfaces. Calibration curves were performed with the three distinct concentrations of alginate.

4.9.3. Image analysis: fluorescence quantification

All acquired images were treated as grey-scale images. Fixed areas of each image were collected and the grey mean intensity of each previously stacked image was measured using the ImageJ software (NIH, USA). These values were then adjusted to the calibration curve and the protein release profiles were calculated.

4.9.4. Control test: validation of the on-chip tests

In order to perform control tests we produced several particles of each combinatorial condition using a superhydrophobic surface. These particles were produced with the same properties as the particles used for the chip assay. We placed two particles in each well of a commercially available white opaque 96-well plate. Each well was used to study one specific time point. We then added 80 µL of PBS to each well and carefully removed the particles from each well in the intended time point. These time-points corresponded to the time-points in which the images were collected in the chip. The control tests were performed for the 3 formulations containing 0.5 mg/mL BSA-FITC in 1% (w/v), 1.5% (w/v) and 2% (w/v) of alginate.

We measured the fluorescence in each well in a microplate reader (Synergie HT, Bio-Tek) at an excitation wavelength of 485/20 nm and at an emission wavelength of 528/20 nm. The values were then adjusted to a calibration curve which contained concentration values from 0.005 mg/mL to 1 mg/mL of BSA-FITC in PBS.

4.10. Statistical analysis

Results in this thesis are expressed as mean ± standard deviation. Statistical analysis was performed using Prism software (Prism 4.0c, GraphPad Software Inc., San Diego, CA, USA). Normality tests were performed using Shapiro–Wilk tests. For normally distributed populations parametric tests were

performed by using a one-way or two-way analysis of variance (ANOVA). In the cases where the population was not normally distributed, we used nonparametric Mann–Whitney analysis. The differences were considered statistically significant for $p < 0.05$.

4.11. Factorial analysis

Design of experiments (DOE) is a tool used for the validation of manufacturing processes, namely in the medical field [64]. It refers to a set of statistical approaches to experiment design and analysis and it is used to model and predict the effect of one or more process factors on the responses. While in traditional experimentation the variation of factors is usually singular, while all others are held constant, using DOE all the factors eventually affecting the output can be investigated in single trials. Consequently, the size of the experiment is decreased and key information is provided regarding process interactions. The study of factors interaction is of high importance, as many responses occurring in the biomedical field occur when different factors interact at different levels. Importantly, this type of information on interactions between factors cannot be easily obtained by investigating the effect of each factor separately.

DOE tests include single factor, two-level, factorial designs, Taguchi methods, mixture methods, and response surface models [65]. The so called "screening trials" or two-level trials only study each factor at a high and low level are useful for determining the important sources of variability for a process. They are particularly useful for highlighting critical factors to be studied later with more detail. Taguchi methods are often applied in the design of reliable processes by hit-spotting operating conditions that minimize product variation. Response surface experiments, used in this thesis in Chapters 7 and 8, are used to map the effect of varying two or more factors across a range of values [66]. The use of DOE approaches increases the efficient use of resources while providing detailed analysis and predictive capability. It reduces the size of the experimental setup and hence the costs.

In Chapter 7, three-factor analysis was performed using the Design of Experiments DesignExpert7 Software (Stat-Ease, Inc). Specific storage modulus and *tan* δ data obtained at 1 Hz was analyzed. The list of individual factors considered were: chitosan concentration, genipin concentration and bioactive nanoparticles concentration. The factors were considered as categorical ordinal and the model was not adjusted to any transformation. Data regarding individual factors effect and combined interference was demanded.

In Chapter 8, three-factor analysis was performed using the Design of Experiments DesignExpert7 Software (Stat-Ease, Inc). Response surface models were generated for the analyzed conditions and the

contribution of each factor was then quantified. The three factors considered were: concentration of chitosan in the scaffold (factor A), type of polymer added to the chitosan scaffolds (factor B), and dilution of such polymer (factor C). The variables were considered as numerical, for factor A and factor C, and nominal for factor B. Three levels were considered for factor A: 1%, 1.5%, and 2%. Three levels were considered for factor B: Alg, k-Carr, and i-Carr. Factor C was analyzed also considering three levels: H—for lower dilution factor (i.e., higher concentration of polymer added to chitosan scaffold: 2%), M—for intermediate dilution factor (concentration of polymer B: 1%), and L—for higher dilution factor (concentration of polymer added to chitosan scaffold: 0.5%). For histology scores analysis, the chitosan concentration 1.5% was isolated, so a three-factor analysis was performed considering a new factor: the volume of chitosan dispensed (factor D): 4 ("1.5% Chi") or 6 mL ("1.5%+ Chi"). We developed three distinct surface response models for each time point: 24 h and 7 days after implantation. Each model was developed according to the quantified number of lymphocytes, scores attributed to on-chip macrophages, and to each part of the histological cuts performed in the tissue collected around the chips. The results were analyzed by the software by ''sequential model sum of squares'' to select the highest order polynomial where terms were significant and the results were not aliased. For most of the models, response surface 2FI models were suggested and further on generated. For lymphocyte and macrophage quantifications after 24 h of implantation, main effect models were generated. Results were then analyzed by analysis of variance (ANOVA). Each model allowed concluding about the percentage contribution of each factor. The effect of each factor and the combined effect of factors were also analyzed.

4.12. REFERENCES

[1] Oliveira NM, Neto AI, Song WL, Mano JF. Two-Dimensional Open Microfluidic Devices by Tuning the Wettability on Patterned Superhydrophobic Polymeric Surface. Appl Phys Express. 2010;3:085205.

[2] Hancock MJ, He JK, Mano JF, Khademhosseini A. Surface-Tension-Driven Gradient Generation in a Fluid Stripe for Bench-Top and Microwell Applications. Small. 2011;7:892-901.

[3] Neto AI, Custodio CA, Song WL, Mano JF. High-throughput evaluation of interactions between biomaterials, proteins and cells using patterned superhydrophobic substrates. Soft Matter. 2011;7:4147-51.

[4] Oliveira MB, Salgado CL, Song WL, Mano JF. Combinatorial On-Chip Study of Miniaturized 3D Porous Scaffolds Using a Patterned Superhydrophobic Platform. Small. 2013;9:768-78.

[5] Salgado CL, Oliveira MB, Mano JF. Combinatorial cell-3D biomaterials cytocompatibility screening for tissue engineering using bioinspired superhydrophobic substrates. Integr Biol-Uk. 2012;4:318-27.

[6] Ma K, Rivera J, Hirasaki GJ, Biswal SL. Wettability control and patterning of PDMS using UV-ozone and water immersion. J Colloid Interf Sci. 2011;363:371-8.

[7] Park JJ, Luo XL, Yi HM, Valentine TM, Payne GF, Bentley WE, et al. Chitosan-mediated in situ biomolecule assembly in completely packaged microfluidic devices. Lab Chip. 2006;6:1315-21.

[8] Schuster E, Eckardt J, Hermansson AM, Larsson A, Loren N, Altskar A, et al. Microstructural, mechanical and mass transport properties of isotropic and capillary alginate gels. Soft Matter. 2014;10:357-66.

[9] Shachar M, Tsur-Gang O, Dvir T, Leor J, Cohen S. The effect of immobilized RGD peptide in alginate scaffolds on cardiac tissue engineering. Acta Biomaterialia. 2011;7:152-62.

[10] Li LB, Fang YP, Vreeker R, Appelqvist I. Reexamining the egg-box model in calcium-alginate gels with X-ray diffraction. Biomacromolecules. 2007;8:464-8.

[11] Smidsrod O. Molecular basis for some physical properties of alginates in the gel state. Faraday Discussions of the Chemical Society. 1974;57:263-74.

[12] Grant GT, Morris ER, Rees DA, Smith PJC, Thom D. Biological interactions between polysaccharides and divalent cations: The egg-box model. FEBS Letters. 1973;32:195-8.

[13] Smidsrod O, Skjakbraek G. Alginate as Immobilization Matrix for Cells. Trends in Biotechnology. 1990;8:71-8.

[14] Borgogna M, Skjak-Braek G, Paoletti S, Donati I. On the Initial Binding of Alginate by Calcium Ions. The Tilted Egg-Box Hypothesis. J Phys Chem B. 2013;117:7277-82.

[15] Ikada Y, Tabata Y. Protein release from gelatin matrices. Adv Drug Deliv Rev. 1998;31:287-301.

[16] Mangione MR, Giacomazza D, Bulone D, Martorana V, Cavallaro G, San Biagio PL. K+ and Na+ effects on the gelation properties Of kappa-Carrageenan. Biophys Chem. 2005;113:129-35.

[17] Mangione MR, Giacomazza D, Bulone D, Martorana V, San Biagio PL. Thermoreversible gelation of kappa-Carrageenan: relation between conformational transition and aggregation. Biophys Chem. 2003;104:95-105.

[18] Rochas C, Rinaudo M. Calorimetric determination of the conformational transition of kappa carrageenan. Carbohydrate Research. 1982;105:227-36.

[19] Popa EG, Gomes ME, Reis RL. Cell Delivery Systems Using Alginate-Carrageenan Hydrogel Beads and Fibers for Regenerative Medicine Applications. Biomacromolecules. 2011;12:3952-61.

[20] Popa EG, Reis RL, Gomes ME. In Vitro Performance of K-Carrageenan Hydrogels Combined with Different Types of Cells Aimed at Applications in Cartilage Regeneration. Int J Artif Organs. 2011;34:683-683.

[21] Pankov R, Yamada KM. Fibronectin at a glance. J Cell Sci. 2002;115:3861-3.

[22] Ugarova TP, Zamarron C, Veklich Y, Bowditch RD, Ginsberg MH, Weisel JW, et al. Conformational Transitions in the Cell-Binding Domain of Fibronectin. Biochemistry-Us. 1995;34:4457-66.

[23] Singh P, Schwarzbauer JE. Fibronectin and stem cell differentiation - lessons from chondrogenesis. J Cell Sci. 2012;125:3703-12.

[24] Martino MM, Mochizuki M, Rothenfluh DA, Rempel SA, Hubbell JA, Barker TH. Controlling integrin specificity and stem cell differentiation in 2D and 3D environments through regulation of fibronectin domain stability. Biomaterials. 2009;30:1089-97.

[25] Hench LL, Paschall HF, Paschall M, Mcvey J. Histological Responses at Bioglass and Bioglass-Ceramic Interfaces. Am Ceram Soc Bull. 1973;52:432-.

[26] Hench LL, Splinter RJ, Allen WC, Greenlee TK. Bonding mechanisms at the interface of ceramic prosthetic materials. J Biomed Mater Res. 1971;5:117-41.

[27] Jones JR. Review of bioactive glass: From Hench to hybrids. Acta Biomaterialia. 2013;9:4457-86.

[28] Luz GM, Mano JF. Preparation and characterization of bioactive glass nanoparticles prepared by sol-gel for biomedical applications. Nanotechnology. 2011;22:494014.

[29] Kaur G, Pickrell G, Kimsawatde G, Homa D, Allbee HA, Sriranganathan N. Synthesis, cytotoxicity, and hydroxyapatite formation in 27-Tris-SBF for sol-gel based CaO-P2O5-SiO2-B2O3-ZnO bioactive glasses. Sci Rep. 2014;4:4392.

[30] Mathew R, Stevensson B, Tilocca A, Eden M. Toward a Rational Design of Bioactive Glasses with Optimal Structural Features: Composition-Structure Correlations Unveiled by Solid-State NMR and MD Simulations. J Phys Chem B. 2014;118:833-44.

[31] Xie J, Blough ER, Wang CH. Submicron bioactive glass tubes for bone tissue engineering. Acta Biomater. 2012;8:811-9.

[32] Vallés Lluch A, Ferrer GG, Pradas MM. Surface modification of P(EMA-co-HEA)/SiO2 nanohybrids for faster hydroxyapatite deposition in simulated body fluid? Colloids and Surfaces B: Biointerfaces. 2009;70:218-25.

[33] Gough JE, Jones JR, Hench LL. Nodule formation and mineralisation of human primary osteoblasts cultured on a porous bioactive glass scaffold. Biomaterials. 2004;25:2039-46.

[34] Bosetti M, Cannas M. The effect of bioactive glasses on bone marrow stromal cells differentiation. Biomaterials. 2005;26:3873-9.

[35] Jones JR, Tsigkou O, Coates EE, Stevens MM, Polak JM, Hench LL. Extracellular matrix formation and mineralization on a phosphate-free porous bioactive glass scaffold using primary human osteoblast (HOB) cells. Biomaterials. 2007;28:1653-63.

[36] Silver IA, Deas J, Erecinska M. Interactions of bioactive glasses with osteoblasts in vitro: effects of 45S5 Bioglass, and 58S and 77S bioactive glasses on metabolism, intracellular ion concentrations and cell viability. Biomaterials. 2001;22:175-85.

[37] Xynos ID, Edgar AJ, Buttery LD, Hench LL, Polak JM. Gene-expression profiling of human osteoblasts following treatment with the ionic products of Bioglass 45S5 dissolution. J Biomed Mater Res. 2001;55:151-7.

[38] Butler MF, Ng Y-F, Pudney PDA. Mechanism and kinetics of the crosslinking reaction between biopolymers containing primary amine groups and genipin. Journal of Polymer Science Part A: Polymer Chemistry. 2003;41:3941-53.

[39] Sung HW, Chang Y, Chiu CT, Chen CN, Liang HC. Crosslinking characteristics and mechanical properties of a bovine pericardium fixed with a naturally occurring crosslinking agent. J Biomed Mater Res. 1999;47:116-26.

[40] Sung HW, Liang IL, Chen CN, Huang RN, Liang HF. Stability of a biological tissue fixed with a naturally occurring crosslinking agent (genipin). J Biomed Mater Res. 2001;55:538-46.

[41] Manickam B, Sreedharan R, Elumalai M. 'Genipin' - the natural water soluble cross-linking agent and its importance in the modified drug delivery systems: an overview. Curr Drug Deliv. 2014;11:139-45.

[42] Yoo JS, Kim YJ, Kim SH, Choi SH. Study on genipin: a new alternative natural crosslinking agent for fixing heterograft tissue. Korean J Thorac Cardiovasc Surg. 2011;44:197-207.

[43] Muzzarelli RAA. Genipin-crosslinked chitosan hydrogels as biomedical and pharmaceutical aids. Carbohyd Polym. 2009;77:1-9.

[44] Tacar O, Sriamornsak P, Dass CR. Doxorubicin: an update on anticancer molecular action, toxicity and novel drug delivery systems. J Pharm Pharmacol. 2013;65:157-70.

[45] Momparler RL, Karon M, Siegel SE, Avila F. Effect of adriamycin on DNA, RNA, and protein synthesis in cell-free systems and intact cells. Cancer Res. 1976;36:2891-5.

[46] Tan ML, Friedhuber AM, Dunstan DE, Choong PF, Dass CR. The performance of doxorubicin encapsulated in chitosan-dextran sulphate microparticles in an osteosarcoma model. Biomaterials. 2010;31:541-51.

[47] Amjadi I, Rabiee M, Hosseini MS, Mozafari M. Synthesis and characterization of doxorubicin-loaded poly(lactide-co-glycolide) nanoparticles as a sustained-release anticancer drug delivery system. Appl Biochem Biotechnol. 2012;168:1434-47.

[48] Griffiths JA (2007). Fourier Transform Infrared Spectrometry (2nd ed.). Wiley-Blackwell. ISBN 0-471-19404-2.

[49] J. Coates, in Encyclopedia of Analytical Chemistry, ed. R. A. Meyers, John Wiley & Sons, 2000, pp. 10815–10837.

[50] Holdsworth DW, Thornton MM. Micro-CT in small animal and specimen imaging. Trends in Biotechnology. 2002;20:S34-S9.

[51] Feldkamp LA, Davis LC, Kress JW. Practical Cone-Beam Algorithm. J Opt Soc Am A. 1984;1:612-9.

[52] Liu Y, Liu H, Wang Y, Wang G. Half-scan cone-beam CT fluoroscopy with multiple x-ray sources. Med Phys. 2001;28:1466-71.

[53] Sasaki N. Viscoelastic Properties of Biological Materials. In: Vicente DJD, editor. Viscoelasticity - From Theory to Biological Applications: InTech; 2012.

[54] Wen JH, Vincent LG, Fuhrmann A, Choi YS, Hribar KC, Taylor-Weiner H, et al. Interplay of matrix stiffness and protein tethering in stem cell differentiation. Nat Mater. 2014;13:979-87.

[55] Engler AJ, Sen S, Sweeney HL, Discher DE. Matrix Elasticity Directs Stem Cell Lineage Specification. Cell. 2006;126:677-89.

[56] Mano JF, Neves, N.M., Reis, R.L. Mechanical Characterization of Biomaterials, in Biodegradable Systems in Tissue Engineering and Regenerative Medicine. In: Reis RL, Román JS, editors.: CRC Press; 2005.

[57] Caridade SG, da Silva RMP, Reis RL, Mano JF. Effect of solvent-dependent viscoelastic properties of chitosan membranes on the permeation of 2-phenylethanol. Carbohyd Polym. 2009;75:651-9.

[58] Silva RM, Silva GA, Coutinho OP, Mano JF, Reis RL. Preparation and characterisation in simulated body conditions of glutaraldehyde crosslinked chitosan membranes. J Mater Sci-Mater M. 2004;15:1105-12.

[59] Schuh CA. Nanoindentation studies of materials. Mater Today. 2006;9:32-40.

[60] Bilezikian JP, Lawrence G. Raisz, and Gideon A. Rodan. Principles of Bone Biology. San Diego: Academic Press, 2002. p.1506.

[61] Ehrbar M, Sala A, Lienemann P, Ranga A, Mosiewicz K, Bittermann A, et al. Elucidating the Role of Matrix Stiffness in 3D Cell Migration and Remodeling. Biophys J. 2011;100:284-93.

[62] Egerton R. The Scanning Electron Microscope. Physical Principles of Electron Microscopy: Springer US; 2005. p. 125-53.

[63] Fischer AH, Jacobson KA, Rose J, Zeller R. Hematoxylin and eosin staining of tissue and cell sections. CSH Protoc. 2008; 4986.

[64] DC Montgomery, Design and Analysis of Experiments, 4th ed. New York: Wiley, 1999, pp. 413.

[65] Alexander K, Clarkson PJ. Good design practice for medical devices and equipment, Part II: Design for validation. J Med Eng Technol. 2000;24:53-62.

[66] Kim JS, Kalb JW (1996) "Design of Experiment, an Overview and Application Example" Medical Device and Diagnostic Industry, Vol. 18, Part 3, pp. 78-88.

SECTION III. SUPERHYDROPHOBIC SURFACES PATTERNED WITH WETTABLE SPOTS AS CHIPS TO PERFORM HIGH-THROUGHPUT TISSUE ENGINEERING STUDIES

CHAPTER 5. COMBINATORIAL CELL-3D BIOMATERIALS CYTOCOMPATIBILITY SCREENING FOR TISSUE ENGINEERING USING BIOINSPIRED SUPERHYDROPHOBIC SUBSTRATES[4]

5.1. ABSTRACT

We report on the development of a new array-based screening flat platform with the potential to be used as a high-throughput device based on biomimetic polymeric substrates for combinatorial cell/3D biomaterials screening assays in the context of tissue engineering. Polystyrene was used to produce superhydrophobic surfaces based on the so-called lotus effect. Arrays of hydrophilic regions could be patterned in such surfaces using UV/ozone radiation, generating devices onto which combinatorial hydrogels spots were deposited. The biological performance of encapsulated cells in hydrogels could be tested in an *in vitro* 3D environment assuming that each site was isolated from the others due to the high contrast of wettability between the patterned spots and the superhydrophobic surroundings. Three different polymers – chitosan, collagen and hyaluronic acid - were combined with alginate in different proportions in order to obtain combinatorial binary alginate-based polymeric arrays. The effect of the addition of gelatin to the binary structures was also tested. The gels were chemically analyzed by FTIR microscopic mapping. Cell culture results varied according to the hydrogel composition and encapsulated cell types (L929 fibroblast cells and MC3T3-E1 pre-osteoblast cells). Cell viability and number could be assessed by conventional methods, such as MTS reduction test and dsDNA quantification. Non-destructive image analysis was performed using cytoskeleton and nuclei staining agents and the results were consistent with the ones obtained by conventional sample-destructive techniques. Briefly, L929 cells showed higher number and viability for higher alginate-content and collagen-containing hydrogels, while MC3T3-E1 showed higher cell viability and cell number in lower alginate-content and chitosan containing hydrogels. The addition of gelatin did not influence significantly cell metabolic activity or cell number in any of the encapsulated cell types.

[4] This chapter was based on the publication: Salgado CL*, Oliveira MB*, Mano JF. Combinatorial cell-3D biomaterials cytocompatibility screening for tissue engineering using bioinspired superhydrophobic substrates. Integr Biol-Uk. 2012;4:318-27 (*the authors contributed equally to this work).

5.2. INTRODUCTION

In tissue engineering, the study of the interactions between three-dimensional (3D) constructs and cells is traditionally limited to a low number of combinations of materials, cell types and external stimuli. Cell response to biomaterials is known to be affected by a wide range of complex interdependent signals [1]. In its majority, the function and interactions between these signals still remain undisclosed and the variation of most of these mechanisms has been usually studied individually. This led to the necessity of developing efficient and cost-saving platforms for the screening of biomaterials that act as artificial extracellular matrices (ECMs) for tissue regeneration, in order to study the systematic variation of diverse factors in a high-throughput manner.

Although combinatorial biomolecular libraries of DNA and drug microarrays have been widely reported [2], the synthesis of polymeric libraries is still a recent challenge, especially if one intends to reproduce the 3D environment felt by cells *in vivo*. High-throughput analysis has allowed for the fast study of arrays of biomaterials physicochemical characteristics [3-5] and cell response to combinatorial arrays of substrates and soluble factors [6-9].

The development of new platforms for high-throughput study of biomaterials and respective interactions with cells must take in consideration three different aspects: (i) the easy fabrication of the platform where the different materials are deposited with controlled volumes; (ii) the easy generation of combinatorial biomaterial arrays and combinations in the desired shape and organizational structure, such as scaffolds or hydrogels, optionally combined with other tissue engineering components such as soluble factors or cells; (iii) the reliable collection of results (either from physicochemical characterization or biological response), ideally avoiding the destruction of the whole final high-throughput platform.

Aiming to obtain substrates for the production of biomaterials arrays, top-down techniques can be used to pattern substrates in which polymeric materials can be further deposited. Regarding this group of techniques, emphasis has been given to lithographic methods, namely photolithography which uses patterned hollow masks that allow for the substrate to be exposed to radiation in some areas leading to selective crosslinking [10] or changes of the wettability of specific regions of the substrate, as suggested herein.

This concept relies on the contrast between surface wettability for the construction of chips and was previously used in 2D studies to investigate the effect of pre-adsorbed proteins in cell adhesion and growth [11] or for the assessment of the osteoconductivity of inorganic nanoparticles [12].

The assessment of cell behavior into flat (2D) biomaterials has been carried out by developing microarray systems to, for example, study the interactions among biomaterials, adsorbed proteins and human embryonic stem cells [13]. However, in tissue engineering field, such tests should ideally be performed in microenvironments that could mimic better the *in vivo* conditions. Therefore, the extension of combinatorial assays to 3D milieus is an important step in the improvement of the reliability of the results obtained in high-throughput platforms [14]. Polymeric 3D arrays of well-characterized biodegradable polymer blends were used to test the ability to efficiently screen different materials with a range of different cell types6 and to study stem cell behavior [15-16] using techniques such as direct writing printing of microliter-sized gels [17]. However, few solutions have been proposed in the case of the comparison between biomaterials exhibiting complex structures. In order to obtain 3D porous scaffolds combinations, commercially available polystyrene (PS) well plates have been proposed [18-19]. Porous gradients with the single-factor variation of some property of the material, e.g. crosslinking extent [20], or calcium phosphates content [19] have also been suggested. The variation of the size and shape of the structures in commercial PS well plates is limited to the size of the wells, as their full characterization inside the wells may be a difficult task in cases where image analysis or insertion of probes may be needed. In the case of gradients, the variation of more than one single factor may be difficult due to the absence of a physical separation between the different regions in the scaffold/hydrogel.

Herein, we propose a new concept of miniaturized device for combinatorial screening of chemical composition and cytocompatibility of 3D biomaterials. The device is based on the use of previously reported superhydrophobic substrates [21], in which cell attachment seems to be decreased [22-24]. UV/ozone (UVO) irradiation could be used to locally modify the wettability of such substrates up to the superhydrophilic regime, using hollow photomasks to generate spot regions onto super-repellent substrates. Different biomaterials can be then dispensed in these regions. The main objective of this work is to develop a combinatorial array-based screening assay using such new polymeric chips to evaluate different biomaterial/cells compositions for tissue engineering applications by dispensing hydrogel-precursor polymeric solutions with encapsulated cells followed by the respective ionic crosslinking over controlled spatially modified superhydrophobic substrates.

Natural-based polymers have been widely used as supports for tissue engineering applications [25]. In this work, combinations of natural macromolecules, including alginate (Alg), chitosan (Chi), collagen (Coll) hyaluronic acid (HA) and gelatin (G) were explored to demonstrate the applicability of the

proposed technology, since different kinds of conjugates with natural polymers have been shown to be favorable for different cell types in tissue repair [26].

5.3. MATERIALS AND METHODS

5.3.1. Processing of superhydrophobic polymeric substrates

Commercially available PS plates (Corning) and PS flakes (Mn=69000, Mw/Mn=1.734) were used. Tetrahydrofuran (THF) was purchased from Fluka (p.a.>99.5%) and ethanol absolute from Panreac. The surfaces were modified according to the protocol described elsewhere [11,21,27-28]. The developed superhydrophobic substrates were treated using a UVO lamp (Bioforce, Nanosciences) for 20 minutes. In order to control the wettability, an aluminum mask with 4 mm^2 open squares, separated by 0.5 mm was used. The wettability of the studied surfaces was assessed by contact angle (CA) measurements. Static CA measurements were carried out using an OCA15+ goniometer (DataPhysics, Germany) using the Sessile drop method. Distilled water (3 µL) was dropped on the surfaces (hydrophilic and superhydrophobic) and pictures were taken after stabilization of the water droplet.

5.3.2. Cell expansion and preparation of the materials for cell culture

A fibroblast cell line (L929, ATCC) and a pre-osteoblast cell line (MC3T3, ATCC) were used as well established cell lines for preliminary biocompatibility studies. Cells were expanded in basal medium consisting of alpha-MEM medium (α-MEM; Gibco, UK) supplemented with 10% heat-inactivated fetal bovine serum (FBS; BiochromAG, Germany) and 1% antibiotic/antimyotic solution (final concentration of penicillin 100 units/mL and streptomycin 100 mg/mL; Gibco, UK). Cells were cultured at 37°C in an atmosphere of 5% CO_2. Prior to cell culture, Alg, Chi and G solutions were sterilized in an autoclave for 15 minutes at 121°C and 1 atm. HA and Coll solutions were filtered, and PS superhydrophobic surfaces were immersed in ethanol 70% solution overnight and then rinsed with sterile phosphate buffer saline (PBS).

5.3.3. Production of 3D structural spots onto the hydrophilic regions of the developed chips

The 3D structures were prepared by dispensing polymeric solutions onto the hydrophilic spots of the PS substrates prepared as described before. The hydrogels were prepared using aqueous solutions of: sodium alginate, 1 wt/v% (Sigma, USA); water soluble chitosan, 1 wt/v% (Novamatrix, Norway); collagen type I, 1 wt/v% (Fluka, Switzerland); gelatin B, 0.2 wt/v% (Aldrich, USA) and hyaluronic acid sodium salt,

1 wt/v% (Sigma, USA). After trypsinisation from the cell culture flask, cells were concentrated and mixed with the liquid polymeric hydrogel precursors at a constant concentration of $5x10^4$ cells/spot. The liquid drops were solidified by the action of crosslinker $CaCl_2$ 0.5 M (Merck) with 4-(2-hydroxyethyl)-1-piperazineethanesulfonic acid (HEPES) 0.1 M (Sigma, USA). In each spot, a total amount of 4 µl of polymeric solutions (which amount depended in the weight proportion of alginate being tested) and 1 µl of crosslinking solution were dispensed using a digital micropipette, in a drop-by-drop logic. Different proportions of the materials were analyzed (40:60; 50:50; 70:30 and 90:10 – weight proportion of different materials/alginate).

5.3.4. Characterization of the material distribution in the hydrogel spots

To assess the presence and distribution of the materials in each spot and to verify if the semi-IPN could maintain its integrity after 24 hours of immersion in a liquid medium, Fourier Transform Infrared (FTIR) analysis was performed to all samples. A whole chip with the polymeric mixtures - with no encapsulated cells - was immersed in PBS for 24 hours. The samples were then air-dried in order to minimize the absorption peaks of water in the FTIR analysis. A whole chip was then placed in a Perkin-Elmer Spectrum Spotlight 200 FTIR Microscope System and each spot was analyzed in reflectance mode.

Characteristic absorption bands of each polymer were selected [29] and identified in FTIR collected data for each control, i.e. the pure polymer dispensed and dried in the platform. The main aim was to assess the polymers distribution in the air-dried structures. In the case of Alg/Coll mixtures, the distribution of both polymers could be assessed. However, in Alg/Chi and Alg/HA the overlapping of the characteristic peaks of alginate did not allow for the simultaneous identification of both polymers in the maps. As a consequence, the distributions of chitosan and hyaluronic acid in the mixtures with chitosan were identified individually. Regarding the gelatin-containing structures, the identification of this polymer in the mixtures containing collagen was not possible due to the protein character of both of them. Since Chi and HA could not be distinguished from alginate, we chose to analyze the Alg/HAG and Alg/ChiG mixtures excluding the chemical mapping of alginate and distinguishing gelatin from HA and Chi. However, these are results that require a careful analysis, since the peaks that identify these polymers are close in the infrared spectrum and overlapping phenomena may be observed. The chemical groups and corresponding infrared peaks, as well as the respective chosen bandwidths used to identify each polymer are specified in Table 5.1.

Table 5.1. – List of the characteristic peaks and restriction bandwidths used to identify each polymer in the FTIR mapping analysis.

Polymer	Identified simultaneously with:	Characteristic group(s)	Corresponding peak (cm^{-1})	Selected bandwidth (cm^{-1})
Chitosan	-	Amine I	~1650	1680-1620
Collagen	Alginate	Amine I (present in Proline) Amine II (present in Glycine)	~1650 ~1550	1680-1620 1580-1520
Hyaluronic acid	-	Ester Amine II	~1045 ~1550	1055-1035 1580-1520
Alginate	Collagen	Ester	~1045	1000-1100
Gelatin	Chitosan and Hyaluronic acid	Amine I Amide	~1650 ~1650	1680-1620

Regarding the colors used in the chemical mapping of the mixtures, for the single identification of chitosan in Alg/Chi mixtures, blue was the chosen color; dark yellow was used for the single identification of HA in Alg/HA mixtures. In the Alg/Coll mixtures, green was chosen for the identification of alginate, while light yellow was used in the identification of collagen. To distinguish gelatin from Chi in Alg/ChiG mixtures, gelatin was considered red, while Chi was considered as blue. In the same logic, in Alg/HAG mixtures, gelatin was considered red while HA remained dark yellow.

Spectra were collected in continuous scan mode for sample areas of 100 x 100 μm2, with a spectral resolution of 16 cm- 1, averaging 15 scans for each spectrum.

5.3.5. Cell culture in the superhydrophobic chips

For cell encapsulation experiments, the chips with the hydrogels and cells were placed in a 6-well plate with 5 mL of complete cell culture medium. PS substrates cut from commercial Petri dishes were used as controls. All seeded samples and controls were incubated for 24 hours in order to evaluate the cell viability and quantify the cell number on the different materials combinations.

5.3.6. Cell response assessment

Destructive tests for viability assessment and cell quantification

After 24 hours of cell culture, the hydrogels were removed from the platform and disaggregated using 5 μL of sodium citrate solution (100mM). The cell viability was determined using the CellTiter

96®AQueous One Solution Cell Proliferation Assay (Promega, USA). This assay is based on the bioreduction of a tetrazolium compound,3-(4,5-dimethylthiazol-2yl)-5-(3-carboxymethoxyphenyl)- 2-(4-sulfofenyl)-2H-tetrazolium (MTS), into a water-soluble brown formazan product. The absorbance was measured at 490 nm in a microplate reader (SynergieHT, Bio-Tek, USA), being related to the quantity of formazan product and directly proportional to the number of living cells in the constructs. Samples were characterized in triplicate.

Cell proliferation was quantified by the total amount of double-stranded DNA (dsDNA), along the culturing time. Quantification was performed using the Quant-iT™ Pico-Green dsDNA Assay Kit (Invitrogen™, Molecular Probes™, Oregon, USA), according to the instructions of the manufacturer. Briefly, cells in the construct were lysed by osmotic and thermal shock and the supernatant was used for the dsDNA quantification assay. The fluorescence of the dye was measured at an excitation wavelength of 485/20 nm and at an emission wavelength of 528/20 nm, in a microplate reader (Synergie HT, Bio-Tek, USA). The dsDNA concentration for each sample was calculated using a standard curve (dsDNA concentration ranging from 0.0 to 1.5 mg/mL) relating quantity of dsDNA and fluorescence intensity. Samples were characterized in triplicate.

Non-destructive image-based tests for cell viability and quantification assessment

After 24 hours of cell culture, cell viability was evaluated by a non-destructive live/dead assay. After washing the samples with PBS, the samples were incubated with 100 µL of calcein AM solution (2 µg/mL) and 100 µL of propidium iodide solution (consisting of 1 µg/mL of propidium iodide and 10 µg/mLof RNAase A in PBS, prepared from stock solutions of 1 mg/mL of propidium iodide in distilled water, and 1 mg/mL of RNAase A in distilled water). The incubation time was of 30 minutes at 37°C for all samples. Cell quantification could be performed by staining the cells nuclei with 4',6-diamidino-2-phenylindole (DAPI – 1 mg/mL). In both cases, fluorescence microscopy (Reflected/Transmitted Light Microscope, Zeiss) was used for image analyses on WCIF Image J software, using 10 images of 200x magnification per sample, and the same threshold criterions were used in all images.

A schematic resume of the procedure performed in this study can be seen in Figure 5.1.

5.4. Results and Discussion

Superhydrophobic biomimetic substrates with a water contact angle of 151.7±3.1° (see contour of the water droplet in Figure 5.1) were obtained by phase-separation of PS [25]. This polymer was used since it is the gold standard material for *in vitro* cell culture. Hydrophilic patterns were obtained after 20 minutes of UVO exposure covered with a photomask, and the contact angle of the treated regions

decreased to 72.4±2.3° (see contour of the water droplet in Figure 5.1). Controlled volumes of liquid precursors with mixed cells could be dispensed in such wettable spots using a micropipette and were kept confined in that area during crosslinking and after 24 hours of immersion in cell culture medium due to the surface tension contrast between the wettable spot and the surrounding superhydrophobic regions (Figure 5.2A). The contrast of hydrophobilicity between the patterned spots and the surrounding area allows for an easy variation of the volume of the hydrogels, as already proven by Neto et al [11] with the deposition of simple liquids in the spots, by the variation of the spots area and volume of the deposited solution. Also, these platforms allow for the sloping and transportation of the whole platform without the mixture of the individual volumes dispensed in each hydrophilic spot.

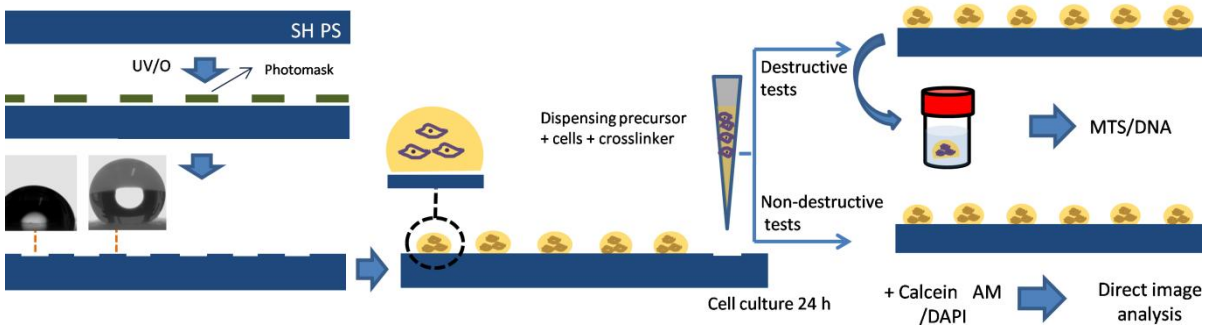

Figure 5.1. – Schematic representation of the process used to create hydrophilic spots in the initially superhydrophobic substrate using a hollow mask to imprint wettable spots by the action of UVO irradiation. Images of the contours of water droplets in the original (superhydrophobic) and surface modified (hydrophilic) substrates are included. The characterization of each construct can be carried out by individual destructive tests or using colorimetric/image analysis in which the biomaterials are kept in the chip.

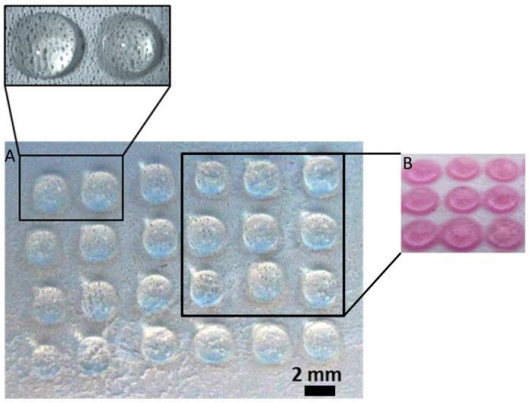

Figure 5.2. – A) Hydrogels samples dropped into the hydrophilic spots. B) Magnified image of the hydrogel alginate based materials after 24h of immersion in culture medium.

In this work, the size of the hydrogels differs from previously referred biological chips proposed systems, in which the dispensed spots have sizes in the micrometric range. In this new platform, the size of material structure can be easily varied, simply by varying the size of the hollows in the masks and the volume of the liquid precursors. The millimetric sizes of the hydrophilic spots open the possibility of, in the future, producing structures with hierarchical organization such as porous scaffolds exhibiting pore sizes adequate for tissue engineering applications.

Volumes of 4 µl of aqueous polymeric solutions with a constant density of encapsulated cells were dispensed in the wettable regions of the platform, and crosslinked afterwards with $CaCl_2$, in order to obtain arrays of hydrogel spots with sizes of ca. 4 mm^2 (Figure 5.2A). The whole chip was incubated in cell culture medium right after the crosslinking reaction (Figure 5.2B). For the proof-of-concept, alginate-based hydrogels were used since alginate is largely used in cell encapsulation [30]. To obtain arrays of alginate-based natural polymer hydrogels, alginate was mixed with Chi, Coll and HA in 40, 50, 70 and 90% (weight/weight) ratios. We also analyzed the effect of the addition of gelatin in all binary alginate-natural polymer mixtures. A total of 24 different combinations of materials were obtained per platform. These were tested with 2 different encapsulated cell types, resulting in a total of 48 cell/polymers combinations, which were tested in triplicate. In order to show the stability of the chips overtime, those were kept in cell culture medium for 3 days and no delamination of the spots was observed.

In a first set of arrays, Alg was mixed with Chi, which is one of the most commonly used polymers in biomaterials production. Chi has already been conjugated with a wide range of polymers, including alginate [31]. Coll was also used to produce a set of arrays; it is the most abundant protein in the body and shows characteristics such as high mechanical strength, good biocompatibility and low antigenicity. Combinations of Coll with several materials have been prepared, such as Coll microsponges impregnated into previously prepared synthetic polymerics caffolds, enhancing biological performance [32]. HA was another polymer tested in binary combinations with Alg. It is a water-soluble and high-swelling polymer which can form hydrogels, which are enzymatically degraded by hyaluronidase, existing in cells and blood serum. It is mainly used in cartilage tissue engineering since it is part of this native tissue. Combined with Alg and Chi, the presence of HA allowed for the production of an artificial ECM that permitted the growth of the embedded chondrocytes [33-34]. We also investigated the potential biological effect of the addition of gelatin - obtained from the denaturation of collagen - to the previously described mixtures, obtaining ternary combinations. Gelatin was reported to improve mesenchymal stem cell attachment for further chondrogenic differentiation in hyaluronic acid hydrogels [35] and to improve cell adhesion [36].

The choice of the processing method for the polymeric structures focused on the easiness, rapidness and compatibility with cell encapsulation. Thereby, the materials were processed as semi-IPNs [37-38], using Alg as the mesh-forming crosslinkable polymer by simple ionic gelling, in a drop-by-drop based technique to spot the hydrogels in the hydrophilic patterns. Besides cytocompatibility studies, the prove of concept of the functionality of this platform opens the path for its use in more complex and long term studies in the future involving, for example, stem cells differentiation.

This study aimed to test the suitability of the developed superhydrophobic platforms by performing a preliminary rapid screening of biomaterials for two different cell types

FTIR mapping analysis was performed in order to (i) check for the distribution of the polymers after 24 hours of immersion in PBS, (ii) observe the differences in the amount of each polymer in the gradients and (iii) check for the existence of vestiges of all polymers in the mixtures after 24 hours of immersion in PBS. In Figure 5.3 the images resulting from the restriction of the infrared bandwidth restriction can be seen for the selected colors for each polymer (corresponding to the bandwidth restrictions indicated in Table 5.1). A first analysis of the FTIR maps can be performed regarding the amount of each polymer in the increasing Alg-content mixtures. Considering Chi single quantification results in the Alg/Chi mixtures, it seems that a decrease in the intensity of the blue color in the FTIR maps occurred with the increase of alginate amount, which is related to the decrease in the amount of polymer in the structure. The same tendency could be seen in Alg/HA mixtures, even in a more clear way, observing the decrease in the dark yellow-colored regions. Regarding Alg/Coll mixtures, the presence of both polymers – Alg and Coll – could be detected. From the mixture with 40% content of alginate to the one with 90% content, a decrease in the yellow color in the maps (correspondent to collagen) can be observed, accompanied by an increase in the ratio of green color (correspondent to alginate).

It was possible to assess the presence of gelatin in the mixtures in the case of the systems containing Chi and HA. However, considering the proximity of the peaks used to identify gelatin from the ones present in these two polymers, the analysis of the results is not straight forward. For these two cases, it seems that in the higher (90%) Alg content mixtures, more spots corresponding to the gelatin color – red - can be seen. This may be explained by the higher crosslinking extent of the network due to a larger amount of crosslinked matrix (Alg), resulting in a more stable retention of the gelatin on the spots. Control spots with 100% Alg were analyzed in the characteristic bandwidths of the mixed polymers and the results show the almost complete absence of color in these FTIR chemical maps. Moreover, the FTIR spectra in Figure 5.3 show the characteristic peaks of the polymers in the mixtures evidenced by grey bars. In general, peaks of higher intensity can be seen in 60% non-crosslinked polymer

formulations (i.e., 60% of Chi, Coll, HA or their mixtures with gelatin), while lower intensity peaks can be seen in 10% non-crosslinked polymer formulations.

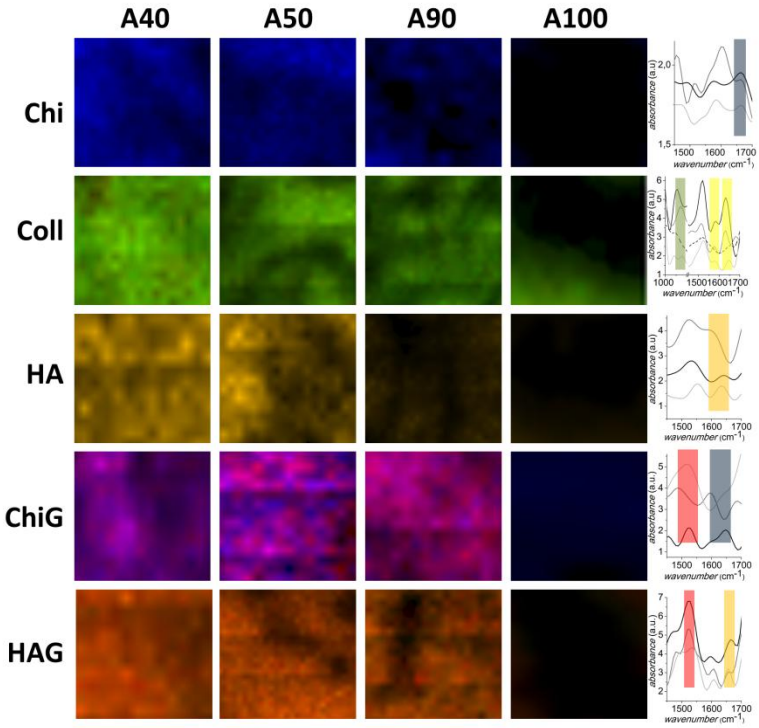

Figure 5.3. – Chemical maps of the 40%, 50%, 90% and 100% alginate (labeled as A) formulations. Respective FTIR spectra of the polymeric mixtures in which ▬ ▬ corresponds to 40% alginate- content hydrogels, ▬ to 50% alginate hydrogels, ▬ to 90% alginate-content hydrogels and ▬ to 100% alginate-content hydrogels. The area of each chemical map corresponds to 100x100 μm^2.

Regarding the distribution of the mixed polymers in the Alg network, apparent phase separation in some materials combinations could be observed. Also, these phase separations presented different sizes according to the type of mixture. For example, in the case of Alg40/Coll60 and Alg40/60HAG mixtures, the size of the aggregates of the phase separation have sizes around 10 μm. In the case of 40Alg/60HA and 40Alg/60ChiG, the phase separation aggregates seem to round 20 μm. This difference of sizes between the aggregates may possibly be explained by the charges of the polymers while they are mixed in the liquid precursor. In the case of Alg/Coll mixtures, the polymers present opposite charges: the net charge of Coll is positive, while the charge of sodium alginate is negative. This may lead to favorable electrostatic interactions between the polymers during their mixing, forming smaller aggregates, resulting in a more homogeneous distribution of the non-crosslinked polymer in the further crosslinked Alg matrix. On the other hand, in cases in which the polymers show equivalent charge (for example,

HA/sodium alginate and Chi/gelatin), the repulsion between the polymeric chains due to the charges may lead to the formation of larger aggregates of each polymer, as could be verified in 40Alg/60HA and 40Alg/60ChiG mixtures.

Two distinct cell types were used in the *in vitro* biological tests: the fibroblast cell line L929, which is widely used for cytotoxicity experiments, and the pre-osteoblast MC3T3-E1 cell line, which is a well-characterized model for osteoblasts since it follows the typical stages of osteogenesis during culture in both 2D and 3D environments [39].

Regarding the risk of crosstalk and cell passage between the different spots, it has been proved that this type of superhydrophobic surfaces impairs the adhesion and inhibits the proliferation of several cell types [22,24,28]. Moreover, in this application the cells are encapsulated in the hydrogels, making their mobility more difficult than if they were simply seeded in the hydrophilic patterned regions.

After 24 hours of cell culture, all the materials were analyzed using both indirect (or image analysis-based) and direct (conventional destructive) methods for cell quantification and cell metabolic activity assessment. According to the 24 different hydrogels compositions, the behavior of both cell types was expected to vary with the presence of specific proteins (such as Coll) and chemical nature. Indirect methods were performed by image analysis of each spot using fluorescent staining for cell nuclei (Figure 5.5) and live (green)/dead (red) for cells cytoskeletons (Figure 5.4).

The direct methods were performed by extracting the cells from the materials spots and incubating them in MTS solution or by quantification of extracted dsDNA from lysed cells, according to the methods usually performed in single scaffold analysis. The results obtained from the indirect tests were treated and are represented as intensity maps in Figure 5.6A1,B1.

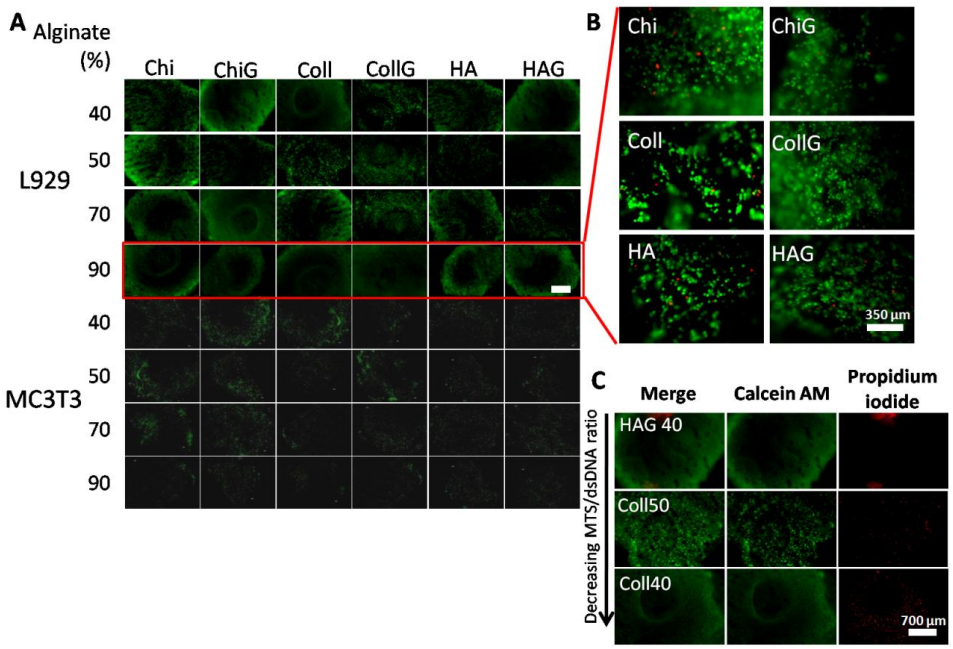

Figure 5.4. – (A) Fluorescent microscopy images of viable cells in the hydrogels stained with calcein AM after 24h of culture. Images scale bar corresponds to 700 µm. (B) Calcein AM (green)/propidium iodide (red) (live/dead) staining with the magnification used for the calcein AM pixel quantification (200x). (C) Live/dead staining images (merged and with the live cells staining and dead cells staining shown separately) of three different polymeric mixtures in which the ratio of viable cells per total amount of cells (which was calculated by the MTS/dsDNA quantification values) is decreasing from the upper mixture to the downer mixture, as indicated by the arrow.

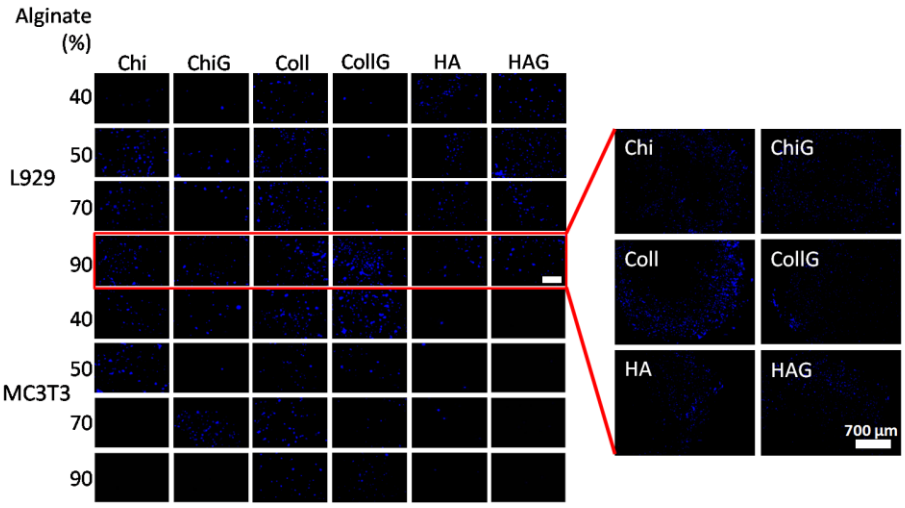

Figure 5.5. – Fluorescent microscopy images of hydrogels stained with DAPI for the cell nuclei blue staining. In left, randomly selected 200x magnification used for DAPI pixel quantification can be observed (the scale bar corresponds to 350 µm). In right, images of 50x magnification can be observed for the conditions 90%Alg, which allows for a general observation of the distribution of the cells in the hydrogels.

The validation of the non-destructive assessment of the data in a high-throughput manner is important since it eliminates the necessity of taking the hydrogels from the platform and decreases analysis time. The hydrogels/cells constructs were evaluated by a dye combination of calcein AM for cellular viability/propidium iodide for dead cells and DAPI for nuclei quantification. The specific biological properties of the spots in the hydrogel arrays could be assessed through image analysis in which the cell number could be quantified. The corresponding heat map of such data is presented in Figure 5.6A2,B2. In Figure 5.4A, the calcein AM staining of viable cells in each hydrogel can be observed in a magnification that allows for the visualization of the whole hydrogel structure. For the visualization of the merged calcein AM and propidium iodide staining, more magnified images - which used for the viable cells quantification - are presented in Figure 5.4B.

In Figure 5.4C, in order to show the live/dead staining for low magnification images (which allow for the observation of the whole hydrogel), we show the merged live/dead images and the independent stainings for 3 different combinations. Since in the images an apparent increase in the number of non-viable cells could be seen from the mixture HAG40 (with low death cells number) to the Coll40 mixture (with an apparent high death cells number), we compared the results with the ratio between MTS reduction test and dsDNA quantification values (MTS/dsDNA), in order to compare the number of viable cells with the total amount of cells in the hydrogels. We could observe that the ratio between death cells and live cells was effectively higher in the Coll40 mixture, followed by the Coll50 mixture, and much lower in the HAG40 mixture.

Most biological results that were observed by fluorescence microscopy (Figure 5.4 and Figure 5.5, with the tendencies represented in the intensity maps of Figure 5.6A2,B2) are consistent with those obtained by MTS and dsDNA extraction protocols (with the tendencies represented in the intensity maps of Figure 5.6A1,B1). Such finding seems to indicate that the indirect colorimetric essays on the spots could provide data consistent with the results obtained by the conventional destructive tests. The findings obtained by the observation of the cellular behavior in quite distinct materials and using two cell types provides a good indication that this methodology could be extended to other cell-3D materials interactions.

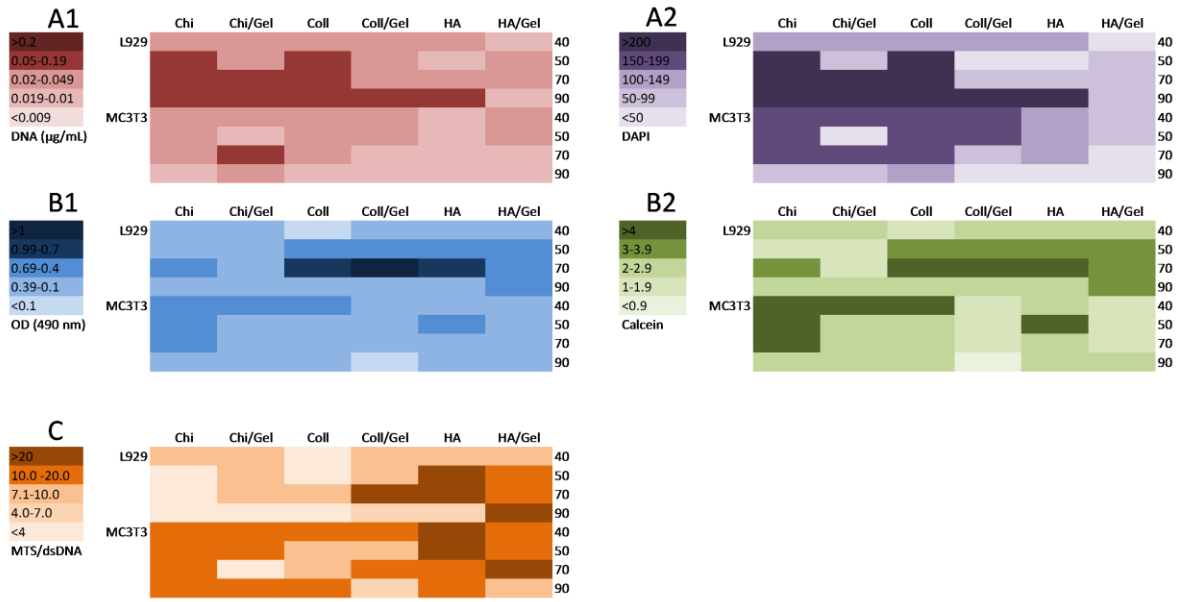

Figure 5.6. – (A1) dsDNA quantification of cell number of fibroblast (L929) and osteoblast (MC3T3-E1) in different hydrogels samples after 24 hours of cell culture. (A2) MTS evaluation of cell metabolic activity of fibroblast cells (L929) and pre-osteoblast cells (MC3T3) in different hydrogels samples after 24 hours of cell culture represented in an intensity map. (B1) dsDNA content (DAPI – blue) calculated using fluorescence microscope images treated with WCIF image J program and (B2) Calcein AM fluorescence (viable cells - green) calculated using fluorescence microscope images treated with WCIF image J program. (C) MTS/dsDNA ratio results intensity map.

For both MTS absorbance results (Figure 5.6B1) and the calcein AM fluorescence microscopy image analysis (Figure 5.6B2), higher number of viable L929 fibroblast cells could be seen in 70%Alg content hydrogels. This tendency could be observed especially in the presence of Coll and HA, which are macromolecules present in connective tissues, highly populated by fibroblasts. In the analyzed formulations hydrogels containing Chi showed the lowest viability results.

MC3T3-E1 cells showed increased cell viability in structures with higher Chi content: Alg40/Chi60, Alg40/ChiGel60 and Alg50/Chi50, which can be seen in both MTS and calcein AM data in Figure 5.6B1,B2. The presence of HA improved MC3T3 viability in the Alg50/HA50 condition up to values correspondent to chitosan-containing hydrogels with lower Alg content. Also, in the lowest ratio of Alg hydrogel (40%), the presence of Coll improved cell viability, which was expectable since Coll fibers constitute the most abundant protein structure in the pre-bone (osteoid) and bone native tissue [40].

Both dsDNA quantification (Figure 5.4B) and analysis of DAPI staining images (Figure 5.5) showed that L929 cells preferred higher Alg content hydrogels (50% to 90%, especially for formulation containing 90% Alg). Oppositely, MC3T3-E1 cells showed higher number in lower alginate content hydrogels, with

prevalent higher number on 40% and 50% of Alg compositions. In general, the intensity corresponding to cell number observed for the L929 cell line was stronger than the one observed for MC3T3-E1 cell line, which is related to the threshold of proliferation of each of the cell lines: L929 typically shows faster proliferation rate than MC3T3-E1.

In the analysis of the ratio between viable cells and total number of cells (MTS/dsDNA; Figure 5.6C), some differences could be verified while comparing these values with the straight analysis of the viable cells in the hydrogels. For example, in the case of MC3T3-E1 cells in the mixtures A90/Chi10, A90/ChiG10 and A90/Coll10, the number of viable cells was apparently low (Figure 5.6B2). However, the ratio of viable cells per number of total cells in the hydrogels is high in the intensity map scale, meaning that although the number of cells in the hydrogels was low these cells were living. This probably means that these hydrogels allow for the maintenance of viable cells, but do not promote cell proliferation. In an opposite case, in the mixture A70/Coll30 in L929 cell line, the high value of the measured optical density measured for MTS reduction test contradicts the low value of the MTS/dsDNA ratio, meaning that in this case, although cell number is high, the correspondent living cells in the hydrogel is proportionally low, meaning that probably cell proliferation occurred in the 24 hours of cell culture, but not all of these cells could remain alive in the hydrogel for this period of time.

In the case of HA-containing mixtures, the MTS and calcein AM single analysis suggested that the HA-containing combinations impaired cell viability. However, the comparison with cell amount (dsDNA) revealed that although Alg/HA mixtures seem not to promote cell proliferation in both cell types, they allow for high cell viability values.

Despite the previously presented cases, in a broad sense the tendencies for cell viability normalized with dsDNA amount in the different compositions was correspondent to the previously discussed MTS and calcein AM staining for both cell types.

For the particular set of studied materials, the presence of gelatin in the hydrogels did not lead to an improvement of biological performance, neither in the viability nor in cell number, in any of the cell lines. The only condition in which the presence of gelatin in the system seemed to improve the cell adhesion was in L929 cell culture in the Alg90/HAG10 condition. Such results clearly demonstrate that the effect of specific combinations of biomaterials may be not evident and combinatorial evaluations are clearly necessary in the tissue engineering field.

The obtained results constitute a proof-of-concept on the development of an innovative method to create a cheap and simple device to evaluate cell-materials interactions (namely, cytocompatibility) using patterns of extreme wettability in a single-polymer flat surface. It was clear that the hydrogel network

chemistry and encapsulated cell type could influence cell number and viability after 24 hours of cell culture. The fabricated arrays are versatile and could be used to explore the influence of other combinations of natural polymeric materials and eventually soluble factors on the viability and proliferation of multiple cell types. A particular advantage of this approach is the ability to screen the influence of different conjugated biomaterials or signals on the behavior of distinct cell types cultured in 3D environment, avoiding the use of complex and costly fabrication techniques. Further approaches could allow for the assessment of the materials degradation and other physicochemical characteristics within each individual spot.

In conclusion, array-based chips, with the potential to be used as high-throughput devices, were obtained by the local treatment of superhydrophobic surfaces, in which polymeric precursors were dispensed in hydrophilic spots, and maintained in the spot due to the contrasting wettability between the spot area and the surrounding area. Two cell types were used in the study of alginate-based hydrogels obtained by the mixture of alginate with other natural polymers and cells, followed by ionic crosslinking. Analysis of cell viability and cell number after 24 hours of cell culture was performed by conventional methods, which require the destruction of the whole chip integrity. Non-destructive methods based in image analysis were also performed and the results of these tests match the tendencies shown by the conventional destructive tests. This new chip allows not only for the performance of several cell tests in new hydrogel combinations encapsulating different cell types, but also for their analysis without the destruction of the whole platform.

5.5. Conclusions

We propose a new concept of miniaturized devices for combinatorial biological screening of 3D biomaterial structures/cells interactions. Those are based on the use of biomimetic superhydrophobic substrates in which UVO modification could be used to locally modify the wettabiliy to hydrophilic characteristics. Masks were used to spot wettable regions where different combinations of natural biomaterials with encapsulated cells were deposited and further ionicalycrosslinked. Chemical mapping showed that the combined polymers were dispersed in the crosslinked matrix and that vestiges of all polymers could be identified in the hydrogels after 24 hours of immersion.

The different materials combinations showed different effects on two encapsulated cell types: L929 and MC3T3-E1 cell lines. Local and non-destructive cytotoxicity and cell number assessment was developed using cell dying agents and an image analysis program. Results corroborate the conventional destructive MTS and dsDNA quantification results, showing that this new method allows for rapid and non-

destructive array-based analysis of the cytotoxicity of biomaterial combinations. Regarding cell culture results a tendency can be seen in both cell types, according to the addition of different biomaterials, especially of collagen in the case of L929 cells, or chitosan in the case of MC3T3-E1 cells. The addition of a highly viscous and highly hydrating material such as HA decreased MC3T3-E1 viability and cell number. Also, L929 culture showed enhanced results in high-content alginate hydrogels, whereas osteoblasts showed opposite tendency. The addition of gelatin to the binary polymeric hydrogels analyzed did not show any effect in biological performance.

Besides cytotoxicity analysis, this platform shows to be promising for more complex analysis of 3D biomaterials-cells interactions for tissue engineering purposes.

5.6. ACKNOWLEDGMENTS

M.B. Oliveira acknowledges Fundação para a Ciência e para a Tecnologia for the PhD grant SFRH/BD/71396/2010.

5.7. REFERENCES

[1] Place ES, Evans ND, Stevens MM. Complexity in biomaterials for tissue engineering. Nat Mater. 2009;8:457-70.

[2] Macarron R, Hertzberg RP. Design and Implementation of High Throughput Screening Assays. Mol Biotechnol. 2011;47:270-85.

[3] Moraes C, Wang G, Sun Y, Simmons CA. A microfabricated platform for high-throughput unconfined compression of micropatterned biomaterial arrays. Biomaterials. 2010;31:577-84.

[4] Kranenburg JM, Tweedie CA, van Vliet KJ, Schubert US. Challenges and Progress in High-Throughput Screening of Polymer Mechanical Properties by Indentation. Adv Mater. 2009;21:3551-61.

[5] Burdick JA, Watt FM. High-throughput stem-cell niches. Nature Methods. 2011;8:915-6.

[6] Khan F, Tare RS, Kanczler JM, Oreffo ROC, Bradley M. Strategies for cell manipulation and skeletal tissue engineering using high-throughput polymer blend formulation and microarray techniques. Biomaterials. 2010;31:2216-28.

[7] Hook AL, Anderson DG, Langer R, Williams P, Davies MC, Alexander MR. High throughput methods applied in biomaterial development and discovery. Biomaterials. 2010;31:187-98.

[8] Chen AA, Underhill GH, Bhatia SN. Multiplexed, high-throughput analysis of 3D microtissue suspensions. Integr Biol. 2010;2:517-27.

[9] Jung JP, Moyano JV, Collier JH. Multifactorial optimization of endothelial cell growth using modular synthetic extracellular matrices. Integr Biol. 2011;3:185-96.

[10] Yuan B, Li Y, Wang D, Xie Y, Liu Y, Cui L, et al. A General Approach for Patterning Multiple Types of Cells Using Holey PDMS Membranes and Microfluidic Channels. Advanced Functional Materials. 2010;20:3715-20.

[11] Neto AI, Custodio CA, Song W, Mano JF. High-throughput evaluation of interactions between biomaterials, proteins and cells using patterned superhydrophobic substrates. Soft Matter. 2011;7:4147-51.

[12] Luz GM, Leite AJ, Neto AI, Song WL, Mano JF. Wettable arrays onto superhydrophobic surfaces for bioactivity testing of inorganic nanoparticles. Mater Lett. 2011;65:296-9.

[13] Mei Y, Gerecht S, Taylor M, Urquhart AJ, Bogatyrev SR, Cho S-W, et al. Mapping the Interactions among Biomaterials, Adsorbed Proteins, and Human Embryonic Stem Cells. Advanced Materials. 2009;21:2781-6.

[14] Griffith LG, Swartz MA. Capturing complex 3D tissue physiology in vitro. Nat Rev Mol Cell Biol. 2006;7:211-24.

[15] Huang NF, Patlolla B, Abilez O, Sharma H, Rajadas J, Beygui RE, et al. A matrix micropatterning platform for cell localization and stem cell fate determination. Acta Biomaterialia. 2010;6:4614-21.

[16] Fisher OZ, Khademhosseini A, Langer R, Peppas NA. Bioinspired Materials for Controlling Stem Cell Fate. Accounts Chem Res. 2010;43:419-28.

[17] Neuss S, Apel C, Buttler P, Denecke B, Dhanasingh A, Ding X, et al. Assessment of stem cell/biomaterial combinations for stem cell-based tissue engineering. Biomaterials. 2008;29:302-13.

[18] Yang Y, Bolikal D, Becker ML, Kohn J, Zeiger DN, Simon CG. Combinatorial polymer scaffold libraries for screening cell-biomaterial interactions in 3D. Advanced Materials. 2008;20:2037-43.

[19] Chatterjee K, Sun L, Chow LC, Young MF, Simon Jr CG. Combinatorial screening of osteoblast response to 3D calcium phosphate/poly(epsilon-caprolactone) scaffolds using gradients and arrays. Biomaterials. 2011;32:1361-9.

[20] Chatterjee K, Lin-Gibson S, Wallace WE, Parekh SH, Lee YJ, Cicerone MT, et al. The effect of 3D hydrogel scaffold modulus on osteoblast differentiation and mineralization revealed by combinatorial screening. Biomaterials. 2010;31:5051-62.

[21] Oliveira N, Neto AI, Song W, Mano JF. Two-Dimensional Open Microfluidic Devices by Tuning the Wettability on Patterned Superhydrophobic Polymeric Surface. Applied Physics Express. 2010;3:085205.

[22] Song W, Veiga DD, Custódio CA, Mano JF. Bioinspired Degradable Substrates with Extreme Wettability Properties. Advanced Materials. 2009;21:1830-4.

[23] Alves NM, Shi J, Oramas E, Santos JL, Tomás H, Mano JF. Bioinspired superhydrophobic poly(L-lactic acid) surfaces control bone marrow derived cells adhesion and proliferation. Journal of Biomedical Materials Research Part A. 2009;91A:480-8.

[24] Ballester-Beltran J, Rico P, Moratal D, Song W, Mano JF, Salmeron-Sanchez M. Role of superhydrophobicity in the biological activity of fibronectin at the cell-material interface. Soft Matter. 2011;7:10803-11.

[25] Mano JF, Silva GA, Azevedo HS, Malafaya PB, Sousa RA, Silva SS, et al. Natural origin biodegradable systems in tissue engineering and regenerative medicine: present status and some moving trends. J R Soc Interface. 2007;4:999-1030.

[26] Discher DE, Mooney DJ, Zandstra PW. Growth Factors, Matrices, and Forces Combine and Control Stem Cells. Science. 2009;324:1673-7.

[27] Oliveira MB, Song W, Martin L, Oliveira SM, Caridade SG, Alonso M, et al. Development of an injectable system based on elastin-like recombinamer particles for tissue engineering applications. Soft Matter. 2011;7:6426-34.

[28] Oliveira SM, Song W, Alves NM, Mano JF. Chemical modification of bioinspired superhydrophobic polystyrene surfaces to control cell attachment/proliferation. Soft Matter. 2011;7:8932-41.

[29] Coates J. Interpretation of Infrared Spectra, A Practical Approach. In: Meyers RA, editor. Encyclopedia of Analytical Chemistry: John Wiley & Sons Lda; 2000. p. 10815-37.

[30] Uludag H, De Vos P, Tresco PA. Technology of mammalian cell encapsulation. Adv Drug Deliv Rev. 2000;42:29-64.

[31] Li ZS, Ramay HR, Hauch KD, Xiao DM, Zhang MQ. Chitosan-alginate hybrid scaffolds for bone tissue engineering. Biomaterials. 2005;26:3919-28.

[32] Chen GP, Ushida T, Tateishi T. A hybrid network of synthetic polymer mesh and collagen sponge. Chem Commun. 2000;16:1505-6.

[33] Miralles G, Baudoin R, Dumas D, Baptiste D, Hubert P, Stoltz JF, et al. Sodium alginate sponges with or without sodium hyaluronate: In vitro engineering of cartilage. J Biomed Mater Res. 2001;57:268-78.

[34] Correia CR, Moreira-Teixeira LS, Moroni L, Reis RL, van Blitterswijk CA, Karperien M, et al. Chitosan Scaffolds Containing Hyaluronic Acid for Cartilage Tissue Engineering. Tissue Eng Part C-Methods. 2011;17:717-30.

[35] Angele P, Muller R, Schumann D, Englert C, Zellner J, Johnstone B, et al. Characterization of esterified hyaluronan-gelatin polymer composites suitable for chondrogenic differentiation of mesenchymal stem cells. J Biomed Mater Res Part A. 2009;91A:416-27.

[36] Young BR, Pitt WG, Cooper SL. Protein adsorption on polymeric biomaterials I. Adsorption isotherms. J Colloid Interface Sci. 1988;124:28-43.

[37] Alvarez-Lorenzo C, Concheiro A, Dubovik AS, Grinberg NV, Burova TV, Grinberg VY. Temperature-sensitive chitosan-poly(N-isopropylacrylamide) interpenetrated networks with enhanced loading capacity and controlled release properties. J Control Release. 2005;102:629-41.

[38] Kim I-Y, Yoo M-K, Kim B-C, Kim S-K, Lee H-C, Cho C-S. Preparation of semi-interpenetrating polymer networks composed of chitosan and poloxamer. International Journal of Biological Macromolecules. 2006;38:51-8.

[39] Shea LD, Wang D, Franceschi RT, Mooney DJ. Engineered Bone Development from a Pre-Osteoblast Cell Line on Three-Dimensional Scaffolds. Tissue Engineering. 2000;6:605-17.

[40] Engler AJ, Sen S, Sweeney HL, Discher DE. Matrix Elasticity Directs Stem Cell Lineage Specification. Cell. 2006;126:677-89.

CHAPTER 6. COMBINATORIAL ON-CHIP STUDY OF MINIATURIZED 3D POROUS SCAFFOLDS USING A PATTERNED SUPERHYDROPHOBIC PLATFORM[5]

6.1. ABSTRACT

One of the main challenges in tissue engineering (TE) is to obtain optimized products, combining biomaterials, cells and soluble factors able to stimulate tissue regeneration. Multiple combinations may be considered by changing the conditions among these three factors. The unpredictable response of each combination requires time-consuming tests. High-throughput methodologies have been proposed to master such complex analysis in TE. Usually, these tests are performed using cells cultured into two-dimensional biomaterials or by dispensing arrays of cell loaded hydrogels. We propose for the first time the on-chip combinatorial study of 3D miniaturized porous scaffolds using a patterned bioinspired superhydrophobic platform. Arrays of biomaterials are dispensed and processed in situ as porous scaffolds with distinct composition, surface characteristics, porosity/pore size and mechanical properties. On-chip porosity, pore size and mechanical properties of scaffolds based on chitosan and alginate are assessed by adapting microcomputed tomography equipment and a dynamic mechanical analyzer - and cell response after 24 hours. The interactions between cell types of two distinct origins – osteoblast-like and fibroblasts - and the scaffolds modified with fibronectin are studied by image-based methods and validated by comparison with conventional destructive methods (dsDNA quantification and MTS tests). Physical and biological on-chip analyses are coherent with the conventional measures, and conclusions about the most favorable conditions for each cell type are taken.

We believe this type of chips will have a wide range of applications in distinct areas such as cell-materials interactions studies, tracking of nanoparticles internalization for cell differentiation or gene therapy and high-throughput analysis of the effect of different types of irradiation and drugs in tumor cell death.

[5]This chapter was based on the publication: Oliveira MB, Salgado CL, Song WL, Mano JF. Combinatorial On-Chip Study of Miniaturized 3D Porous Scaffolds Using a Patterned Superhydrophobic Platform. Small. 2013;9:768-78.

6.2. INTRODUCTION

The achievement of the fast regeneration of injured tissues is the ultimate goal of tissue engineering (TE). Although in the last decades the research in this area undergone significant progress, the achievement of fully effective systems for the regeneration of body tissues is still unaccomplished. This research is mainly based in trial/error logic and usually a low number of conditions are tested in each study. However, the complete understanding of the therapeutic potential of a given system requires the full study of all possible combinations as each of them lead to unpredictable results.[1,2] The large number of combinations of biomaterials, cells and other stimuli that can be varied during a TE system development make this area especially resource spending.

In order to facilitate the rapid and effective study of complex TE systems, the miniaturization and automation of experimental systems to a lab-on-chip scale has been proposed.[3,4] Nonetheless, most manufacturing approaches for high-throughput analysis involve costly setups, lengthy fabrication processes and non-versatile platforms. Most of cell-biomaterials combinatorial assays have been performed in 2D substrates, that is: biomaterials are dispensed as thin coatings in specific regions of chips and cells are put over such spots [5]. However, in the physiological environment cells are located in three-dimensional (3D) media, interacting with the extracellular matrix and with neighboring cells. Several studies have shown that most adherent cells respond differently if cultured in 2D or 3D substrates, according to the physicochemical properties of the substrate [6-10]. As such, the sought response of a cell may be dependent on a specific 3D niche. Therefore, in this work emphasis will be mainly to combinatorial assays of cell/3D biomaterials relationships study.

The design of 3D biomaterials for TE has been proposed most commonly as hydrogels and porous scaffolds. Hydrogels are the most commonly used biomaterials for the study of cell response in array-based high-throughput analysis systems since they allow for cell encapsulation [11], permitting a one-step preparation of the arrayed spots. However, their network properties may be difficult to optimize in order to have adequate mechanical strength, permit cell migration and proliferation and allow for nutrients/waste transport in the matrix [12,13], which may impair the biocompatibility of the structures [14] Porous scaffolds have a structural organization with interconnected pores having pore sizes in the order of 100 μm or higher, in order to allow simultaneously cell proliferation and migration, as well as efficient nutrients and waste exchanges in the structure [15-17]. Their mechanical properties can be modulated as a function of a wide diversity of factors, such as porosity and pores architecture control, crosslinking, crystallization degree and materials compositions. The high-throughput combinatorial study of 3D porous scaffolds has been mainly performed using commercially available well plates,

although they present stiff and high walls, impairing analysis that require the insertion of probes, passage of beams through the biomaterials or image analysis.

We propose the use of a completely flat platform based on micro- and nano-textured superhydrophobic surfaces patterned with hydrophilic spots for the innovative on-chip study of 3D porous scaffolds. This platform - in which the size and shape of the spots containing biomaterials can be varied simply by modifying the patterning of the exposing regions of a photomask - allows for the fabrication of miniaturized scaffolds owning representative number of pores suitable for TE applications. We consider that the size of the 3D porous samples should be in the millimetric order so that a representative number of pores can exist in the structure. The liquid precursor(s) of the biomaterials are aqueous solutions dispensed in the hydrophilic patterns, which are kept in the hydrophilic region due to the contrast of surface tension between the hydrophilic region and the surrounding superhydrophobic surface.

To prove the suitability of the developed platform in the study of porous scaffolds, we propose the fabrication of combinatorial chitosan (Chi)/alginate (Alg) scaffolds by a complexation reaction and in-situ neutralization, followed by freeze-drying. Both polymers are widely used for TE purposes [18]. Furthermore, the addition of Alg to Chi was proven to improve elastic modulus values and porosity in scaffolds [19]. For the analysis of the porosity and pore size of the scaffolds in the chips, a microcomputed tomography (μCT) equipment was adapted for the rapid, in situ, and non-destructive assessment of this information. Adherent cells have shown to respond to mechanical characteristics of the substrates [6,20]. For the analysis of the viscoelastic behavior of the polymeric scaffolds, conventional dynamic mechanical analysis (DMA) equipment was modified and adapted for rapid, non-destructive in situ testing of the different scaffolds.

For the proof-of-concept, we report the study of 18 Chi:Alg combinations using the bioinspired combinatorial platform. After a first screening step restricted to physical properties of the scaffolds, a new array was prepared based in the previously selected conditions with gradients of adsorbed fibronectin (Fn), in order to demonstrate that the proposed methodology may be used to test scaffolds with multiple compositions and distinct surface treatments. Finally, the cytocompatibility of the scaffolds for fibroblast and osteoblast-like cell lines was studied by image-based methods that allowed keeping the chip integrity, and validated with conventional chip-destructive techniques.

6.3. RESULTS

6.3.1. Preparation of the superhydrophobic patterned chips with 3D porous scaffolds

A platform consisting of a superhydrophobic biomimetic substrate with hydrophilic patterns described in previous studies [21,22] was used to test the mechanical/morphological properties of 3D porous scaffolds, as well as their cytocompatibility using two cell lines. Briefly, PS was treated by phase-separation in order to present a contact angle higher than 150° simply by the introduction of micro- and nano-roughness, without any chemical modification of the polymeric structure [23]. Hydrophilic patterns were obtained after 20 minutes of UVO exposure through a photomask.

Porous scaffolds were prepared using two polymers of natural marine origin: Chi and Alg. Both were previously used in a wide range of studies for TE purposes [24-26] and present opposite charges. These characteristics were used in order to promote complexation between both polymers. In Figure 6.1B an image of the LMW Chi array can be seen after eosin staining (which stains Chi), whose intensity is higher for the scaffolds richer in Chi. Nomenclature and abbreviations for scaffolds' combinations are explained in Experimental Section.

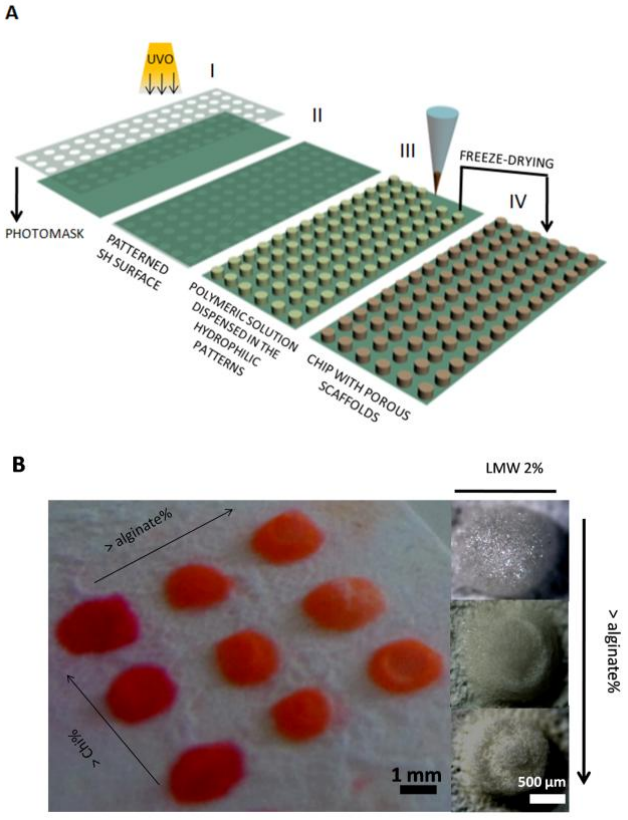

Figure 6.1. – (A) Schematic representation of the procedure performed to obtain patterned superhydrophobic surfaces with arrayed hydrophilic patterns by UVO exposure, followed by deposition of polymeric solutions: I and II) generation of the PS superhydrophobic surface with patterned hydrophilic spots by exposure to UV/Ozone

irradiation through the hollows for a plastic mask; III) deposition of polymeric solutions in the hydrophilic spots and IV) freeze-drying of the polymeric solutions, resulting in porous scaffolds. (B) Picture of part of an array of LMW Chi scaffolds stained with eosin (left) and zoom view of LMW 2% scaffolds (right).

6.3.2. On-chip mechanical and porosity/pore size characterization of the scaffolds

A gutter was assembled on the DMA equipment, as a well as a probe to establish contact with the scaffolds (see Figure 6.2, scheme).

Chips of 9 scaffolds produced either with low molecular weight (LMW) Chi or medium molecular weight (MMW) Chi were tested in µCT equipment. The values of porosity obtained directly in the chip were validated by two controls. The first control aimed to exclude the effect of the relative position of the 3D porous scaffold in the chip; a chip composed of 3 equal scaffolds in 3 distinct positions distributed in a horizontal line was tested both for compressive dynamic elastic modulus (*E'*) by DMA and for porosity/pore size using a µCT. The second control measure aimed to check for the representativeness of the miniaturized scaffolds built on the chip; 3D scaffolds with analogous composition to the miniaturized ones were prepared in 96 well-plates (Figure 6.3), a conventional scaffold preparation method.

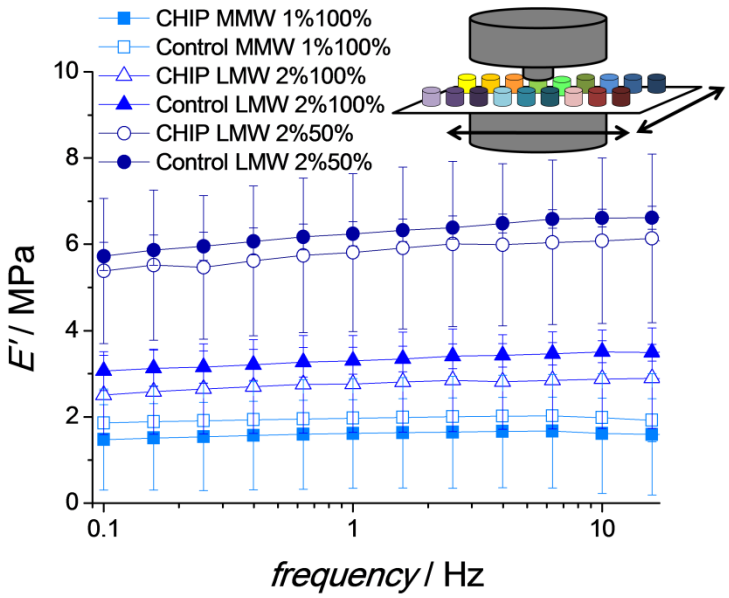

Figure 6.2. – *E'* of the scaffolds conditions analyzed in Figure 6.2, using on-chip samples and control samples produced using commercially available 96 well plates. Schematic representation of the modification performed in the DMA equipment for the in-situ analysis of the scaffolds dispensed in the chip (up).

The *E'* values at 1 Hz for each sample - both in-chip (Figure 6.5A) and in control samples fabricated in 96-well plates (Figure 6.5B) - are presented in Figure 6.5 as intensity maps. For all polymeric combinations the *E'* measured in-chip and in control samples processed by a conventional method follows similar tendencies and presents similar values. Considering the slight increase of the *E'* with increasing frequency, the behavior of on-chip tested samples and the behavior of conventionally processed controls is similar (see plot from Figure 6.3).

Regarding the study of the relative position of the scaffolds in the chip, *E'* values were acquired for three MMW1% Chi 100Chi:0Alg scaffolds disposed in a horizontal line in a chip. Scaffolds in different positions showed similar *E'* values (see Figure 6.4A).

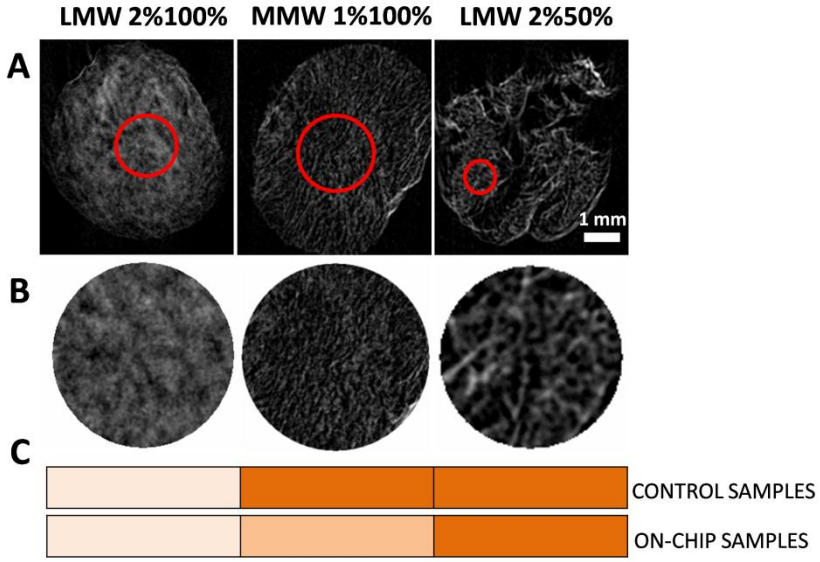

Figure 6.3. – (A) Tomographs obtained by µCT of three different control scaffolds produced in commercially available 96 well plates, (B) respective different sized selected zones used for the generation of slice replicas for the reconstruction of the structure and calculation of porosity and (C) intensity map corresponding to the interval of values for the porosity of the analyzed samples, according to the values/colour relationship defined in Figure 6.5.

Figure 6.5 shows general tendencies in *E'* values for both LMW100%Chi and MMW100%Chi samples. The increase in Chi concentration from 1% to 2%Chi led to an increase in the average *E'*. *E'* tends to increase with the addition of Alg, although with different tendencies in LMW and MMW Chi formulations. In LMW Chi combinations, the addition of Alg to Chi led to an increase in *E'* of the structures, mainly in the 50Chi:50Alg conditions. Regarding MMW Chi combinations, in 1% Chi scaffolds the highest *E'* value

was registered in the 50Chi:50Alg condition. In 1.5% and 2% Chi condition the stiffer conditions were 75Chi:25Alg, although in the 2%Chi conditions all the structures presented high *E'*.

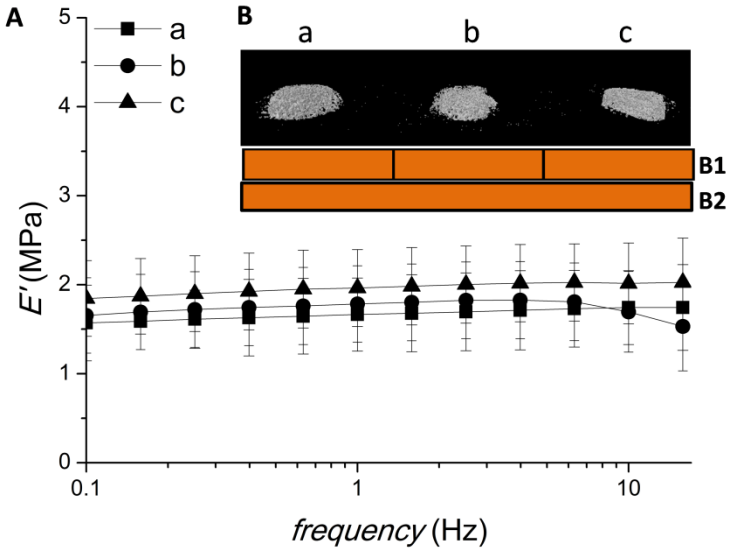

Figure 6.4. – (A) On-chip determined *E'* of the three scaffolds of the control chip. (B) µCT reconstruction of the scaffolds of the condition MMW 1% 100Chi:0Alg produced in the control chip with 3 equivalent scaffolds. In the lower part of the reconstructions the color corresponding to the interval of the porosity of the intensity map of Figure 6.2 is represented for (B1) the three equal scaffolds evaluated in the control chip and (B2) the scaffold evaluated in the combinatorial chip containing the 9 formulations of LMW Chi scaffolds.

Regarding the analysis of the porous structure of each scaffold, the values obtained on-chip for LMW and MMW scaffolds can be seen in Figure 6.5. Figure 6.5I, obtained by µCT, shows representative binary images obtained for the reconstruction of the LMW Chi-containing scaffolds on-chip.

Similar porosity values were obtained in the control chip containing 3 equally produced scaffolds aligned horizontally (Figure 6.4B1). Also, the values obtained for 3 randomly selected control scaffolds produced in 96 well plates ranged the same interval of values of the on-chip produced scaffolds (Figure 6.3 and 6.5, respectively).

In the case of 100Chi:0Alg scaffolds, the increasing Chi concentration led to lower porosity values, both in LMW and MMW compositions. Regarding the LMW Chi compositions containing Alg, in the 75Chi:25Alg formulation the increasing concentration of Chi – from 1% to 1.5% and 2% - led to an increase of porosity from 40-50% to 60-70%. In the 50Chi:50Alg formulation, the increase of porosity was observed from the 1.5%Chi formulation to the 2%Chi formulation.

In the MMW Chi compositions, a gradual increase in porosity was verified in the 75Chi:25Alg formulation from 1% to 2%Chi. In the 50Chi:50Alg formulations, the 1%Chi scaffold presented a high porosity (60-70%), as well as the 2%Chi formulation. The 1.5%Chi formulation presented a lower porosity value, in the 50-60% interval.

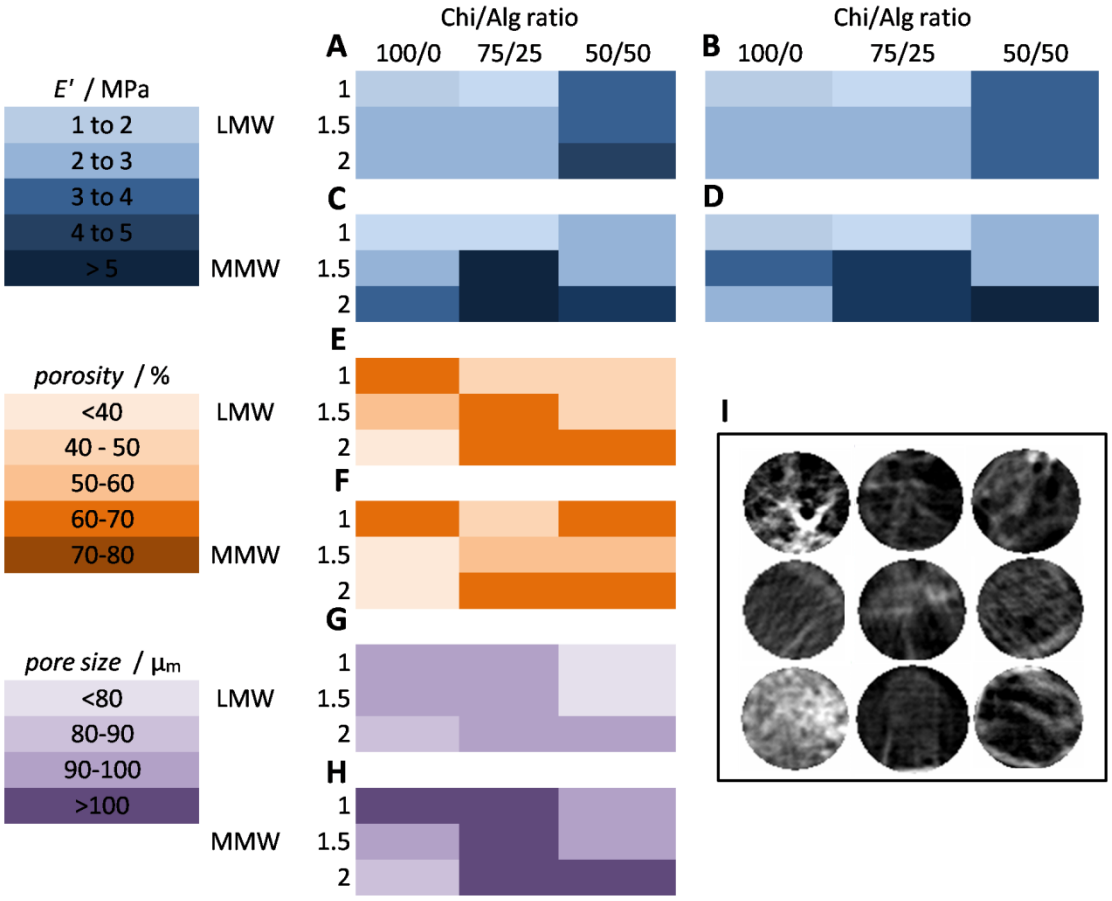

Figure 6.5. – (A) Intensity map with the interval values of *E'* obtained on DMA on-chip for scaffolds produced with LMW Chi; (B) intensity map with the interval of *E'* values obtained on-chip for scaffolds produced with MMW Chi. Intensity map with the interval of (C) *E'* values obtained for scaffolds produced in 96 well plates (conventional method) for scaffolds produced with LMW Chi; (D) *E'* values obtained for scaffolds produced in 96 well plates for scaffolds produced with MMW Chi; (E) porosity values obtained on-chip by µCT for scaffolds produced with LMW Chi (F) porosity values obtained on-chip by µCT for scaffolds produced with MMW Chi; (G) pore size values obtained on-chip by µCT for scaffolds produced with LMW Chi; (H) pore size values obtained on-chip by µCT for scaffolds produced with MMW Chi. (I) Representative replicas of the slices obtained by cone beam acquisition performed during the on-chip µCT analysis for the scaffolds produced with LMW Chi.

Pore size values obtained for the scaffolds using µCT are represented in Figure 6.5G,H.

A graphic correlating the *E'* and porosity values and respective standard deviations for both LMW and MMW Chi formulations is shown in Supporting Information (Figure 6.S1).

6.3.3. Fn adsorption on 3D porous scaffolds

Fn was labeled with a red fluorescent molecule in order to qualitatively study the protein adsorption in different concentrations in each formulation - see Figure 6.6A. Figure 6.6B presents the image-based fluorescence quantification in each image. Increasing fluorescence intensity can be observed with increasing amount of Chi in all formulations exposed to Fn. We could observe that in 100Chi:0Alg samples, the amount of adsorbed Fn seems to increase with the increasing concentration of the Fn solution. A similar tendency can be seen in the 75Chi:25Alg combination. However, higher concentration of Fn is needed to reach a maximum level of adsorption, which is lower than the one achieved in the 100Chi:0Alg condition. In the case of 50Chi:50Alg condition, the adsorption of Fn was kept in the lowest levels, even with increasing concentration of Fn.

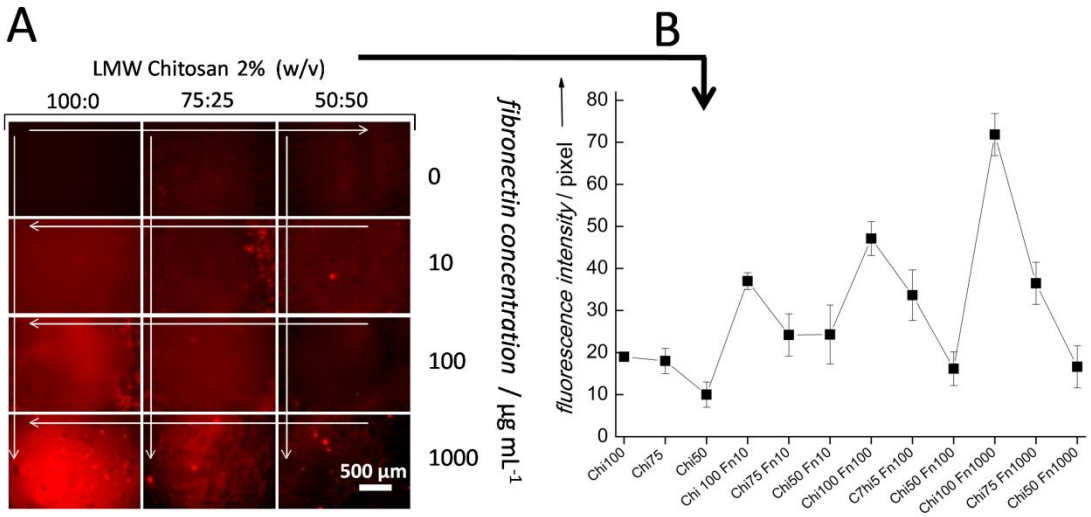

Figure 6.6. – (A) Fluorescence microscopy images of the array LMW 2%Chi scaffolds after physical adsorption of Fn in different concentration. (B) Pixel intensities of the Fn adsorption images, measured in ImageJ software.

6.3.4. On-chip cell culture of fibroblast and osteoblast-like cell lines

The behavior of two cell types – L929 fibroblast and SaOs-2 osteoblast-like cell lines – was assessed using techniques compatible with the maintenance of the integrity of the samples in the chip. In order to validate these techniques – based on image analysis – the scaffolds were removed from the platform and analyzed individually by conventional tests in order to assess cell metabolic activity and cell number. For this comparison, L929 cells were seeded in a rate of $9x10^4$ cells/spot. The tendencies between dsDNA quantification (Figure 6.7 A1) and image-based quantification of cell nuclei through DAPI staining (Figure 6.7 A2) were similar. In the case of cell seeding in scaffolds not exposed to Fn, the cell number registered in the 100Chi:0Alg scaffolds was lower than the one observed in 75Chi:25Alg scaffolds, which, by its turn, was lower than the one registered in 50Chi:50Alg scaffolds. Fn adsorption

promoted a significant increase in cell number for 100Chi:Alg0 and 50Chi:50Alg scaffolds, with the use of more concentrated solutions of Fn: 100 µg/mL and 1 mg/mL. In all conditions cell death presented low values: cell viability was higher than 96% in all formulations.

The behavior of L929 and SaOs-2 cell lines was compared using a lower cell seeding number: $1.5x10^4$ cells/spot. In general, the number of SaOs-2 cells adhered to the scaffolds was lower than the number of L929 cells in the same conditions. Regarding L929 cells, in the absence of Fn the cell number was lower in the 75Chi:25Alg condition. In general, in the whole experiment, the condition that led for lower cell number for L929 cell line was also this one. Nonetheless, Fn concentrations of 100 µg/mL and 1 mg/mL allowed for an increase in cell adhesion. In 100Chi:0Alg condition, an increase in cell adhesion was verified in 1 mg/mL Fn condition. In 50Chi:50Alg conditions, adsorption with solutions of 10 µg/mL and higher concentrations of Fn increased cell adhesion (Figure 6.8).

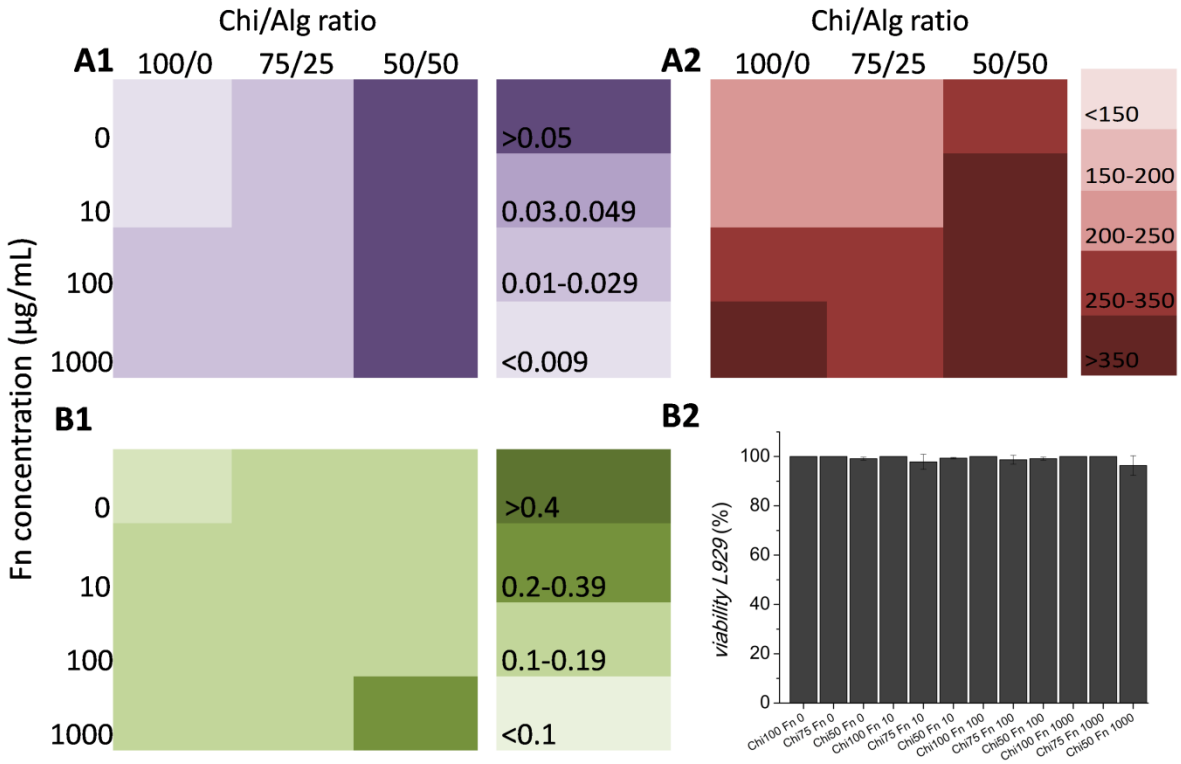

Figure 6.7. – Intensity maps of the values of (A1) dsDNA quantification of the individual scaffolds of the 2%LMW Chi chip with gradients of adsorbed Fn using L929 cell line with a cell seeding number of $9x10^4$/scaffold, (A2) image-based nuclei quantification on the 2%LMW Chi chip with gradients of adsorbed Fn using L929 cell line with a cell seeding number of $9x10^4$/scaffold, (B1) MTS reduction test of the individual scaffolds of the 2%LMW Chi chip with gradients of adsorbed Fn using L929 cell line with a cell seeding number of $9x10^4$/scaffold, (B2) on-chip calculated cell viability on each scaffold of the 2%LMW Chi chip with gradients of adsorbed Fn using L929 cell line with a cell seeding number of $9x10^4$/scaffold, obtained by image-based quantification of dead cells.

In the absence of Fn, SaOs-2 number was higher in the 50Chi:50Alg condition and lower in 75Chi:25Alg scaffolds (Figure 6.8). In all conditions, in 100 µg/mL condition, the higher number of cells was observed in the scaffolds. In the 100Chi:0Alg condition, Fn adsorption from 10 µg/mL showed a positive effect in the number of cells in the scaffolds, while in 75Chi:25Alg and 50Chi:50Alg conditions the positive effect of protein adsorption was only verified in 100 µg/mL and 1 mg/mL conditions.

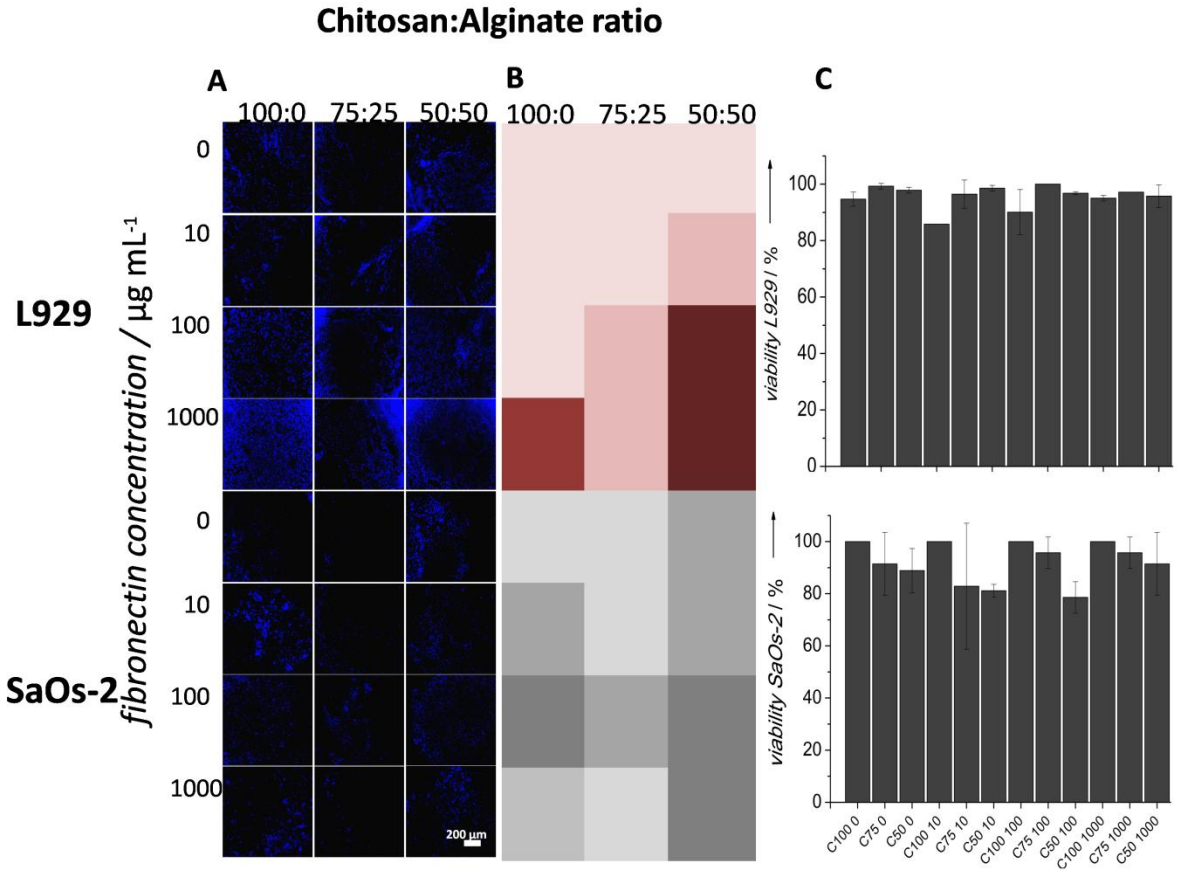

Figure 6.8. – (A) Images of the on-chip produced scaffolds (2%LMW Chi scaffolds with gradients of adsorbed Fn) with L929 and SaOs-2 cell nuclei stained with DAPI with a cell seeding number of 1.5x10^4/scaffold. (B) Intensity maps of image-based quantification of cell nuclei. (C) On-chip calculated cell viability on each scaffold of the 2%LMW Chi chip with gradients of adsorbed Fn with a cell seeding number of 1.5x10^4/scaffold, obtained by the image-based quantification of dead cells.

Comparing both essays performed with L929 cell line, the effect of the cell seeding number can be observed. In the experiment performed with 9x10^4 cells/scaffold, the cell number quantified in each scaffolds was, in general for all conditions, higher than the cell number quantified in the experiment performed with 1.5x10^4 cells/scaffold. However, in the 50Chi:50Alg conditions with 100 µg/mL and 1 mg/mL of Fn, the values obtained in both experiments are equally high. The general tendencies of cell behavior are similar for both experiments (Figure 6.7 A2 and 6.8B).

The exact numerical values and respective standard deviations of the experiments with the L929 and SaOs-2 cell lines are registered in Supplementary Data (Figures 6.S2 and 6.S3).

6.3.5. Balance of costs and time saving

The performance of mechanical and morphological characterization as well as cell response studies in 3D porous scaffolds using patterned flat superhydrophobic platforms was time and cost saving. The total volume of solutions used to produce each scaffold in the chip corresponded to 1/50 of the volume of solution used for the preparation of the controls in 96 well plates. The cost reduction permitted by the use of the platform was not only applicable to the amount of biomaterials, but also to the proteins and biological materials, which amount is also proportional to the size of the scaffolds.

An effective time saving of 9x was achieved during the μCT analysis during image acquisition step: the individual acquisition of each control took about 90 minutes and the on-chip acquisition permitted the simultaneous acquisition of 9 samples. By the reduction of samples size as well as by a controlled decreased in image resolution, this analysis may be up-scalable by increasing the number of scaffolds analyzed simultaneously.

6.4. Discussion

We propose the use of polystyrene (PS) superhydrophobic surfaces patterned with hydrophilic regions for the study of 3D porous biomaterials-cells combinations. The liquid biomaterial precursors were restricted in the hydrophilic regions due to the contrast of surface tensions, as proven before in studies of protein-cells interactions in two-dimensional (2D) environment [21] and in a study with 3D cell-laden hydrogels [22]. This method is versatile and overcomes several drawbacks of array platforms reported in the state of the art, as discussed previously [22]. Microarrays developed for high-throughput analysis – obtained, for example, by techniques such as contact printing [27] or ink-jet printing [28] – are usually composed of array-unit with sizes correspondent to a single pore of a porous scaffold for TE. As such, the possibility of having a significant number of pores in a structure is incompatible with these techniques. The proposed solutions for this problem are combinatorial studies of porous biomaterials have been performed in commercially available well plates [29], leading to high amounts of used materials and samples manipulation, increasing contamination probability.

The platform proposed herein is composed only by pure PS: the gold-standard for two-dimensional *in vitro* cell culture studies. The superhydrophobic surfaces are obtained by a phase-inversion reaction, as previously described [23], and the final product is physically-treated PS showing micro and nano-

roughness. The introduction of molecules or the release of toxic leachables is totally avoided in this process. PS superhydrophobic surfaces were reported to weaken cell adhesion [30,31] and to impair the proliferation of several cell types [30]. The risk of cell crosstalk or cell passage is decreased due to the anti-adherent and anti-proliferative characteristics of the surface in between the spots containing the porous scaffolds.

Mechanical analysis of biomaterials in high-throughput chips is usually performed using nanoindentation equipment [32]. However, conventional nano-/micro-indentation methods for calculation of modulus of elasticity are limited to linear, isotropic materials and cannot be used in porous millimetric-sized structures. Problems associated with the "pile-up" or "sink-in" of the material on the edges of the indent during the indentation process remains a problem [33]. Traditional mechanical analysis equipments provide information about the stiffness of the tested material (such as the elastic modulus) and the brittleness of the materials (such as maximum tension). Dynamic mechanical analysis (DMA) equipments allow for a sensitive and complementary non-destructive characterization of mechanical/viscoelastic properties of the materials. DMA equipments also enable testing the materials' properties in wet or physiological-like conditions [34], permitting to get a better perception on the performance of the device *in vivo*.

Regarding the essays consisting of the on-chip measurements of E' of 3 scaffolds aligned in an x-axis, we concluded that the relative positions of the scaffolds did not have significant influence in the measured value of the E' (Figure 6.4).

An increase in E' both in LMW100%Chi and MMW100%Chi with the increasing Chi concentration from 1% to 2%Chi was expected due to the lower porosity generated by the higher concentration of material in the scaffold. In fact, a tendency for decreasing porosity from 1% to 2%Chi scaffolds was verified, along with an increase in E' values (see Figure 6.5A).

Also as expected, addition of Alg to Chi led to an increase in compressive E' values [19]. However, this increase was observed in different extents comparing both molecular weight Chi scaffolds. In the 1%Chi LMW Chi combinations, the increase in E' could be observed with the increasing amount of Alg added to Chi. This was accompanied by a decrease in porosity, suggesting that the increase of E' resulted probably from a collapse of the porous structure. Increasing E' was also observed with increasing amounts of Alg in the case of 1.5%Chi scaffolds. In the 75Chi:25Alg condition, the increase of E' was accompanied by an increase in porosity. However, in the 50Chi:50Alg condition, a decrease in porosity of the scaffolds was again verified, suggesting that for 1.5%Chi scaffolds the collapse of the porous

structure occurs. Also, for both 1%Chi and 1.5%Chi scaffolds, the pore size of the 50:50 scaffolds decreased, corroborating the scaffold collapse hypothesis (Figure 6.5G,H).

In the sub-array consisting of scaffolds produced from 2%Chi, an increase in *E'* is observed with the increasing content of Alg in the scaffold - mainly in the 50Chi:50Alg condition - and the porosity of the structures is higher in the Alg-containing formulations. As such, in this sub-array the mechanical properties of the scaffolds seem to be independent of the porosity of the scaffold, being essentially influenced by its chemical composition. The higher *E'* in 50Chi:50Alg condition may be explained by the higher degree of complexation between the two polyelectrolytes, comparing with 75Chi:25Alg conditions. Due to the stoichiometric ratio between polymers in this condition, the degree of complexation reaction is expected to be lower than in 50Chi:50Alg. It has been shown that structures obtained by complexation, due to the tight ionic bond formed between polymers [35] and depending on the variation of processing variables, may present high mechanical properties suitable for potential application in tissue regeneration [36,37].

LMW2%Chi sub-array scaffolds present distinct properties- Figure 6.5: a scaffold exhibiting low *E'* and low porosity (100Chi:0Alg), a scaffold with low *E'* and high porosity (75Chi:25Alg) and a scaffold with high *E'* and high porosity (50Chi:50Alg).

Regarding MMW Chi combinations, the collapse of the structures seem to have been avoided in all the formulations, since the increase in the *E'* of the scaffolds with increasing amounts of Alg was accompanied with increasing porosity values. Moreover, pore size values did not decrease with the increasing amount of Alg in any of the conditions. In the 1%Chi and 1.5%Chi conditions, the stiffer conditions were the ones of 75Chi:25Alg formulations. In the 2%Chi conditions, all the structures presented high *E'*, and only 100Chi:0Alg conditions presented a low porosity, as expected, due to the absence of Alg in its composition.

Regarding μCT analysis, a chip with three equally produced scaffolds of the condition MMW1%Chi 100Chi:0Alg was used as a control. This was performed to exclude the possibility of the relative position of the scaffolds in the platform affect the image acquisition of each structure. We concluded that the values obtained for the three scaffolds were consistent and similar. Moreover, these were consistent with the value of porosity measured for the condition MMW1%Chi 100Chi:0Alg measured in the chip containing all the 9 different MMW Chi conditions.

For the samples prepared using 96 commercially available well plates, the obtained results for both on-chip collected results and individual control samples were in general consistent (Figure 6.5).

As the LMW2%Chi sub-array presented a high diversity of porosity/*E'* properties, it was selected for further analysis in terms of protein adsorption and cell response.

In the biological environment, biomaterials interact with many different components. Proteins are of prime importance for the biointerface since most cell structures and functions depend on protein assembly and activity. The interactions between proteins and material surfaces involve a variety of intermolecular interactions, namely hydrophobic interactions, electrostatic interactions, coordination bonding and molecular recognition. Protein adsorption is also influenced by surface topography and is generally observed that protein adsorption increases with increasing surface hydrophobicity [38]. Surface modification of biomaterials by physical adsorption avoids complicated reactions using toxic reagents. Fn contains the site for αv-β3 integrin-binding: the arginine-glycine-aspartic acid (RGD) domain [39], involved in an effective cell adhesion, which determines cell survival and further proliferation. The effect of physical adsorption of Fn was investigated using the array-based methodology.

The progressive increasing proportion of Alg in the formulations led to an apparent decrease in the adsorption of Fn in the scaffolds (Figure 6.6). This may be explained by the higher hydrophobicity of Chi compared to Alg. Chi films were reported to show water contact angles around 80°, while Alg showed a higher hydrophilicity, with a contact angle around 20° [40]. Moreover, while in 75Chi:25Alg formulations the increasing amount of Fn in the adsorption solutions leads to a higher apparent adsorption in the structures, in the 50Chi:50Alg formulations, - except for 100 μg/mL Fn conditions which presents a higher fluorescence intensity - the adsorption of Fn in the surface of the scaffolds does not seem to depend on the concentration of Fn in solution. This may be explained by a full saturation of the scaffolds with physically adsorbed Fn in the case of immersion with the lowest protein concentration solution, since the affinity of the structure with Fn is lower than in scaffolds with higher amount of Chi.

Cell number and viability were analyzed after 24 hours for L929 cell line, both on-chip by image analysis-based techniques, as well as by methods usually applied in the analysis of single samples. Regarding image-based analysis - which did not require the removal of the scaffolds from the platform - cell number was assessed by counting cell nuclei stained with DAPI in each scaffold using image analysis. Cell viability was assessed by counting the number of cells stained with propidium iodide using a similar methodology. The conventional testing consisted of the analysis of cell metabolic activity by MTS reduction test and dsDNA quantification, which is proportional to cell number in each scaffold. These tests required the removal of the scaffolds from the chip and their individual analysis in separated containers.

The comparison between destructive and non-destructive methods showed that image analysis of DAPI staining of L929 cell line (Figure 6.7) was overall coherent with the dsDNA quantification performed on individual samples. Regarding the ratio of viable and dead cells in the samples the observed cell death was very low in all samples in the case of L929 cell line. The maximum rate of dead cells in these samples corresponded to less than 4% of the total number of cells, showing the non-cytotoxicity of the developed scaffolds. In the absence of cell death in the scaffolds a proportional increase in reduced MTS with increasing cell number would be expectable, considering that all cells are equally metabolically active. However, the values of MTS test were similar for all conditions, except for the condition 50Chi:50Alg 1 mg/mL of Fn. Several studies have reported the limitations of reduction tests with the production of formazan, such as MTS reduction test, in the detection of cell viability [41]. The reduction of the compound is dependent on the metabolic activity of cells, which can vary, as many different conditions can increase or decrease metabolic activity. Also, these tests have been proved to be sensitive in the presence of some agents (including proteins present in the cell culture medium), influencing the final result [42,43]. We conclude that image analysis of dead cells stained with DAPI/propidium iodide gives a more precise indication of effective ratio of adhered/dead cells in samples.

The same parameters were evaluated for L929 and SaOs-2 cell lines seeded in lower number in the scaffolds using image-based criteria. In general, the scaffolds allowed for high cell viability values for both cell lines (Figure 6.8), showing their non-cytotoxicity.

Considering the scaffolds which were not exposed to Fn, the similarity of results of L929 cells observed in all conditions contrasted with the differences observed in the SaOs-2 cell line. SaOs-2 are osteoblast-like cells, and were proven to adhere and proliferate preferably in stiffer substrates [20]. As expected, SaOs-2 cell number was higher in the stiffer condition: 50Chi:50Alg. However, this conclusion was dependent on an analysis of independency between variables affecting the scaffolds. Firstly, the porosity of the samples 75Chi:25Alg and 50Chi:50Alg is similar, excluding the effect of the porosity in the higher cell number present in the 50Chi:50Alg condition. Moreover, the surface chemistry of the scaffolds could also be responsible for more favorable cell-biomaterials interactions. However, if cell behavior was strictly dependent on surface chemistry generated by the presence of Alg in the mixtures, 75Chi:25Alg condition would also present higher cell number than 100Chi:0Alg. As such, we can conclude that SaOs-2 showed a preferable attachment to 50Chi:50Alg non-treated scaffolds due to their higher mechanical properties.

The exposure of the scaffolds of the chips to Fn in different concentrations had different effects according to each cell type. In the case of L929 cells, in the conditions 100Chi:0Alg and 75Chi:25Alg only adsorption of Fn with the most concentrated solution – 1 mg/mL - showed positive effects in the cell number in the scaffolds. In the 50Chi:50Alg condition, the lowest Fn concentration – 10 μg/mL – was enough to cause an increase in cell number, followed by higher cell number in the scaffolds for adsorption with 100 μg/mL and 1 mg/mL solutions (Figure 6.8B). Although the intensity of Fn labeling was lower in the 50Chi:50Alg (Figure 6.8B), the protein in this condition may be in a correct conformation, with a higher number of RGD domains available for the cell membrane integrins. The lack of control over protein conformation resulting of adsorption processes is one of the main drawbacks associated with this technique [44].

In the case of SaOs-2 cells (Figure 6.8), the adsorption of 10 μg/mL of Fn in the 100Chi:0Alg condition led to values of cell number similar to the ones of 50Chi:50Alg without any treatment. In 100 μg/mL Fn conditions, both 100Chi:0Alg and 75Chi:25Alg showed the highest cell numbers. In the condition 50Chi:50Alg, the effect of the adsorption of Fn was noticed in conditions 100 μg/mL and 1 mg/mL, in which the highest values of cell number in the chip were observed. Nonetheless, regarding SaOs-2 seeding in the Chi/Alg scaffolds, it can be concluded that non-linear and theoretically unpredictable tendencies were observed regarding Alg addition to Chi, in scaffolds without any surface modification. Also, adsorption of Fn using low concentrations of the protein allowed increasing the cell number in scaffolds that, without any surface treatment, showed unfavorable interaction with cells.

The possibility of studying 3D porous biomaterials on-chip was proven using arrays of Chi/Alg porous scaffolds produced in patterned superhydrophobic PS surfaces. This study included the in-situ mechanical and morphological characterization of the arrays and their validation by comparison with conventional samples and characterized also using the equipment in a conventional mode. The conclusion from the physical characterization of the scaffolds allowed for a screening of a sub-array of wide mechanical and porosity properties. With this screening, a second cycle of tests was performed, by the development of an array with different amounts of adsorbed Fn in the structures. Protein adsorption qualitative studies were performed, followed by studies on the behavior of two distinct cell types in the structures, which could be performed using image-based techniques.

6.5. Conclusions

We herein proposed the use of a flat platform consisting of a PS superhydrophobic surface patterned with hydrophilic spots for the on-chip study of mechanical, morphological and cell behavior on 3D

miniaturized porous scaffolds for TE. The adaptation of both DMA and μCT was achieved successfully for the data acquisition directly from the elements on the chip. Control tests allowed to conclude that the 3D porous scaffolds produced in the arrayed platform are valid in comparison with scaffolds produced in conventional conditions and sizes. Moreover, these tests also showed that the relative position of the scaffolds in the chip is not relevant for the data collection or analysis. A two-step screening process was carried out: firstly, an array of 3D porous scaffolds was studied on-chip, providing mechanical and morphological information. A sub-array was selected from this selection, and based on these conditions a new array of porous scaffolds with different amounts of adsorbed Fn was prepared. Cell response of two cell types was studied in such array using image-based analysis for assessment of cell number and viability. These measures were validated with conventional destructive tests for cell metabolic activity and quantification of dsDNA. The tendencies observed allowed to conclude which were the most favorable conditions for the culture of each cell type: L929 and SaOs-2. We concluded that this technique allowed for the collection of reliable and valid data, while reducing the experimentation time, costs and samples manipulation.

6.6. EXPERIMENTAL SECTION

6.6.1. Processing of superhydrophobic polymeric substrates

PS flakes were cut from commercially available PS plates (Corning). Tetrahydrofuran (THF) was purchased from Fluka (p.a.>99.5%) and ethanol absolute from Panreac. The surfaces were modified according to the protocol described elsewhere.[13] The wettability of the studied surfaces was assessed by contact angle (CA) measurements, using an OCA15+ goniometer (DataPhysics, Germany) using the Sessile drop method. To produce the patterned chips, the obtained superhydrophobic substrates were treated using a UV/Ozone (UVO) lamp (Bioforce, Nanosciences) for 20 minutes through an aluminum mask with 4 mm2 open squares, separated by 1 mm (Figure 6.1A).

6.6.2. Preparation of the chips and control samples

A solution of 1% (w/v) of low viscosity alginate sodium salt (Sigma) in 1 M sodium hydroxide (NaOH) (Sigma) was prepared. Solutions of both low molecular weight (LMW; 50-190 kDa, as referred by the supplier) and medium molecular weight (MMW; 190-310 kDa, as referred by the supplier) Chi (Sigma) were prepared in concentrations of 1% (w/v), 1.5% (w/v) and 2% (w/v) in 0.33 M acetic acid (Sigma). Both chitosans present a similar degree of decetylation (75-85%).

Control samples were prepared using commercially available 96-well plates. Different amounts of the Chi solutions were dropped in each well, and further mixed with different amounts of Alg leading to 18 different combinations of Alg/Chi in weight proportions of 50%, 75% and 100% of Chi, herein named as: 50Chi:50Alg, 75Chi:25Alg and 100Chi:0Alg, respectively. The prepared solutions were dispensed in each well in individual volumes of 200 μl.

The same Alg:Chi proportions used for the controls were also dispensed in the chips prepared using the patterned superhydrophobic platform. The polymeric solutions were dispensed in the hydrophilic patterns in a drop-by-drop logic, in individual volumes of 4 μl. Control chips with 3 similar scaffolds of MMW 1%Chi 100Chi:0Alg, separated by 2 mm, were prepared.

After the dispensing of the solutions, the chips and the control well-plates were frozen at -20°C for 1 hour, and then kept at -80°C overnight. The samples were then freeze-dried at -80°C for 48 hours. After freeze-drying, the individual controls prepared on the well-plates were removed from the wells. The 100% Chi samples were neutralised by immersion in a solution of 1 M NaOH, and then washed with distilled water, renewed three times. All other samples (Alg/Chi samples) were immersed three times in excess of renewed distilled water for 30 minutes per immersion, right after the removal from the wells, in order to remove the excess of NaOH. In the chips, the 100% Chi samples were neutralized with 2 μl of 1 M NaOH, and right after all the chip was immersed in excess of distilled water in the same conditions as the individual controls. All the samples were then frozen at -20°C for 1 hour, and frozen at -80°C, followed by freeze-drying in the same conditions as described before.

6.6.3. Mechanical characterization: Dynamic mechanical analysis (DMA)

The viscoelastic measurements of the scaffolds were performed using a TRITEC8000B DMA from Triton Technology (UK), equipped with the compressive mode. The cylindrical controls produced in the 96 well plates were measured using the standard protocol for the tests in compression mode. Regarding on-chip experiments, a steel cylindrical probe of 3.8 mm of diameter especially fabricated to perform non-destructive compression tests to the individual scaffolds in the chip. This piece was inserted in the fixed upper plate of the DMA equipment. The superhydrophobic platform containing the scaffolds was fixed in the down plate of the DMA equipment in a gutter previously assembled in this part of the apparatus, which allowed the platform to move two-dimensionally. In each essay, the individual scaffolds were vertically aligned with the cylindrical steel probe.

The DMA spectra were obtained during a frequency scan between 0.1 and 15 Hz. The experiments were performed under constant strain amplitude, corresponding to approximately 1% of the original

height of the sample. In control samples produced by conventional means, the applied strain amplitude was of 50 μm, while in the on-chip samples the applied strain amplitude was of 10 μm. A small preload was applied to each sample to ensure that the entire scaffold surface was in contact with the compression plates before testing. At least three samples were used for each condition.

6.6.4. Morphological analysis: μCT

The architecture of the scaffolds was evaluated using a high-resolution micro-CT Skyscan 1072 scanner (Skyscan, Kontich, Belgium). The X-ray source was set at 31 keV and 179 μA. Data sets were reconstructed using standardised cone-beam reconstruction software (NRecon v1.4.3, SkyScan). The output format for each sample was serial 1024 -1024 bitmap images. Representative data set of the slices was segmented into binary images with a dynamic threshold of 40–255 (grey values). The binary images were used for morphometric analysis (CT Analyser, v1.5 SkyScan) and to build the 3D models (ANT 3D creator, v2.4, SkyScan) for the MMW 1%Chi 100Chi:0Alg condition. Three samples were tested for each condition. Due to dimension specificities, the controls produced in 96 well plates and the chips with 3 scaffolds from the same condition (MMW 1%Chi 100Chi:0Alg) were acquired with a pixel size of 11.3 μm. The chips with 9 different scaffolds (either LMW or MMW chips) were acquired with a pixel size of 19.1 μm.

6.6.5. Surface modification: Fn adsorption on the 3D porous scaffolds

The effect of pre-adsorption of Fn in the scaffold samples disposed in the chips was also investigated. Fn (Millipore) was labelled with Alexa Fluor 488 (eBioscience), according to the manufacturer's instructions. Solutions of Fn in phosphate buffer saline (PBS) of 10 μg/mL, 100 μg/mL and 1mg/mL were prepared. Droplets of 0.5 μl of each solution were dispensed in each scaffold of the array and kept at 37°C during 30 minutes. The whole platform was then washed in distilled water three times during 30 minutes. The scaffolds in the platform with adsorbed Fn, as well as controls consisting of the scaffolds in contact with PBS without Fn, were then observed in a reflected/transmitted light microscope (Zeiss) in red filter fluorescence mode. All scaffolds images were acquired using a constant exposure time.

6.6.6. *In vitro* cell testing

Cell expansion and cell culture

A fibroblast cell line (L929) and a osteoblast-like cell line (SaOs-2) were used as well established cell lines for preliminary cytocompatibility studies. Cells were expanded in basal medium consisting of alpha-MEM medium (Gibco, UK) supplemented with 10% heat-inactivated fetal bovine serum (FBS; BiochromAG, Germany) and 1% antibiotic/antimycotic solution (final concentration of penicillin 100 units/mL and streptomycin 100 mg/mL; Gibco, UK). Cells were cultured at 37oC in an atmosphere of 5% CO2. The entire chips were placed in a 6-well plate with 5 mL of complete cell culture medium (DMEM). All seeded samples and controls were incubated for 24 hours in order to evaluate the cell metabolic activity and quantify the cell number on the different materials combinations.

Cell behavior analysis: conventional chip-destructive testing

After 24 hours of cell culture, the scaffolds were removed from the platform. The cells metabolic activity was determined using the CellTiter 96®AQueous One Solution Cell Proliferation Assay (Promega, USA), a MTS reduction test, according to the instructions of the manufacturer. The absorbance was measured at 490 nm in a plate reader (SynergieHT, Bio-Tek, USA). Samples were characterized in triplicate.

Cell number was quantified by the total amount of double-stranded DNA (dsDNA), along the culturing time. Quantification was performed using the Quant-iT™ Pico-Green dsDNA Assay Kit (Invitrogen™, Molecular Probes™, Oregon, USA), according to the instructions of the manufacturer. Briefly, cells in the construct were lysed by osmotic and thermal shock and the supernatant was used for the dsDNA quantification assay. The fluorescence of the dye was measured at an excitation wavelength of 485/20 nm and at an emission wavelength of 528/20 nm, in a plate reader (Synergie HT, Bio-Tek, USA). The dsDNA concentration for each sample was calculated using a standard curve (dsDNA concentration ranging from 0.0 to 1.5 mg/mL) relating quantity of dsDNA and fluorescence intensity. Samples were characterized in triplicate.

Cell behavior analysis: image-based analysis

After 24 hours of cell culture, cell mortality was evaluated by a non-destructive assay. After washing the samples with PBS, the samples were incubated with 5 µL of propidium iodide 1 µg/mL solution in each spot. All samples were incubated for 30 minutes at 37°C.

Cell quantification was performed by staining the cells nuclei with 4',6-diamidino-2-phenylindole (DAPI, diluted 1000x). In both cases, fluorescence microscopy was used for image analyses on WCIF Image J

software, using 18 images of 200x200 pixel2 per sample acquired with the same magnification (50x). The same threshold criterions were used in all images.

6.7. ACKNOWLEDGEMENTS

M.B. Oliveira acknowledges Fundação para a Ciência e para a Tecnologia for the PhD grant SFRH/BD/71396/2010.

6.8. SUPPORTING INFORMATION

The numerical values obtained on-chip from mechanical, porosity and cell quantification are represented with their respective standard deviations in the following figures.

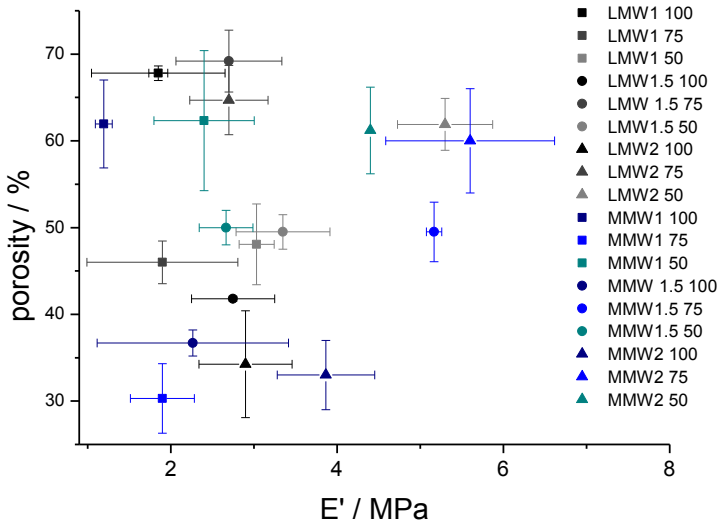

Figure 6.S1 – Numerical values obtained on-chip by dynamic mechanical analysis (DMA) at the frequency1Hz and porosity value obtained by µCT for scaffolds. These values are represented in Figures 6.5A and 6.5E, respectively, as intensity maps.

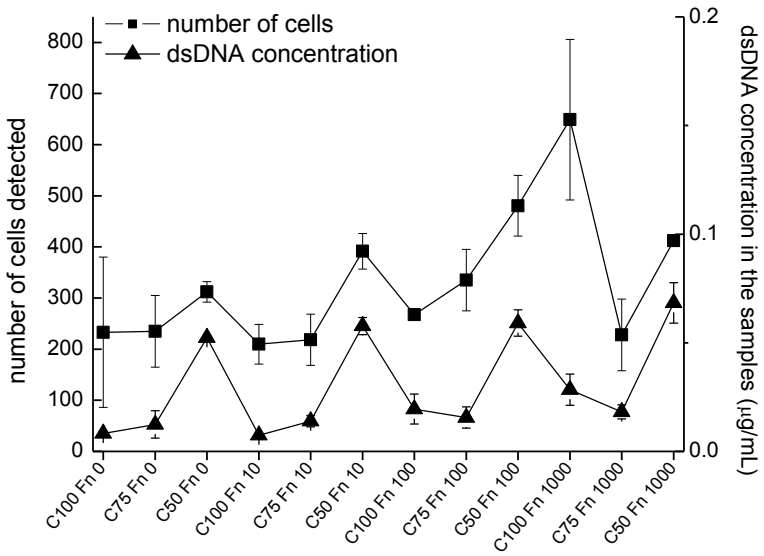

Figure 6.S2 - Number of L929 cells obtained by image analysis of the cell nuclei staining with DAPI and dsDNA concentrations obtained by chip-destructive analysis. These values are represented in the paper in Figures 6.7A1 and 6.7A2, respectively, as intensity maps.

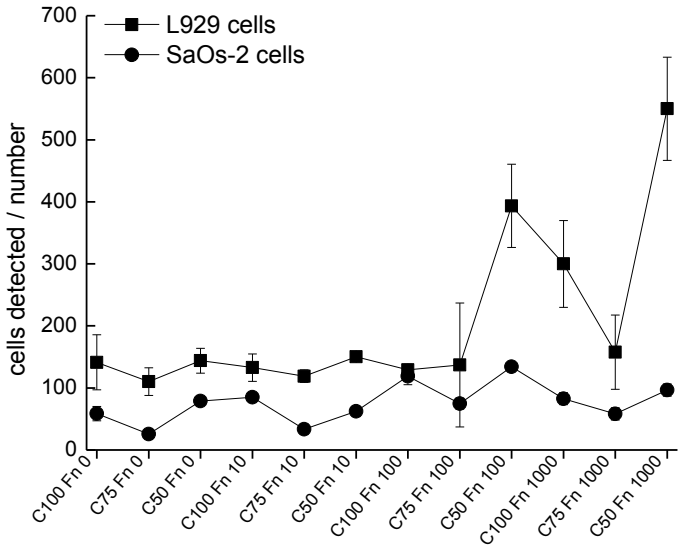

Figure 6.S3 – Number of L929 and SaOs-2 cells obtained on-chip by image analysis of cell nuclei staining with DAPI. These values are represented in the paper in Figure 6.8B as intensity maps.

6.9. REFERENCES

[1] van der Meer A, van den Berg A. Organs-on-chips: breaking the in vitro impasse. Integrative Biology. 2012;4:461-70.

[2] Lee K, Silva EA, Mooney DJ. Growth factor delivery-based tissue engineering: general approaches and a review of recent developments. Journal of The Royal Society Interface. 2011;8:153-70.

[3] Hook AL, Anderson DG, Langer R, Williams P, Davies MC, Alexander MR. High throughput methods applied in biomaterial development and discovery. Biomaterials. 2010;31:187-98.

[4] Power KA, Fitzgerald KT, Gallagher WM. Examination of cell-host-biomaterial interactions via high-throughput technologies: A re-appraisal. Biomaterials. 2010;31:6667-74.

[5] Neto AI, Custodio CA, Song W, Mano JF. High-throughput evaluation of interactions between biomaterials, proteins and cells using patterned superhydrophobic substrates. Soft Matter. 2011;7:4147-51.

[6] Engler AJ, Sen S, Sweeney HL, Discher DE. Matrix Elasticity Directs Stem Cell Lineage Specification. Cell. 2006;126:677-89.

[7] Evans ND, Minelli C, Gentleman E, LaPointe V, Patankar SN, Kallivretaki M, et al. Substrate stiffness affects early differentiation events in embryonic stem cells. Eur Cell Mater. 2009;18:1-13.

[8] Ghosh K, Ingber DE. Micromechanical control of cell and tissue development: Implications for tissue engineering. Advanced Drug Delivery Reviews. 2007;59:1306-18.

[9] Karamichos D, Skinner J, Brown R, Mudera V. Matrix stiffness and serum concentration effects matrix remodelling and ECM regulatory genes of human bone marrow stem cells. Journal of Tissue Engineering and Regenerative Medicine. 2008;2:97-105.

[10] Orr AW, Helmke BP, Blackman BR, Schwartz MA. Mechanisms of Mechanotransduction. Developmental Cell. 2006;10:11-20.

[11] Fedrorovich NE AJ, Wijn JR, Hennink WE, Verbout AJ, Dhert WJA. Hydrogels as Extrecellular Matrices for Skeletal Tissue Engineering: State-of-the-Art and Novel applications in Organ Printing. Tissue Engineering. 2007;13:1905-25.

[12] Tan H, Marra KG. Injectable, Biodegradable Hydrogels for Tissue Engineering Applications. Materials Letters. 2010;3:1746-67.

[13] Drury JL, Mooney DJ. Hydrogels for tissue engineering: scaffold design variables and applications. Biomaterials. 2003;24:4337-51.

[14] Williams DF. On the mechanisms of biocompatibility. Biomaterials. 2008;29:2941-53.

[15] Adachi T, Osako Y, Tanaka M, Hojo M, Hollister SJ. Framework for optimal design of porous scaffold microstructure by computational simulation of bone regeneration. Biomaterials. 2006;27:3964-72.

[16] Hollister SJ. Porous scaffold design for tissue engineering. Nat Mater. 2005;4:518-24.

[17] Karageorgiou V, Kaplan D. Porosity of 3D biomaterial scaffolds and osteogenesis. 2005;26:5474-91.

[18] Mano JF, Silva GA, Azevedo HS, Malafaya PB, Sousa RA, Silva SS, et al. Natural origin biodegradable systems in tissue engineering and regenerative medicine: present status and some moving trends. J R Soc Interface. 2007;4:999-1030.

[19] Li Z, Ramay HR, Hauch KD, Xiao D, Zhang M. Chitosan–alginate hybrid scaffolds for bone tissue engineering. Biomaterials. 2005;26:3919-28.

[20] Oliveira MB, Song WL, Martin L, Oliveira SM, Caridade SG, Alonso M, et al. Development of an injectable system based on elastin-like recombinamer particles for tissue engineering applications. Soft Matter. 2011;7:6426-34.

[21] Neto AI, Custodio CA, Song WL, Mano JF. High-throughput evaluation of interactions between biomaterials, proteins and cells using patterned superhydrophobic substrates. Soft Matter. 2011;7:4147-51.

[22] Salgado CL, Oliveira MB, Mano JF. Combinatorial cell-3D biomaterials cytocompatibility screening for tissue engineering using bioinspired superhydrophobic substrates. Integrative Biology. 2012;4:318-27.

[23] Oliveira NM, Neto AI, Song WL, Mano JF. Two-Dimensional Open Microfluidic Devices by Tuning the Wettability on Patterned Superhydrophobic Polymeric Surface. Appl Phys Express. 2010;3:085205.

[24] Di Martino A, Sittinger M, Risbud MV. Chitosan: A versatile biopolymer for orthopaedic tissue-engineering. Biomaterials. 2005;26:5983-90.

[25] Kumar MNVR, Muzzarelli RAA, Muzzarelli C, Sashiwa H, Domb AJ. Chitosan Chemistry and Pharmaceutical Perspectives. ChemInform. 2005;36:6017-84.

[26] Augst AD, Kong HJ, Mooney DJ. Alginate hydrogels as biomaterials. Macromol Biosci. 2006;6:623-33.

[27] Mei Y, Gerecht S, Taylor M, Urquhart AJ, Bogatyrev SR, Cho S-W, et al. Mapping the Interactions among Biomaterials, Adsorbed Proteins, and Human Embryonic Stem Cells. Advanced Materials. 2009;21:2781-6.

[28] Roth EA, Xu T, Das M, Gregory C, Hickman JJ, Boland T. Inkjet printing for high-throughput cell patterning. Biomaterials. 2004;25:3707-15.

[29] Simon CG, Lin-Gibson S. Combinatorial and High-Throughput Screening of Biomaterials. Advanced Materials. 2011;23:369-87.

[30] Oliveira SM, Song W, Alves NM, Mano JF. Chemical modification of bioinspired superhydrophobic polystyrene surfaces to control cell attachment/proliferation. Soft Matter. 2011;7:8932-41.

[31] Ballester-Beltran J, Rico P, Moratal D, Song WL, Mano JF, Salmeron-Sanchez M. Role of superhydrophobicity in the biological activity of fibronectin at the cell-material interface. Soft Matter. 2011;7:10803-11.

[32] Tweedie CA, Anderson DG, Langer R, Van Vliet KJ. Combinatorial Material Mechanics: High-Throughput Polymer Synthesis and Nanomechanical Screening. Adv Mater. 2005;17:2599-604.

[33] Poon B, Rittel D, Ravichandran G. An analysis of nanoindentation in linearly elastic solids. International Journal of Solids and Structures. 2008;45:6018-33.

[34] Mano JF. Viscoelastic properties of chitosan with different hydration degrees as studied by dynamic mechanical analysis. Macromolecular Bioscience. 2008;8:69-76.

[35] Lin Y-C, Tan F-j, Marra KG, S-S; J, Liu D-C. Synthesis and characterization of collagen/hyaluronan/chitosan composite sponges for potential biomedical applications. Acta Biomaterialia 2009;5:2591-600.

[36] Hariri HH, Schlenoff JB. Saloplastic Macroporous Polyelectrolyte Complexes: Cartilage Mimics. Macromolecules. 2010;43:8656-63.

[37] Porcel CH, Schlenoff JB. Compact Polyelectrolyte Complexes: “Saloplastic” Candidates for Biomaterials. Biomacromolecules. 2009;10:2968-75.

[38] Yuan L, Yu Q, Li D, Chen H. Surface Modification to Control Protein/Surface Interactions. Macromolecular Bioscience. 2011;11:1031-40.

[39] Pierschbacher MD, Ruoslahti E, Sundelin J, Lind P, Peterson PA. The cell attachment domain of fibronectin. Determination of the primary structure. Journal of Biological Chemistry. 1982;257:9593-7.

[40] Hsu S-h, Whu S, Tsai C-L, Wu Y-H, Chen H-W, Hsieh K-H. Chitosan as Scaffold Materials: Effects of Molecular Weight and Degree of Deacetylation. Journal of Polymer Research. 2004;11:141-7.

[41] Wang P, Henning SM, Heber D. Limitations of MTT and MTS-Based Assays for Measurement of Antiproliferative Activity of Green Tea Polyphenols. PLoS ONE. 2010;5:e10202.

[42] Wang S, Yu H, Wickliffe JK. Limitation of the MTT and XTT assays for measuring cell viability due to superoxide formation induced by nano-scale TiO2. Toxicology in Vitro. 2011;25:2147-51.

[43] Funk D, Schrenk H-H, Frei E. Serum albumin leads to false-positive results in the XTT and the MTT assay. BioTechniques. 2007;43.

[44] Custódio CA, Alves CM, Reis RL, Mano JF. Immobilization of fibronectin in chitosan substrates improves cell adhesion and proliferation. J Tissue Eng Regen Med. 2010;4:316-23.

CHAPTER 7. COMBINATORIAL STUDY OF NANOCOMPOSITE HYDROGELS: ON-CHIP MECHANICAL/VISCOELASTIC AND PRE-OSTEOBLASTS INTERACTIONS CHARACTERIZATION[6]

7.1. ABSTRACT

Nanocomposite hydrogels were prepared in a combinatorial way with chitosan, bioglass nanoparticles (BG-NP) and distinct amounts of crosslinker (genipin), in a total of 30 formulations. Such miniaturized hydrogels were prepared by dispensing the precursor solutions in wettable spots previously patterned onto superhydrophobic surfaces. The chips were used as platforms to analyze the biomaterials on-chip both for mechanical/viscoelastic and cell-biomaterials interactions. We adapted a mechanical dynamic analyzer (DMA) in order to perform the in-situ totally unconfined solid-state rheological characterization of biomaterials under physiological-like conditions. We concluded that the viscoelastic properties of the hydrogels are dependent on the three factors studied. Besides influencing biomaterials' mechanical properties, bioglass fillers also confer bioactivity. We immersed the chips with 20 distinct biomaterials formulations in a cell suspension of MC3T3-E1 pre-osteoblasts and quantified - using image analysis compatible with the maintenance of the integrity of the chip – selective cell adhesion after 1 day of cell culture, as well as cell proliferation and cell morphology at day 3. Linear regression studies showed that for the range of conditions studied herein, neither cell adhesion nor proliferation depended directly on the biomaterials mechanical/viscoelastic properties. Rather, cell proliferation was favoured in the presence of an intermediate amount of BGNP (12.5% w/w) for all chitosan/genipin conditions, especially in softer hydrogels (2% (w/v) chitosan, 2.5% (w/w) genipin). This hit-spotted condition also favoured cell spreading. Interestingly, the elastic modulus measured for this formulation meets the values reported for the granulation tissue occurring during bone regeneration, where fibroblasts lay producing collagen. We believe that this approach will facilitate the totally on-chip rapid and complete study of miniaturized biomaterials, in order to get more adequate formulations to be used in tissue engineering or other biomedical applications.

[6] This chapter was based on the publication: Oliveira MB, Luz GM, Mano JF. A combinatorial study of nanocomposite hydrogels: on-chip mechanical/viscoelastic and pre-osteoblast interaction characterization. Journal of Materials Chemistry B. 2014;2:5627-38.

7.2 Introduction

Bone is the main structural tissue of the skeletal system as it carries major loads in vertebrate animals. It is constituted by a ceramic composite whose components are primarily collagen (organic component) and hydroxyapatite (inorganic component) [1,2]. Through the actions of remodelling by cells, bone's composite structure repairs fatigue damage and continuously adapts to changes in mechanical usage. While it is essentially brittle, bone has a degree of significant elasticity contributed by its organic components [3].

In the development of biomaterials for bone regeneration an adequate balance of chemical and physical properties is of great importance. Chemical cues were reported to direct biological responses such as cell adhesion, differentiation and matrix production by processes of osteoinduction and osteoconduction [4]. Physical properties, namely mechanical properties, were reported to be responsible for the success of the integration of the implant in the native bone during the early stages of the regeneration process and were also proved to modulate cell response through mechanisms of mechanosensing [5,6]. Polymer-based nanocomposites emerged as a promising route to mimic complex natural structures [7,8]. Namely, composites based on biodegradable polymers containing bioactive ceramics or glasses were reported to be effective in preserving the structural and biological functions of damaged hard tissues as they mimic more closely the natural system in comparison to polymers or ceramics taken separately [7,8].

Herein, we perform a combinatorial study in order to optimize formulations of a three-factor hydrogel system targeting bone regeneration applications constituted by: polymer-based

nanocomposites based in a chitosan (Chi) scaffolds prepared from 3 distinct concentrations, with addition of bioactive glass nanoparticles (BG-NP) in 5 different amounts and crosslinked with two distinct amounts of genipin,. As an organic part of the system we used Chi, a natural polysaccharide obtained from the desacetylation of chitin, that is arguably the most widely used biopolymer for biomedical applications [9-12]. The use of nature-derived polymers has been widely proposed for tissue regeneration purposes, as in general such polymers are similar to macromolecules present in the biological environment and produce degradation products that are recognizable and metabolically processed by the body [9]. The structure of Chi has structural similarity to glycosaminoglycans, making it a potential candidate for connective tissue engineering. Its biological properties include non-cytotoxicity and biodegradability to harmless products [10].

Nanosized glass/ceramic bioactive fillers have been incorporated in polymeric matrixes in order to obtain biomaterials with increased elastic modulus [13-15]. It has also been previously reported that,

besides conferring higher stiffness to polymeric materials, the incorporation of BG-NP in certain conditions did not compromise the strength of the biomaterial [16]. Furthermore, their chemical interaction with surrounding bone tissue i*n vivo* promotes osteointegration by the formation of a calcium phosphate layer in the interface, increasing bone-bonding [17-21]. The ionic release from bioactive glasses may stimulate gene expression, promoting osteoinduction [22]. Nanocomposites with BG-NP with alginate were suggested as biocompatible materials for periodontal regeneration, as well as mixtures of BG-NP nanoparticles with beta-chitin [23,24]. Caridade et al. showed that the Young modulus of Chi/BG-NP membranes was higher than the one of pure Chi membranes, for a particular formulation presented in that study [25]. Dynamic mechanical analysis (DMA) scans also showed increased storage modulus (*E'*) of Chi membranes upon incorporation of BG-NPs [26]. Besides affecting mechanical properties, the incorporation of BG-NPs in Chi was already proven to be successful in conferring bioactivity to the composite, as a calcium phosphate layer was formed *in vitro* upon immersion in a simulated body fluid [26,27].

A key property that researchers commonly seek to modulate in biomaterials is stiffness, as it affects biomaterials' integration in the tissue after implantation, and it was also proven to modulate osteoblast-like cells response [5]. In the case of polymeric biomaterials, the increase in stiffness has been achieved by the variation of polymers' molecular weight and polymer concentration in the hydrogel [28,29] crosslinking degree or by the blending with other polymers with higher elastic modulus [30].

Although mechanical characterization of biomaterials is of utter importance to understand their potential of integration in tissues after implantations and eventual mechanisms of mechanosensing, few works have been developed so far to increase the throughput of such methods. The most common high-throughput approach to assess biomaterials' stiffness is by nanoindentation, mainly applied in thin films [31]. Tweedie *et al.* [32] synthesized 576 polyacrylate compositions and subsequently tested them on-chip by depth-sensing indentation. The modulus obtained for the copolymers was not always an expected value from the volume fraction and modulus of its pure constituents, as microstructural and phase changes influenced the stiffness. Simon *et al.* [33] also used nanoindentation to study a gradient library of poly(L-lactic acid) and poly(*D,L*-lactic acid). Stafford *et al.* [34] developed a method to obtain the elastic modulus of polymer films from the buckling wavelength of bilayers consisting of a stiff, thin polymer film with known thickness, coated onto a relatively softsubstrate.

Regarding nano-/micro-indentation, these methods are limited to linear, isotropic materials and cannot be used in porous or anisotropic millimetric-sized structures, as they do not provide information on bulk properties of materials. Problems associated with the "pile-up" or "sink-in" of the material on the edges

of the indent during the indentation were also described, as they have been widely reported to increase the values of the elastic modulus artificially [35].

Although stiffness of biomaterials is commonly discussed, living tissues show a viscoelastic nature. Living tissues like skin, cartilage and bone are viscoelastic, and thus exhibit time-dependent mechanical response and energy-dissipation ability [31,35]. Recently, the effect of energy dissipation ability of scaffolds was proven to affect chondrogenic expression of ephiphyseal chondro-progenitor cells upon cyclic stimulation [36]. As such, the combined study of materials stiffness as well as damping properties is certainly valuable for the full characterization of biomaterials' performance. Dynamic mechanical analysis (DMA) equipments allow for a sensitive and complementary non-destructive characterization of mechanical/viscoelastic properties of materials. DMA equipments also enable testing the materials' properties in wet or physiological-like conditions [37], in a closer environment to the *in vivo* conditions. Moreover, this technique allows measuring the bulk properties of hydrogels and other three-dimensional materials, while nanoindentation characterization is mainly adequate to the study of thin films.

In this work we developed an on-chip methodology to assess mechanical and viscoelastic properties of biomaterials in physiological-like conditions, by adapting a dynamic mechanical analyzer. With the proposed method, a high number of conditions can be studied while the total amount of material used in the experiment is decreased, when compared to the conventional techniques for biomaterials study [29]. Such method not only allows for a faster data collection but also result in less expensive and resource-saving experimentation [38-42].

We performed on-chip cell-biomaterials interaction studies to discover the mostly predominant effects affecting pre-osteoblasts response in the formulations developed herein. We aimed hit-spotting formulations favorable for cell attachment and growth, and eventually correlate these features with materials' properties.

7.3. Results and Discussion

7.3.1. Preparation of on-chip samples

Miniaturized Chi/BG-NP hydrogels were prepared in a chip consisting of a polystyrene superhydrophobic surface patterned with hydrophilic spots. The materials' precursors were dispensed in the hydrophilic spots and the surrounding superhydrophobicity prevented their spreading, as shown previously for studies with cell-laden hydrogels and porous scaffolds for tissue engineering *in vitro* biomaterials-cells interactions assessment.29,40 The materials used herein were based on a Chi matrix crosslinked with

genipin, in a reaction carried out in water-saturated atmosphere, preventing the evaporation of the water contained in the precursor Chi solution. While compared with traditional methods for hydrogels preparation – e.g. the use of 96 well plates to prepare hydrogel disks - this procedure allowed a saving of 33 fold of volume of material.

7.3.2. On-chip Dynamic Mechanical Analysis

We assessed the mechanical and viscoelastic properties of 30 biomaterials prepared in a combinatorial manner, as represented in Figure 7.1B. We varied 3 distinct factors: polymer concentration used to prepare the hydrogel, concentration of crosslinker used to prepare the matrix and addition of bioglass nanoparticles to the structure. We used a DMA to assess the storage modulus, E' – that gives a measure of the stiffness of the materials – and the loss factor, $tan\ \delta$ – that gives a measure of the damping ability of the materials. Such tests were performed on-chip, by using an adequate adaptor that allowed measuring the properties of miniaturized samples. We inserted a stainless steel cylinder in the upper fixed part of the DMA equipment and attached the chip in a gutter that allowed the samples to be moved two-dimensionally, as indicated in Figure 7.1A. The conditions used in the tests were adjusted in order to mimic the physiological environment regarding temperature, wetting conditions and pH; the assays were carried out at 37°C in physiological buffered saline (PBS).

In order to compare materials accurately, taking in consideration their different mass and density, as well as eventual different swelling properties under physiological environment, the density of the samples was measured after immersion in PBS at 37°C until equilibration. Figure 7.2 depicts an Ashby plot, where the density values obtained for each sample are counterpoised with the E' measured for the samples at 1 Hz. We observed that materials' density was dependent not only on the total dry mass of the materials, but also on the swelling of each formulation. The highest densities were registered for 3%Chi2.5%genipin conditions, while 4%Chi2.5%genipin groups showed lowest densities. The percentage of Chi (% w/v) refers to the mass of chitosan in the hydrogel; percentage of genipin and BG-NP (% w/w of Chi) refer to their mass relatively to the total mass of chitosan in the hydrogel.

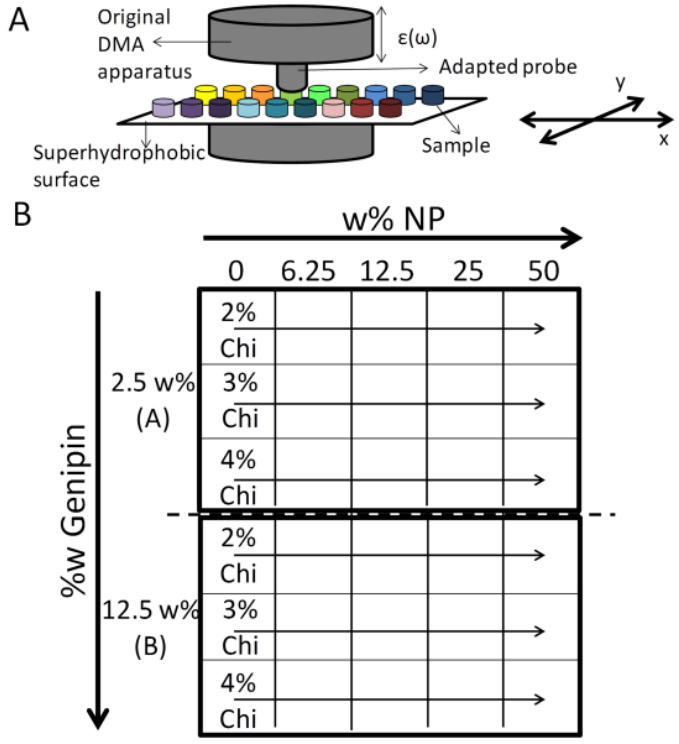

Figure 7.1. – A. Schematic representation of the adaptation performed to the original DMA equipment, where a probe was attached to the upper fixed part of the measuring system, in order to contact each hydrogel on the chip individually. The gutter fixed in the lower part of the DMA equipment allowed the chips to be moved two-dimensionally, in the x and y axes. B. Experimental design used to process the hydrogels with combined compositions (30 formulations) on the chips. NP are the bioglass nanoparticles incorporated on the hydrogels (BG-NP).

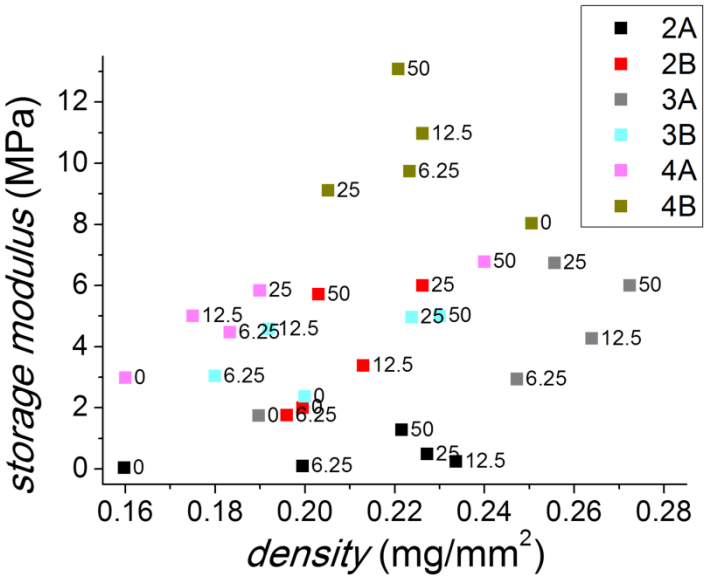

Figure 7.2. – Ashby plot obtained by the measurement of the storage modulus (*E'*) at 1 Hz and density of the distinct biomaterial formulations (upon swelling in PBS at 37°C). The nomenclature of the biomaterials in this

plot is given by Chi concentration (2, 3 or 4, corresponding to 2%, 3% and 4% (w/v)), genipin concentration (A for 2.5% (w/w of Chi) and B for 12.5% (w/w of Chi)) and percentage of BG-NP incorporated in the matrix (0, 6.25, 12.5, 25 or 50% (w/w of Chi)).

As density did not vary linearly with the total dry mass of the materials and the effect was also determined by the swelling capability of the hydrogels, the most accurate way to compare the hydrogels' properties was by determining their specific modulus at 1 Hz, given by E´/density. Results are shown in Figure 7.3A. The significant differences between conditions and sets of conditions are indicated according to the bars in Figure 7.3 and in Figure 7.4.

Regarding studies dealing with the effect of the incorporation of bioglass and ceramic nanoparticles in polymeric matrixes, it was previously reported that, in certain conditions, they lead to an increase in materials' stiffness [13-15,43-46]. It is also know that high amounts of these materials may lead to the formation of brittle structures, as they introduce breaking points in the polymeric structure. Nonetheless, such studies are limited to very low numbers of formulations, and further study in order to tailor and fully understand the role of the incorporation of such nanoparticles in polymeric matrixes is needed. Caridade et al. proved that the incorporation of nano-sized bioactive particles in Chi membranes shows advantages over conventional (micron-sized) bioactive glasses, as a result of the larger surface area obtained with the incorporation of bioglass nanoparticles; Chi/BG-NP composite membranes presented higher *E'* values in tensile mechanical tests, as well as enhanced bioactivity [24]. Herein, we observed (Figure 7.3A) that the specific storage modulus of the samples crosslinked

with 2.5% (w/w of Chi) genipin increased significantly with the incorporation of 50 % (w/w of Chi) BG-NP comparing to all other conditions prepared both with 2% (w/v) and 4% (w/v) of Chi. In the condition 3% (w/v) Chi, only the formulations with 50% (w/w of Chi) BG-NP and 0% (w/w of Chi) BG-NP showed significant differences. Regarding hydrogels crosslinked with 12.5% (w/w of Chi) genipin, in 2% (w/v) Chi samples the addition of 50% (w/w of Chi) BG-NP led to a significant increase of the specific modulus compared to samples containing 0%, 6.25% and 12.5% (w/w of chi) BG-NP. For hydrogels prepared with 3% (w/v) Chi, 50%, 25% and 12.5% (w/w of Chi) BG-NP led to a significant increase in the samples' specific modulus, when compared to the samples that did not contain BG-NP. In the samples prepared with 4% (w/v) Chi and crosslinked with 12.5% (w/w of Chi) genipin, the addition of BG-NP did not lead to a significant increase in the specific modulus value.

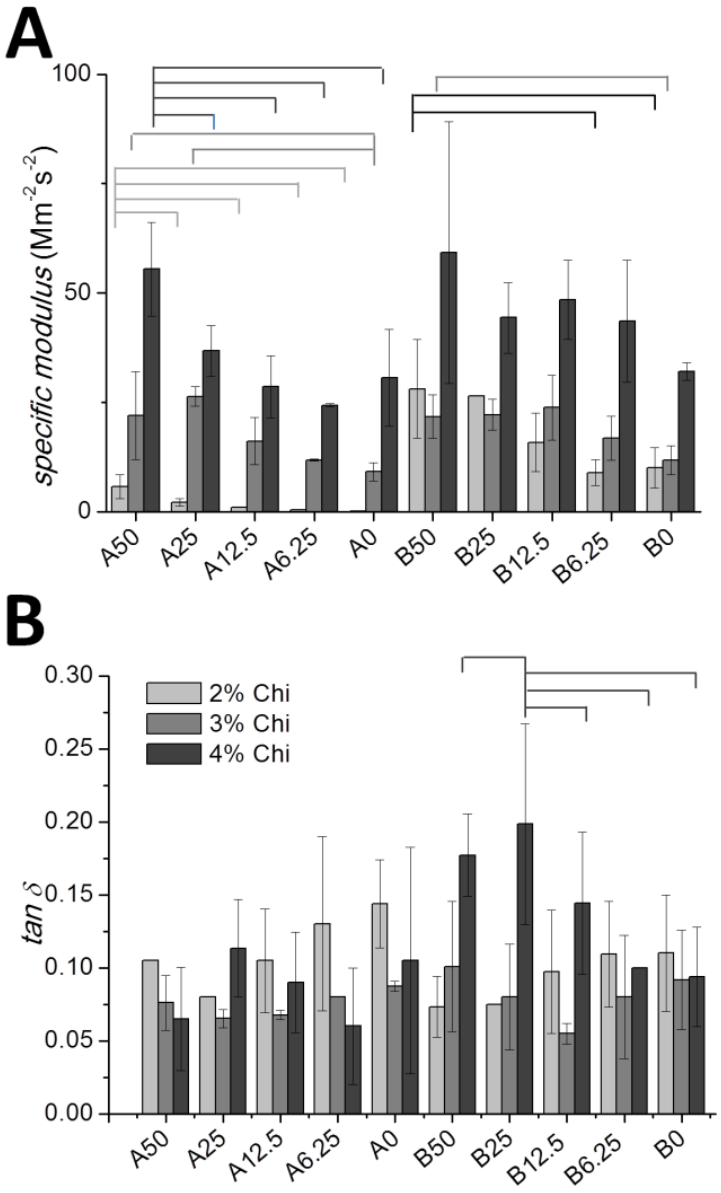

Figure 7.3. – A. Specific storage modulus of the biomaterials studied on-chip (given as *E'*/density). B. Loss factor (*tan* δ) of the biomaterials studied on-chip (given by E´´ (loss modulus)/E´ (storage modulus). In both plots the nomenclature refers to the genipin concentration (A for 2.5% (w/w of Chi) and B for 12.5% (w/w of Chi)) and percentage of BG-NP incorporated in the matrix (0, 6.25, 12.5, 25 or 50% (w/w of Chi)). Significant differences (considered for $p<0.05$, by one-way ANOVA followed by Tukey's post test) between hydrogels with fixed Chi and genipin concentrations, but different BG-NP amounts, are given by the colored bars on the top of the plot columns. Significant differences regarding the factors "Chi concentration" and "genipin concentration" can be found in Figure 7.4.

A

% BGNP	2% 2.5 vs 2% 12.5	3% 2.5 vs 3% 12.5	4% 2.5 vs 4% 12.5
50	**	ns	ns
25	***	ns	ns
12.5	ns	ns	**
6.25	ns	ns	**
0	ns	ns	ns
	2% 2.5 vs 3% 2.5	**3% 2.5 vs 4% 2.5**	**2% 2.5 vs 4% 2.5**
50	*	***	***
25	***	ns	***
12.5	ns	ns	***
6.25	ns	ns	***
0	ns	**	***
	2% 12.5 vs 3% 12.5	**3% 12.5 vs 4% 12.5**	**2% 12.5 vs 4% 12.5**
50	ns	***	***
25	ns	**	*
12.5	ns	***	***
6.25	ns	***	***
0	ns	**	**

B

% BGNP	2% 2.5 vs 2% 12.5	3% 2.5 vs 3% 12.5	4% 2.5 vs 4% 12.5
50	ns	ns	ns
24	ns	ns	ns
12.5	ns	ns	*
6.25	**	ns	**
0	ns	ns	ns
	2% 2.5 vs 3% 2.5	**3% 2.5 vs 4% 2.5**	**2% 2.5 vs 4% 2.5**
50	ns	ns	ns
24	ns	ns	ns
12.5	ns	ns	ns
6.25	***	ns	ns
0	ns	ns	*
	2% 12.5 vs 3% 12.5	**3% 12.5 vs 4% 12.5**	**2% 12.5 vs 4% 12.5**
50	ns	ns	ns
25	ns	ns	ns
12.5	ns	*	ns
6.25	ns	***	***
0	ns	ns	ns

Figure 7.4. – Conditions regarding significant differences (by two-way ANOVA followed by Bonferroni's post test) observed for A. the specific modulus and B. *tan* δ values measured on-chip for the factors "Chi concentration" and "genipin concentration". "*", "**", "***" and "ns" refers to significant differences for $p<0.05$, $p<0.01$, $p<0.001$ and non significant differences, respectively.

The independent effect of polymer concentration in the hydrogel system was also studied. It was previously reported that increasing polymer concentrations usually lead to stiffer hydrogels [29] due to the lower amount of water entrapped in the hydrogel. We observed significant differences in specific storage modulus between all samples of 2% (w/v) Chi and 4% (w/v) Chi, regardless of the amount of crosslinker used (Figure 7.4), where the higher concentration of Chi led to higher specific storage modulus values. The same happened for 3% (w/v) Chi and 4% (w/v) Chi samples crosslinked with 12.5% (w/w of Chi) genipin (Figure 7.4). Differences between 2% (w/v) Chi and 3% (w/v) Chi samples were observed mainly in samples containing higher levels of BG-NP (Figure 7.3A and Figure 7.4).

The use of distinct concentrations of genipin – 2.5% or 12.5% (w/w of Chi) was expected to lead to different stiffness of the hydrogels due to the establishment of covalent bonds between amine groups of the Chi molecules. Significant differences in specific modulus values while using distinct crosslinker concentrations were observed in the 2% (w/v) Chi formulations, namely in the conditions containing more than 12.5% (w/w of Chi) of BG-NP. For 4% (w/v) Chi formulations, we observed significant differences in specific modulus of materials in conditions with the incorporation of 6.25% and 12.5% (w/w of Chi) BG-NP.

The frequency scans of some selected conditions are represented in Figure 7.5A. The hydrogels, either with the incorporation of the highest amount of BG-NP (50% (w/w of Chi)) or without any addition of BG-NP showed, in general, constant specific storage modulus up to frequencies of 10 Hz. A slight increase in E' values with increasing frequency was observed mostly in the lower Chi concentration formulations (2% (w/v) Chi). This may be explained by the effect of the water entrapment in the hydrogel structure and low compressibility of water, as previously suggested for similar phenomena [47].

In order to be aware of the relative effect of each factor in the whole system regarding specific storage modulus values, we performed factorial analysis. Expert-Design® (Stat-Ease, Inc.) software was used to produce a model based in the evolution of the specific storage modulus with the variation of the three factors varied in this approach. This was performed to evaluate the contribution of each factor to specific modulus values and also to detect eventual combined contribution of factors. Factors were considered as ordinal categorical, i.e. the factors were labelled in an ordinal scale as, e.g., lowest, low, medium, high and highest. By treating the average results of specific modulus in the software, a model with an insignificant lack of fit was obtained (R^2 value of 0.89 and F-value of 12.33 characterized the model as significant with 99.5% confidence). All the independent factors studied in this experiment – "Chi" (concentration of Chi, studied with 3 levels), "BG-NP" (concentration of BG-NP, studied with 5 levels) and "G" (concentration of genipin, studied with 2 levels) – affected significantly the model (Table 7.1). Quantitatively, the estimated effect of a given main effect or interaction and its rank relative to other main effects and interactions is given via least squares estimation. We observed that the factor affecting specific storage modulus with a higher relevance was Chi concentration (66% effect). The incorporation of BG-NP was the second most influencing factor (14% effect), followed by the effect of the amount of genipin added to the hydrogels (9% effect). The combined effect of Chi concentration and genipin concentration (3% effect) was also significant, as expected, since the crosslinking kinetics is expected to depend on the amount of free amines in the polymer (higher in higher concentrations of Chi) and in the amount of genipin molecules (higher in the highest concentration of genipin). Nanoparticles

concentration effect did not show any combined effect with any other factor. This suggests that an eventual phenomenon of complexation of the BG-NP (negatively charged, as evaluated by zeta potential measurement) [48] with the free Chi molecules prior and during the crosslinking reaction had no significant influence in the final stiffness of the structures.

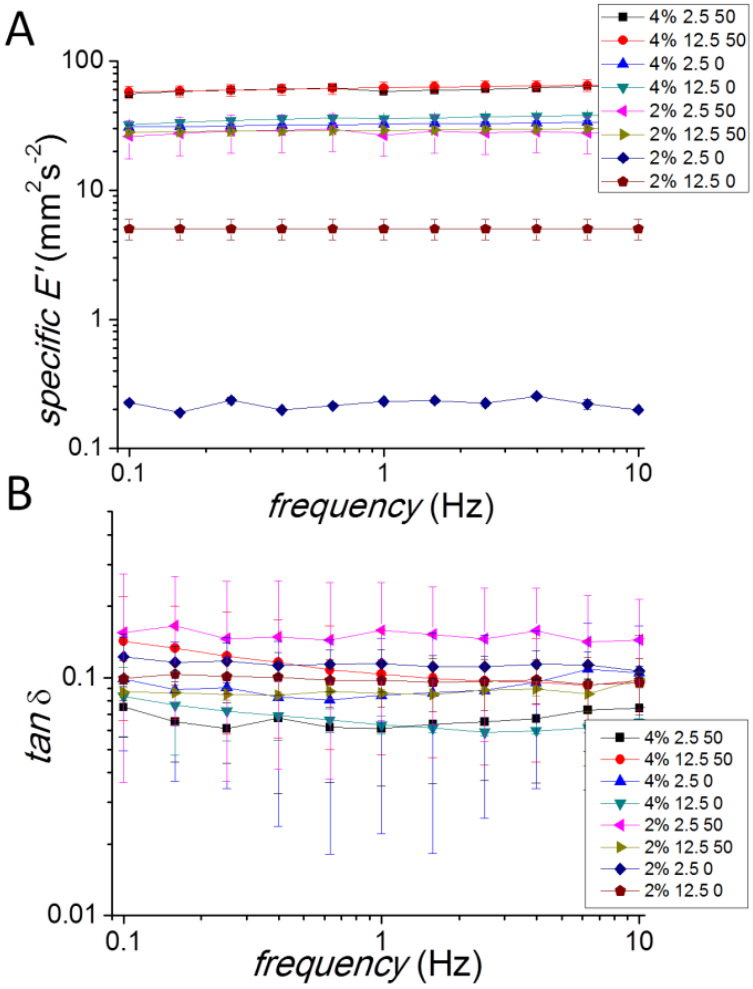

Figure 7.5. – Frequency dependent scans of the (A) specific storage modulus and (B) loss factor of the biomaterials studied on-chip, for the conditions 2% (w/v) Chi and 4% (w/v) Chi without any BG-NP or with the maximum amounts tested (50% (w/w of Chi) of BG-NP). The nomenclature in the plots is given by Chi concentration (2 or 4% (w/v)), genipin concentration (2.5 or 12.5% (w/w of Chi)) and BG-NP concentration (0 or 50% (w/w of Chi)).

Table 7.1. – Percentage effect of the individual and combined factors affecting the specific storage modulus of the biomaterials measured on-chip.

Factor	Effect on Specific Modulus (%)	Effect on loss factor (%)
Chi	66.1	-
BG-NP	14.1	21.3
G	9.1	-
Chi/G	3.2	29.9
Chi/BG-NP	-	13.7
Residual and non-significant factors	7.5	27.5

Regarding damping properties, it was previously reported that in specific formulations *tan* δ exhibited higher values for Chi/BG-NP than for Chi membranes [24,46]. This could be the result of the larger area covered by the interface between the polymeric matrix and the particles for the former composite, that could contribute more for the dissipation of mechanical energy. We herein observed that the loss factor values for the hydrogels increased significantly in 4% (w/v) Chi 12.5% (w/w of Chi) genipin condition for formulations with higher BG-NP amount, namely for 25% (w/w of Chi) BG-NP condition. For the other formulations, with fixed Chi and crosslinker concentrations, the addition of BG-NP to the hydrogels did not affect significantly the loss factor values (Figure 7.3B). However, as indicated in Figure 7.4B, we observed that only in the presence of BG-NP significant differences in the damping ability of the hydrogels - prepared both with 2.5% and 12.5% (w/w of Chi) of genipin - were observed with the variation of Chi concentration. Also, in the comparison of the loss factors of the hydrogels prepared with the same Chi concentration, but with distinct genipin amounts, we observed that only hydrogels with incorporation of 12.5% and 25% (w/w of Chi) of BG-NP showed significant differences in *tan* δ values. Interestingly, in general, the loss factor values registered for the hydrogels developed herein are in a close range to the native values measured in native bone, ranging from 0.02 to 0.10 [49,50]. Those were namely registered in all conditions prepared with 2.5% genipin, and 2% (w/v) Chi and 3% (w/v) Chi prepared with 12.5% (w/w of Chi) genipin.

The *tan* δ values were, in general, constant while exposed to distinct frequencies (Figure 7.5B). It was also previously reported that, upon mineralization, the damping properties of Chi/BG-NP membranes were not significantly altered [26], which indicates that the hydrogels would keep their energy dissipation properties after implantation in a bone defect.

By treating the average values of *tan* δ with Expert-Design® Software (Stat-Ease, Inc.) in a similar way as previously performed for the values of *E'*, we obtained a model with an insignificant lack of fit (R^2 of 0.76 and F-value of 6.87, with an interval of confidence of 99.8%). We observed that the main factor

affecting *tan* δ of the biomaterials studied herein was the amount of BG-NP, with an effect of 21.3%. The other individual effects, namely the amount of Chi and concentration of genipin, were not significant to the model. Moreover, the results were significantly affected by the combined action of Chi and genipin (effect of 29.9%), as well as by the interaction of Chi with BG-NP (effect of 13.7%), as shown in Table 7.1.

7.3.3. Control study with conventional sized hydrogels and comparison with nanoindentation results

Control studies were performed with hydrogels prepared on chips with round hydrophilic patterns with 8 mm width, in order to have a size commonly used in biomaterials' studies and compatible with DMA measuring without any equipment modifications. After crosslinking, the samples were removed from the chips and measured. Four conditions were studied, including formulations with distinct chitosan concentrations (2% w/v and 3% w/v), absence and 25% (w/w) of BG-NP and distinct genipin amounts (2.5% and 12.5% w/w). Values of stiffness in the same order of magnitude were obtained for the samples prepared conventionally and on-chip (Figure 7.6). However, samples measured on-chip showed - especially for samples containing BG-NP - lower values than the ones obtained for samples without any incorporated BG-NP. Although the tendencies and order of magnitude of the *E'* values observed from the on-chip analysis were the same as the ones obtained by conventional use of DMA, results suggest that the output of on-chip measurements on miniaturized samples must be carefully analyzed, as in certain conditions results may be slightly higher than the value obtained for a conventionally-sized hydrogel, probably due to size effect-related phenomena.

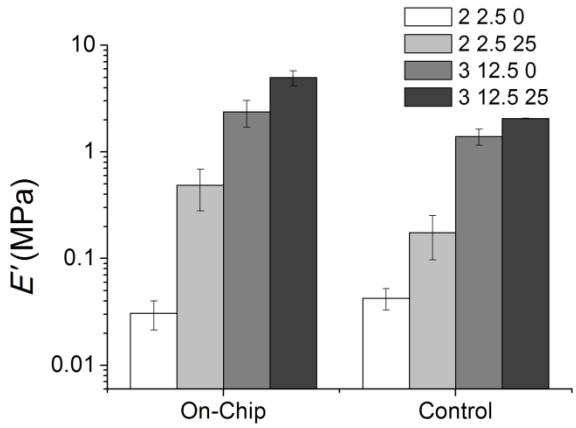

Figure 7.6. – Storage modulus at 1 Hz measured for the on-chip samples and control samples consisting of conventional sized hydrogels. Those were hydrogels prepared in the form of cylinder with approximately 8 mm

diameter x 2 mm height). The nomenclature in the plots is given by Chi concentration (2 or 3% (w/v)), genipin concentration (2.5 or 12.5% (w/w of Chi)) and BG-NP concentration (0 or 25% (w/w of Chi)).

As nanoindentation is the most commonly applied method to study biomaterials' mechanical behavior in a high-throughput manner,[32-34] we performed such tests in some of the materials of the chips. However, we were only able to perform them in dry state. As such, the absolute values of reduced modulus (*Er*, Table 7.2) and *E'* were not amenable to be compared due to the distinct hydrations states of the samples. We analysed the accuracy of the measurements in the isotropic (formulations with 100% chitosan; 0% BG-NP) and anisotropic samples (composed by chitosan and BG-NP). We tested 3 points/samples, with 50 μm of distance. In the samples with 0%BG-NP, we observed a standard deviation (S.D.) of less than 1% of the measured *Er* value. However, in samples containing 25%BG-NP, this value increased to 10% to 14%, as the difference of *Er* measured in distinct points of the samples increased. With a 50%BG-NP sample (5 points studied in the same sample) we observed a S.D. of 92% of the *Er* value. This variation in the same sample corroborates that nanoindentation is not an adequate tool to study anisotropic samples, such as the composite hydrogels developed herein.

7.3.4. Pre-osteoblasts selective adhesion and proliferation on-chip

We prepared chips with 20 formulations (all formulations with 2% w/v Chi and 4% w/v Chi) from the initial ones studied by DMA analysis. We seeded a cell suspension in the chips with a density of $1x10^6$ cells/mL, in order to promote a selective adhesion of the cells to the surface of the hydrogels. The number of adhered cells after 1 day of cell culture per hydrogel, quantified by cell nuclei image analysis (ImageJ, NIH), is depicted in Figure 7.7A. We observed higher cell number after 1 day of cell culture in the conditions 2%Chi2.5%G50NP, 4%Chi2.5%G12.5%NP, 4%Chi2.5%G50%NP, 4%Chi12.5%G12.5%NP and 4%Chi12.5%G25%NP. We performed factorial analysis to all results of cell adhesion performed on-chip. However, we found no correlations between individual factors (Chi concentration, BG-NP concentration or genipin amount) and the number of adhered cells. By performing linear and polynomial regressions to the array of results against *E'* and specific *E'* values, we also did not find any correlation. This result was surprising, as mechanosensing phenomenon has been reported before for MC3T3-E1 cells [41,52]. Nonetheless, the order of magnitude of materials' stiffness at which previous studies were performed [41,52] were lower than the ones studied herein.

Table 7.2. – Analysis of 4 distinct formulations on-chip with a nanoindenter. Each sample was measured in 3 distinct spots (**5 distinct spots), separated by 50 μm. *Er* is the average of the reduced modulus measured in different points of the same sample. S.D. is the standard deviation observed inside the same sample, considering the measurement of the 3 distinct spots of the sample. "Average *Er*" is the average of the *Er* measured in 3 distinct samples. s.e.m. is the standard error of the mean, considering the average values measured for 3 distinct samples. The curves where the values of *Er* were taken from can be consulted in Supporting Information (Figures 7.S1 – 7.S4).

Formulation	Sample	*Er* (GPa)*	S.D.	% S.D.	*Average Er* (GPa)	S.E.M.
2%C12.5%G25NP	#1	4.31	0.36	9.99±0.6	3.66	0.35
	#2	3.53	0.33			
	#3	3.14	0.38			
4%C2.5%G25NP	#1	3.56	0.34	14.4±9.5	3.76	0.16
	#2	3.96	0.93			
	#3	3.42	0.35			
4%C2.5%G0NP	#1	2.81	0.014	0.81±0.3	3.21	0.38
	#2	2.89	0.031			
	#3	3.93	0.034			
4%C2.5%G50NP**	#1	5.05	4.66	92.28	-	-

As cell number at day 1 was compared with *tan* δ values, a second order polynomial correlation with a R^2=0.45 (plot as Supporting Information, Figure 7.S5) was found. Although the correlation was weak, it suggests that the adhesion of MC3T3-E1 cells to these materials in this range of values depends non-linearly on the damping of the materials, with specific formulations for optimized cell adhesion.

After 3 days of cell culture, a clear tendency in cell number on the hydrogels was observed. Formulations with 6.25% (w/w) and 12.5% (w/w) of BG-NP showed higher number of cells (Figure 7.7B). While performing factorial analysis to the whole array of results, no significant effect of any of the factors was found. Linear and polynomial regressions outputs against *E'*, specific *E'* and *tan* δ also did not show any strong correlation between these properties and the number of cells in the hydrogels after 3 days of cell culture.

Regarding cell proliferation occurring between day 1 and day 3 (Figure 7.7C), it was observed that its highest value (150%) was hit spotted for the condition 2%Chi2.5%G12.5%NP (Figure 7.7C). Moreover, all conditions containing 12.5% BG-NP were the only that, regardless of the biomaterials' formulation, guaranteed positive proliferation ratio for the cells (Figure 7.7C).

Interestingly, the condition providing a higher cell proliferation was also the one where cells showed a more spread morphology, as shown by F-actin staining analysis (using ImageJ software, NIH, USA), used for cell area quantification (Figure 7.7D). This was also depicted in scanning electron microscopy micrographs (Figure 7.8).

7.3.5. Biological relevance of the results

During bone healing after a fracture, the extent to which the injured bone regains stability and strength depends on the mechanical properties of the callus, a dynamic tissue formed during the healing process. In the regenerative step of such complex process, the granulation tissues formed during a primary inflammatory phase is converted into hyaline cartilage (chondroid tissue), which performs a role as a mechanical stabilizer of the fracture. After this stage, it was proven that the strength of callus is increased as mineralization of the tissue occurs [53-54]. Indentation modulus obtained for studied callus showed values of 0.61–1.27 MPa (median = 0.99 MPa) to the granulation tissue, 1.39–4.42 MPa (median = 2.89 MPa) to the chondroid tissue and 26.92–1010.00 MPa (median = 132.00 MPa) for the mineralized tissue, depending on the time of mineralization allowed to occur [55].

By varying the formulation of the composite hydrogels developed in this study, we were able to obtain materials storage modulus in the range of the chondroid tissue and more reinforced transition tissue structures. Specifically, conditions where crosslinking occurred with 12.5% genipin for all Chi concentrations, or 3% Chi formulations prepared with 2.5% genipin (ranging from approximately 2 to 6 MPa) were in the range of the modulus measured for chondroid tissue (Figure 7.2). In the case of 4% Chi formulations crosslinked with 12.5% genipin, the average storage modulus values (ranging from approximately 7 to 14 MPa) are higher than the range indicated for chondroid tissue, suggesting that they may be in the range of mineralized tissue in its early form, which may allow for a better stabilization of the hydrogels upon implantation in a bone defect. Moreover, Chi/BG-NP composites previously shown to be able to mineralize after some hours in the presence of simulated body fluid [26]. As such, the development of the mechanical properties and inorganic phase in these materials would be expected to be similar to the one occurring during the natural healing process, but in an accelerated and stronger manner, as the acellular mineralization of such materials occurs fast, as well as an increase of their stiffness (in membranes, an increase for 20 MPa in non-mineralized samples to 90 MPa for samples immersed in simulated body fluid for 14 hours was observed) [26].

The specific formulation of the biomaterials developed herein that promoted the highest cell proliferation rate along with a spread morphology for pre-osteoblasts – 2%Chi2.5%G12.5%NP – showed a storage

modulus of 240 kPa. This value is in the range of values measured for granulation tissue [56]. MC3T3-E1 cells are pre-osteoblasts with a fibroblast-like phenotype. Moreover, the ECM of granulation tissue is known to be secreted and modified by fibroblast cells, which may explain the preference of undifferentiated MC3T3-E1 cells for this material [57].

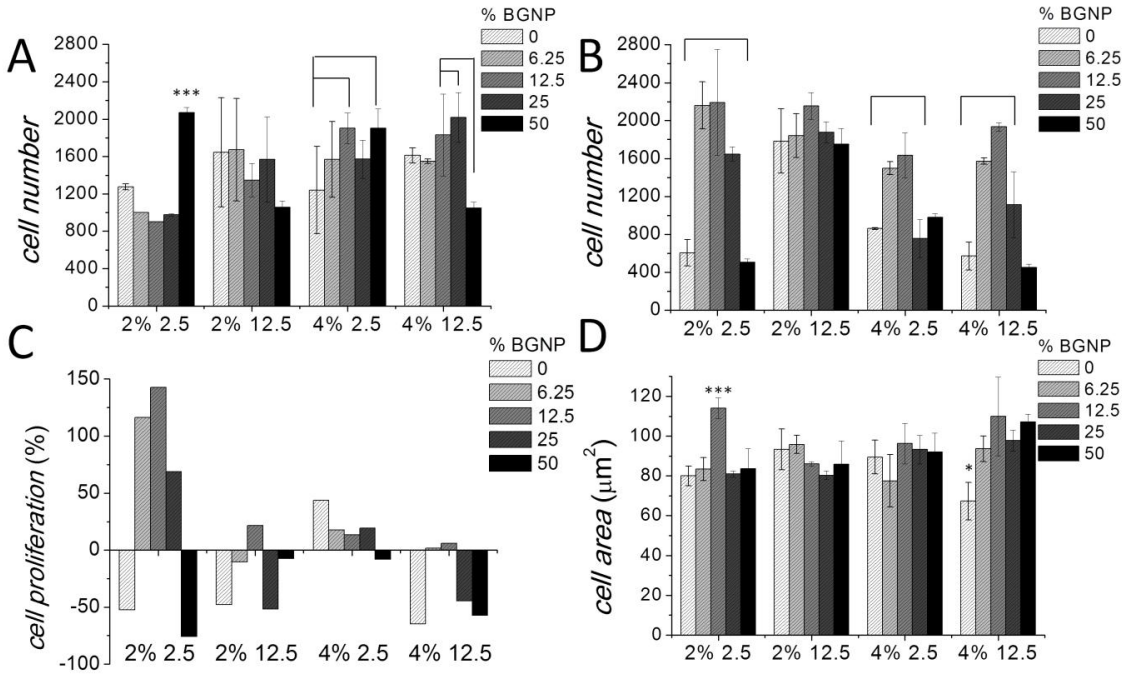

Figure 7.7. – (A) Cell number present in each formulation on-chip after 1 day of cell culture, after fixation. (B) Cell number present in each formulation on-chip after 3 days of cell culture, after fixation. The number of cell was quantified by the number of nuclei present in each hydrogel, by analysis of DAPI staining using ImageJ software (NIH, USA). (C) Cell proliferation ratio, from day 1 to day 3, calculated considering the average values shown on (A) and (B). (D) Average cell area in each formulation of the chip. The area occupied by each cell was calculated the analysis of cell F-actin staining in each biomaterial formulation using ImageJ software (NIH, USA). All values represent mean ± standard deviation.

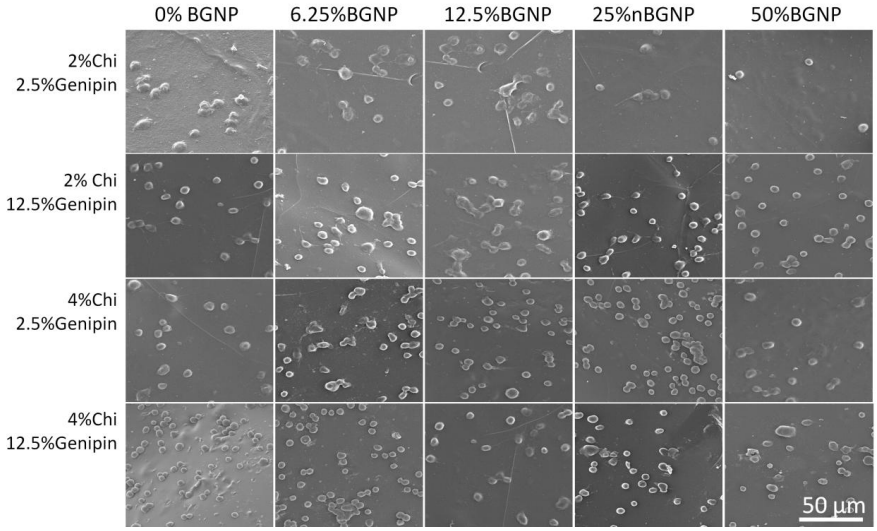

Figure 7.8. – Scanning electron microscopy micrographs of representative areas of all formulation studied for MC3T3-E1 response after 3 days of cell culture.

7.4. EXPERIMENTAL SECTION

7.4.1. Development of the superhydrophobic chips

Polystyrene flaks were cut from commercially available Petri dishes (Corner). Stickers of polyvinyl chloride (PVC) (Oracal® 614) were cut in a squared-shaped shape with 2x2 mm^2 in an A4 sheet in a typography service using a CNC laser cutting machine. Arrays of 30 squared-shaped stickers separated by 2 mm were printed in the polystyrene flaks. The polystyrene surfaces were then treated using a phase-separation method, as described by Oliveira et al.10,13 and dried under a flow of nitrogen. Tetrahydrofuran (THF) was purchased from Fluka and absolute ethanol from Panreac. The stickers were removed after the drying of the surfaces.

7.4.2. Preparation of BG-nanoparticles

To prepare the BG-NPs a protocol based on previous work was followed [18,58]. The procedure to obtain nanoparticles with the composition SiO_2:CaO:P_2O_5 (mol.%) = 55:40:5 consisted of sequential reagent dissolution that resulted in hydrolysis and polycondensation reactions. TEOS (99.90% pure) was used as the silicon precursor, ammonium phosphate dibasic as the phosphorus precursor, calcium nitrate tetrahydrate (99%) as the calcium precursor, citric acid monohydrate (99–100%) to promote hydrolysis, absolute ethanol, ammonium hydroxide (maximum 33% NH3) as the gelling agent and

polyethylene glycol 20,000 (PEG) as the surfactant. The BG-NPs were sintered at 700°C for 5 h to obtain spherical particles with sizes below 50 nm.

7.4.3. Development of the hydrogels

Solutions of low molecular weight Chi (Sigma; molecular weight of 50-190 kDa, as referred by the supplier; degree of deacetylation 75-85%) were prepared in acetic acid (2% v/v) in concentrations of 2% (w/v), 3% (w/v) and 4% (w/v). Parts of these solutions were mixed with BG-NP in amounts of 0%, 6.25%, 12.5%, 25% and 50% relatively to the Chi total mass in the solution (w/w of Chi). An amount of 4 µl of each solution was dropped in each hydrophilic well. Amounts of 2 µl of genipin in concentrations of either 2.5% or 12.5% (in a 10 ethanol/90 water mixture), relatively to the total mass of Chi in the well, were dropped on the top of each droplet of Chi/BG-NP. The crosslinking reaction occurred during 4 hours at 37°C in a humidity saturated environment. The chips were then immersed in ethanol in order to clean the genipin residues, and afterwards in PBS at 37°C for 1 hour.

7.4.4. Determination of the density of the biomaterials

The density of the biomaterials was determined by weighting each hydrogel after 1 hour of immersion in PBS at 37°C, and by measuring its dimensions in the same conditions, in order to calculate the hydrogels' volume. Density was calculated by weight/volume.

7.4.5. On-chip mechanical and viscoelastic characterization of the biomaterials

The viscoelastic measurements of the scaffolds were performed using a TRITEC8000B DMA from Triton Technology (UK), equipped with the compressive mode, in PBS at 37°C. A steel cylindrical probe of 3.8 mm of diameter was especially fabricated to perform non-destructive compression tests to the individual scaffolds in the chip. This piece was inserted in the fixed upper plate of the DMA equipment. The superhydrophobic platform containing the scaffolds was fixed in the down plate of the DMA equipment in a gutter previously assembled in this part of the apparatus, which allowed the platform to move two-dimensionally (Figure 7.1A). In each assay, the individual scaffolds were vertically aligned with the cylindrical steel probe.

The DMA spectra were obtained during a frequency scan between 0.1 and 10 Hz. The experiments were performed under constant strain amplitude, corresponding to approximately 1% of the original height of the sample. At least four samples were used for each condition.

7.4.6. Assessment of dynamic mechanical/viscoelastic properties of "bulk" conventional sized hydrogels: a control study

Control samples were prepared using chips with round hydrophilic spots with 8 mm width. The prepared solutions were dispensed in each well in individual volumes of 100 µl. In control samples produced by conventional means, the applied strain amplitude was of 30 µm. A small preload was applied to each sample to ensure that the entire scaffold surface was in contact with the compression plates before testing. At least three samples were used for each condition.

7.4.7. Nanoindentation

Nanoindentation tests were carried out at room temperature using air-dried samples. A Berkovich diamond indenter was used. A loading rate of 0.01mN/s was applied until a maximum load of 10 mN was reached. Three to five indentations were made in random locations on each side of the air-dried hydrogels.

7.4.8. Cell studies: MC3T3-E1 pre-osteoblasts adhesion, proliferation and morphology analysis

Cell culture and expansion

A pre-osteoblast cell line (MC3T3-E1, ATCC) was used to study cells-biomaterials interaction on-chip. Cells were expanded in basal medium consisting of alpha-MEM (Gibco, UK) supplemented with 10% heat-inactivated fetal bovine serum (BiochromAG, Germany) and 1% antibiotic/antimycotic solution (penicillin 100 units/mL and streptomycin 100 mg/mL; Gibco, UK). Cells were grown in 150 cm2 tissue culture flasks and incubated at 37 °C in a humidified air atmosphere of 5% CO_2. Every 3–4 days, fresh medium was added. At 90% of confluence, cells grown in tissue culture flasks were washed with PBS and subsequently detached by a chemical procedure with 0.05% trypsin-EDTA solution for 5 min at 37 °C in a humidified air atmosphere of 5% CO_2. To inactivate the trypsin effect, cell culture medium was added. The cells were then centrifuged at 300 g and 25 °C for 5 min and the medium was decanted. A cell suspension with a density of $1x10^6$ cells/mL was prepared. Prior to the contact with cell suspension, the platforms were sterilized with ethanol 70% (v/v) for 2 hours, rinsed with sterile phosphate buffered saline (PBS) 3 times. The chips were put in contact with 5 mL of cell suspension.

Cell analysis on-chip

Cell quantification was performed after washing the whole chips with PBS and fixing the cells with formalin, after 1 and 3 days of cell culture. Cells' nuclei were stained with 4',6-diamidino-2-phenylindole

(DAPI, Sigma, diluted 1000x). F-actin was stained with phalloidin-tetramethyl rhodamine isothiocyanate (Sigma, diluted 1000x). Cell number was quantified through cell nuclei counting using particle analysis of ImageJ software (NIH). Cell area was calculated by particle analysis of the F-actin staining. Each condition was analyzed in quadruplicate. All results are represented by average ± S.D..

Cells' morphology was assessed with more detail by scanning electron microscopy (JEOL JSM-6010LV). The whole chips were assessed after dehydration using sequential ethanol immersions, from 30% to 90%, followed by air drying and sputtering of the samples with a gold layer.

7.4.9. Statistical and factorial analysis

All data is presented as mean ± S.D. for triplicate sets. The data obtained for E' and $tan\ \delta$ at the frequency of 1 Hz was analyzed by two-way analysis of variance (ANOVA) test, followed by Bonferroni's pos-test for $p<0.05$, for the factors "genipin concentration" and "polymer concentration". The differences between distinct BG-NP amounts in the hydrogels with fixed amounts of Chi and genipin were tested by one-way ANOVA, followed by Tukey's post test with significance for $p<0.05$.

Regarding factorial analysis, specific storage modulus data obtained at 1 Hz was analyzed in the Design-Expert 7 software. The factors were considered as categorical ordinal and the model was not adjusted to any transformation. Data regarding single factors effect and combined interference was demanded.

7.5. Conclusions

We developed an on-chip strategy based on superhydrophobic chips and on the adaptation of a DMA to test the mechanical and viscoelastic properties of miniaturized hydrogels. Those were produced in a combinatorial and resource-saving logic to be used as biomaterials for bone tissue engineering. Factorial analysis was performed to independently study the effect of the concentration of the polymer used as the main matrix in the hydrogels (Chi), as well as the effect of the addition of two distinct relative amounts of crosslinker (genipin). We also assessed the effect of addition of BG-NP in the mechanical and viscoelastic properties of the material formulations. Storage modulus, as well as specific storage modulus of hydrogels, was mostly affected by Chi concentration, as higher concentrations led to higher modulus. The addition of BG-NP was the second most relevant effect to the system; addition of such nanoparticles in amounts higher than 12.5% (w/w of Chi) – namely 25% and 50% (w/w of Chi) - led, in general, to significant increase in the storage modulus and specific storage modulus of the hydrogels. The concentration of genipin used to crosslink Chi also affected the storage modulus of the hydrogels, although in a lower extent than the previously referred factors. The interaction of this factor with Chi

concentration also affected the storage modulus outcomes in the hydrogels. Regarding the loss factor of the hydrogels, formulations where values were maintained in the range of the native bone tissue were obtained.

The response of MC3T3-E1 pre-osteoblast cell line was also assessed on-chip. Such cells showed selective preferential adhesion to specific conditions on the chip. Their proliferation and spreading was increased mainly in formulations with lower amount of chitosan (2% w/v), with intermediate concentrations of BG-NP, especially 12.5% (w/w) BG-NP, with an *E'* value of 240 kPa and a *tan* δ value of 0.10.

7.6. ACKNOWLEDGEMENTS

The authors acknowledge the financial support from the FCT- Fundação para a Ciência e para a Tecnologia through the Ph.D. and Post-Doctoral grants with the references SFRH/BD/71396/2010 and SFRH/BPD/91681/2012. We also acknowledge the financial support of FEDER through the program Operacional Factores de Competitividade - COMPETE and from FCT – under the projects PTDC/FIS/115048/2009 and PTDC/CTM-Bio/1814/2012.

7.7. SUPPORTING INFORMATION

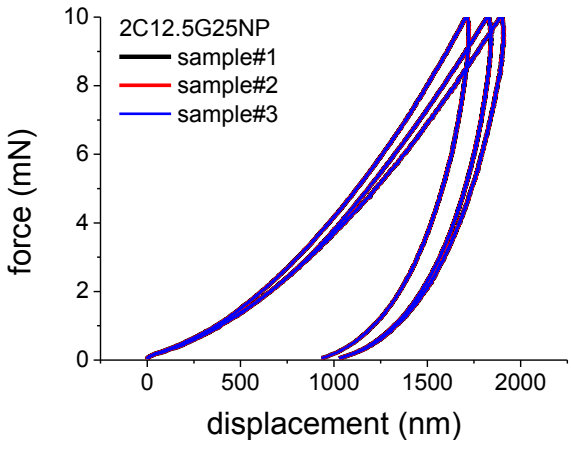

Figure 7.S1 – Load/displacement curve obtained with nanoindentation performed on-chip in dry conditions for the formulation 2%Chi12.5%G25NP, in three distinct points of three distinct samples.

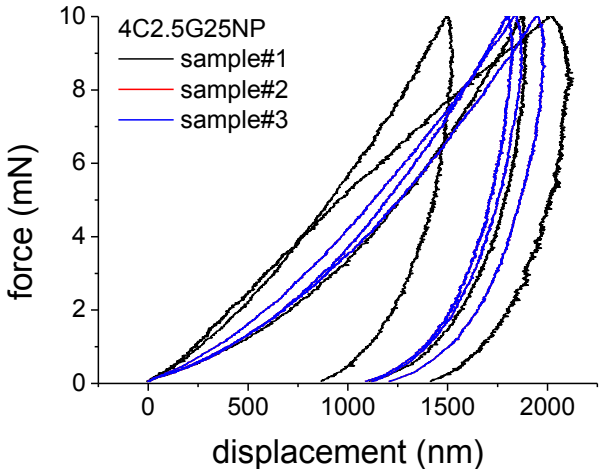

Figure 7.S2 – Load/displacement curve obtained with nanoindentation performed on-chip in dry conditions for the formulation 4%Chi2.5%G25NP, in three distinct points of three distinct samples.

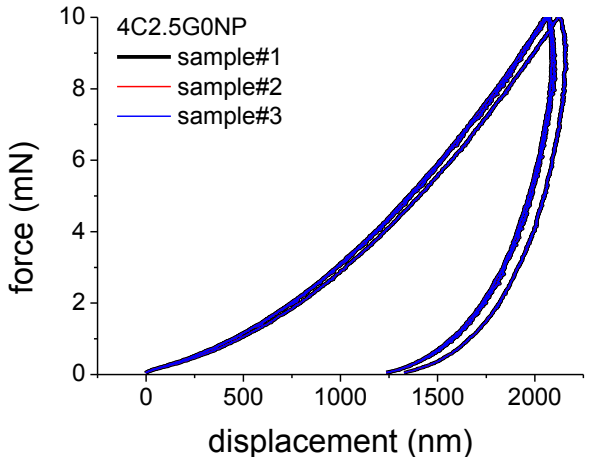

Figure 7.S3 – Load/displacement curve obtained with nanoindentation performed on-chip in dry conditions for the formulation 4%Chi2.5%G0NP, in three distinct points of three distinct samples.

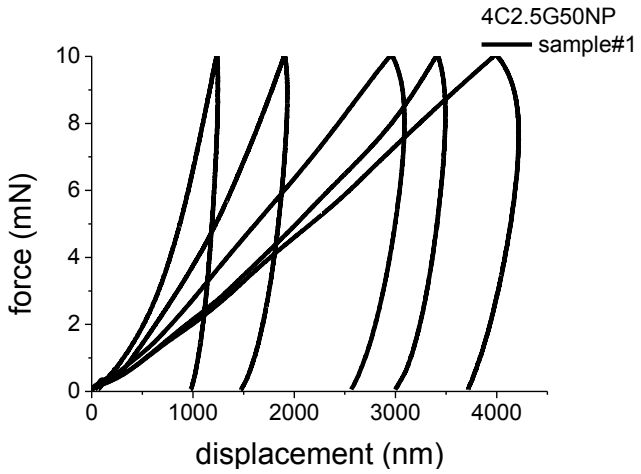

Figure 7.S4 – Load/displacement curve obtained with nanoindentation performed on-chip in dry conditions for the formulation 4%Chi2.5%G50NP, in five distinct points a single sample.

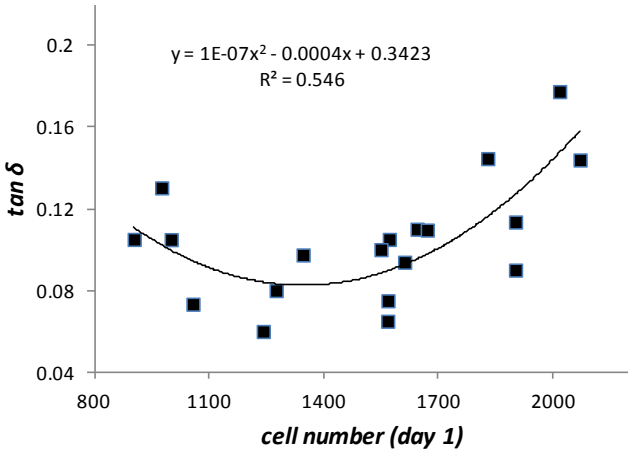

Figure 7.S5 – Average values of *tan* δ measured on-chip and respective cell number adhered to each formulation after 1 day of cell culture, and respective polynomial fitting.

7.7. REFERENCES

[1] Porter JR, Ruckh TT, Popat KC. Bone tissue engineering: A review in bone biomimetics and drug delivery strategies. Biotechnology Progress. 2009;25:1539-60.

[2] Salgado AJ, Coutinho OP, Reis RL. Bone Tissue Engineering: State of the Art and Future Trends. Macromolecular Bioscience. 2004;4:743-65.

[3] Sikavitsas VI, Temenoff JS, Mikos AG. Biomaterials and bone mechanotransduction. Biomaterials. 2001;22:2581-93.

[4] Albrektsson T, Johansson C. Osteoinduction, osteoconduction and osseointegration. Eur Spine J. 2001;10:S96-S101.

[5] Oliveira MB, Mano JF. Polymer-Based Microparticles in Tissue Engineering and Regenerative Medicine. Biotechnol Progr. 2011;27:897-912.

[6] Engler AJ, Sen S, Sweeney HL, Discher DE. Matrix elasticity directs stem cell lineage specification. Cell. 2006;126:677-89.

[7] Paul DR, Robeson LM. Polymer nanotechnology: Nanocomposites. Polymer. 2008;49:3187-204.

[8] Luz GM, Mano JF. Mineralized structures in nature: Examples and inspirations for the design of new composite materials and biomaterials. Composites Science and Technology. 2010;70:1777-88.

[9] Mano JF, Silva GA, Azevedo HS, Malafaya PB, Sousa RA, Silva SS, et al. Natural origin biodegradable systems in tissue engineering and regenerative medicine: present status and some moving trends. J R Soc Interface. 2007;4:999-1030.

[10] Muzzarelli RAA. Chitins and chitosans for the repair of wounded skin, nerve, cartilage and bone. Carbohydr Polym. 2009;76:167-82.

[11] Di Martino A, Sittinger M, Risbud MV. Chitosan: A versatile biopolymer for orthopaedic tissue-engineering. Biomaterials. 2005;26:5983-90.

[12] Silva SS, Mano JF, Reis RL. Potential applications of natural origin polymer-based systems in soft tissue regeneration. Crit Rev Biotechnol. 2010;30:200-21.

[13] Boccaccini AR, Erol M, Stark WJ, Mohn D, Hong Z, Mano JF. Polymer/bioactive glass nanocomposites for biomedical applications: A review. Composites Science and Technology. 2010;70:1764-76.

[14] Misra SK, Mohn D, Brunner TJ, Stark WJ, Philip SE, Roy I, et al. Comparison of nanoscale and microscale bioactive glass on the properties of P(3HB)/Bioglass® composites. Biomaterials. 2008;29:1750-61.

[15] Xu HHK, Sun L, Weir MD, Takagi S, Chow LC, Hockey B. Effects of incorporating nanosized calcium phosphate particles on properties of whisker-reinforced dental composites. Journal of Biomedical Materials Research Part B: Applied Biomaterials. 2007;81B:116-25.

[16] Heinemann S, Ehrlich H, Knieb C, Hanke T. Biomimetically inspired hybrid materials based on silicified collagen. International Journal of Materials Research. 2007;98:603-8.

[17] Lu HH, El-Amin SF, Scott KD, Laurencin CT. Three-dimensional, bioactive, biodegradable, polymer–bioactive glass composite scaffolds with improved mechanical properties support collagen synthesis and mineralization of human osteoblast-like cells in vitro. J Biomed Mater Res A. 2003;64A:465-74.

[18] Alves NM, Leonor IB, Azevedo HS, Reis RL, Mano JF. Designing biomaterials based on biomineralization of bone. J Mater Chem. 2010;20:2911-21.

[19] Hong Z, Reis RL, Mano JF. Preparation and in vitro characterization of novel bioactive glass ceramic nanoparticles. Journal of Biomedical Materials Research Part A. 2009;88A:304-13.

[20] Hong Z, Luz GM, Hampel PJ, Jin M, Liu A, Chen X, et al. Mono-dispersed bioactive glass nanospheres: Preparation and effects on biomechanics of mammalian cells. Journal of Biomedical Materials Research Part A. 2010;95A:747-54.

[21] Rezwan K, Chen QZ, Blaker JJ, Boccaccini AR. Biodegradable and bioactive porous polymer/inorganic composite scaffolds for bone tissue engineering. Biomaterials. 2006;27:3413-31.

[22] Jell G, Stevens MM. Gene activation by bioactive glasses. J Mater Sci: Mater Med. 2006;17:997-1002.

[23] Srinivasan S, Jayasree R, Chennazhi KP, Nair SV, Jayakumar R. Biocompatible alginate/nano bioactive glass ceramic composite scaffolds for periodontal tissue regeneration. Carbohyd Polym. 2012;87:274-83.

[24] Sowmya S, Sudheesh Kumar PT, Chennazhi KP, Nair SV, Tamura H, Jayakumar R. Biocompatible β-chitin Hydrogel/Nanobioactive Glass Ceramic Nanocomposite Scaffolds for Periodontal Bone Regeneration. Trends in Biomaterials & Artificial Organs. 2011;25:1-11.

[25] Mota J, Yu N, Caridade SG, Luz GM, Gomes ME, Reis RL, et al. Chitosan/bioactive glass nanoparticle composite membranes for periodontal regeneration. Acta Biomaterialia. 2012;8:4173-80.

[26] Caridade SG, Merino EG, Alves NM, Bermudez VdZ, Boccaccini AR, Mano JF. Chitosan membranes containing micro or nano-size bioactive glass particles: evolution of biomineralization followed by in situ dynamic mechanical analysis. Journal of the Mechanical Behavior of Biomedical Materials. 2013;20:173-83.

[27] Luz GM, Boesel L, Campo Ad, Mano JF. Micropatterning of Bioactive Glass Nanoparticles on Chitosan Membranes for Spatial Controlled Biomineralization. Langmuir. 2012;28:6970-7.

[28] Lin S, Sangaj N, Razafiarison T, Zhang C, Varghese S. Influence of Physical Properties of Biomaterials on Cellular Behavior. Pharm Res. 2011;28:1422-30.

[29] Oliveira MB, Salgado CL, Song W, Mano JF. Combinatorial On-Chip Study of Miniaturized 3D Porous Scaffolds Using a Patterned Superhydrophobic Platform. Small. 2013;9:768-78.

[30] Correlo VM, Boesel LF, Pinho E, Costa-Pinto AR, Alves da Silva ML, Bhattacharya M, et al. Melt-based compression-molded scaffolds from chitosan–polyester blends and composites: Morphology and mechanical properties. Journal of Biomedical Materials Research Part A. 2009;91A:489-504.

[31] Tweedie CA, Anderson DG, Langer R, Van Vliet KJ. Combinatorial Material Mechanics: High-Throughput Polymer Synthesis and Nanomechanical Screening. Adv Mater. 2005;17:2599-604.

[32] Simon CG, Eidelman N, Deng Y, Washburn NR. High-Throughput Method for Determining Modulus of Polymer Blends. Macromolecular Rapid Communications. 2004;25:2003-7.

[33] Stafford CM, Harrison C, Beers KL, Karim A, Amis EJ, Vanlandingham MR, et al. A buckling-based metrology for measuring the elastic moduli of polymeric thin films. Nat Mater. 2004;3:545-50.

[34] Rojo FJ, Páez JMG, Jorge-Herrero E, Atienza JM, Millán I, Rocha A, et al. Optimal selection of biological tissue using the energy dissipated in the first loading cycle. Journal of Biomedical Materials Research Part B: Applied Biomaterials. 2010;95B:414-20.

[35] Sasaki N. Viscoelastic Properties of Biological Materials, In Vicent (ed.) Viscoelasticity – from theory to biological applications, InTech, 2012, pp. 99-122.

[36] Abdel-Sayed P, Darwiche SE, Kettenberger U, Pioletti DP. The role of energy dissipation of polymeric scaffolds in the mechanobiological modulation of chondrogenic expression. Biomaterials. 2014;35:1890-7.

[37] Poon B, Rittel D, Ravichandran G. An analysis of nanoindentation in linearly elastic solids. International Journal of Solids and Structures. 2008;45:6018-33.

[38] Coutinho DF, Sant SV, Shin H, Oliveira JT, Gomes ME, Neves NM, et al. Modified Gellan Gum hydrogels with tunable physical and mechanical properties. Biomaterials. 2010;31:7494-502.

[39] Salgado CL, Oliveira MB, Mano JF. Combinatorial cell-3D biomaterials cytocompatibility screening for tissue engineering using bioinspired superhydrophobic substrates. Integrative Biology. 2012;4:318-27.

[40] Oliveira MB, Mano JF. On-Chip Assessment of the Protein-Release Profile from 3D Hydrogel Arrays. Analytical Chemistry. 2013;85:2391-6.

[41] Neto AI, Custodio CA, Song WL, Mano JF. High-throughput evaluation of interactions between biomaterials, proteins and cells using patterned superhydrophobic substrates. Soft Matter. 2011;7:4147-51.

[42] Luz GM, Leite AJ, Neto AI, Song WL, Mano JF. Wettable arrays onto superhydrophobic surfaces for bioactivity testing of inorganic nanoparticles. Mater Lett. 2011;65:296-9.

[43] Duarte ARC, Caridade SG, Mano JF, Reis RL. Processing of novel bioactive polymeric matrixes for tissue engineering using supercritical fluid technology. Materials Science and Engineering: C. 2009;29:2110-5.

[44] Gentile P, Mattioli-Belmonte M, Chiono V, Ferretti C, Baino F, Tonda-Turo C, et al. Bioactive glass/polymer composite scaffolds mimicking bone tissue. J Biomed Mater Res A. 2012;100A:2654-67.

[45] Lei B, Shin K-H, Noh D-Y, Koh Y-H, Choi W-Y, Kim H-E. Bioactive glass microspheres as reinforcement for improving the mechanical properties and biological performance of poly(ε-caprolactone) polymer for bone tissue regeneration. Journal of Biomedical Materials Research Part B: Applied Biomaterials. 2012;100B:967-75.

[46] Ghosh S, Gutierrez V, Fernández C, Rodriguez-Perez MA, Viana JC, Reis RL, et al. Dynamic mechanical behavior of starch-based scaffolds in dry and physiologically simulated conditions: Effect of porosity and pore size. Acta Biomaterialia. 2008;4:950-9.

[47] Luz GM, Mano JF. Chitosan/bioactive glass nanoparticles composites for biomedical applications. Biomedical Materials. 2012;7:054104.

[48] Caridade SG, Merino EG, Alves NM, Bermudez VdZ, Boccaccini AR, Mano JF. Chitosan membranes containing micro or nano-size bioactive glass particles: evolution of biomineralization followed by in situ dynamic mechanical analysis. Journal of the Mechanical Behavior of Biomedical Materials. 2013;20:173-83.

[49] Guedes RM, Simões JA, Morais JL. Viscoelastic behaviour and failure of bovine cancellous bone under constant strain rate. Journal of biomechanics. 2006;39:49-60.

[50] Lakes RS, Katz JL, Sternstein SS. Viscoelastic properties of wet cortical bone—I. Torsional and biaxial studies. Journal of biomechanics. 1979;12:657-78.

[51] Ehrbar M, Sala A, Lienemann P, Ranga A, Mosiewicz K, Bittermann A, et al. Elucidating the role of matrix stiffness in 3D cell migration and remodeling. Biophys J. 2011;100:284-93.

[52] Keogh MB, O'Brien FJ, Daly JS. Substrate stiffness and contractile behaviour modulate the functional maturation of osteoblasts on a collagen–GAG scaffold. Acta Biomaterialia. 2010;6:4305-13.

[53] Claes LE, Cunningham JL. Monitoring the Mechanical Properties of Healing Bone. Clin Orthop Relat Res. 2009;467:1964-71.

[54] Moorcroft CI, Ogrodnik PJ, Thomas PBM, Wade RH. Mechanical properties of callus in human tibial fractures: a preliminary investigation. Clinical Biomechanics. 2001;16:776-82.

[55] Leong PL, Morgan EF. Measurement of fracture callus material properties via nanoindentation. Acta Biomaterialia. 2008;4:1569-75.

[56] Claes LE, Heigele CA, Neidlinger-Wilke C, Kaspar D, Seidl W, Margevicius KJ, et al. Effects of mechanical factors on the fracture healing process. Clin Orthop Relat Res. 1998:S132-47.

[57] Ina K, Kitamura H, Tatsukawa S, Miyazaki T, Abe H, Fujikura Y. Intracellular formation of collagen microfibrils in granulation tissue. Experimental and Molecular Pathology. 2005;79:244-8.

[58] Luz GM, Mano JF. Preparation and characterization of bioactive glass nanoparticles prepared by sol–gel for biomedical applications. Nanotechnology. 2011;22:494014.

CHAPTER 8. *IN VIVO* HIGH-CONTENT EVALUATION OF THREE-DIMENSIONAL SCAFFOLDS BIOCOMPATIBILITY[7]

8.1. ABSTRACT

While developing tissue engineering strategies, inflammatory response caused by biomaterials is an unavoidable aspect to be taken in consideration, as it may be an early limiting step of tissue regeneration approaches. We demonstrate the application of flat and flexible films exhibiting patterned high-contrast wettability regions as implantable platforms for the high-content *in vivo* study of inflammatory response caused by biomaterials. Screening biomaterials by using high-throughput platforms is a powerful method to detect hit spots with promising properties and to exclude uninteresting conditions for targeted applications. High-content analysis of biomaterials has been mostly restricted to *in vitro* tests where crucial information is lost, as *in vivo* environment is highly complex. Conventional biomaterials implantation requires the use of high numbers of animals, leading to ethical questions and costly experimentation. Biomaterials' inflammatory response has also been highly neglected in high-throughput studies. We designed an array of 36 combinations of biomaterials based in an initial library of four polyssacharides. Biomaterials were dispensed onto biomimetic superhydrophobic platforms with wettable regions and processed as freeze-dried three-dimensional scaffolds with a high control of the array configuration. These chips were afterwards implanted subcutaneously in Wistar rats. Lymphocyte recruitment and activated macrophages were studied on-chip, by performing immunocytochemistry in the miniaturized biomaterials after 24 hours and 7 days of implantation. Histological cuts of the surrounding tissue of the implants were also analyzed. Localized and independent inflammatory responses were detected. The integration of this data with control data proved that these chips are robust platforms for the rapid screening of early-stage *in vivo* biomaterials' response.

[7]This chapter was based on the publication: Oliveira MB, Ribeiro MP, Miguel SP, Neto AI, Coutinho P, Correia IJ, et al. *In Vivo* High-Content Evaluation of Three-Dimensional Scaffolds Biocompatibility. Tissue Eng Part C Methods (in press). doi: 10.1089/ten.tec.2013.0738

8.2. INTRODUCTION

The choice of biocompatible materials in the development of tissue engineering strategies is crucial, as the lack of adequate immune response caused by biomaterials is one of the most common causes of failure of implants due to tissue damage and chronic response [1,2]. Although inflammatory response is commonly responsible for implants failure, it was also reported to contribute for the triggering of tissue regeneration. It is known that altered levels of TNF-α, IL-1 and other proinflammatory molecules have a major effect on the healing of bone fractures [3]. Inflammation is required in neural regeneration for enhancing the proliferation of neural progenitors and neurogenesis, [4] and has also a necessary involvement in salamanders' limb regeneration, a process dependent on the presence of macrophages [5]. Regeneration using mesenchymal stem cells was also proven to be dependent on recipient T lymphocytes, through the interferon gamma (IFN-γ)-induced downregulation of Runx-2 and enhancement of tumor necrosis factor alpha (TNF-α) signaling in cells [6]. In order to discover optimized formulations of biomaterials for tissue regeneration it is important to screen different and high numbers of combinations of materials. In this complex process, one of the key aspects to take in consideration is the inflammatory response caused by such materials, and its role in implant rejection or as regeneration adjuvants.

High-content approaches to study cells-biomaterials interactions have allowed collecting large amounts of data about single and combined molecular interactions affecting tissue regeneration. The ultimate goal of these approaches is to perform assays in a resource- and time-saving manner [7,8]. Biomaterials with beneficial properties for stem cells culture [10-15] and bacterial attachment prevention [16] were spotted using micro-array methods [17]. Over time arrayed platforms for high-content studies matured from platforms that allowed studying cells-2D materials interactions to platforms compatible with cell encapsulation in hydrogels, allowing for a closer *in vivo*-like approach. These studies were carried out in *in vitro* environment. As such, information was lost on inflammatory response of these materials, as well as other phenomena resulting from the complexity of the *in vivo* environment. The lack of established methods for *in vivo* combinatorial analysis led us to develop the method described herein.

Hereby, we propose the implantation of superhydrophobic flexible and flat platforms with patterned arrays of wettable regions where combinations of biomaterials are dispensed and processed as independent porous scaffolds. These chips are used to study foreign body response in localized spots in a high-throughput manner [18.20]. Similar platforms were used *in vitro* for the study of protein-cells interactions in 2D environment, cell-laden 3D hydrogels and 3D scaffolds [19-21]. We hypothesize that

the miniaturized size of the patterned biomaterials and the gap maintained between them would be sufficient to observe distinct inflammatory cells recruitment, while allowing for isolated responses in each spot. Moreover, the low cell adhesion reported in superhydrophobic surfaces would improve the independency between spots [18-22]. For the proof-of-concept, we designed an array of 36 combinations of biomaterials from a small library of four materials: chitosan (Chi), alginate (Alg) and two carrageenans: k-carrageenan (k-Carr) and ι-carrageenan (ι-Carr), the later having a higher number of sulfate groups. We aimed to study the effect of distinct anionic surfaces combined with Chi, as they were reported to promote higher levels of macrophages and adherent lymphocytes, compared to materials with distinct chemical features [23]. The individual inflammatory response of Chi [24] and Alg [25] applied as biomaterials was previously investigated. For carrageenans, inflammatory response in the form of implantable biomaterials is still poorly described. However, carrageenan solutions with high number of sulfate groups (ι-Carr and λ-carrageenan) are widely used to trigger inflammation for *in vivo* studies [26]. Our proposed methodology has the potential to be adapted to diversified combinations of biomaterials, allowing saving high numbers of animals. The direct application of the method would result in an important ethical achievement, along with the consequent optimization of costs adjacent to animal experimentation.

8.3. Materials and Methods

8.3.1. Superhydrophobic surfaces with wettable transparent spots

Polystyrene films (ST311190, Goodfellow) were cut in 4 x 4 cm^2 squares. 6x6 arrays of polyvinyl stickers (Oracal) were patterned in the surfaces. The arrays were constituted by squares of 4 mm^2, separated by 2 mm in all sides (Figure 8.1). The surfaces were treated by a phase-separation method, as described elsewhere [27]. Briefly, a solution of commercial grade polystyrene in THF (Sigma) (70 mg/mL) and ethanol absolute (in proportions of 2:1.3) was poured onto the polystyrene films. The solution was then removed and the surfaces were immersed in ethanol absolute. After one minute under immersion, the surfaces were let to dry at room temperature. The stickers were then totally removed and the whole surface washed with pure ethanol to remove possible traces of the stickers' glue. The chips were afterwards cut in 4 geometrically equal squares with 9 biomaterials per square (3x3 array) for implantation.

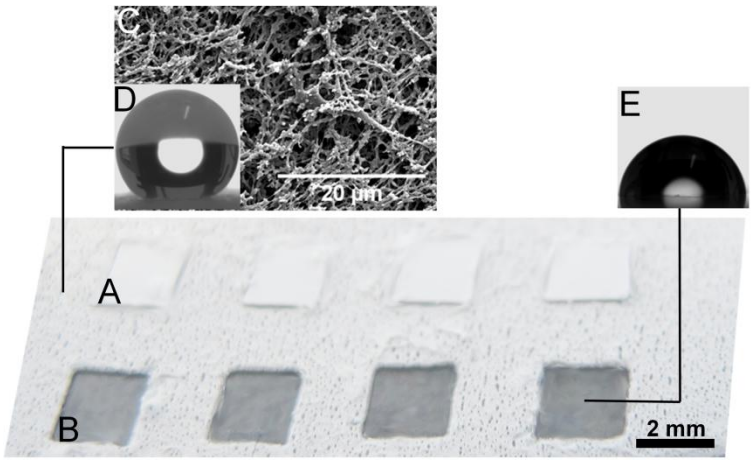

Figure 8.1. – Image of a part of an array of patterns on the chip with A) protective stickers and B) after removing the protective stickers, with transparent wettable spots. C) Scanning electron microscopy image of superhydrophobic domain of the chip. D) Representative profile of a water droplet on the superhydrophobic domain of the chip (contact angle of 156.2°±0.3). E) Representative profile of water droplet on the non-treated part of the chip - wettable region (contact angle of 90.5°±4.7).

8.3.2. Biomaterials array deposition

Our experimental design consisted in a matrix of 36 combinations of biomaterials. The processing of biomaterials followed two steps: firstly, we prepared freeze-dried genipin-crosslinked scaffolds, with distinct concentrations of Chi ("A", in Figure 8.2D,E) in acetic acid (2% v/v) solution: 1%, 1.5% and 2% (w/v). We previously proved that these Chi concentrations are adequate for the preparation of porous scaffolds on such chips [21]. Nine scaffolds of each concentration were prepared in the chips (Figure 8.2D). After freeze-drying the Chi structures, solutions of other polymers (labeled "polymer B") were dispensed on the top of these porous scaffolds in distinct concentrations (Figure 8.2E).

Medium molecular weight Chi (ref. 448877, batch MKBJ9698V, Sigma), with 75% to 85% of desacetylation, was purified according to a re-precipitation method. A solution of crosslinker was prepared with 4% (w/v) genipin (Comercial Rafer, S.L.) in distilled water and ethanol (90:10 v/v). The Chi scaffolds were prepared by pipetting 4 µl of Chi solutions and 2 µl of genipin in each wettable spot of the chip. One additional condition of 1.5% (w/v) of Chi was added to the array, where the volume of Chi dispensed in the wettable regions was 6 µl. This condition is referred as "1.5%+". Crosslinking occurred at 37°C in water saturated environment. Afterwards, the chips were frozen at -20 °C for 2 hours and -80°C overnight. Freeze drying occurred at -80°C, 0.3 bar. Polymers B (Figure 8.2E) were added afterwards to the Chi freeze-dried scaffolds in amounts of 2 µl. Polymers B were Alg (ref. W201502, Sigma), k-Carr (ref. 22048, Sigma) and ι-Carr (ref. 22045, Sigma), in concentrations of 2%

(H), 1% (M) and 0.5% (L) (w/v). They were used as received. They were crosslinked with KCl for k-Carr (JMGS) or $CaCl_2$ (VWR) for ι-Carr and Alg, both at concentration 1M. The chips were again frozen at -20°C for 2 hours and -80°C overnight. Freeze-drying occurred at -80°C, 0.03 bar.

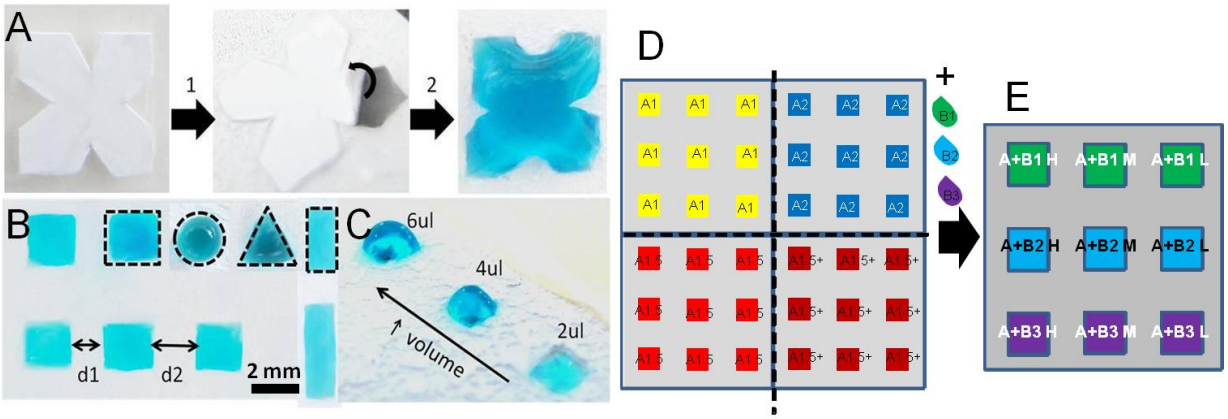

Figure 8.2. – A) Preparation of superhydrophobic patterned chips using removable stickers B) allowing to imprint complex geometrical wettable features surrounded by superhydrophobic domains (step 1 refers to the stickers in the polystyrene untreated film; step 2 shows the superhydrophobic polystyrene chip where the protecting sticker is being removed so the wettable area is exposed). Liquid precursors can be dispensed in wettable regions with distinct sizes and shapes B) (see examples delimited by dashed lines) and with different volumes C). D) Setup used to prepare the implanted chips, where Chi ("A") was patterned in distinct concentrations (1%, 1.5%, 2% and 1.5+%) and separated by different distances (d1, d2), as described in Results section. E) Biomaterials ("B") were added to the previously freeze-dried Chi scaffolds in distinct dilutions (H, M, L for lower, medium and highest dilution factor of polymer "B"), in order to obtain chips with distinct combinations of biomaterials. The implanted chips with 9 scaffolds were cut from the previous chip with 36 scaffolds.

8.3.3. Control samples

On-chip controls: On-chip control samples were processed in an equivalent manner to the standard chips. Biomaterials were dispensed in a randomized configuration, indicated in Table 8.S1, in Supporting Information.

Implantable plugs: Two random conditions were selected from the array of biomaterials: Chi1% ι-Carr2%H and Chi1% Alg2%H. Plugs with 5 mm diameter x 3 mm height of these conditions were processed in commercially available 96 well plates. A volume of 200 µl of Chi solutions was dropped in each well, followed by 100 µl of genipin solution, in the same proportions and concentrations used for on-chip experiments. The well plate was then placed at 37°C for 3 hours, while the crosslinking reaction took place. The samples were then frozen and freeze-dried, in the same conditions as the on-chip ones.

The solutions of polymer B were dispensed on the top of the previously prepared Chi sponges according to the proportions used on-chip, and then crosslinked with 50 µl of the crosslinking solutions. Freeze-drying was repeated. The samples were washed and sterilized using the same procedure of on-chip samples.

Sterilization of the chips and control plugs: The chips with the scaffolds in their final stage of processing were immersed in ethanol 70% (Panreac) for 30 minutes. Before implantation, they were washed with sterile physiological buffer solution (PBS, Fluka) for 15 minutes, three times. The same procedure was performed for the plugs implants prepared without the superhydrophobic film, and to the empty chips.

8.3.4. Implantation of the chips and control samples in Wistar rats

The 36 spot chips were cut in 4 parts (with 9 miniaturized scaffolds per part), the chips boarders were cut with rounded shape as close to the scaffolds as possible, and a mark was made on each chip, in order to identify of the relative position of the biomaterials after explantation. The chips were then implanted subcutaneously in Wistar rats for 24 hours and 7 days with the configuration indicated in Figure 8.2D,E.

To perform the *in vivo* assays a total of 27 Wistar rats (8-10 weeks old) weighing between 150-200 g, were used. The project was conducted in accordance with the international guidelines set for animal research. This study was conducted in the animal research facility of the University of Beira Interior. Housing and animal care were provided according to procedures set for animal research. Animals were individually anesthetized with an intra-peritoneal injection of ketamine (40 mg/kg) and xylazine (5 mg/kg). Subsequently, each animal was immobilized and the dorsum was shaved, washed and disinfected with ethanol (96%). To perform chip implantation, a 1.5-2 cm skin incision was done in four different sites of animal dorsum (Figure 8.3A). The animals were divided in several groups. The first group corresponded to animals where the 4 different chips (with Chi in the different concentration: 1%, 1.5%, 2% and 1.5+%) were implanted ($n \geq 4$). All biomaterials faced the muscle side of the cut. Four chips with random configuration of the spotted biomaterials (as indicated in Table 8.S1, Supporting Information) were implanted in rats (n=3). The second group was similar to the first group; however, in these animals the chip with the condition "1.5+%" was substituted by a chip without any spotted biomaterials (empty chip) (n=2). Control groups were set as one group with 2 empty chips implanted (n=2). One biomaterial plug was implanted by animal (n=2) to be explanted after 24 hours and 7 days of implantation. Subsequently to samples implantation, the skin flaps were sutured. During the study

animals were kept in separate cages and fed with commercial rat food and water *ad libitum*. Animals were sacrificed by CO_2 asphyxiation after 24 hours and 7 days.

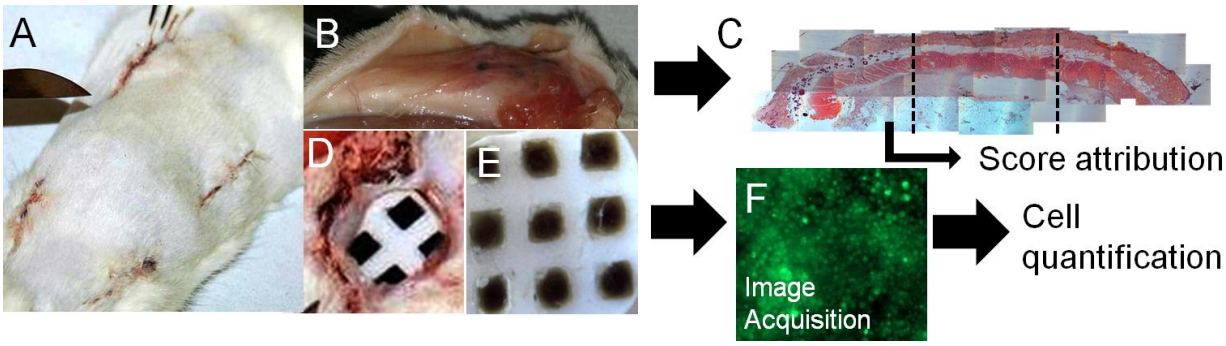

Figure 8.3. – A) Dorsal view of an animal after the implantation of the four chips in the used configuration. B) Tissue surrounding the chip after 7 days of implantation. C) Example of a histological cut performed to explanted tissue around the chip. D) Removal of one chip after 1 day of implantation. E) Explanted chip after 24 hours of implantation. F) Image of immunocytochemistry performed to lymphocytes in one of the conditions of the chip after 24 hours of implantation.

8.3.5. Immunocytochemistry

After the explants of the 4 chips in each animal, the chips were fixed and kept in paraformaldehyde (Figure 8.3E). The explanted chips were incubated with primary antibodies CD25 (AbD Serotec) (specific for IL-2 produced by lymphocytes) or CD163 (AbD Serotec) (specific for macrophages) in concentration of 1:100 overnight, at 4°C. Non-specific binding was blocked by incubation with 3% bovine serum albumin (BSA) solution in PBS for 30 min, at room temperature. After 1 h of incubation with AlexaFluor488 (Alfagene) for CD25, or AlexaFluor594 (Alfagene) for CD163, both at a concentration of 1:250, in BSA 1%, at room temperature, the cells were washed in PBS and counterstained with DAPI (Invitrogen) nuclear staining. The presence of surface markers was analyzed using an Axioplan Imager Z1 fluorescence microscope (Zeiss). Images in a total height of 500 µm were acquired in 20 layers of 25 µm. The images used for the analysis were the ones corresponding to the final stacking of the 20 layers.

8.3.6. Histological analysis

Tissue specimens were obtained from the implantation area by sharp dissection at 24 hours and 7 days, and then fixed with paraformaldehyde and paraffin embedded. In order to obtain a full analysis of all materials present in the chips, different perpendicular sections to the chip were obtained from the tissue

in contact with different samples. Histological cuts were performed in the first 2 mm of the tissue in contact with the chip, followed for 4 mm cuts. A 3 µm section obtained from each paraffin block was stained with hematoxylin and eosin (H&E).

8.3.7. Lymphocytes quantification

Images acquired by microscopy (Axiovision, Zeiss) with a 50x magnification were cut in 4 equal images. Using ImageJ (NIH) software the background caused by the natural fluorescence of natural polymer in each image was removed or minimized. Automatic nuclei counter (ITCN, ImageJ, NIH) was used to quantify the lymphocytes. Images with the green staining were analyzed considering cells with 6 µm of diameter and a separation dependent on the density of cells, varying from 2 to 6 µm. Representative images of the steps performed for the cell quantification can be consulted in Figure 8.S1, in Supporting Information.

8.3.8. Score attribution for histological cuts and macrophages immunocytochemistry

For histological sections, scoring was attributed to each part of the histological cuts (divided according to Figure 8.3C) according to the following scale: 0 – absence of inflammatory cells; 1 - presence of lymphocytes and polymorphonuclear (PMN) cells; 2 - higher presence of lymphocytes and PMN, and low amount of macrophages; 3 - higher presence of lymphocytes; 4 - high concentration of macrophages and presence of lymphocytes; 5 - very high density of macrophages; 6 – vascularization with very high concentration of macrophages. Images of on-chip macrophages were scored (0-6) according to the relative amount of macrophages in the scaffold, where 0 corresponded to the lowest relative amount, and 6 to the highest relative amount.

8.3.9. Generation of intensity maps

The color attributed to each spot of the intensity maps corresponded to the average values of the studied variables (e.g. quantified cell number or attributed score). Numerical values and respective standard deviations can be consulted in Figures 8.S2-8.S7, in Supporting Information. The colors of the intensity maps were generated with Microsoft Office Excel (Microsoft®) according to the following criteria: lower value corresponded to turquoise blue and higher value to bright red. The middle color was allocated to the 50% value of the distribution of the maximum and minimum values registered in the groups of values analyzed. This attribution was performed according to groups of results presented in the same figure or section of figures.

8.3.10. Factorial analysis

Exploratory factor analysis is a technique within factor analysis statistic methods used to uncover the underlying structure of sets of variables. Three-factor analysis was performed using the Design of Experiments DesignExpert7 Software (Stat-Ease, Inc.). Response surface models were generated for the analyzed conditions and the contribution of each factor was then quantified. The three factors considered were: concentration of Chi in the scaffold (%Chi, factor A), type of polymer "B" (polymer, factor B) and dilution of polymer B (dilution, factor C). The variables were considered as numerical, for factor A and factor C, and nominal for factor B. Three levels were considered for factor A: 1%, 1.5% and 2%. Three levels were considered for factor B: Alg, k-Carr and ι-Carr. Factor C was analyzed also considering three levels: H – for lower dilution factor (i.e. higher concentration of polymer B: 2%), M – for intermediate dilution factor (concentration of polymer B: 1%) and L – for higher dilution factor (concentration of polymer B: 0.5%). For histology scores analysis, the Chi concentration 1.5% was isolated, so a three-factor analysis was performed considering a new factor: the volume of Chi dispensed (factor D): 4 (1.5%Chi) or 6 µl (1.5%+Chi).

We developed three distinct surface response models for each time point: 24 hours and 7 days after implantation. Each model was developed according to the quantified number of lymphocytes, scores attributed to on-chip macrophages, and to each part of the histological cuts performed to the tissue collected around the chips. The results were analyzed by the software by "sequential model sum of squares" in order to select the highest order polynomial where terms were significant and the results were not aliased. For most of the models, response surface 2FI models were suggested and furtheron generated. For lymphocytes and macrophages quantifications after 24 hours of implantation, main effect models were generated. Results were then analyzed by ANOVA. Each model allowed concluding about the percentage contribution of each factor. The effect of each factor as well as combined effect of factors were also analyzed.

8.3.11. Statistical analysis

Two-way ANOVA with Bonferroni post test was performed to the results of standard chips (main experiment), resulting from the implantation in the first group of animals, considering the results of lymphocyte quantification and scoring of macrophages on-chip, as well as of histology images. Three distinct variables were considered: effect of polymer B, effect of dilution of polymer B and effect of Chi

concentration. The results of significant differences can be consulted in Table 8.S2, in Supporting Information.

8.4. Results and Discussion

We implanted 36 miniaturized combinations of biomaterials in single animals using chips based on extreme water repellency (Figures 8.1, 8.2 and 8.3) with patterned arrays of wettable regions (Figure 8.1, 8.2A-C and Figure 8.2D,E) where combinations of biomaterials (Figure 8.2D,E) were dispensed and processed as independent porous scaffolds (Figure 8.3E). The chips are versatile, allowing patterning a high diversity of shapes, sizes (Figure 8.2A,B) and amounts of biomaterials (Figure 8.2C), processed by several techniques and with the possibility of showing anisotropic features and distinct and geometrical configurations between them (Figure 8.2B). These chips - where the surface of biomaterials is totally exposed to the *in vivo* environment (Figure 8.3E) - were used to study foreign body response in localized spots in a high-throughput manner. The liquid biomaterial precursors were strongly restricted in the wettable regions due to the high contrast of surface tensions (Figure 8.2A-C) [18-20]. Superhydrophobic surfaces prepared by phase separation methods showed low cell adhesion, [18] including substrates prepared using polystyrene [22]. Therefore we expect that the scaffolds spots could be maintained relatively isolated from each other, avoiding cell passage between spots and minimizing the interaction of the platform with the *in vivo* milieu.

All biomaterials patterned in the chips remained attached to the wettable regions of the chip after 24 hours of implantation (an example of an explanted chip can be observed in Figure 8.3E). After 7 days of implantation, a small percentage of the scaffolds was integrated in the animals muscle, as the majority of the scaffolds remained attached to the chip. The response to biomaterials that remained attached to the chip was studied by immunocytochemistry along with the histological cuts performed to tissue surrounding the chip.

From here on, the set of polymers added to the Chi scaffolds – Alg, k-Carr or ι-Carr - will be labeled as polymer B, and the dilution of such polymers will be indicated as H (indicating the lowest dilution; 2% w/v polymer concentration), M (indicating an intermediate dilution; 1% w/v polymer concentration) and L (indicating the highest dilution; 0.5% w/v polymer concentration).

8.4.1. Analysis of on-chip immunocytochemistry

After being explanted, scaffolds were analyzed on-chip by immunocytochemistry, both for lymphocytes and macrophages presence. The lymphocytes were labeled with a green secondary antibody, and

macrophages with a red one. Figure 8.4 depicts representative examples of fluorescence microscopy performed to the chips where the presence of both cell types can be seen after 24 hours and 7 days of implantation. Lymphocytes present on each formulation were quantified by image analysis using ImageJ software; the procedure is explained in Figure 8.S1 (Supporting Information). The presence of macrophages in each formulation was evaluated according to a score explained previously in the Materials and Methods section. After the quantification of lymphocytes and score attribution to macrophages presence in each condition, an intensity map was built (Figure 8.6). By color analysis of the maps in Figure 8.6, all conditions on-chip can be rapidly compared in terms of average mean values obtained for lymphocytes quantification and macrophages scores. The numerical values with respective standard deviations can be found in Figures 8.S2-8.S7 (Supporting Information). Further on, the results will also be reported and discussed taking in consideration the statistical analysis of such results. Both on-chip data and histological sections results were analyzed with two-way ANOVA with Bonferroni post-test. For the on-chip data obtained from the quantification of immunocytochemistry images, analysis was performed to all combinations of the ionic networks with both 1% Chi and 2% Chi. All conditions from the histological examination were analyzed for statistical significance (results in Table 8.S2, Supporting Information).

After 24 hours of implantation, the presence of lymphocytes in the scaffolds was very similar in all conditions containing ι-Carr; no significant differences were observed between any of these conditions. The effect of dilution factor of polymer B was observed between H and M, H and L, as well as M and L, mainly for Alg-containing conditions, where L led to lower lymphocytes number than M, and those to lower scores than H conditions. Conditions containing ι-Carr were significantly different from both conditions containing k-Carr and Alg, and k-Carr conditions were different from those containing Alg. ι-Carr conditions showed higher lymphocytes numbers, followed by k-Carr and Alg. For k-Carr and Alg-containing conditions, significant differences were registered with 1% Chi and 2% Chi. Higher concentration of Chi (2%) was responsible for higher concentration of lymphocytes. Lymphocytes have been shown to adhere to surfaces *in vitro* [28]. In lymphocyte/macrophage co-cultures, lymphocytes have been observed to associate with macrophages and foreign body giant cells [1]. Regarding the presence of macrophages in the biomaterials after 24 hours of implantation, no significant differences were observed between the conditions.

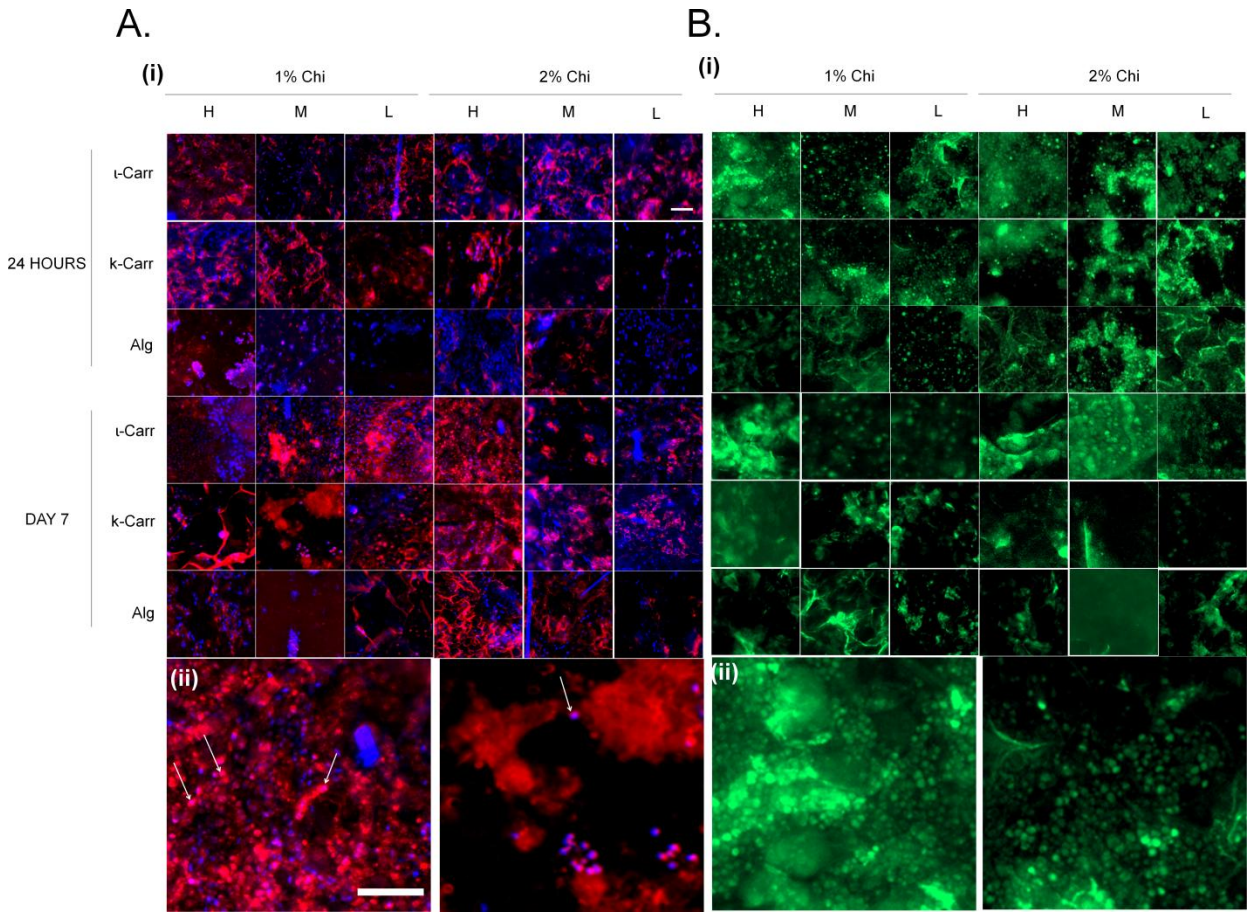

Figure 8.4. – A) i. Immunocytochemistry pictures of macrophages (in red) in each scaffold of the chips. ii. Magnified pictures of conditions D1 1%Chi ι-Carr H (left) and D1 1%Chi k-Carr L (right) where the morphology of the lymphocytes can be observed. B) i. Immunocytochemistry pictures of lymphocytes (in green) and staining of the nucleus (DAPI, in blue) present in each scaffold of the chips. ii. Magnified pictures of conditions D7 2%Chi ι-Carr H (left) and D7 1%Chi k-Carr M (right), where the morphology of the macrophages can be observed. Some macrophages are indicated with white arrows. Scale bar = 50 µm.

We observed a transient presence of lymphocytes after 24 hours of implantation. The evolution of inflammatory response until day 7 was also monitored by analysis of different inflammatory cells present in the distinct biomaterials. Lymphocytes registered a transition from 24 hours to 7 days: their amount decreased significantly in all conditions, mainly in the ones containing Alg, where their presence was almost inexistent (Figure 8.6A). Their presence was also very low in k-Carr containing conditions. Increasing concentrations of Chi in the substrate scaffold led to higher number of lymphocytes attached to the biomaterials, namely in the 2% k-Carr condition and in ι-Carr conditions. We also observed that the lymphocytes withdrawal gave place to the increase of macrophages in the biomaterial. Lymphocytes were previously reported to be transiently present at the implant site [23]. They have been shown to

interact with monocytes and macrophages resulting in mutual effects on each other in terms of activation and enhanced inflammatory responses. The conditions with more concentration of macrophages were the ones with k-Carr and ι-Carr. These results were consistent with the dilution of polymer B present in the combinatorial biomaterials, since H and M materials showed higher amount of macrophages than those with dilution factor L.

8.4.2. Analysis of histological cuts

After collecting the chips from the animals, the tissue that surrounded each chip was also collected for histological analysis. The analysis of the tissues was performed by the attribution of histological scores to three different parts of the histological cuts (performed in the tissue perpendicularly to the chip position during implantation), exemplified in Figure 8.3C. Figure 8.5 shows representative images of the parts of the histological parts that were in contact/closer to each biomaterial patterned on the chips. The scoring scale is explained in the Materials and Methods section. An intensity map with colors corresponding to the ranking of the average values attributed to each region of the histological cuts can be observed in Figure 8.5B. Average scores values, standard deviations and significant differences between all conditions can be found in Supporting Information (Figures 8.S2, 8.S3 and Table 8.S2).

According to the general tendencies observed in Figure 8.6B, after 24 hours of implantation higher histology scores were attributed to the conditions containing ι-Carr and k-Carr, when compared to the ones containing Alg. Biomaterials conditions with lower dilution factor (H) were significantly different between ι-Carr and Alg, and k-Carr and Alg. We did not observe any significant differences between biomaterials containing ι-Carr and k-Carr. The increase of dilution factors of the polymer B (from H to L) led to a decrease in the general tendencies of histology scores in all conditions, regardless of polymer B. The majority of statistical differences were observed while comparing H with L dilution factors. Conditions containing k-Carr as polymer B were the ones more sensitive to changes in the dilution factor from H to M (intermediate dilution

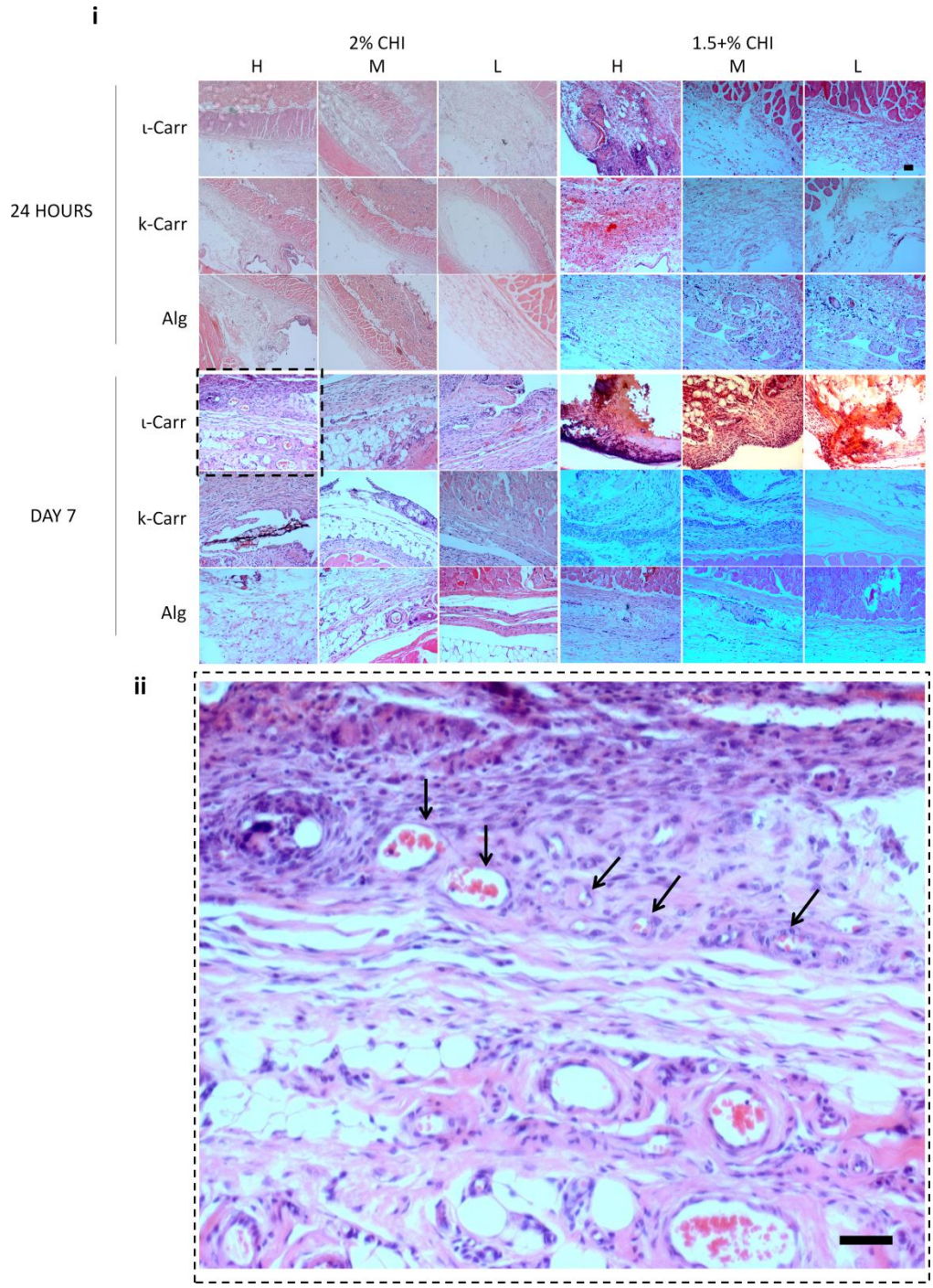

Figure 8.5. – i. Pictures of histological sections of 2% Chi and 1.5%+ Chi conditions. ii. Magnification of the condition 2% ι-Carr in 2% Chi scaffold (image framed in i). The presence of higher amount of blood vessels (indicated by black arrows) can be observed in this condition. Scale bars = 50 µm. The nomenclatures H, M, and L correspond to high, medium and low dilution factors of polymer B, respectively. More detailed information on cell type identification can be observed in Figure 8.9.

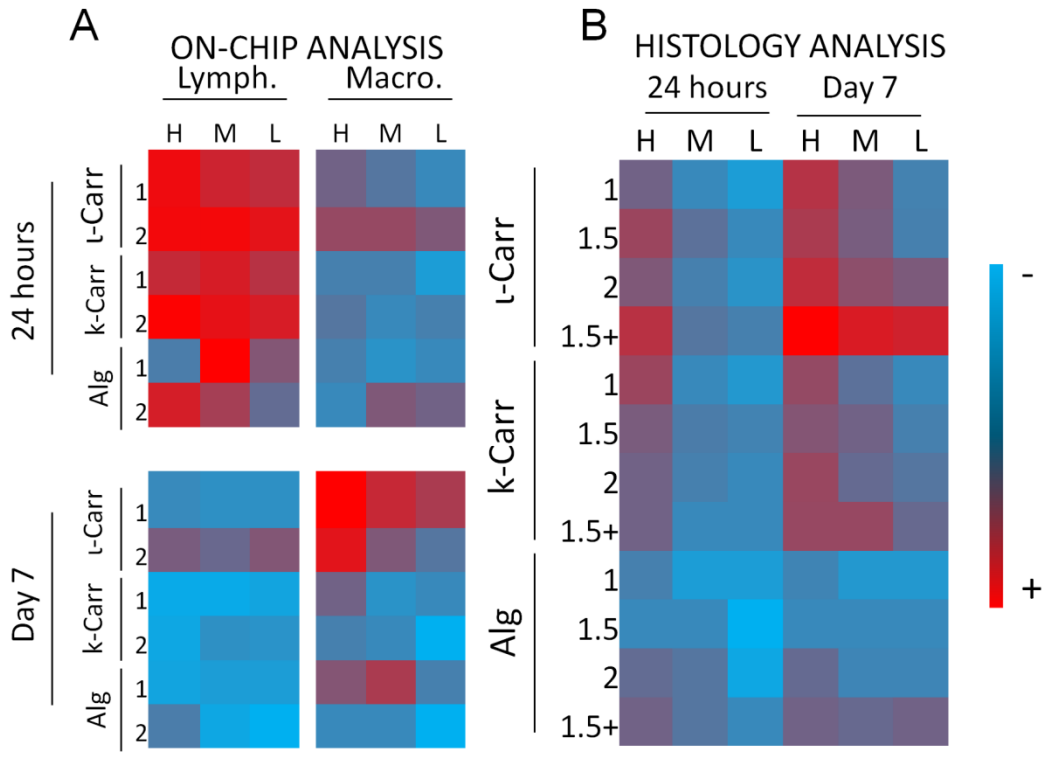

Figure 8.6. – Intensity map, according to the color gradient (right), with colors attributed to average values obtained for A) the quantification of lymphocytes (Lymph.), macrophages (Macro.) and B) for scores attributed to histological analysis, after 24 hours and 7 days of implantation.

factor) and M to L. The presence of distinct polymers B in the biomaterials combinations also led to differences in the histology scores, namely in the H dilution condition. Statistical differences were found between biomaterials containing ι-Carr/k-Carr and biomaterials containing Alg. No statistical differences between materials with ι-Carr and k-Carr were observed.

After 7 days of implantation significant differences between H and M dilution factors were observed in biomaterials containing ι-Carr. Materials with M dilution factor were attributed with lower histological scores. No other correlations between the dilution factors were observed. In several dilution conditions and Chi concentration biomaterials containing ι-Carr were attributed with higher scores than the ones with k-Carr and Alg. No statistically relevant differences between materials containing k-Carr or Alg were found.

8.4.3. Factorial analysis

We developed three distinct factorial analysis models for each time point: 24 hours and 7 days after implantation. Each model was developed according to the quantified number of lymphocytes (obtained

from microscopy images as the ones represented in Figure 8.4B), scores attributed to macrophages analyzed on-chip (attributed to microscopy images as the ones represented in Figure 8.4A), or to the histological scores attributed to each part of the histological cuts (as the ones represented in Figure 8.5) performed to the tissue collected around the chips. The analysis was performed considering the average values for each of these parameters (as represented in Figure 8.6). Each model allowed concluding about the percentage contribution of each factor affecting the results. For the models generated from the data collected on 24 hours time point, histology scores allowed obtaining a robust surface response model (with 99.9% of confidence), where not only the main effects but the effect of interacting factors could be analyzed. The contribution of each factor and interactions between factors for each time point can be seen in Figure 8.7.

For lymphocytes and macrophages analyses after 24 hours of implantation, the model was not significant in order to analyze the effects of combined factors, so a model analyzing only the main effects was applied. For the case of histological scores, all individual factors contributed significantly to the variation of inflammatory phenomena. The main effect contributing was the dilution of polymer B (factor C, in Figure 8.7), with 63% of contribution, followed by the type of polymer B (factor B), with 17% of contribution. Regarding the analysis of lymphocytes after 24 hours of implantation, the only factor considered relevant to the results was the type of polymer B present in the biomaterials. For macrophage scores, both percentage of Chi (factor A) and type of polymer B (factor B) were considered significant for the surface response model.

After 7 days of implantation, data obtained both from on-chip and histological scores analysis allowed obtaining robust models, with 99.9% of confidence. All individual factors showed a significant effect in the histological scores attributed to the distinct biomaterials. The individual factor with more relevance was the dilution of polymer B (factor C), with 48% of contribution to the model. The effect of Chi percentage of the substrate porous scaffold (factor A) contributed with 6%, and the dilution of polymer B (factor B), with 34%. Moreover BC interactions were also considered as statistically relevant, although with less impact than individual factors. Regarding on-chip analysis, lymphocytes number was affected mainly by factor A (27%) and B (46%), while macrophages score was affected by factors B (48%) and C (31%).

A

		Lymph.	Macro.	Histology
24 hours	%Chi - A	10	29	2
	PolymerB - B	25*	35	17*
	Dilution - C	9	4	63*
	AB	x	x	6
	AC	x	x	2
	BC	x	x	5
Day 7	%Chi - A	27*	7	6*
	PolymerB - B	46*	48*	34*
	Dilution - C	2	31*	48*
	AB	10	4	1
	AC	3	1	0
	BC	5	4	6*

B

	Histology
Volume Chi-D	4*
PolymerB - B	21*
Dilution - C	55*
DB	9*
DC	2*
BC	10*
Volume Chi-D	32*
PolymerB - B	43*
Dilution - C	10*
DB	8*
DC	1
BC	5*

Figure 8.7. – Contribution of the effect (%) of each factor and combination of factors in the surface response models. Data to generate the surface response models was obtained for lymphocyte, macrophage and histological scores evaluation with distinct biomaterials after 24 hours and 7 days of implantation. A) Models considering factor A as %Chi and B) models considering factor A as volume of Chi for the 1.5% and 1.5+% conditions. Significant effects are labeled with "*". The total value of the addition of factor contribution is not 100%, as the values attributed to residues of the model are not shown herein.

Regarding the factorial analysis performed to the histological scores of conditions 1.5%Chi and 1.5%+Chi – which is a condition where the scaffolds were not prepared from 4 µL volume of chitosan, but from a higher volume of 6 µL - (Figure 8.7B), the main effects affecting the inflammatory response observed after 24 hours of implantation were the type of polymer B (with 21% of contribution) and the dilution of polymer B (with 55% of contribution). In this time point, all factors and combined effects were statistically relevant for the scores attributed. After 7 days of implantation, the main effects contributing for the attributed scores of the histology images were the type of polymer B in the biomaterials (43%), as well as the volume of Chi (factor D) used in the Chi scaffold (32%). Except for the interaction DC, all factors and combined effects were significantly relevant for the developed surface response model.

8.4.4. Correlation between on-chip and histology results

For 24 hours of implantation, the results obtained for on-chip analysis and histology analysis were not directly correlated. This may be explained by the lack of robustness of the models obtained for on-chip cell analysis (for macrophages analysis, a low value for predicted R^2 - 0.20 – was obtained). Moreover, after 24 hours of implantation cells involved in inflammatory response may have not reached the

material, and may still be migrating to the materials. Histology showed that, in fact, lymphocytes along with PMN and some macrophages were present in the tissue around the biomaterials (Figure 8.5).

After 7 days of implantation, the effect of the factors on-chip and obtained from the analysis of histological scores were easily correlated (Figure 8.7). The effects obtained for the histological analysis were similar to the combined analysis of the effect of both lymphocytes and macrophages. Therefore, after 7 days of implantation, the results can probably be directly obtained from on-chip image-based methods, without the loss of any important information. This is an important outcome of the method that permits assessing information on biomaterials/tissues interaction in a high-throughput form, without the need of time-consuming histology analysis.

8.4.5. General analysis of biomaterials' inflammatory response

Regarding the general response from the explanted chips no fibrotic capsule or macroscopic signs of inflammation were observed (Figure 8.3D). The histology analysis performed to the tissue around the chips (Figure 8.10C) suggests that the reaction observed in each chip is totally independent between the four implanted chips. Moreover, animals showed a normal behavior during the implantation period.

Chi crosslinked with genipin was used as the base material for all biomaterials studied in this approach. Chi inflammatory response was previously described for the mice model [29]. In this work, histological assessment indicated marked neutrophil accumulation within the implant and antibody-specific analysis showed a very low incidence of Chi-specific reactions [24]. It was then described as a relatively inert biomaterial that does not elicit a chronic immune response. The inflammatory response to Alg crosslinked with $CaCl_2$ was previously reported with contradictory conclusions. Some studies described it as a material with high immunogenicity [30] as after 14 days of its implantation fibroblasts began to secrete collagen and macrophages were still present in the tissue [25]. However, in other studies it has been described as a material with no specific inflammation or reactive granuloma formation [31]. Carrageenans biocompatibility has been questioned in the literature [32,33]. Carrageenan is used to induce paw edema in the rat and mouse and induces IL-8 production through distinct Bcl10 pathway in normal human colonic epithelial cells [32,33].

We concluded that the presence of Chi in the combinatorial conditions explored in this approach produces a concentration-dependent effect. Porous Chi scaffolds with concentration of 2% led generally to significantly higher inflammatory responses than the ones with 1% or 1.5% (Table 8.S2). However, the major effect observed with Chi scaffolds was not their concentration, but the volume of solution used to process the biomaterials. In the conditions 1.5%+Chi (prepared with 6 µL of Chi, instead of 4 µL, as in

other conditions) the amount of polymer B was maintained. Regardless of the type of polymer B added to the Chi scaffold, the 1.5%+ Chi condition led to higher inflammatory responses regarding histology analysis. We believe that the increase in inflammation with the volume of Chi solution used to prepare the scaffold would be related with the higher biomaterial surface area exposed to the animal tissue. For this, we consider that the total surface exposure of the scaffolds is a major advantage of the system proposed herein, as it allows studying biomaterial volume-dependent phenomena.

Alg was the polymer present in the studied array of materials that led to lower inflammatory responses. k-Carr led to a slightly higher response, in most conditions not significantly different from Alg. Such polymers showed concentration-dependent effects on inflammatory response. ι-Carr was the material that showed a higher inflammatory response. This effect was concentration-dependent: 2% Chi was the condition that triggered higher inflammatory responses. This fact, along with the lower inflammatory response observed in k-Carr samples, suggests that the inflammatory response triggered by ι-Carr is related to its higher amount of sulfate groups.

Another interesting feature observed in scaffolds containing ι-Carr in all concentrations was the higher amount of blood vessels present in the tissue sections that surrounded the biomaterial after 7 days of implantation (Figure 8.5II). The method could be probably extended to studies of crossed effects of inflammation, vascularization and regeneration of tissues.

8.4.6. Validation of the method

Chips with scaffolds disposed in re-arranged positions randomly were generated (as indicated in Table 8.S1); on-chip immunocytochemistry images can be seen in Figures 8.S8 and 8.S9, in Supporting Information). This allowed confirming that the obtained results were not dependent on the relative position of the scaffolds in the chips evidencing the independence of the tissue reaction to the biomaterials with respect to their relative location (Figures 8.8A and 8.8B), both for histological analysis and immunocytochemistry results.

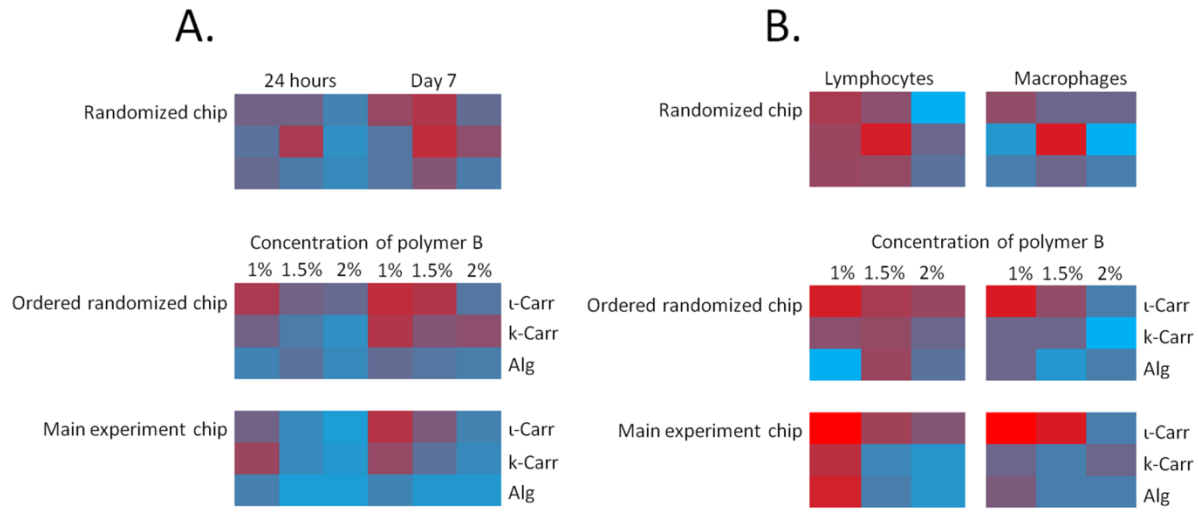

Figure 8.8. – A) Intensity maps of the scores attributed to histological analysis of the tissue surrounding the implanted control chips with biomaterials in a random configuration, according to Table 8.S1. The results obtained according to the configuration of the chip (randomized chip), the same results ordered according to the order of the conventional chips (ordered randomized chip) and the results obtained in the normal chips (main experiment chip), for the same conditions (1%Chi, 24 hours of implantation). B) On-chip analysis of the results obtained for lymphocyte analysis (left) and macrophages scores (right) after 24 hours of implantation, for 1% Chi conditions. The conditions in "Randomized chips" are the ones as indicated in Table 8.S1.

Implantation of single scaffolds with conventional size was carried out in order to compare the response observed with the implant of 4 chips with distinct biomaterials in a single animal with two randomly chosen conditions. This step of validation of the method consisted in the direct implantation of 2 distinct biomaterials without using the superhydrophobic platform, with the size of conventionally implanted plugs in tissue engineering field (5 mm diameter x 3 mm height). This was performed in single animals, i.e. one plug/animal. Results regarding implantation of biomaterial plugs can be seen in Figure 8.9. We observed that the adherence of lymphocytes to the scaffold containing ι-Carr was higher and more evenly distributed than to the one containing Alg. Images of histology sections showed that for 24 hours of implantation PMN cells were prevalent around the biomaterial in the Alg-containing scaffolds. For scaffolds containing ι-Carr, the presence of PMN cells was similar to the Alg-containing scaffolds. However, the presence of lymphocytes was detected around the implanted material (blue arrows for lymphocytes and green arrows indicating the material, Figure 8.9). After 7 days of cell culture, in the Alg-containing scaffold the presence of PMN cells (orange arrows, Figure 8.9) was still prevalent. In the scaffold ι-Carr, histology showed macrophages adhered to the biomaterial (black arrows, Figure 8.9). These results were consistent with the results observed on-chip, both for on-chip lymphocyte analysis

and histology analysis. After 24 hours of implantation, the amount of lymphocytes detected on-chip was lower for Alg-containing scaffolds, compared to the ones with ι-Carr. The amount of macrophages after 24 hours of implantation on both conditions studied on-chip was not significantly different. After 7 days of implantation, the amount of macrophages adhered to the scaffolds containing ι-Carr was clearly higher than in the ones containing Alg, as was corroborated by the plugs results. As such, we conclude that the results obtained for on-chip analysis with miniaturized scaffolds was coherent with the implantation of single plugs without the superhydrophobic film.

Polystyrene chips without biomaterials were also implanted in the rats. We verified that general cell adhesion to the superhydrophobic side of the chip was much lower than to the wettable domains on both time points (see DAPI blue staining of cell nuclei). Regarding the adhered cells, we could see that after 24 hours of implantation, the lymphocyte adhesion on the wettable spots occurred, while in the superhydrophobic domains of the chip was almost totally avoided. After 7 days of implantation, no macrophages were detected in the superhydrophobic domain of the chips (Figure 8.10A). Histological analysis (Figure 8.10B) showed that inflammatory response observed after 24 hours (Figure 8.10B1) of implantation was very mild. The presence of a low amount of PMN cells was registered very close to the site of implantation. After 7 days of implantation (Figure 8.10B2), the inflammatory response seemed to increase slightly around the chips. The cells present around the chip were PMN, along with some lymphocytes and macrophages. Also in the empty chips implanted in one animal along with 3 chips with biomaterials with the conditions 1% Chi, 1.5% Chi and 2% Chi the observed inflammatory response was very mild. After 24 hours (Figure 8.10C1) of implantation a low presence of macrophages and PMN cells was observed.

After 7 days of implantation (Figure 8.10C2) a very low presence of inflammatory cells was registered. This suggests that the water repellence that characterizes these surfaces and its propensity to decrease protein adhesion [29] lowers the tissue response in the superhydrophobic sites. The lower surface contact between the tissue and the materials was previously reported to decrease inflammatory response [33]. Along with the previously described control results these observations strengthen the idea that the response between patterned biomaterials will be independent from spot to spot in the chip.

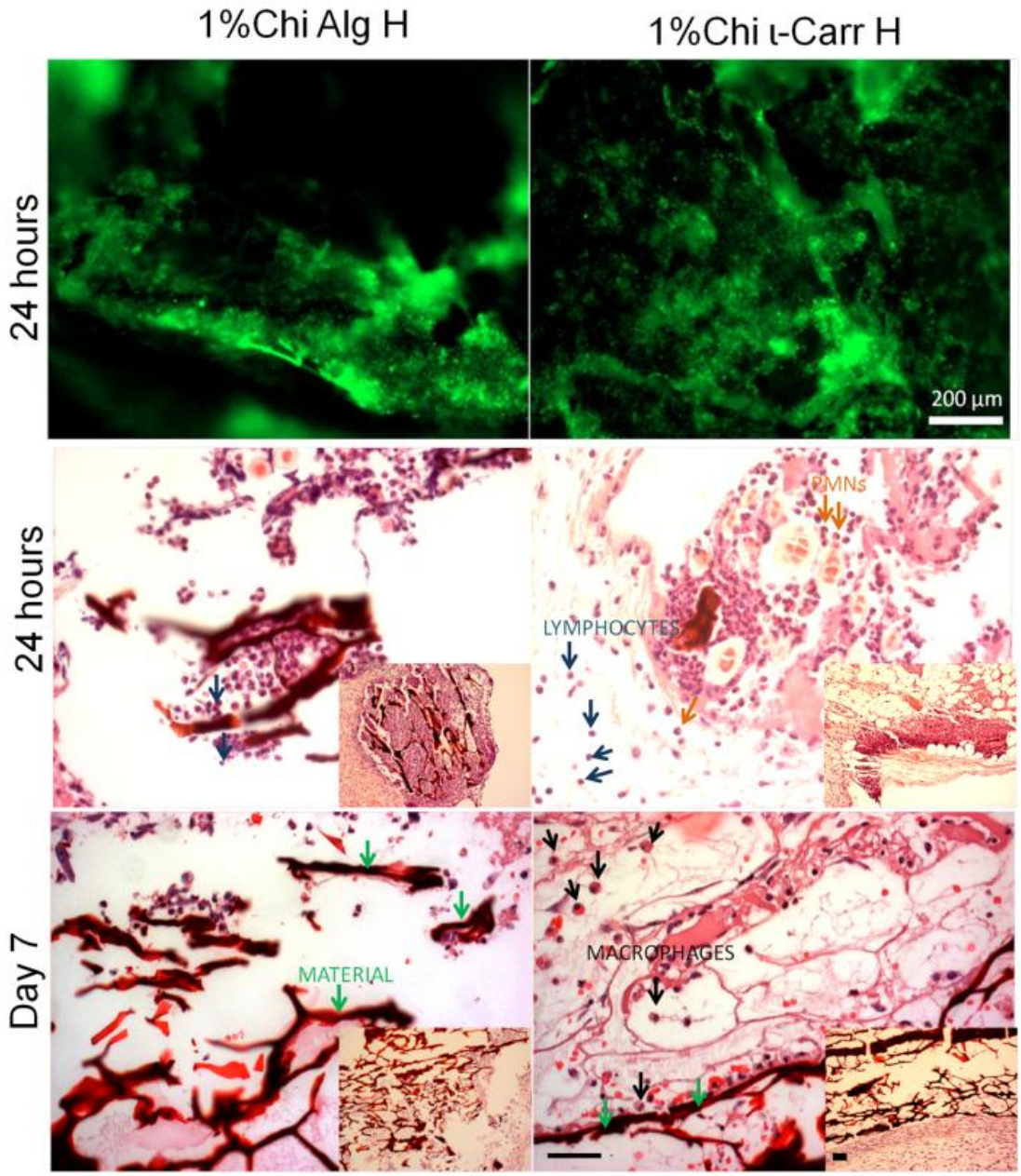

Figure 8.9. – Results obtained from the analysis of implanted scaffold plugs with conventional sizes (5mm x 3mm). Lymphocyte immunocytochemistry images (upper line images). Images of histology sections (middle and lower lines images) after 24 hours and 7 days of implantation. Blue arrows indicate lymphocytes and green arrows indicate the biomaterial. PMN cells are indicated with orange arrows and the scaffold is indicated with black arrows, for 7 days images. Scale bars in histological cuts figures = 200 µm.

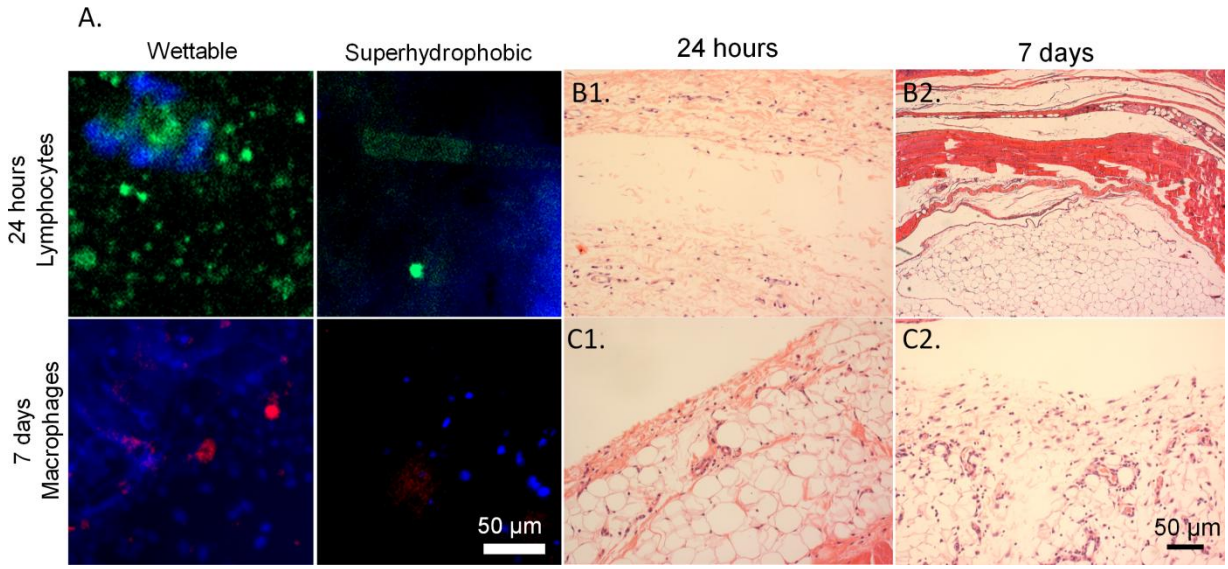

Figure 8.10. – A) Immunocytochemistry images for lymphocytes (after 24 hours of implantation) and macrophages (after 7 days of implantation) of empty chips, without any biomaterials spotted in the wettable regions. Two identical chips were implanted by animal. B) Histological (H&E staining) sections of the tissue surrounding a chip (without any biomaterial spotted in the wettable regions). Two identical chips were implanted by animal. C) – Histological (H&E staining) sections of the tissue surrounding empty chips (without any biomaterial spotted in the wettable regions). These chips were implanted along with 3 chips with biomaterials with the conditions 1% Chi, 1.5% Chi and 2% Chi. We observed that after 24 hours and 7 days of implantation.

8.4.7. Significance of the method

High-throughput methods are increasing and expanding their areas of application, allowing rapidly answering complex questions in the field of biomaterials. We demonstrated the possibility of performing high-throughput *in vivo* analysis of inflammatory response to distinct biomaterials using affordable superhydrophobic patterned thin and flat surfaces. We validated the method by distributing the arrays of biomaterials randomly and by comparing the results from implanting conventional-size biomaterial plugs in individual animals. This approach allowed studying new combinations of biomaterials and assessing their inflammation-triggering potential. The patterning of biomaterials in the proposed platforms allowed having biomaterials with total surface exposure, to maximize the contact with the *in vivo* environment. We saw that a combined analysis of on-chip and histology observation leads to an accurate evaluation of the materials' performance. Moreover, after 7 days of implantation the on-chip analysis was correspondent to the histology scores attribution. This may allow, in the future, shortening the time of results analysis, working solely with on-chip results that can be assessed rapidly through direct image analysis. This method allows reducing the number of animals while screening biomaterials for inflammatory response.

This work demonstrated the feasibility of the method by analyzing different combinations of a few polyssacharides, a class of natural materials widely used in biomedical application [35]. These studies could be easily extended to many combinations of other materials and may be complemented with long-term regeneration studies, where the combined effect of inflammation may be beneficial for the vascularization and regeneration of the implants. In such studies, biomaterials that promote an ideal balance of inflammatory cells recruitment in order to promote tissue regeneration and do not induce the rejection of the biomaterial by the host would be hit-spotted. Biomaterials with distinct shapes and anisotropic features may also be patterned and implanted, and the performance of the materials in both sides of the chips may also be studied to assess the response of distinct tissues in contact with two faces of the film. Moreover, we foresee the development of new chips with distinct flexibility and stiffness. Those would be useful not only as subcutaneous implants but also to be used in other anatomic sites where tissues require adaptation of the shape of the chip, such as cardiac, vascular tissue or bone.

8.5. CONCLUSION

We demonstrated the application of superhydrophobic chips patterned with wettable regions as implantable platforms for the high-content *in vivo* study of inflammatory response caused by biomaterials. We tested 36 combinations of biomaterials in the form of freeze-dried three-dimensional scaffolds simultaneously in one animal. The integration of the data obtained from the on-chip lymphocyte and macrophages analyses, as well as histological analysis of the surrounding tissue, with control data showed the applicability of these chips as platforms for the rapid screening of *in vivo* biomaterials' response. We believe that in the future such methodology may be applied in distinct approaches regarding, for example, complex multivariable tissue regeneration studies.

8.6. ACKNOWLEDGEMENTS

M.B. Oliveira acknowledges Fundação para a Ciência e para a Tecnologia for the PhD grant SFRH/BD/71396/2010. The research leading to these results has received funding from the European Union's Seventh Framework Programme (FP7/2007-2013) under grant agreement n° REGPOT-CT2012-316331-POLARIS. The research was also funded by FEDER through the Competitive Factors Operation Program – COMPETE and by National funds through FCT – Fundação para a Ciência e a Tecnologia in the scope of the projects PTDC/CTM-BIO/1814/2012, Pest-C/SAU/UI0709/2011 and PEst-OE/EGE/UI4056/2011.

8.7. SUPPORTING INFORMATION

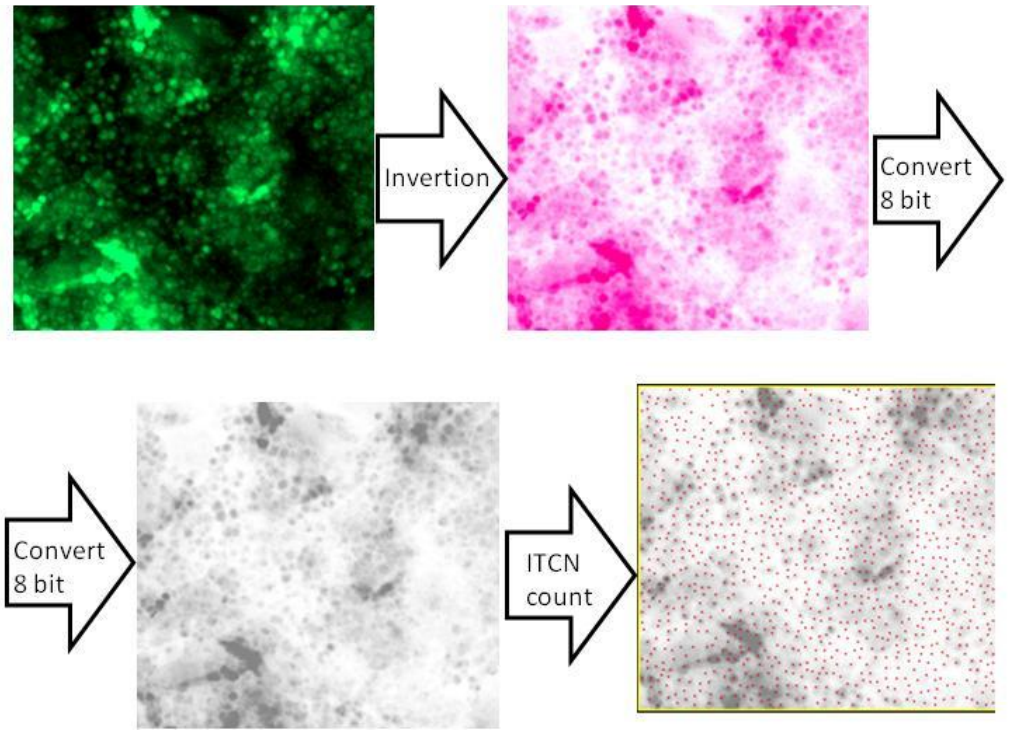

Figure 8.S1 – Sequential steps for the quantification of lymphocytes from microscopy images. The original image is treated in order to have the lowest background from natural polymers as possible. It is then inverted and converted to 8-bit image. The size of the cells and mean distance expected between them is inserted in the ITCN software, and an output image is generated with red dots in the spots counted as cells.

Note 1: The quantification of macrophages was not performed by the method indicated in Figure 8.S1. The shape of macrophages varies during the time of implantations, while lymphocytes are kept as round cells. Moreover, the natural polymers background in most of the polymeric combinations made the application of image techniques for the quantification of such cells difficult. As such, we attributed a score system for the quantification of macrophages on-chip, as indicated in the manuscript.

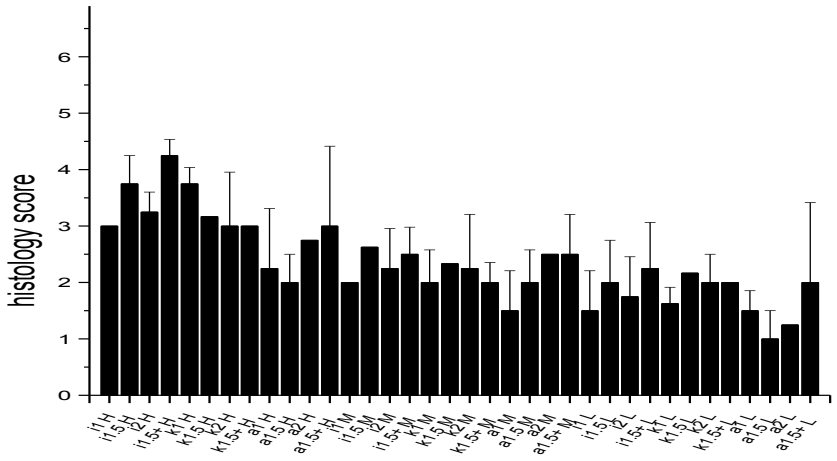

Figure 8.S2 – Histology scores attributed to the histology cuts performed to the tissue around the implanted chips after 24 hours of implantation (average value + S.D., n≥4). The conditions are abbreviated according to: A – Alg, k – k-Carr, ι - ι-Carr. The percentage of Chi is indicated with 1, 1.5, 2 and 1.5+, for 1%, 1.5%, 2% and 1.5+%, respectively. The dilutions of polymer B are indicated according to the nomenclature adopted in the manuscript.

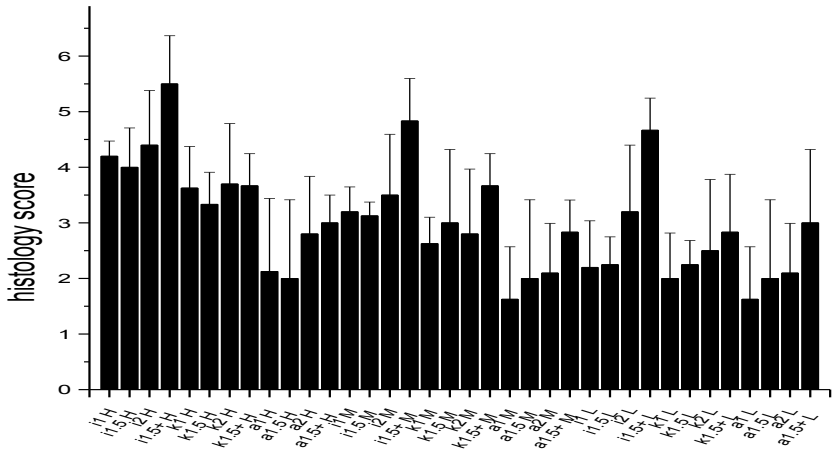

Figure 8.S3 - Histology scores attributed to the histology cuts performed to the tissue around the implanted chips after 7 days of implantation (average value + S.D., n≥4). The conditions are abbreviated according to: A – Alg, k – k-Carr, ι - ι-Carr. The percentage of Chi is indicated with 1, 1.5, 2 and 1.5+, for 1%, 1.5%, 2% and 1.5+%, respectively. The dilutions of polymer B are indicated according to the nomenclature adopted in the manuscript.

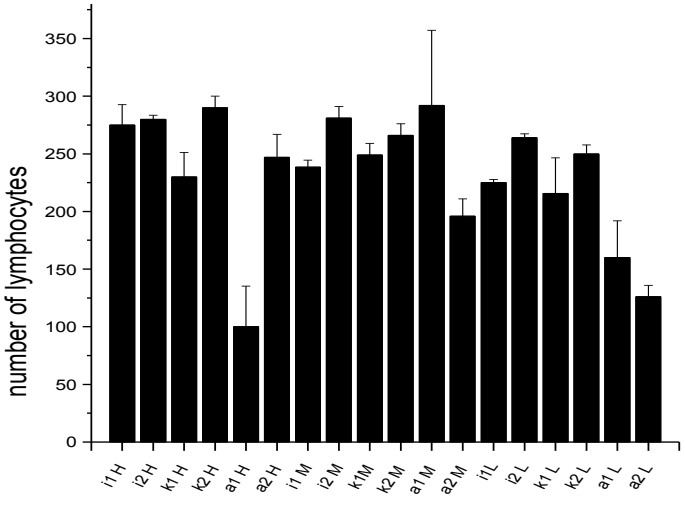

Figure 8.S4 – Quantification of lymphocytes on-chip (cells/100x100 pixel^2) after 24 hours of implantation. Bars indicate the cell number average value + S.D. (n≥4). The conditions are abbreviated according to: A – Alg, k – k-Carr, ι - ι-Carr. The percentage of Chi is indicated with 1, 1.5, 2 and 1.5+, for 1%, 1.5%, 2% and 1.5+%, respectively. The dilutions of polymer B are indicated according to the nomenclature adopted in the manuscript.

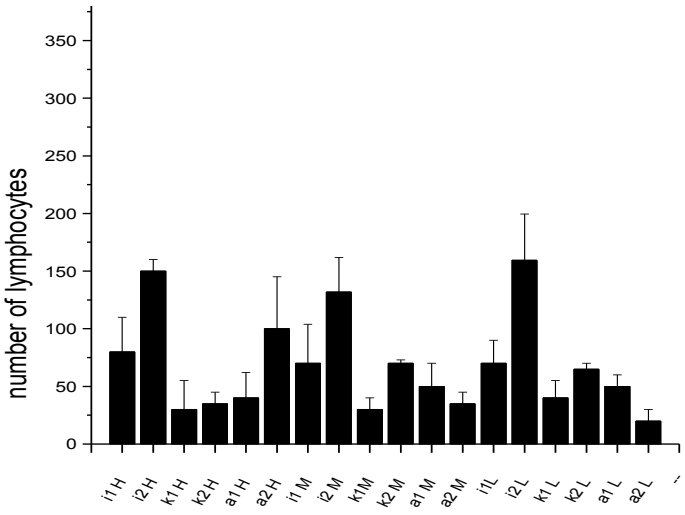

Figure 8.S5 - Quantification of lymphocytes on-chip (cells/100x100 pixel^2) after 7 days of implantation. Bars indicate the cell number average value + S.D. (n≥4). The conditions are abbreviated according to: A – Alg, k – k-Carr, ι - ι-Carr. The percentage of Chi is indicated with 1, 1.5, 2 and 1.5+, for 1%, 1.5%, 2% and 1.5+%, respectively. The dilutions of polymer B are indicated according to the nomenclature adopted in the manuscript.

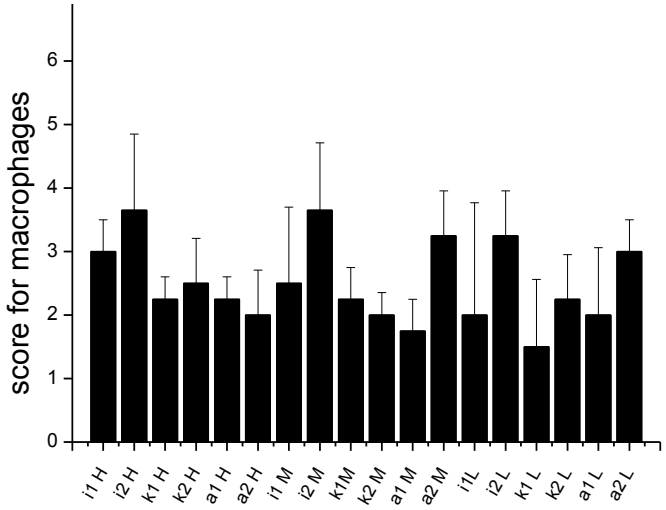

Figure 8.S6 – Score attributed to on-chip immunocytochemistry images of macrophages after 24 hours of implantation. Bars indicate the score average value + S.D. (n≥4). The conditions are abbreviated according to: A – Alg, k – k-Carr, ι - ι-Carr. The percentage of Chi is indicated with 1, 1.5, 2 and 1.5+, for 1%, 1.5%, 2% and 1.5+%, respectively. The dilutions of polymer B are indicated according to the nomenclature adopted in the manuscript.

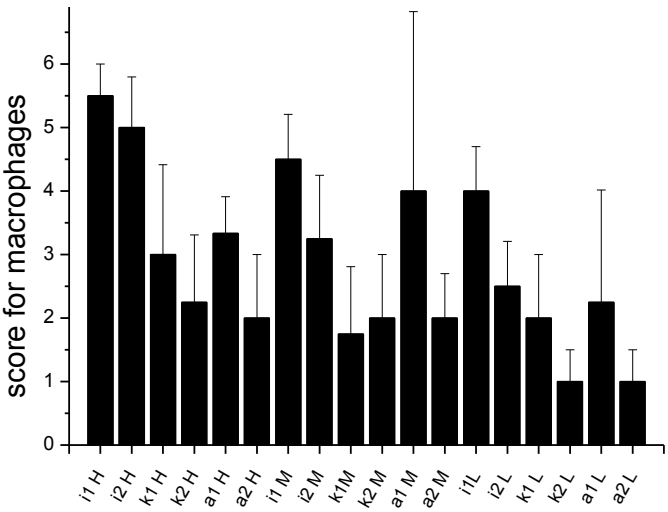

Figure 8.S7 - Score attributed to on-chip immunocytochemistry images of macrophages after 7 days of implantation. Bars indicate the score average value + S.D. (n≥4). The conditions are abbreviated according to: A – Alg, k – k-Carr, ι - ι-Carr. The percentage of Chi is indicated with 1, 1.5, 2 and 1.5+, for 1%, 1.5%, 2% and 1.5+%, respectively. The dilutions of polymer B are indicated according to the nomenclature adopted in the manuscript.

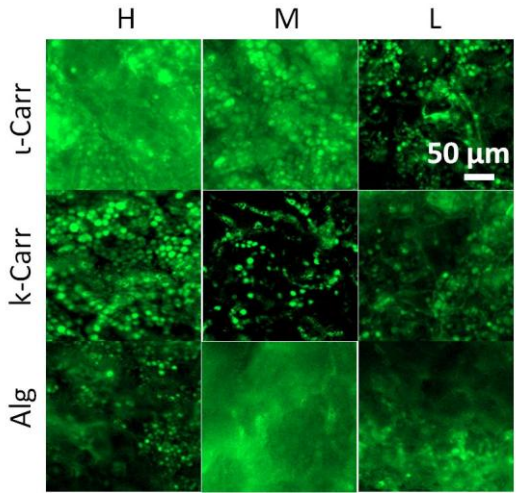

Figure 8.S8 – Lymphocytes immunocytochemistry images (in green) from a control chip (1% Chi) after 24 hours of implantation. The biomaterials conditions were disposed in the chip randomly, according to the configuration in Table 8.S1. Results regarding lymphocytes quantification in control chips and comparison with normal chips can be found in Figure 8.8., in the manuscript.

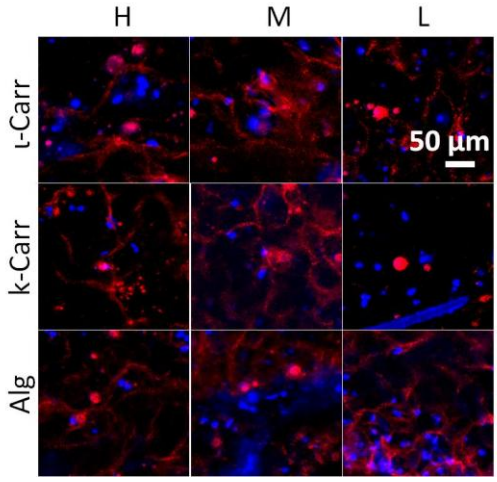

Figure 8.S9 - Macrophages immunocytochemistry images (in red) from a control chip after 24 hours of implantation, where the biomaterials conditions in the chip were disposed randomly, according to the configuration in Table 8.S1. Results regarding macrophages scoring in control chips and comparison with normal chips can be found in Figure 8.8., in the manuscript.

Note 2: The color distribution on the intensity maps was generated using Microsoft Office Excel (Microsoft®) according to the following criteria: lower value is turquoise and higher value is red. The middle intensity color is allocated to the 50% value of the distribution of the maximum and minimum values registered in the groups of

values analyzed. This attribution was performed according to groups of results presented in the same figure or section of figures.

Table 8.S1 – a. Configuration of the chip implanted during the main experiment. b. Configuration of the control chip with randomly generated positions of the biomaterials. All conditions were prepared from 1% Chi.

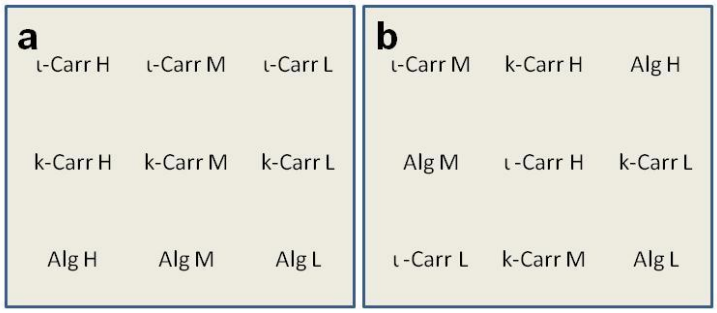

Table 8.S2 – Statistically relevant differences (considered for $p<0.05$) between on-chip conditions according to two-way ANOVA with Bonferroni post-test. "X" indicated the inexistence of statistically significant differences between conditions. The conditions are abbreviated according to: A – Alg, k – k-Carr, ι - ι-Carr. The percentage of Chi is indicated with 1, 1.5, 2 and 1.5+, for 1%, 1.5%, 2% and 1.5+%, respectively. The dilutions of polymer B are indicated according to the nomenclature adopted in the manuscript.

	24 hours			Day 7		
	Histology	Lymph.	Macro.	Histology	Lymph.	Macro.
H vs M	ι1.5+, k1, k1.5	A1, A1.5	X	X	A2	X
H vs L	ι1, ι1.5, ι2, ι1.5+, k1, A2	A1, A1.5, A2	X	ι1, ι1.5	A2	X
M vs L	k1.5	k1, A1, A2	X	X	X	X
ι-Carr vs k-Carr	X	X	X	1.5+H, 1.5+L	ι2, k2, A2	X
ι-Carr vs Alg	1.5H	1H, 2H, 1M, 1.5M, 2L	X	1H, 1.5H, 1.5+M	ι2, a2	1H, 1.5H, 2H, 1.5+H
k-Carr vs Alg	1H	1H, 2H, 1M, 1.5M, 2L	X	X	X	X
1%Chi vs 1.5% Chi	X	X	X	X	X	X
1%Chi vs 2%Chi	X	AH, kM, kL, AM, AL	X	X	ιH, kH, AH, ιL	X
1%Chi vs 1.5%+Chi	X	X	X	X	X	ιM
1.5%Chi vs 2%Chi	X	X	X	X	X	X
1.5%Chi vs 1.5%+Chi	X	X	X	X	X	ιM
2%Chi vs 1.5%+Chi	X	X	X	X	X	X

8.8. REFERENCES

[1] Anderson JM, Rodriguez A, Chang DT. Foreign body reaction to biomaterials. Seminars in Immunology. 2008;20:86-100.

[2] Remes A, Williams DF. Immune-response in biocompatibility. Biomaterials. 1992;13(11):731-43.

[3] Mountziaris PM, Mikos AG. Modulation of the inflammatory response for enhanced bone tissue regeneration. Tissue Eng Part B-Rev. 2008 Jun;14(2):179-86.

[4] Kyritsis N, Kizil C, Zocher S, Kroehne V, Kaslin J, Freudenreich D, et al. Acute Inflammation Initiates the Regenerative Response in the Adult Zebrafish Brain. Science. 2012;338(6112):1353-6.

[5] Godwin JW, Pinto AR, Rosenthal NA. Macrophages are required for adult salamander limb regeneration. Proc Natl Acad Sci USA 2013 110(23):9415-20.

[6] Liu Y, Wang L, Kikuiri T, Akiyama K, Chen CD, Xu XT, et al. Mesenchymal stem cell-based tissue regeneration is governed by recipient T lymphocytes via IFN-gamma and TNF-alpha. Nat Med. 2011; 17(12):1594-601.

[7] MacLean D, Kamoun S. Big data in small places. Nat Biotechnol. 2012;30(1):33-4.

[8] Ebert AD, Svendsen CN. Human stem cells and drug screening: opportunities and challenges. Nat Rev Drug Discov. 2010;9(5):367-72.

[9] McCoy JP. High-content screening: getting more from less. Nat Methods. 2011;8(5):390-1.

[10] Brafman DA, Chien S, Willert K. Arrayed cellular microenvironments for identifying culture and differentiation conditions for stem, primary and rare cell populations. Nat Protoc. 2012;7(4):703-17.

[11] Burdick JA, Watt FM. High-throughput stem-cell niches. Nat Methods. 2011;8(11):915-6.

[12] Desbordes SC, Studer L. Adapting human pluripotent stem cells to high-throughput and high-content screening. Nat Protoc 2013;8(1):111-30

[13] Gobaa S, Hoehnel S, Roccio M, Negro A, Kobel S, Lutolf MP. Artificial niche microarrays for probing single stem cell fate in high throughput. Nat Methods. 2011;8(11):949-55.

[14] Lecault V, VanInsberghe M, Sekulovic S, Knapp D, Wohrer S, Bowden W, et al. High-throughput analysis of single hematopoietic stem cell proliferation in microfluidic cell culture arrays. Nat Methods. 2011;8(7):581-86.

[15] Mei Y, Saha K, Bogatyrev SR, Yang J, Hook AL, Kalcioglu ZI, et al. Combinatorial development of biomaterials for clonal growth of human pluripotent stem cells. Nat Mater. 2010;9(9):768-78.

[16] Hook AL, Chang CY, Yang J, Luckett J, Cockayne A, Atkinson S, et al. Combinatorial discovery of polymers resistant to bacterial attachment. Nat Biotechnol. 2012;30(9):868-75.

[17] Curtarolo S, Hart GLW, Nardelli MB, Mingo N, Sanvito S, Levy O. The high-throughput highway to computational materials design. Nat Mater. 2013;12(3):191-201.

[18] Song WL, Veiga DD, Custodio CA, Mano JF. Bioinspired Degradable Substrates with Extreme Wettability Properties. Adv Mater. 2009;21(18):1830-36.

[19] Neto AI, Custodio CA, Song WL, Mano JF. High-throughput evaluation of interactions between biomaterials, proteins and cells using patterned superhydrophobic substrates. Soft Matter. 2011;7(9):4147-51.

[20] Salgado CL, Oliveira MB, Mano JF. Combinatorial cell-3D biomaterials cytocompatibility screening for tissue engineering using bioinspired superhydrophobic substrates. Integr Biol. 2012;4(3):318-27.

[21] Oliveira MB, Salgado CL, Song WL, Mano JF. Combinatorial On-Chip Study of Miniaturized 3D Porous Scaffolds Using a Patterned Superhydrophobic Platform. Small. 2013;9(5):768-78.

[22] Ballester-Beltran J, Rico P, Moratal D, Song WL, Mano JF, Salmeron-Sanchez M. Role of superhydrophobicity in the biological activity of fibronectin at the cell-material interface. Soft Matter. 2011;7(22):10803-11.

[23] Chang DT, Colton E, Matsuda T, Anderson JM. Lymphocyte adhesion and interactions with biomaterial adherent macrophages and foreign body giant cells. J Biom Mat Res A. 2009;91A(4):1210-20.

[24] Kim H, Tator CH, Shoichet MS. Chitosan implants in the rat spinal cord: Biocompatibility and biodegradation. J Biom Mat Res A. 2011;97A(4):395-404.

[25] Nunamaker EA, Purcell EK, Kipke DR. In vivo stability and biocompatibility of implanted calcium alginate disks. J Biom Mat Res A. 2007;83A(4):1128-37.

[26] Masferrer JL, Zweifel BS, Manning PT, Hauser SD, Leahy KM, Smith WG, et al. Selective inhibition of inducible cyclooxygenase 2 in vivo is antiinflammatory and nonulcerogenic. Proc. Natl Acad Sci USA.1994;91(8):3228-32.

[27] Oliveira NM, Neto AI, Song WL, Mano JF. Two-Dimensional Open Microfluidic Devices by Tuning the Wettability on Patterned Superhydrophobic Polymeric Surface. Appl Phys Express. 2010;3:085205.

[28] Chang D, Saidel G, Anderson J. Dynamic Systems Model for Lymphocyte Interactions with Macrophages at Biomaterial Surfaces. Cel Mol Bioeng. 2009;2(4):573-90.

[29] VandeVord PJ, Matthew HWT, DeSilva SP, Mayton L, Wu B, Wooley PH. Evaluation of the biocompatibility of a chitosan scaffold in mice. J Biom Mat Res. 2002;59(3):585-90.

[30] Smidsrød O, Skjåk-Braek G. Alginate as immobilization matrix for cells. Trends Biotech. 1990;8(0):71-8.

[31] Lima AC, Batista P, Valente TAM, Silva AS, Correia IJ, Mano JF. Novel Methodology Based on Biomimetic Superhydrophobic Substrates to Immobilize Cells and Proteins in Hydrogel Spheres for Applications in Bone Regeneration. Tissue Eng Pt A. 2013;19(9-10):1175-87.

[32] Morris C. Carrageenan-Induced Paw Edema in the Rat and Mouse. In: Winyard P, Willoughby D, editors. Inflammation Protocols: Humana Press; 2003. p. 115-21.

[33] Borthakur A, Bhattacharyya S, Dudeja PK, Tobacman JK. Carrageenan induces interleukin-8 production through distinct Bcl10 pathway in normal human colonic epithelial cells. American Journal of Physiology - Gastrointestinal and Liver Physiology. 2007;292(3):G829-G38.

[34] Mahdavi A, Ferreira L, Sundback C, Nichol JW, Chan EP, Carter DJD, et al. A biodegradable and biocompatible gecko-inspired tissue adhesive. Proc Natl Acad Sci USA. 2008;105(7):2307-12.

[35] Mano JF, Silva GA, Azevedo HS, Malafaya PB, Sousa RA, Silva SS, et al. Natural origin biodegradable systems in tissue engineering and regenerative medicine: present status and some moving trends. J R Soc Interface. 2007;4(17):999-1030.

CHAPTER 9. ON-CHIP ASSESSMENT OF THE PROTEIN-RELEASE PROFILE FROM 3D HYDROGEL ARRAYS[8]

9.1. ABSTRACT

As the formation of healthy tissue and the treatment of several diseases is often dependent on an effective and prolonged action of bioactive agents, the delivery of molecules for therapeutic or induction purposes in a tissue is a common procedure. The correct administration of those agents is often dependent on tailored delivery mechanisms from hydrogel or polymeric matrices. To the best of our knowledge, methods for the high-throughput monitoring of bioactive agents delivery are nonexistent. The methods for the *in vitro* monitoring of molecules release are resource spending and laborious. As a simplifying alternative to these methods we propose the imprinting of superhydrophobic biomimetic surfaces with ring-shaped transparent spots with concentric superhydrophobic millimetric regions to be used as bioactive agents release study platforms. We designed an array where polymeric precursors mixed with a growth-factor model protein labeled with a fluorescent tag could be dispensed in the concentric highly repellent regions and crosslinked afterwards, generating a polymeric protein-loaded sphere. The ring-shaped region was then filled with a physiological-like fluid that covered the polymeric sphere. The acquisition of sequential images of each spot over time using microscopy methods allowed monitoring easily the protein release by image-based fluorescence quantification. As the platform is easily adaptable and amenable for future automation in order to mimic standardized organs dynamics, we concluded that the device shows applicability for rapid and efficient *in vitro* bioactive agents release studies.

[8]This chapter was based on the publication: Oliveira MB, Mano JF. On-Chip Assessment of the Protein-Release Profile from 3D Hydrogel Arrays. Anal Chem. 2013;85:2391-6.

9.2. INTRODUCTION

The success of tissue engineering, gene therapy and drug delivery strategies is often dependent on the effective delivery of bioactive molecules *in vivo* [1-3]. In *in vitro* situations - both when cells are cultured in 2D or in 3D milieus - controlled delivery may only be beneficial for the saving of high amounts of expensive molecules during the cell culture period. In an *in vivo* situation, the systematic delivery of these factors is usually of low profit since low amount or no molecule can reach the implant site. Besides being costly, the systematic delivery of factors may be dangerous for the patient, since as some of these factors are necessary for tissue formation, they are toxic for other tissues [4]. As such, before implantation, the study of the delivery rate of bioactive molecules from biomaterials and the assurance of the desirable release rate is a crucial step in the development of these constructs.

Hydrogels are often used as space-filling agents in tissue engineering strategies. Nonetheless, their application as bioactive molecules stabilizers and delivery agents, as well as carriers of cells capable of producing such molecules, has been of increasing interest [5,6]. This strategy helps in stabilizing such molecules and enables their localized delivery, avoiding the administration of high doses, enzymatic degradation and nonspecific uptake by other tissues. By tailoring polymers properties and by choosing specific combinations of materials – whose behavior may be difficult to predict - the release behavior of the hydrogel/active molecule system can be modulated in order to satisfy the requirements of different strategies [7]. These can rely in hydrogels as drug delivery systems, gene therapy vehicles or tissue engineering constructs with bioactive molecules, among others [8-11].

One of the most efficient hydrogel forms for molecules delivery is as micro- and milli-range particles, which show high surface area and enable a fast response to environmental stimuli [12]. The methods chosen for the processing of particles determine their shape, mean size and distribution, porosity, topography and drug entrapment efficiency [13]. Most particles processing methods involve the use of organic solvents, high temperature and allow for low encapsulation efficiency. Moreover, most methods lead to the partial loss of bioactive molecule to a liquid medium and, consequently, the complete encapsulation is unachieved. In order to solve this limitation, Song *et al.* [10] developed a method based on the properties of superhydrophobic surfaces with similar properties to the Lotus leaf. In this method, liquid polymeric droplets containing bioactive molecules were dispensed as spheres and hardened as hydrogel structures under mild conditions in a solid/air interface [14,15]. This method was also used to produce particles used as cell carriers and scaffolds-precursors in constructs formed by cells and beads [10,16].

Regarding the *in vitro* actual methods for assessing bioactive molecules release from biomaterial matrices, they mostly rely in laboring and resource/space-wasting methods to obtain a cumulative release profile [13]. For the automation of this type of assays, complex and large mechanical systems would be needed. High performance liquid chromatography (HPLC) also holds popularity in quantifying drugs by directly reading their characteristic UV absorbance, refractive index, electrical conductivity or fluorescence emission upon elution from a proper HPLC column. HPLC thus lacks the real-time monitoring capability and suffers from high operational costs, lengthy training requirement and usually lack of a universal sensitive detector. The use of high-throughput platforms for the monitoring of biomolecules-cells interactions has been widely used [17-20]. However, to the best of our knowledge, high-throughput array methodologies are herein proposed for the first time aiming to be applied in studies of biomolecules release from biomaterial matrices.

Polystyrene superhydrophobic surfaces were not only proposed to produce drug-loaded particles with high encapsulation efficiency, but also to be used as high-throughput platforms for 2D and 3D tissue engineering constructs analysis [14,15]. These platforms consist of superhydrophobic surfaces in which wettable regions were patterned by exposure to UV/ozone irradiation through a photomask. Combinations of biomaterials were dispensed in the arrays of wettable spots in the form of adsorbed proteins and hydrogels. Cell behavior in these materials could be studied using validated image-based methodologies, relying usually in fluorescence quantification.

Quantification methods using image-acquired fluorescence were proposed in studies regarding the dynamic measurement of the height and volume of cells [21]: this study was based in the negative staining where a fluorescent non-cell-permeant dye was added to the extracellular medium. Since the fluorescent signal is dependent on the thickness of the emitting layer, the decrease of fluorescent signal in respect to the background was higher as the cell's height increased. The calibration curve for that study was performed using microfabricated patterns with steps and the obtained results were validated by comparison with atomic force microscopy (AFM) measurements. An opposite concept was used to measure the osmotic water permeability of cells. The method was based on confocal recording of the fluorescence intensity emitted by calcein-loaded adherent cells during osmotic shock. Permeability was calculated as a function of the time constant in the fluorescence intensity change, the cell surface-to-volume ratio and the fractional content of the osmotically active cell volume [22]. Fluorescence polarization was conjugated with a droplet-based microfluidics device for the rapid analysis of protein-protein interactions [23] and fluorescent-tagged molecules were also used as a qualitative indicator of the dispersion of fluorescent molecules in hydrogels [24]. Nonetheless, quantification and calibration of

images in fluorescence microscopy are considered methods to be performed carefully taking in consideration the wide variety of factors that may introduce error to the final results [25].

We herein propose a chip up-scalable for high-throughput analysis based on wettability contrast with ring-shaped hydrophilic transparent regions positioned in an array. A superhydrophobic circle was maintained concentrically to these wettable regions, so the hydrogels were processed as protein-loaded spheres with minimum protein loss. A combinatorial system of fluorescein isothiocyanate labelled bovine serum albumin (BSA-FITC) – a commonly used growth-factor model – encapsulated in alginate hydrogels was designed for the proof-of-concept. Ionically crosslinked alginate was used as the hydrogel matrix since it is relatively noncytotoxic, nondegradable and can be gelled under mild conditions [26]. Moreover, the release profile of bioactive molecules can be easily modeled in these hydrogels by changing parameters such as polymer source, concentration, crosslinking method, molecular weight and initial amount of loaded bioactive agent [3,27,28]. BSA-FITC release from alginate hydrogels was monitored by resource, space and labor-saving image-based methods.

9.3. Experimental Section

9.3.1. Development of polystyrene superhydrophobic surfaces with ring-shaped transparent patterns

Polystyrene flaks in the form of 3x3 cm squares were cut from commercially available Petri dishes (Corner). Stickers of polyvinyl chloride (PVC) (Oracal® 614) were cut in a ring-shaped shape with 5 mm of outer diameter and 2 mm of inner diameter in an A4 sheet in a typography service using a CNC laser cutting machine. Arrays of 3x3 ring-shaped stickers separated by 2 mm were printed in the polystyrene flaks.

The polystyrene surfaces were then treated using a phase-separation method, as described elsewhere [10,13] and dried under a flow of nitrogen. Tetrahydrofuran (THF) was purchased from Fluka and ethanol absolute from Panreac. The stickers were removed after the drying of the surfaces.

9.3.2. Design of the combinatorial hydrogel matrix

We designed an array of combinatorial conditions for protein-release aiming to control two variables: the concentration of the polymer that constitutes the hydrogel matrix and the concentration of the protein initially encapsulated in the hydrogel matrix. We used alginate sodium salt compatible with cell encapsulation (Sigma) as hydrogel matrix material and BSA-FITC (Sigma) as the protein model, since it is well-known as a model for proteins release studies.

Solutions of 1%, 1.5% and 2% (w/v) of alginate were prepared using distilled water. Each of these solutions was divided in three equal parts and, to each portion, amounts of BSA-FITC in concentrations of 0.1 mg/mL, 0.5 mg/mL and 1 mg/mL were added. A total of 9 combinatorial hydrogel precursors mixed with BSA-FITC were prepared.

9.3.3. Deposition of combinatorial hydrogel microparticles in the chips and set-up for the protein-release studies

An amount of 2 µL of each liquid precursor was dropped in each concentric superhydrophobic spot inside the ring-shaped wettable spot. To fix the polymeric droplets, an indentation was previously made in the center of the superhydrophobic circle using a 22G needle. Each droplet was then crosslinked with 0.8 µL of 10 M $CaCl_2$ during 10 minutes in a water saturated environment. After the crosslinking reaction an amount of 40 µL of PBS was dropped in the ring-shaped hydrophilic spot, covering the particle. The maximum amount of loaded BSA-FITC – 1 mg/mL per particle – leads to a maximum proportion of 0.05 mg/mL of protein in PBS in case of total protein release to the 40 µL of medium (PBS). This value is lower than the limit solubility provided by the supplier (around 0.1 mg/mL in water).

9.3.4. Image acquisition and calibration curves

Images of each spot were acquired before the addition of PBS to the wettable regions and then sequentially after the addition of the PBS to each ring-shaped wettable spot. After studying the evaporation of PBS in each spot at room temperature (20°C), we concluded that there was an average evaporation of 20% of the total volume after 30 minutes. As such, we added 2.7 µl of PBS to each spot every 10 minutes. The final images consisted of the stacking of 28 layers acquired every 25 µm on the particle z axis; those were acquired using the microscope Axiovision Rel. 4.8 program (Zeiss). The images were composed of whole particles and some surrounding area. The images were acquired every 5 minutes until 30 minutes of protein release. After an interval of 30 minutes, images were also collected at 60 minutes after the addition of PBS to the particles.

The exposure time of the fluorescence lamp of the reflected/transmitted light microscope (Zeiss) was maintained in each experiment. Calibration curves with pre-defined concentrations from 1 mg/mL to 0.025 mg/mL of BSA-FITC were performed. Droplets of 2 µL of alginate solutions with the distinct amounts BSA-FITC and crosslinked with $CaCl_2$ were dispensed in superhydrophobic surfaces. Calibration curves were performed with the three distinct concentrations of alginate.

9.3.5. Fluorescence quantification

All acquired images were treated as grey-scale images. Fixed areas of each image were collected and the grey mean intensity of each previously stacked image was measured using the ImageJ software (NIH, USA). These values were then adjusted to the calibration curve and the protein release profiles were calculated.

9.3.6. Control test: validation of the on-chip tests

In order to perform control tests we produced several particles of each combinatorial condition using a superhydrophobic surface. These particles were produced with the same properties as the particles used for the chip assay. We placed two particles in each well of a commercially available white opaque 96-well plate. Each well was used to study one specific time point. We then added 80 μL of PBS to each well and carefully removed the particles from each well in the intended time point. These time-points corresponded to the time-points in which the images were collected in the chip. The control tests were performed for the 3 formulations containing 0.5 mg/mL BSA-FITC in 1% (w/v), 1.5% (w/v) and 2% (w/v) of alginate.

We measured the fluorescence in each well in a microplate reader (Synergie HT, Bio-Tek) at an excitation wavelength of 485/20 nm and at an emission wavelength of 528/20 nm. The values were then adjusted to a calibration curve which contained concentration values from 0.005 mg/mL to 1 mg/mL of BSA-FITC in PBS.

9.3.7. Statistical Analysis

All data is presented as mean ± standard deviation (S.D.) for triplicate sets. Data obtained for the time points 5 minutes and 10 minutes (burst release analysis) and for 60 minutes (final acquired release value) was analyzed by one-way analysis of variance (ANOVA) test, followed by Tukey's pos-test for $p<0.05$. The adopted nomenclature was the following: α - 1% alginate vs 1.5% alginate; β - 1% alginte vs 2% alginate; γ - 1.5% alginate vs 2% alginate; * - 0.5 mg/mL BSA-FITC vs 1 mg/mL BSA-FITC (in 1% alginate; # - 0.1 mg/mL BSA-FITC vs 0.5 mg/mL BSA-FITC (in 1.5% alginate); § - 0.1 mg/mL BSA-FITC vs 1 mg/mL BSA-FITC (in 1.5% alginate). The repetition of symbols refers to: single symbol – $p<0.05$; double symbol: $p<0.01$; triple symbol: $p<0.001$.

9.4. RESULTS AND DISCUSSION

By developing transparent and wettable patterns on polystyrene superhydrophobic surfaces we created a platform that allowed producing alginate beads loaded with BSA-FITC. The protein release profiles could be studied using images acquired in real-time. High encapsulation efficiency was achieved since this technique uses the superhydrophobicity of treated polystyrene surfaces – which were previously used to high efficient molecules encapsulation in polymeric matrices [13] and in high-throughput strategies [14,15] – in order to produce loaded particles in an air-solid interface. Wettable spots were patterned in the superhydrophobic surfaces and combinatorial conditions of particles were dispensed in the same platform (Figure 9.1A1,2 and Figure 9.2A), using the array for an increased-throughput rapid analysis (Figure 9.1B2).

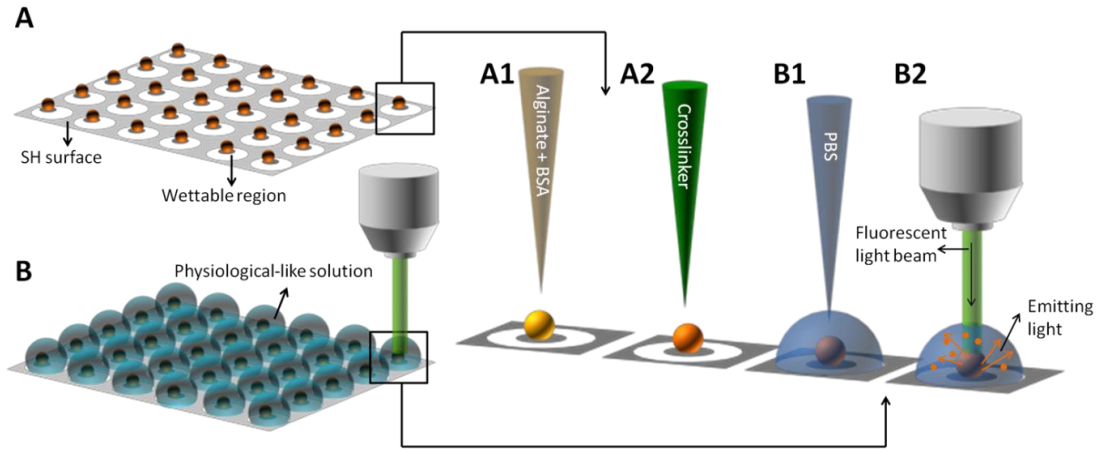

Figure 9.1. – A) Schematic representation of the superhydrophobic platform patterned with ring-shaped transparent spots with alginate crosslinked particles dispensed in each concentric superhydrophobic (SH) area. Details of the processing of the particles regarding the dispensing of the (A1) polymeric precursors and (A2) crosslinking of the particle in the chip. B) Schematic representation of the superhydrophobic platform patterned with ring-shaped transparent spot with alginate crosslinked particles after the dispensing of PBS in each wettable region and exposure to reflected fluorescent light in each individual spot. Details of the (B1) dispensing of the physiological-like fluid in the wettable region and (B2) of the particles' analysis by fluorescent light microscopy: the fluorescent light targets the particle and emission of light from the particles occurs.

The use of polystyrene superhydrophobic surfaces allows for the rapid generation of non-expensive platforms for combined studies. The platforms are prepared in a time frame of less than 2 hours and can be easily stored since they are totally flat. Moreover, the high contrast of wettability between the transparent region and the surroundings allow dispensing high volumes of physiological-like solutions in

the transparent regions, corresponding to semi-drops higher than a semi-sphere (Figure 9.1B1 and Figure 9.2B). This allows having volumes compatible with the full dissolution of the encapsulated agent in a stable and robust platform. The high stability of the liquid droplets facilitates the transport and manipulation of the entire chip. Moreover, it permits to vary individually the liquid volumes dispensed along time, such as performing the extraction and addition of precise volumes of liquids in the spots.

The phase separation treatment introduces permanently micro- and nano-roughness in the initially smooth polystyrene, avoiding the chemical modification of the material. Due to the merely physical modification of the surface, the cytocompatibility of the platform is kept [15], which opens the possibility of their future application in complex studies involving cells and controlled release of bioactive agents. The stickers used to protect polystyrene from the phase-separation treatment were cut from commercially available PVC adhesive sheets in an inexpensive process.

A total of nine conditions of polymeric matrix properties/protein concentration were studied simultaneously in the same array platform for the proof of concept of the functionality of this system. A two-factor array was developed by combining conditions of polymer concentration for the production of polymeric spheres with the amount of protein mixed with the polymer. The polymeric matrix chosen for the tests was alginate, which can easily be hardened by the addition of divalent ions under mild conditions, shows low toxicity and is readily available [26]. BSA-FITC was used as a model molecule, since this protein shows a similar molecular weight of those of growth factors, whose controlled delivery is often desired in tissue engineering strategies, and also of other proteins with therapeutic action.

In order to monitor the release of protein from the alginate matrices, sequential images of whole particles were acquired from each particle in the distinct array spots every time point (Figure 9.2E). The number of layers acquired per image and fluorescent light exposure time of the lamp are parameters that determine the time that the analysis of each spot will take. As such, they must be optimized according to the number of samples to be analyzed and the time point interval intended to be studied.

Usually the acquisition of fluorescent-tagged molecules distributed in hydrogels is used for qualitative analysis of the distribution and amount of bioactive agents in biomaterials [3]. We acquired images of the particles with some surrounding area (see Figure 9.2C) and observed the distribution of BSA-FITC over time in the alginate beads (Figure 9.2F). Calibration curves were prepared using a series of alginate beads prepared on superhydrophobic surfaces and crosslinked with $CaCl_2$ containing distinct BSA-FITC contents (Figure 9.2D). The volumes of such beads are the same as the ones dispensed in the chip, as the fluorescence intensity value is dependent on the height of the emitting sample [21]. In each repetition of the assays a new calibration curve was performed due to the possible wear of the lamp and

re-adjustments of the fluorescent light exposure time. An example of a calibration curve can be observed in Figure 9.2D; the measured values allowed to perform a linear fitting with a R^2=0.985.

Although in this proof-of-concept the quantification method used to analyze the protein release profiles is image-based fluorescence quantification, we believe that the platforms proposed herein may be adapted to other types of image-based quantification methods. Since the wettable area of the chip is transparent, quantification methods based in the amount of molecules released to the medium could be used, instead of the method proposed herein that relies in the quantification of the remaining molecule inside the hydrogel structure. As such, the versatility of the platforms would be broader if absorbance-based methods were adapted by exposing the chip to visible or UV light.

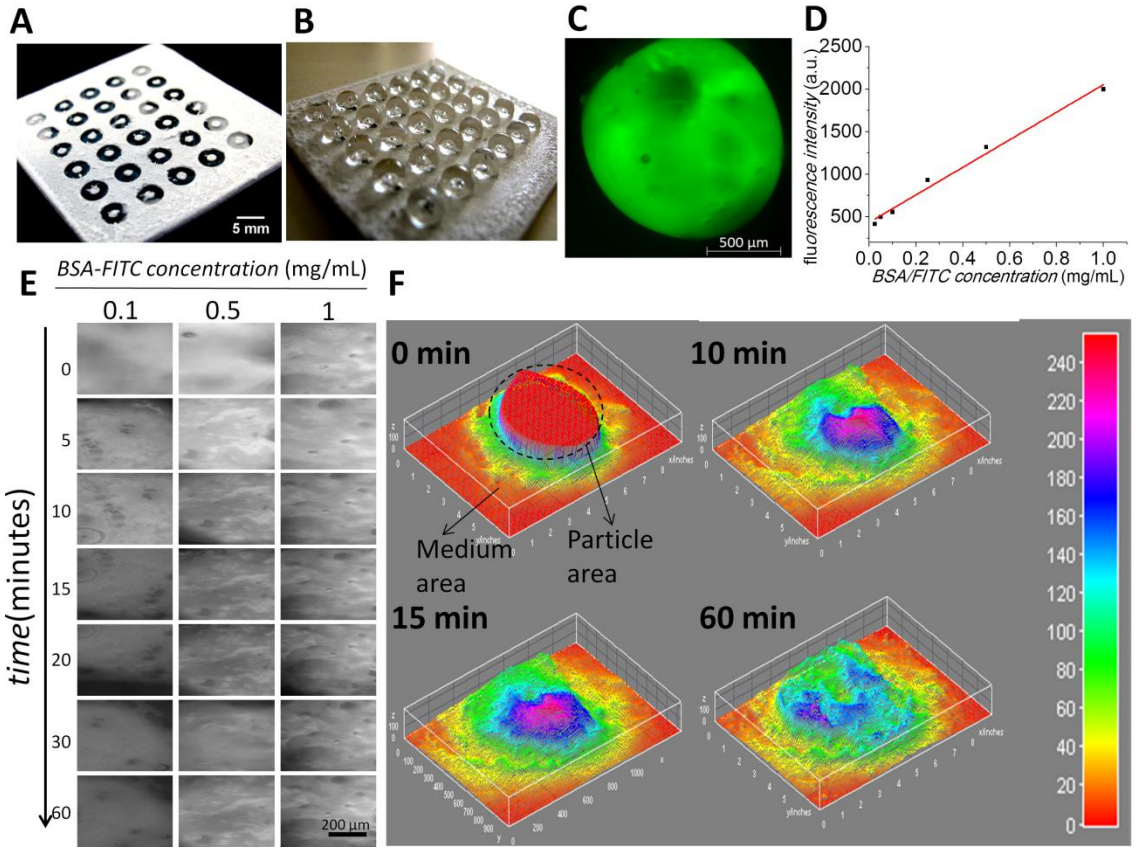

Figure 9.2. – A) Picture of the superhydrophobic polystyrene surface after the removal of the PVC stickers; B) Picture of the superhydrophobic polystyrene surface after the dispensing of the particles and PBS C) Microscope image of BSA-FITC-loaded alginate particles under green fluorescent light exposure; D) Example of a fluorescence intensity/BSA-FITC concentration calibration curve; E) Microscope images of a region in the lower left part of the particles prepared with 2% alginate with concentrations of 0.1, 0.5 and 1 mg/mL of BSA-FITC during the protein release experiment time points; F) Surface plots obtained

by ImageJ software of 2% alginate 0.5 mg/mL BSA-FITC condition in distinct time points of the protein release experiment and respective intensity map of the fluorescence intensities in a 0-255 pixel scale.

The release profiles of BSA-FITC measured directly on the chip are shown in Figure 9.3. The effect of alginate concentration was one of the studied varying factors. Higher alginate concentrations were expected to create tighter polymeric networks in which the protein would be entrapped [7]. As expected, 2% alginate hydrogels promoted significantly slower BSA-FITC release and less amount of released protein after 60 minutes in PBS, for all loading conditions. For the lower amount of encapsulated BSA-FITC, 1.5% alginate hydrogels led to slower burst release of protein, compared to the 1% alginate condition (Figure 9.3).

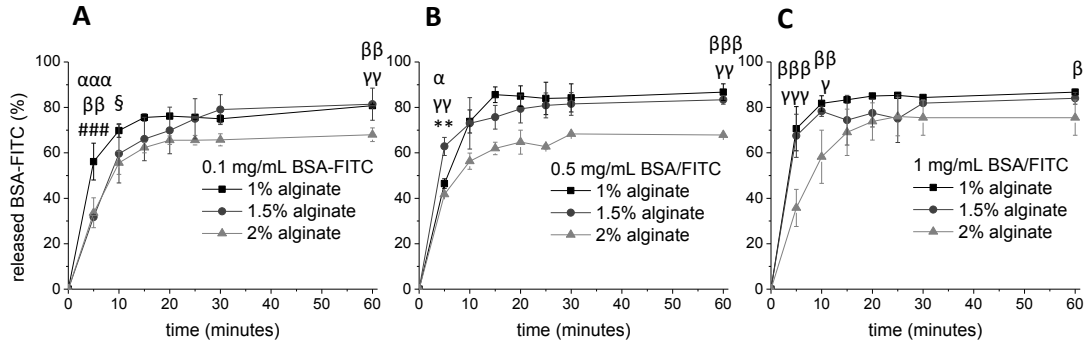

Figure 9.3. – BSA-FITC release profiles from alginate particles of the A) 0.1 mg/mL BSA-FITC condition, B) 0.5 mg/mL BSA-FITC condition, C) 1 mg/mL BSA-FITC condition performed by image-based analysis.

The concentration gradient is the driving force for protein diffusion. High BSA-FITC concentration gradient between the hydrogel surface and the release medium during the very early stage of contact was expected to lead to a higher initial burst release and fast release rate [7]. After 60 minutes of protein release no significant differences in the total amount of release protein could be observed. Nonetheless, regarding burst release, in some conditions the effect of protein concentration gradient was statistically significant: in 1.5% alginate hydrogels, the burst release in 1 mg/mL BSA-FITC loading condition was faster than in 0.1 mg/mL and 0.5 mg/mL loading conditions (Figure 9.3A,B,C). Also, in the 1% alginate hydrogels, 1 mg/mL BSA-FITC condition led to faster burst release than 0.5 mg/mL BSA-FITC loading condition.

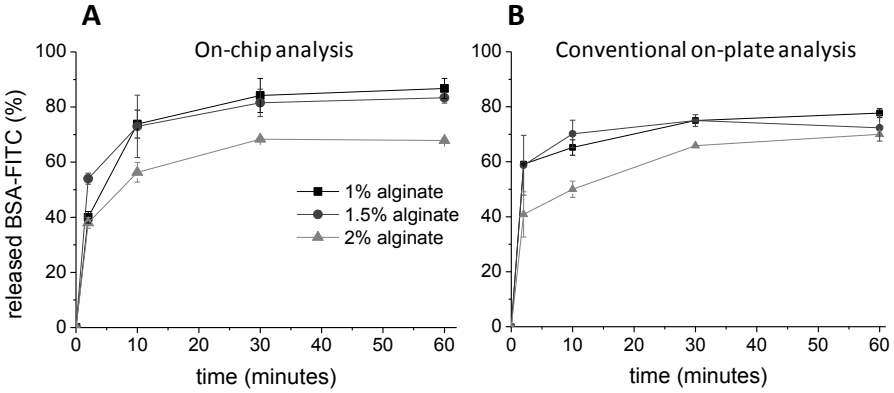

Figure 9.4. – BSA-FITC release profiles from alginate particles of the 0.5 mg/mL BSA-FITC condition in experiments performed by A) image-based analysis and B) conventional on-plate control test.

Besides allowing the quantification of protein inside the particles, the proposed method can also be used to performa general overview of the distribution of the protein and its amount in the particles over time taking in consideration the fluorescence intensity in the surface plot generated by the ImageJ software (Figure 9.2F).

In order to validate the method, alginate particles of 1%, 1.5% and 2% alginate with 0.5 mg/mL of loaded BSA-FITC were prepared in superhydrophobic surfaces. Particles of each condition were placed in opaque white wells. Two particles were placed in each well, which corresponded to a different time point to be studied. PBS was added to each well and the particles were removed carefully from the well after each time point. The fluorescence in each well was then measured and adjusted to a calibration curve (Figure 9.4B). Results obtained by both methods showed similar tendencies in the release kinetics of BSA-FITC from the alginate matrices (Figure 9.4A,B).

The demand for more efficient and functional delivery vehicles has been increasing, as new biomaterials systems conjugated with bioactive molecules show more complexity and advanced properties [29]. We believe the herein proposed platforms may be of great usefulness in the preliminary and fast study of biomaterials-bioactive molecules interactions and release kinetics studies. In principle, these platforms are compatible with most types of biomaterials/molecules release systems: either the molecules' release driving force is the diffusion gradient, the biomaterial swelling, degradation or response to some stimulus [30,31]. With the discovery of RNA interference, gene therapy for the treatment of diseases has been a widely studied subject and nanomaterials were proposed as nanocarriers for its effective cell delivery.[8] We believe our platforms may be, as well, used in the study of internalization of nanocarriers by cells in 3D tissues, by combining their use with confocal microscopy analysis.

The easy accessibility of the polymeric particles and of the medium insights the possibility of studying of bioactive molecule release kinetics from biomaterial matrices in changing conditions along time. For example, pH or ionic concentration of the release media may be altered easily during the release study by simply adding drops of solutions to the medium. For future applications with increased reliability, the platform shows the potential to be adapted to dynamic conditions and maintenance of medium diffusion conditions according to standard rules by introducing rotating movements using, for example, orbital shakers with controlled rotation frequency and exchanging physiological medium during experiment time by, for example, using microarray tips.

9.5. Conclusion

We used superhydrophobic surfaces for the development of an innovative high-throughput device for molecules' release assessment. We patterned transparent regions in polystyrene flakes and treated the regions out of the patterns with a phase separation method to make their wettability extremely low. Using a method of production of particles that allows for the nearly total encapsulation of biomolecules in a polymeric matrix, we generated an array of combinatorial alginate hydrogels with encapsulated BSA-FITC in distinct amounts. Using the fluorescent properties of the FITC-labeled BSA, we could study the release profiles of the BSA-FITC from the alginate matrices in the chip by image-analysis methods. The effect of alginate concentration and BSA-FITC loading in the particles could be observed. These results were coherent with the protein release profiles obtained by a conventional method in similar conditions. As such, we conclude that the use of the developed chip for combinatorial high-throughput studies of molecules release is validated.

9.6. Acknowledgements

M.B. Oliveira acknowledges Fundação para a Ciência e para a Tecnologia for the PhD grant SFRH/BD/71396/2010.

9.7. REFERENCES

[1] Santo VE, Gomes ME, Mano JF, Reis RL. From nano- to macro-scale: nanotechnology approaches for spatially controlled delivery of bioactive factors for bone and cartilage engineering. Nanomedicine. 2012;7:1045-66.

[2] Gabriel D, Dvir T, Kohane DS. Delivering bioactive molecules as instructive cues to engineered tissues. Expert Opin Drug Deliv. 2012;9:473-92.

[3] Lee K, Silva EA, Mooney DJ. Growth factor delivery-based tissue engineering: general approaches and a review of recent developments. J R Soc Interface. 2011;8:153-70.

[4] Tayalia P, Mooney DJ. Controlled Growth Factor Delivery for Tissue Engineering. Advanced Materials. 2009;21:3269-85.

[5] Seliktar D. Designing Cell-Compatible Hydrogels for Biomedical Applications. Science. 2012;336:1124-8.

[6] Lee KY, Yuk SH. Polymeric protein delivery systems. Progress in Polymer Science. 2007;32:669-97.

[7] Lin C-C, Metters AT. Hydrogels in controlled release formulations: Network design and mathematical modeling. Advanced Drug Delivery Reviews. 2006;58:1379-408.

[8] Tan SJ, Kiatwuthinon P, Roh YH, Kahn JS, Luo D. Engineering Nanocarriers for siRNA Delivery. Small. 2011;7:841-56.

[9] Whitehead KA, Langer R, Anderson DG. Knocking down barriers: advances in siRNA delivery. Nat Rev Drug Discov. 2009;8:129-38.

[10] Song WL, Lima AC, Mano JF. Bioinspired methodology to fabricate hydrogel spheres for multi-applications using superhydrophobic substrates. Soft Matter. 2010;6:5868-71.

[11] Lima AC, Song WL, Blanco-Fernandez B, Alvarez-Lorenzo C, Mano JF. Synthesis of Temperature-Responsive Dextran-MA/PNIPAAm Particles for Controlled Drug Delivery Using Superhydrophobic Surfaces. Pharm Res. 2011;28:1294-305.

[12] Peppas NA, Hilt JZ, Khademhosseini A, Langer R. Hydrogels in Biology and Medicine: From Molecular Principles to Bionanotechnology. Advanced Materials. 2006;18:1345-60.

[13] Lima AC, Sher P, Mano JF. Production methodologies of polymeric and hydrogel particles for drug delivery applications. Expert Opin Drug Del. 2012;9:231-48.

[14] Neto AI, Custodio CA, Song WL, Mano JF. High-throughput evaluation of interactions between biomaterials, proteins and cells using patterned superhydrophobic substrates. Soft Matter. 2011;7:4147-51.

[15] Salgado CL, Oliveira MB, Mano JF. Combinatorial cell-3D biomaterials cytocompatibility screening for tissue engineering using bioinspired superhydrophobic substrates. Integrative Biology. 2012;4:318-27.

[16] Oliveira MB, Song WL, Martin L, Oliveira SM, Caridade SG, Alonso M, et al. Development of an injectable system based on elastin-like recombinamer particles for tissue engineering applications. Soft Matter. 2011;7:6426-34.

[17] Fang Y. Ligand-receptor interaction platforms and their applications for drug discovery. Expert Opin Drug Discov. 2012;7:969-88.

[18] Metz A, Ciglia E, Gohlke H. Modulating Protein-Protein Interactions: From Structural Determinants of Binding to Druggability Prediction to Application. Curr Pharm Design. 2012;18:4630-47.

[19] Zhu XC, Zheng Q, Yang H, Cai J, Huang L, Duan YW, et al. Recent advances in inkjet dispensing technologies: applications in drug discovery. Expert Opin Drug Discov. 2012;7:761-70.

[20] Xia X, Wong ST. Concise review: a high-content screening approach to stem cell research and drug discovery. Stem Cells. 2012;30:1800-7.

[21] Bottier C, Gabella C, Vianay B, Buscemi L, Sbalzarini IF, Meister J-J, et al. Dynamic measurement of the height and volume of migrating cells by a novel fluorescence microscopy technique. Lab on a Chip. 2011;11:3855-63.

[22] Zelenina M, Brismar H. Osmotic water permeability measurements using confocal laser scanning microscopy. European Biophysics Journal. 2000;29:165-71.

[23] Choi J-W, Kang D-K, Park H, deMello AJ, Chang S-I. High-Throughput Analysis of Protein–Protein Interactions in Picoliter-Volume Droplets Using Fluorescence Polarization. Analytical Chemistry. 2012;84:3849-54.

[24] Lee AG, Arena CP, Beebe DJ, Palecek SP. Development of Macroporous Poly(ethylene glycol) Hydrogel Arrays within Microfluidic Channels. Biomacromolecules. 2010;11:3316-24.

[25] Baskin DS, Widmayer MA, Sharpe MA. Quantification and calibration of images in fluorescence microscopy. Anal Biochem. 2010;404:118-26.

[26] Augst AD, Kong HJ, Mooney DJ. Alginate hydrogels as biomaterials. Macromol Biosci. 2006;6:623-33.

[27] Al-Musa S, Abu Fara D, Badwan AA. Evaluation of parameters involved in preparation and release of drug loaded in crosslinked matrices of alginate. Journal of Controlled Release. 1999;57:223-32.

[28] Censi R, Di Martino P, Vermonden T, Hennink WE. Hydrogels for protein delivery in tissue engineering. Journal of Controlled Release. 2012;161:680-92.

[29] Kim S, Kim J-H, Jeon O, Kwon IC, Park K. Engineered polymers for advanced drug delivery. European Journal of Pharmaceutics and Biopharmaceutics. 2009;71:420-30.

[30] Mano J. Stimuli-Responsive Polymeric Systems for Biomedical Applications. Advanced Engineering Materials. 2008;10:515-27.

[31] Balmayor ER, Azevedo HS, Reis RL. Controlled Delivery Systems: From Pharmaceuticals to Cells and Genes. Pharmaceutical Research. 2011;28:1241-58.

CHAPTER 10. SUPERHYDROPHOBIC CHIPS FOR CELL SPHEROIDS HIGH-THROUGHPUT GENERATION AND DRUG SCREENING[9]

10.1. ABSTRACT

We suggest the use of biomimetic superhydrophobic patterned chips produced by a bench-top methodology as low-cost and waste-free platforms for the production of arrays of cell spheroids/microtissues by the hanging drop methodology. Cell spheroids have a wide range of applications in biotechnology fields. For drug screening, they allow studying 3D models in structures resembling real living tissues/tumors. In tissue engineering, they are suggested as building blocks of bottom-up fabricated tissues. We used the wettability contrast of the chips to fix cell suspension droplets in the wettable regions and evaluated on-chip drug screening in 3D environment. Cell suspensions were patterned in the wettable spots by three distinct methods: (1) by pipetting the cell suspension directly in each individual spot, (2) by the continuous dragging of a cell suspension on the chip, and (3) by dipping the whole chip in a cell suspension. These methods allowed working with distinct throughputs and degrees of precision. The platforms were robust and we were able to have static or dynamic environments in each droplet. The access to cell culture media for exchange or addition/removal of components was versatile and opened the possibility of using each spot of the chip as a mini-bioreactor. The platforms' design allowed for samples visualization and high-content image-based analysis on-chip. The combinatorial analysis capability of this technology was validated by following the effect of doxorubicin at different concentrations on spheroids formed using L929 and SaOs-2 cells.

[9] Oliveira MB, Neto AI, Correia CR, Rial-Hermida MI, Alvarez-Lorenzo C, Mano JF. Superhydrophobic Chips for Cell Spheroids High-Throughput Generation and Drug Screening. Acs Appl Mater Inter. 2014;6:9488-95.

10.2. INTRODUCTION

High-throughput studies in biotechnology areas such as drug screening and tissue engineering have been carried out mainly in two-dimensional (2D) environment. Such models are routinely used for evaluating the effectiveness and safety of libraries of drugs and other bioactive or potentially therapeutic molecules. However, biological phenomena in living organisms clearly take place in three-dimensional (3D) environments. In 2D techniques, cell-to-plastic interactions prevail rather than the crucial cell-to-cell and cell-to-extracellular matrix (ECM) interactions that form the basis for normal cell function. Tissue culture polystyrene is an unnaturally stiff substrate compared to the softer mechanical environment that cells experience *in vivo*. The stiffness of the substrates used for cell growth is well known to alter cell function. For example, mesenchymal stem cells differentiation can be directed into certain lineages simply by altering the stiffness of the substrates they were cultured on [1]. In nature cells lie in a 3D configuration organized in the self-secreted microenvironment, the ECM, both in organs and tumor masses. In this milieu, cells interact in a totally natural manner, without the intervention of foreign factors, such as biomaterials. The demand for studies using organotypic models is increasing, in order to improve the relevance of the findings achieved in these areas of study.

The use of cell spheroids has been suggested as a potential link to bridge the gap between monolayer cultures and animal model studies [2-6]. A solution to create organotypic models is the *in vitro* construction of cell spheroids. Multicellular tumor spheroids were described as 'spherically symmetric aggregates of cells analogous to tissues, with no artificial substrate for cell attachment'. Such cell structures resemble tumors *in vivo* in many ways. It is known that the expression of antigens, pH and oxygen gradients within the spheroid, as well as penetration rate of growth factors and distribution of proliferating/quiescent cells within the spheroid is similar to those of a real tumor [7,8]. Resembling the *in vivo* environment, in those micromasses cells tend to attach each other in an organized structure constituted by cells in combination with ECM. Some types of spheroids are grown in order to mimic tumor models: the living spheroid structure contains a necrotic core, similarly to the native tumors [9]. As such, the accessibility of cytotoxic agents into the spheroids may be limited by hypoxia and poor vascularization within the microregions of the cultures [10] as occurs in solid tumors [11-13]. Cell growth in 3D organization has been reported to induce significant variations in the bioenergetics of osteosarcoma cells (MG-63) [14]. In the cancer research field, cell spheroids have been widely applied as *in vitro* systems to investigate specific microenvironment factors

associated with tumor therapy, such as the mechanism of action of chemotherapy, radiotherapy, [15,16] and drug toxicity [17]. Cell spheroids are also useful as models for the development of complex microtissues and can also be used as building blocks of larger tissues [18-20].

Several methods to produce cell spheroids can be found in literature [5]. The hanging drop technique is an advantageous method since it can be applied to distinct cell types, it enables the control of the spheroid size control, and the micromass is exposed to low shear stress [21]. The cells are pulled to the concave bottom of a hanging droplet by gravity effect, and tend to start the natural organization by cell-cell attachment and production of ECM. To make spheroids by the hanging drop technique, usually volumes of about 20-30 μL of a cell suspension are pipetted onto the inside lid of a tissue culture plate [22]. Advances into high throughput production of spheroids using the hanging drop method have been made, producing up to 384 spheroids in a single array [23]. However, the platforms developed in that previous work were fabricated by injection molding, requiring specific processing machinery.

Herein, we suggest the use of superhydrophobic surfaces patterned with wettable regions as platforms produced by a bench-top methodology for the affordable and scale-up production and analysis of cell spheroids/microtissues by the hanging drop technique. Platforms based on wettability contrast were previously used for the high-content study of cells-biomaterials interactions [24-26]. In such studies, the patterning of wettable regions in superhydrophobic polystyrene and poly(lactic acid) was performed by exposure to UV/Ozone or plasma gas [27,28]. In both cases, the wettability of the patterns was controlled by the time of exposure of the superhydrophobic surfaces to the UV/Ozone or plasma treatments through a photomask. More recently, instead of patterning wettable regions in the polystyrene surfaces after the phase-separation treatment that leads to their superhydrophobicity, the authors suggested the protection of untreated commercial polystyrene with poly(vinyl chloride) (PVC) stickers, followed by the phase separation treatment of the polymeric surface [29]. The area protected by the stickers remained with the original contact angle of untreated polystyrene, as the surroundings were treated in order to be superhydrophobic. The patterning of wettable regions in other superhydrophobic polymeric surfaces was also reported for biotechnology applications. Accardo *et al.* reported the production of poly(methyl methacrylate) superhydrophobic surfaces by lithography and plasma etching for the X-ray scattering of protein solutions drying in surfaces with distinct topographies [30]. Such surfaces were more recently used for droplet mixing controlled by electrowetting, with great avoidance of contact between the droplets and the surface [31]. We adapted polystyrene superhydrophobic platforms - with transparent wettable regions and the hanging drop

surface totally exposed to the external media allowing its facilitated manipulation – as high-throughput screening platforms for drug testing and on-chip high-content cell response analysis by microscopy. In this approach, cell spheroids were produced by three methods, with distinct throughput abilities and adaptable to the needs of the user: (1) by manual pipetting of cell suspensions in each wettable regions, (2) by dragging a cell suspension on the chip and (3) by dipping the whole chip in a cell suspension.

For the proof-of-concept we dispensed cell suspensions of distinct cell types (L929 and SaOs-2) with different cell densities in the array of wettable regions of the chips. After the formation of cell spheroids, we tested the effect of a cytostatic agent used in clinical practice (doxorubicin - Dox), also dispensed in a combinatorial way in each individual spot of the chip. By on-chip microscopy analysis we proved the suitability of such platforms for direct drug screening using tumor-like models. The presence of transparent patterns in the chips allowed monitoring spheroids formation in real-time without the need of any staining, simply by using transmitted light microscopy. Moreover, the platforms were robust allowing for successive tilting, as the droplets do not slip from the wettable spot. We also proved that besides working directly in the wettable spots by pipetting, it was possible to perforate the superhydrophobic surfaces and feed/remove media from the spots by holes where needles were inserted. With this in mind, we also showed the compatibility of this easily prepared and versatile system with dynamic media exchange and possible configurations that may allow in the future, for example, controlling the delivery of molecules over time, or to use each spot as a mini-bioreactor.

10.3. Materials and Methods

10.3.1. Superhydrophobic chips for manual pipetting technique (methodology (1))

Polystyrene flakes were cut from commercially available polystyrene plates (Corning). PVC stickers (Oracal, USA) were glued in the polystyrene surface in the form of an array of 1x1 mm^2 squares separated by 4 mm. Tetrahydrofuran (THF) was from Fluka (p.a.>99.5%) and ethanol absolute from Panreac. The surfaces were modified according to a phase separation protocol described elsewhere [32]. The wettability of the surfaces was evaluated by contact angle (CA) measurements in an OCA15+ goniometer (DataPhysics, Germany) using the sessile drop method. The stickers were then removed from the surface of the chip. The protected regions remained untreated and, consequently, wettable and transparent (Figure 10.1A,B). Prior to the

contact with cell suspension, the platforms were sterilized with ethanol 70% (v/v) for 2 hours, rinsed with sterile phosphate buffered saline (PBS) 3 times and let to dry at room temperature.

10.3.2. Cell expansion and cell culture

A fibroblast (L929) and an osteosarcoma cell line (SaOs-2) were used for spheroids formation and drug screening studies. Cells were expanded in basal medium consisting of DMEM (Gibco, UK) supplemented with 10% heat-inactivated fetal bovine serum (BiochromAG, Germany) and 1% antibiotic/antimycotic solution (penicillin 100 units/mL and streptomycin 100 mg/mL; Gibco, UK). Cells were grown in 150 cm^2 tissue culture flasks and incubated at 37 °C in a humidified air atmosphere of 5% CO_2. Every 3–4 days, fresh medium was added. At 90% of confluence, cells grown in tissue culture flasks were washed with PBS and subsequently detached by a chemical procedure with 0.05% trypsin-EDTA solution for 5 min at 37 °C in a humidified air atmosphere of 5% CO_2. To inactivate the trypsin effect, cell culture medium was added. The cells were then centrifuged at 300 g and 25 °C for 5 min and the medium was decanted. Cell suspensions with distinct densities were prepared.

10.3.3. Spheroids formation for drug screening

The chips were fixed to the lids of tissue culture plates using commercially available tape. The lower part of the plate was filled with sterile PBS, so the environment was saturated with water, in order to avoid the cell suspension droplets evaporation. A volume of 5 µl of cell suspensions of $4x10^6$ and $8x10^6$ cells/mL was dispensed in each wettable spot of the chip, as indicated in Figure 10.2. Each condition was processed in triplicate in each chip. The spheroids were let to form during 24 hours, after turning the platforms 180°, by closing the tissue culture plate with the lid where the platform was fixed with tape. We were able to monitor the spheroids by transmitted light microscopy (Axio Imager Z1m, Zeiss), as the visible light was able to pass through the polystyrene transparent window in the chip.

10.3.4. Drug screening: studies with doxorubicin

After 24 hours of cell culture for spheroid formation, a volume of 1 µl of solutions of doxorubicin in water was added to each spot in the concentrations of 0, 0.1, 1, 10 µM (based on concentrations previously used) [33]. As live/dead microscopy images from fluorescence microscopy showed a high resistance from L929

cells to these drug concentrations (Figure 10.S1, Supporting Information), a new experiment was carried out with these cells with 0, 1, 10 and 100 µg/mL of Dox (based on concentrations previously used) [34].

10.3.5. Fluorescence microscopy and confocal microscopy

For fluorescence reflected light microscopy as well as for confocal microscopy, live dead staining was carried out using calcein AM and propidium iodide. A volume of 2 µl of solution of PBS with 10% (v/v) of each reagent was added to the spheroids, after 3 µl of the culture medium (from a total volume of 5 µl) was removed from the spots. The samples were left to incubate at 37°C during 30 minutes, and then washed 3 times with 3 µl of PBS. Spheroids diameter quantification was carried out using ImageJ software (NIH, USA).

10.3.6. Viability study: image quantification

Confocal microscopy images were used to determine cell viability. As such, we could determine the number of viable cells in each stack, even if the distribution of dead cells was not uniform in the spheroid. We used the particle analysis application of ImageJ software and analyzed the multiimages (multitiff) in the form of images stacks. The total number of cells in the analyzed spheroids was assumed to be the sum of cells counted in all stacks. Cell viability was determined as:

$$cell\ viability\ (\%) = \frac{\sum live\ cells}{\sum (live\ cells + \ dead\ cells)} \text{x}\ 100\%$$

10.3.7. Superhydrophobic chips for higher-throughput techniques and respective spheroids formation

We treated the polystyrene chips with the PVC stickers, prepared as previously described for manual pipetting, with a layer of WX2100™ (Cytonix, USA), an air-cured fluoro-urethane alkyd, according to the manufacturer's indications. This product has been previously used for cell studies without any report of cytotoxic effect [35]. For these studies, we used chips with stickers with 3x3 mm^2, separated by 3 mm. The surfaces were then let dry for 48 hours. We then removed the stickers.

For the method (2) – as indicated in Figure 10.3A,B – we used a L929 cell line cell suspension with a density of $1x10^7$ cells/mL. We dragged the cell suspension with a speed of approximately 1 wettable spot/second. To measure the average volume of cell suspension fixed in each wettable spot, we used a

micropipette and removed the medium from each individual spot. The chips were turned 180°, as for method (1), and the spheroids were let to form during 24 and 72 hours. Live dead staining was carried out using calcein AM and propidium iodide, as described for method (1). The spheroids were then observed using reflected light fluorescence microscopy (Axio Imager Z1m, Zeiss), and their diameter was quantified using ImageJ software (NIH, USA).

For the method (3) – as indicated in Figure 10.3A,B – we used a L929 cell suspension with a density of $5x10^6$ cells/mL. We dipped the whole chip in cell suspension during 5 seconds. After removing the chip, we tilted it so the remaining cell suspension was removed from the superhydrophobic part of the chip. To measure the average volume of cell suspension fixed in each wettable spot, we used a micropipette and removed the medium from each individual spot. The chips were turned 180°, as in method (1), and the spheroids were let to form during 24 hours. Live dead staining was carried out in the same conditions as for method (1). The spheroids were then observed using reflected light fluorescence microscopy (Axio Imager Z1m, Zeiss), and their diameter was quantified using ImageJ software (NIH, USA).

10.3.8. Increasing the versatility of the superhydrophobic patterned chips: improving the access to cell culture medium

Polystyrene surfaces prepared for drug screening studies (method (1)) were perforated both in the center of the transparent spot (configuration D, Figure 10.2) or at 1 mm from the border of the transparent squares (configurations E and F, Figure 10.2), using a 27G needle for perforation. The needle tips were cut in order to be straight. They were introduced in the chip spot from the upper surface of the chip, as indicated in Figure 10.2, for medium exchange and circulation. We performed and tested the three configurations shown in Figure 10.2E-G. The liquid flows were adjusted to 60 µl/min using a peristaltic pump.

10.3.9. Statistical Analysis

All cell spheroids diameter and cell viability quantification results were analyzed by one-way ANOVA with Tukey's post-test using GraphPad Prism software.

10.4. Results and Discussion

By using the wettability contrast of the superhydrophobic patterned chip, we dispensed droplets of cell suspensions and kept them restricted and fixed in the wettable spot due to the difference in surface tension

compared with the superhydrophobic surrounding regions (Figure 10.1A). It was previously shown that protein adsorption in the wettable regions of the chips is higher than in the superhydrophobic parts.[27,36] Moreover, cell adhesion and proliferation were, as well, diminished in the superhydrophobic parts of chips constituted by different polymers. Such results were observed for fibroblast and osteoblast-like cell lines in polystyrene, bone marrow stem cells in poly(lactic acid), NIH 3T3 fibroblasts in poly(methyl methacrylate), polyether ether ketone and poly-1,8- octanediol-co-citric acid surfaces, as well as for HEK 293 cells in poly(butyl methacrylate- *co*-ethylene dimethacrylate) surfaces [26.27,37-39].

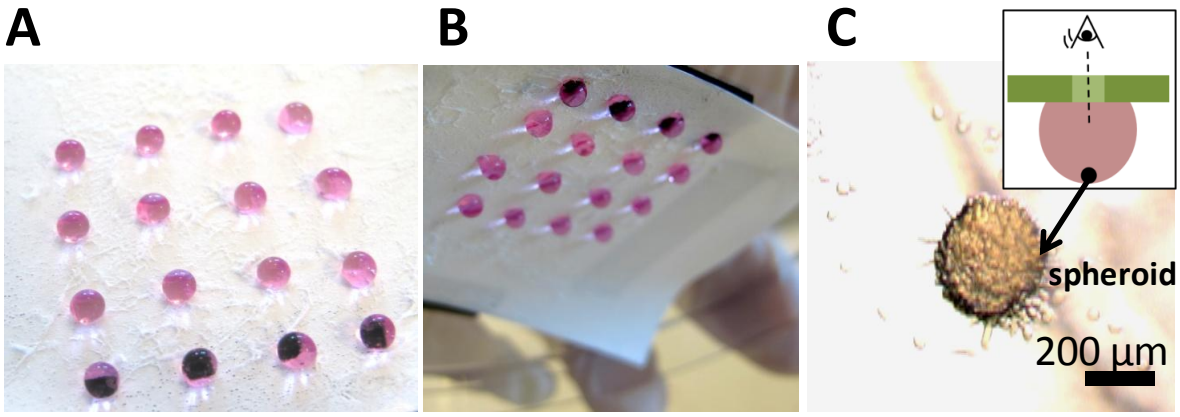

Figure 10.1. – Pictures of the chips with the cell suspensions turned (A) upside and (B) tilted down. (C) Transmitted light microscopy image of a spheroid, observed from the top of the chip, through the transparent spot (as indicated in the schematic representation).

10.4.1. Patterning of cell suspensions in the chips

Cell suspensions were patterned in the wettable spots by manual pipetting of the cell suspension in each individual wettable pattern (Figure 10.2, describing method (1)), dragging of a cell suspension in the array (Figure 10.3A,B, method (2)) or dipping of the whole platform in the cell suspension (Figure 10.3A,B, method (3)). The working principle behind all strategies is the wettability contrast in the chips, where the cell suspensions remain attached to the wettable spots and are repelled from the superhydrophobic regions due to its self-cleaning properties. However, their diversity allows choosing a higher-throughput and time-saving method for microtissues preparation - in the case of methods (2) and (3) -, or higher degree of control of the composition of each individual spot, in the case of method (1). The methods may also be combined. For example, cell spheroids may be prepared by method (2) - if distinct types of spheroids are needed in

replicate in the chips -, or by method (3) - if we aim to produce or study a single type of cell spheroid. Afterwards, distinct drug formulations or other components may be dispensed in each individual spot by pippeting (method (1)).

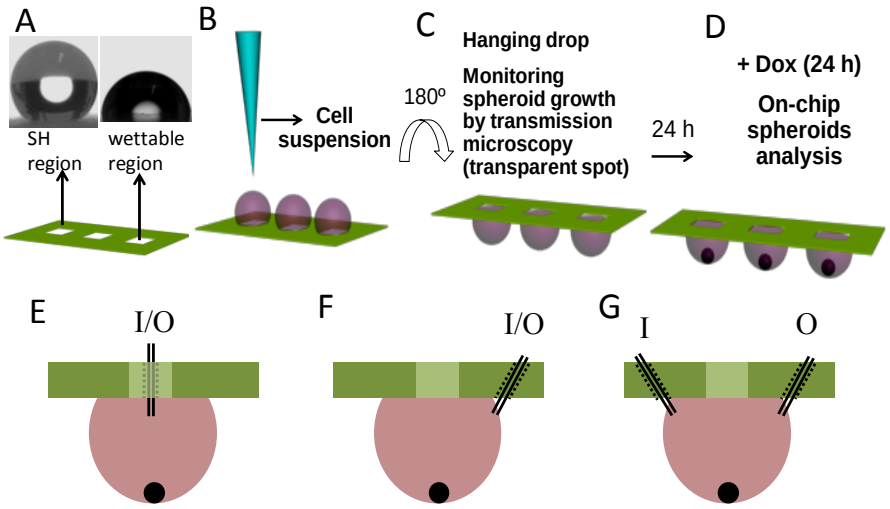

Figure 10.2. – Schematic representation of the procedure for the production of spheroids in (A) superhydrophobic surfaces patterned with wettable transparent spots (water droplet profiles on the superhydrophobic region – left, and wettable region – right). (B) Addition of a cell suspension into the wettable spots of a superhydrophobic patterned chip by pipetting (method (1)). (C) Turning of the platform 180° to create a hanging-drop setup. The spheroids were let to form for 24 hours. (D) Dox was added to each well in combinatorial logic. The addition of Dox to the spots was performed by pipetting after tilting the chips (around 110°). However, the system was also adapted in order to avoid moving the platform, which may disturb the normal formation of the spheroids. We modified the system by making small holes (represented in dashed lines), in order to achieve multiple configurations with the same platform. The medium was reached by a needle tip (represented in black lines, inside the holes). (E) We perforated the inner part of the wettable regions of the array, in order to add and remove medium directly from the spot. (F) In another configuration, in order to avoid evaporation and contamination of the medium, we drilled the superhydrophobic region of the chip, 1 mm away from the wettable spot. As such, we accessed the medium laterally. (G) The number of holes in the system could be increased, and their position could be changed. For example, we created a two-entrance system, with an inlet (I) and an outlet (O), so the medium had a dynamic composition over time (configuration F).

We observed that the chip could be rotated and tilted several times without any movement of the droplets (Figure 10.1B). This proved that the handling of the chip, medium exchange and drug delivery to the droplet could be carried out easily, by simply tilting the culture plate lid, as shown in method (1). The

superhydrophilic-superhydrophobic interactions in polystyrene superhydrophobic surfaces patterned with superhydrophilic channels were previously shown to be stable and resistant even to dynamic environment inside the channels. On the other hand, hydrophobic-superhydrophilic interactions in polystyrene did not allow restricting the liquid in the wettable patterns [32].

For method (2), using a micropipette to drag the cell suspension at an approximated rate of 1 wettable spot/second, we observed that the volume fixed in each spot ranged from 6 µl to 7 µl. Cell spheroids were obtained from a cell suspension of L929 (cell line generated from mice muscle fibroblasts), with a density of $1x10^7$ cells/mL. After 24 hours of cell culture we obtained spheroids with mean sizes of 520.0±48 µm (n=20), and after 72 hours of cell culture with 800.3±18 µm (n=20). As observed by the standard deviation of the spheroids size, a low size distribution was obtained using this approach. For method (3), we used chips with the same dimensions and immersed them for 5 seconds. We observed that after dipping the volume of medium in each individual spot was also in the range of 6-7 µl. The cell suspension was in a concentration of $5x10^6$ cells/mL. After 24 hours of cell culture, we obtained spheroids with an average size of 205.6±26 µm (n=20). With this method, the number of spheroids obtained in 5 seconds is solely dependent on the number of wettable regions on the chip.

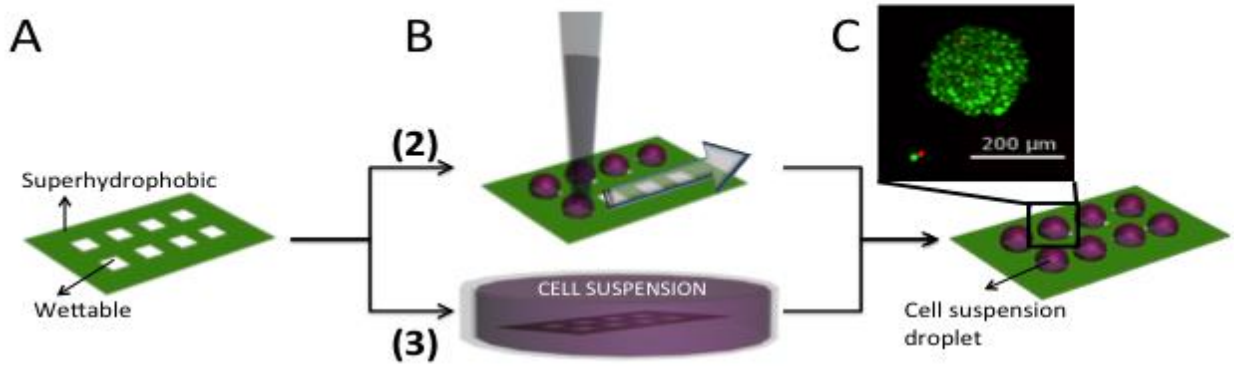

Figure 10.3. – Schematic representation of the higher throughput methodologies (described as method (2) and method (3) in the text). A. In both methodologies the superhydrophobic chip based on wettability contrast is used. B. In methodology (2) a cell suspension is dragged through chip, and the droplets are fixed in the wettable spots due to the wettability contrast. In methodology (3) the whole chip is immersed in a cell suspension. When the chip is removed from the cell suspension, droplets are fixed in the wettable regions and the remaining liquid is repelled from the superhydrophobic parts of the surface due to its self-cleaning properties. C. A chip with droplets of cell culture

medium is obtained and then turned 180° for the formation of cell spheroids, in the same way as in methodology (1). Live/dead staining image of a cell spheroid obtained using the methodology (3).

As the wettable spots of the chips were transparent, the formation of spheroids was amenable to be monitored using transmitted light microscopy (Figure 10.1C), avoiding any cell staining or labeling using toxic labels. It also prevented excessive manipulation/opening of the lid, consequently decreasing the risk of contamination of the whole setup (Figure 10.2).

10.4.2. On-chip cell-drug interactions tests

For the proof of concept of drug screening assays, L929 cells were firstly dispensed at distinct densities in the wettable spots (Figure 10.4A). After 24 hours of incubation, we concluded that the densities that allowed forming cell spheroids were $4x10^6$ and $8x10^6$ cells/mL (Figure 10.4A). Using these conditions we produced spheroids of two cell types: L929 and SaOs-2 (cell line generated from a human osteosarcoma). Spheroids diameter was dependent on both cell number and cell type. For both cell types, after 48 hours of incubation $8x10^6$ cells/mL suspensions led to the formation of larger spheroids. Moreover, SaOs-2 spheroids were smaller than the ones constituted by L929 cells (Figure 10.4B).

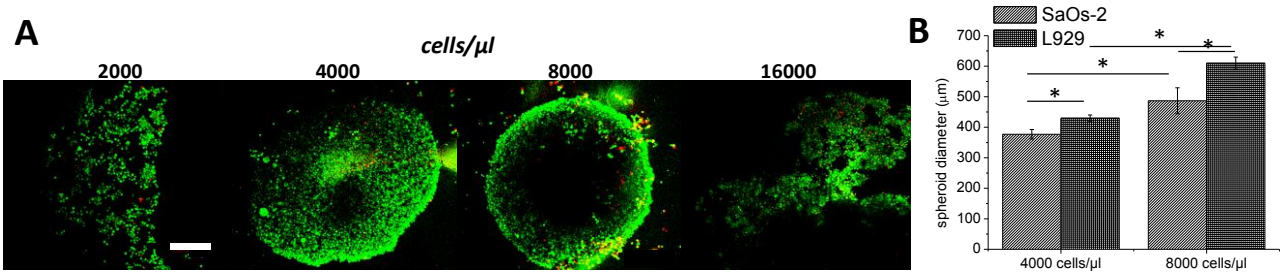

Figure 10.4. – (A) Confocal assembly microscopy images of the cells after 24 hours in the hanging drop system, dispensed in the wettable spots by manual pipetting. We observed that the conditions $4x10^6$ and $8x10^6$ cells/mL were the most favorable for spheroid formation. Scale bar = 200 µm. (B) Average diameter of the spheroids after 48 hours of cell culture, without the addition of any drug. The symbol "*" indicates significant differences for $p<0.05$.

The cell culture media was maintained static during spheroid formation time (24 hours). Afterwards, a cytostatic agent commonly used in clinical practice - Dox – was added in increasing doses. The influence of cell type, cell density of the suspension used to form the spheroid and drug concentration on cells viability

was evaluated. Fluorescence microscopy pictures of live/dead staining of the spheroids are shown in Figure 10.S1 (Supporting Information). Confocal microscopy stack images were used for an accurate cell number-based quantification; images resulting from the assembly of the stacks can be seen in Figure 10.5. For the firstly used Dox concentrations (0.1, 1 and 10 μM), SaOs-2 cells showed concentration-dependent cell viability. With increasing Dox concentration, the area corresponding to red cells (stained with propidium iodide) increased (Figure 10.S1, Supporting Information). However, we observed that for such concentrations the viability of L929 was maintained up to 48 hours (Figure 10.S1, Supporting Information). A decrease in L929 viability was only observed after 72 hours of exposure to Dox. It was previously described that Dox does not kill L929 cells at concentrations that profoundly reduce clonogenic survival (5 μg/mL), corresponding to the range of concentrations used firstly in the work presented herein. Instead, the cell and nuclear volume progressively increase for at least 1 week following drug exposure leading to the production of characteristic giant cells. The increase in nuclear volume results from a continued DNA synthesis and increase in chromosome number without entry into mitosis [40]. As such, we performed the assays with higher concentrations, effective on L929 viability decrease, according to values reported elsewhere [28]. On the other hand, Dox was found to induce reactive oxygen species formation, mitochondrial membrane depolarization, mitochondrial cytochrome c release, caspase-3 activation, and apoptosis in SaOs-2 cells. As such, these cells are well known as highly sensitive to Dox, even at low concentrations [41].

We increased the amount of Dox added to L929 cell spheroids in the order of a million times, compared to the originally used concentrations, and kept the values of the concentration used for SaOs-2. Then the percentage of living cells in the spheroids was quantified by analyzing the stacks of confocal microscopy images, with live/dead staining (Figure 10.5). Even with 10^6-fold higher concentration of Dox (1, 10 and 100 μg/mL), L929 cells were still significantly more resistant to this cytostatic than SaOs-2 cells. SaOs-2 cells viability showed a concentration-dependent behavior (Figure 10.6). For both cells types, $8x10^6$ cells/mL spheroids showed lower viability than $4x10^6$ cells/mL spheroids, even without the addition of Dox (Figure 10.6). This may be explained by the necrotic core formed in the $8x10^6$ cells/mL spheroids after 24 hours of cell culture (Figure 10.6), as they are much more compact than the $4x10^6$ cells/mL spheroids: for a cell number twice as high, the diameter of the spheroids showed to be similar to the ones formed from the $4x10^6$ cells/mL suspension. This fact probably limited oxygen and nutrients diffusion to the center of the cell mass.

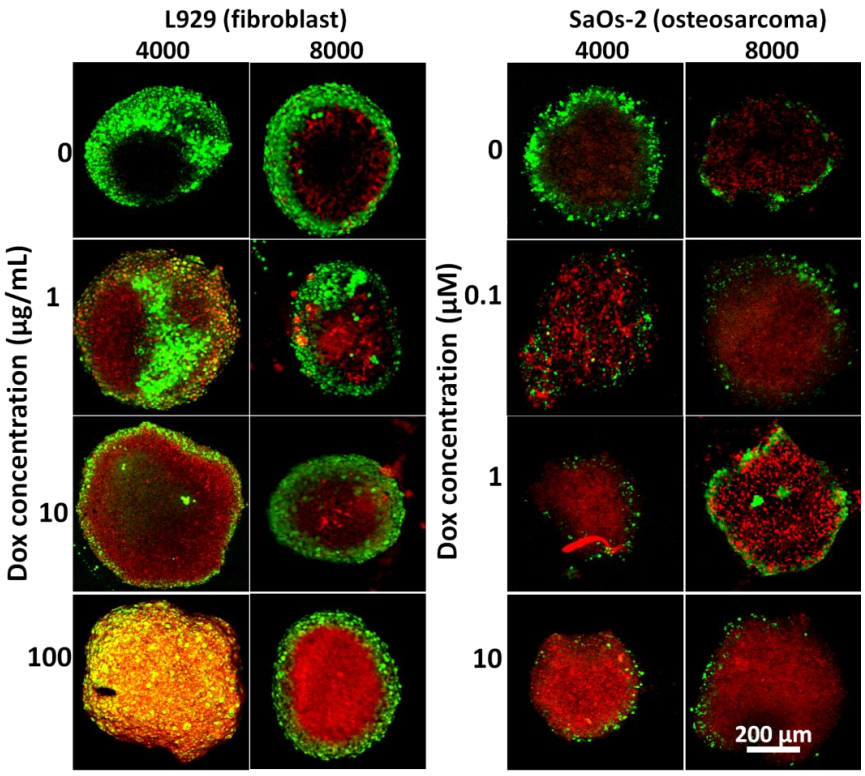

Figure 10.5. – Confocal microscopy assembled images of the cell spheroids formed by L929 and SaOs-2 cells, with live (green)/dead (red) staining (calcein AM/propidium iodide).

10.4.3. Adaptation of the chips for dynamic cell environment

We adapted the chips in order to open the possibility of having dynamic cell environments where, for example, physiological-like drug delivery conditions and clearance properties could be mimicked. Three different possible configurations were tested. The first one (depicted in Figure 10.2E) consisted of holes in the middle part of the wettable regions of the chips, allowing exchanging medium in a direct manner by the introduction of a needle. However, such design may increase the evaporation of the medium from the spots and also increase contamination risk due to cell medium exposure to the outer environment. The second approach (shown in Figure 10.2F) consisted of a hole equivalent to the one of the configuration in Figure 10.2E, with the exception that the drilling was performed in the superhydrophobic part of the chip, 1 mm away from the border of the wettable spots. Such configuration also allows expanding the number of inlets to the system, as shown in the third configuration (depicted in Figure 10.2G), where one of the holes is used as an inlet, and the second hole is used as an outlet. This configuration allows several approaches, such as

recirculation of medium, physiological clearance mimetics, controlled drug delivery to the system, among others. We adjusted the flow of the inlets to 60 µl/min and were able to fill independently each well without having to turn the chip upsides. We additionally tested the system by filling and emptying the wettable spot with a red colorant.

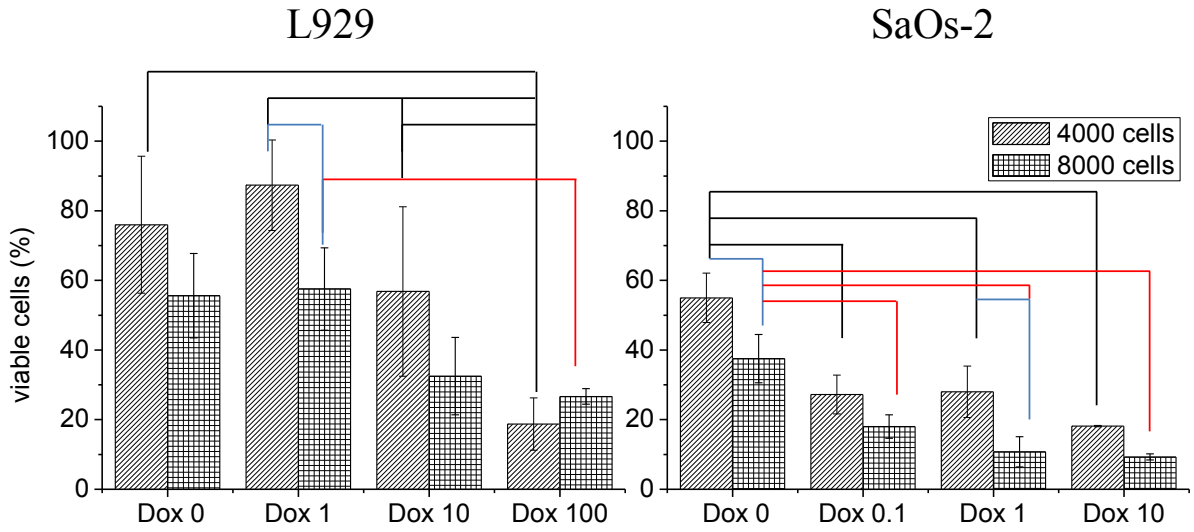

Figure 10.6. – Quantification of viable cells by image analysis for L929 and SaOs-2 spheroids. The black lines indicate significant differences between distinct Dox concentrations for $4x10^6$ cells/mL conditions, while red lines indicate significant differences between distinct Dox concentrations for $8x10^6$ cells/mL conditions. Blue lines indicate significant differences between spheroids prepared using cell suspensions with distinct cell densities, but exposed to the same Dox concentration. Statistically differences were considered for $p<0.05$.

10.4.4. Advantages of the method and future perspectives

In resume, superhydrophobic surfaces patterned with wettable regions are herein proposed as chips for the high-throughput generation and image acquisition of cell spheroids. We were able to pattern cell suspensions with precision in wettable spots by three distinct methods, with distinct throughputs. The superhydrophobic/wettable contrast in the chips allowed having stable droplets, whose volume was amenable to be varied by varying the size of the wettable spots. Due to the transparency of the wettable spots where cell suspensions were dropped, the platform is compatible with reflected light microscopy as well as transmitted light microscopy. The number of spheroids to be prepared was totally controlled by cutting the flexible polystyrene platform with a specific number of wettable regions, making the technique

waste-free. The platform was totally two-dimensional, facilitating sterilization process and eventual re-use. After immersion in 70% ethanol (v/v) and drying at room temperature the chips remained superhydrophobic. Moreover, the boarders of the wettable patterns designed in the chips remained defined, allowing re-using the platforms.

We studied the effect of the addition of a cytostatic drug in different concentrations on the viability of two distinct cell types cultured in the form of spheroids. The platform is versatile as it allowed working with distinct types of cells, drug solutions and stainings. In future studies, it may be adapted for the study of complex heterotypical spheroids, composed by two or more cell types, in contact with distinct drugs, mixtures of drugs and agents released into the medium in a controlled fashion. We also proved that these chips are amenable to be adapted to bioreactor logic, where the flow of medium in each spot could be controlled independently. Clearance and renovation of solutions may be easily achieved by this method.

The transparent window may also be useful in the future to monitor tissue formation and organization using cells transfected with fluorescent molecules. For example, the formation of Janus-like structures may be studied. Moreover, the ideal conditions that lead to the self-assembly of tissues mimicking their natural behavior *in vivo*, namely their vascularization, may also be evaluated using these platforms [42,43].

10.5. Conclusions

Superhydrophobic surfaces patterned with wettable spots were successfully used as improved and versatile platforms for high-throughput spheroids formation and drug screening in such *in vitro*-constructed tissues. These affordable chips are easy to design and can be produced by a bench-top strategy. They are totally cytocompatible and allow working in contamination-preventing visualization conditions. We proved that they are robust and adequate for combinatorial high-throughput drug screening tests. Moreover, we were able to modify them as mini-bioreactors with several configurations that may be used to distinct applications needs, with distinct behaviors in each spot. We believe these platforms may find application in future works regarding not only drug screening but also microtissues formation for tissue engineering purposes.

10.6. Acknowledgements

The authors acknowledge Fundação para a Ciência e para a Tecnologia (FCT) for the PhD grants SFRH/BD/71396/2010 (M.B. Oliveira), SFRH/BD/73119/2010 (A.I. Neto) and SFRH/BD/69529/2010 (C.R. Correia). The research leading to these results has received funding from the European Union's

Seventh Framework Programme (FP7/2007-2013) under grant agreement n° REGPOT-CT2012-316331-POLARIS. The research was also funded by FEDER through the Competitive Factors Operation Program – COMPETE, Portugal National funds through FCT (PTDC/CTM-BIO/1814/2012) and Spain MINECO (SAF 2011-22771 and PRI-AIBPT-2011-1211).

10.7. REFERENCES

[1] Engler AJ, Sen S, Sweeney HL, Discher DE. Matrix elasticity directs stem cell lineage specification. Cell. 2006;126:677-89.

[2] Minchinton AI, Tannock IF. Drug penetration in solid tumours. Nat Rev Cancer. 2006;6:583-92.

[3] Pampaloni F, Reynaud EG, Stelzer EHK. The third dimension bridges the gap between cell culture and live tissue. Nat Rev Mol Cell Biol. 2007;8:839-45.

[4] Kunz-Schughart LA, Freyer JP, Hofstaedter F, Ebner R. The use of 3-D cultures for high-throughput screening: The multicellular spheroid model. J Biomol Screen. 2004;9:273-85.

[5] Breslin S, O'Driscoll L. Three-dimensional cell culture: the missing link in drug discovery. Drug Discov Today. 2013;18:240-9.

[6] Meli L, Jordan ET, Clark DS, Linhardt RJ, Dordick JS. Influence of a three-dimensional, microarray environment on human Cell culture in drug screening systems. Biomaterials. 2012;33:9087-96.

[7] Hirschhaeuser F, Menne H, Dittfeld C, West J, Mueller-Klieser W, Kunz-Schughart LA. Multicellular tumor spheroids: An underestimated tool is catching up again. J Biotechnol. 2010;148:3-15.

[8] Kim JB. Three-dimensional tissue culture models in cancer biology. Semin Cancer Biol. 2005;15:365-77.

[9] Peck Y, Wang D-A. Three-dimensionally engineered biomimetic tissue models for in vitro drug evaluation: delivery, efficacy and toxicity. Expert Opinion on Drug Delivery. 2013;10:369-83.

[10] Jang SH, Wientjes MG, Lu D, Au JLS. Drug delivery and transport to solid tumors. Pharm Res. 2003;20:1337-50.

[11] Sutherland RM, Durand RE. Growth and cellular characteristics of multicell spheroids. Rec Res Camcer Res. 1984;95:24-49.

[12] Santini MT, Rainaldi G, Indovina PL. Apoptosis, cell adhesion and the extracellular matrix in the three-dimensional growth of multicellular tumor spheroids. Crit Rev Oncol/Hematol. 2000;36:75-87.

[13] Elliott NT, Yuan F. A Review of Three-Dimensional In Vitro Tissue Models for Drug Discovery and Transport Studies. J Pharm Sci. 2011;100:59-74.

[14] Santini MT, Rainaldi G, Romano R, Ferrante A, Clemente S, Motta A, et al. MG-63 human osteosarcoma cells grown in monolayer and as three-dimensional tumor spheroids present a different metabolic profile: a H-1 NMR study. Febs Letters. 2004;557:148-54.

[15] Dubessy C, Merlin JL, Marchal C, Guillemin F. Spheroids in radiobiology and photodynamic therapy. Crit Rev Oncol/Hematol. 2000;36:179-92.

[16] Santini MT, Rainaldi G, Indovina PL. Multicellular tumour spheroids in radiation biology. Int J Radiat Biol. 1999;75:787-99.

[17] Durand RE, Olive PL. Resistance of tumor cells to chemo- and radiotherapy modulated by the three-dimensional architecture of solid tumors and spheroids. Methods in Cell Biology, Vol 64. 2001;64:211-33.

[18] Mironov V, Visconti RP, Kasyanov V, Forgacs G, Drake CJ, Markwald RR. Organ printing: Tissue spheroids as building blocks. Biomaterials. 2009;30:2164-74.

[19] Ulloa-Montoya F, Verfaillie CM, Hu WS. Culture systems for pluripotent stem cells. J Biosci Bioeng. 2005;100:12-27.

[20] Schon BS, Schrobback K, van der Ven M, Stroebel S, Hooper GJ, Woodfield TBF. Validation of a high-throughput microtissue fabrication process for 3D assembly of tissue engineered cartilage constructs. Cell and Tissue Research. 2012;347:629-42.

[21] Achilli T-M, Meyer J, Morgan JR. Advances in the formation, use and understanding of multi-cellular spheroids. Expert Opinion on Biological Therapy. 2012;12:1347-60.

[22] Lin R-Z, Lin R-Z, Chang H-Y. Recent advances in three-dimensional multicellular spheroid culture for biomedical research. Biotechnology journal. 2008;3:1172-84.

[23] Hsiao AY, Tung Y-C, Qu X, Patel LR, Pienta KJ, Takayama S. 384 Hanging Drop Arrays Give Excellent Z-factors and Allow Versatile Formation of Co-culture Spheroids. Biotechnol. Bioeng. 2012;109:1293-304.

[24] Salgado CL, Oliveira MB, Mano JF. Combinatorial cell-3D biomaterials cytocompatibility screening for tissue engineering using bioinspired superhydrophobic substrates. Integrative Biology. 2012;4:318-27.

[25] Oliveira MB, Salgado CL, Song W, Mano JF. Combinatorial On-Chip Study of Miniaturized 3D Porous Scaffolds Using a Patterned Superhydrophobic Platform. Small. 2013;9:768-78.

[26] Tsougeni K, Bourkoula A, Petrou P, Tserepi A, Kakabakos SE, Gogolides E. Photolithography and Plasma Processing of Polymeric Lab on Chip for Wetting and Fouling Control and Cell Patterning. Microelectron. Eng. 2014;124:47-52.

[27] Neto AI, Custodio CA, Song WL, Mano JF. High-throughput evaluation of interactions between biomaterials, proteins and cells using patterned superhydrophobic substrates. Soft Matter. 2011;7:4147-51.

[28] Song W, Veiga DD, Custódio CA, Mano JF. Bioinspired Degradable Substrates with Extreme Wettability Properties. Advanced Materials. 2009;21:1830-4.

[29] Oliveira MB, Ribeiro MP, Miguel SP, Neto AI, Coutinho P, Correia IJ, et al. In Vivo High-Content Evaluation of Three-Dimensional Scaffolds Biocompatibility. Tissue Eng Part C Methods. 2014 (in press) doi: 10.1089/ten.tec.2013.0738.

[30] Accardo A, Gentile F, Mecarini F, De Angelis F, Burghammer M, Di Fabrizio E, et al. In situ X-ray scattering studies of protein solution droplets drying on micro- and nanopatterned superhydrophobic PMMA surfaces. Langmuir. 2010;26:15057-64.

[31] Accardo A, Mecarini F, Leoncini M, Brandi F, Di Cola E, Burghammer M, et al. Fast, active droplet interaction: coalescence and reactive mixing controlled by electrowetting on a superhydrophobic surface. Lab Chip. 2013;13:332-5.

[32] Oliveira NM, Neto AI, Song WL, Mano JF. Two-Dimensional Open Microfluidic Devices by Tuning the Wettability on Patterned Superhydrophobic Polymeric Surface. Appl Phys Express. 2010;3:085205.

[33] Tan ML, Friedhuber AM, Dunstan DE, Choong PFM, Dass CR. The performance of doxorubicin encapsulated in chitosan-dextran sulphate microparticles in an osteosarcoma model. Biomaterials. 2010;31:541-51.

[34] Amjadi I, Rabiee M, Hosseini MS, Mozafari M. Synthesis and Characterization of Doxorubicin-Loaded Poly(Lactide-co-glycolide) Nanoparticles as a Sustained-Release Anticancer Drug Delivery System. Appl Biochem Biotechnol. 2012;168:1434-47.

[35] Hancock MJ, He J, Mano JF, Khademhosseini A. Surface-tension-driven gradient generation in a fluid stripe for bench-top and microwell applications. Small. 2011;7:892-901.

[36] Tsougeni K, Petrou PS, Papageorgiou DP, Kakabakos SE, Tserepi A, Gogolides E. Controlled protein adsorption on microfluidic channels with engineered roughness and wettability. Sensors and Actuators B: Chemical. 2012;161:216-22.

[37] Alves NM, Shi J, Oramas E, Santos JL, Tomas H, Mano JF. Bioinspired superhydrophobic poly(L-lactic acid) surfaces control bone marrow derived cells adhesion and proliferation. J Biomed Mater Res A. 2009;91:480-8.

[38] Oliveira SM, Song W, Alves NM, Mano JF. Chemical modification of bioinspired superhydrophobic polystyrene surfaces to control cell attachment/proliferation. Soft Matter. 2011;7:8932-41.

[39] Ueda E, Levkin PA. Micropatterning hydrophobic liquid on a porous polymer surface for long-term selective cell-repellency. Adv Healthc Mater. 2013;2:1425-9.

[40] Lanks KW, Lehman JM. DNA Synthesis by L929 Cells following Doxorubicin Exposure. Cancer Research. 1990;50:4776-8.

[41] Graat HCA, Witlox MA, Schagen FHE, Kaspers GJL, Helder MN, Bras J, et al. Different susceptibility of osteosarcoma cell lines and primary cells to treatment with oncolytic adenovirus and doxorubicin or cisplatin. Br J Cancer. 2006;94:1837-44.

[42] Grellier M, Bordenave L, Amedee J. Cell-to-cell communication between osteogenic and endothelial lineages: implications for tissue engineering. Trends Biotechnol. 2009;27:562-71.

[43] Rivron NC, Liu J, Rouwkema J, de Boer J, van Blitterswijk CA. Engineering vascularised tissues in vitro. Eur Cells Mater. 2008;15:27-40.

SECTION IV. CONCLUDING REMARKS AND FUTURE PERSPECTIVES

CHAPTER 11. CONCLUSIONS AND FUTURE PERSPECTIVES.

The development of arrays of miniaturized biomaterials evoked the perspective for an efficient and rapid discovery of materials for implantation, namely aiming to be used in tissue regeneration strategies. During the last decade, such systems have seen significant development to meet specific needs of TE development, where the importance of reproducing biological niche-like 3D environments has been widely reported.

This thesis aimed at validating flat polystyrene superhydrophobic surfaces patterned with wettable regions as platforms for the high-throughput study of miniaturized 3D biomaterials and systems for TE/biotechnology purposes. The first experimental work presented in this thesis – Chapter 5 – proved the first hypothesis of this thesis: the wettability contrast-based platforms are adequate tools for the on-chip high-throughput analysis of 3D biomaterials. Alginate-based semi-interpenetrated networks - where other natural polymers were mixed with alginate/cells mixtures – were successfully patterned in the wettable spots of the chips. The hydrogels were kept stable in the hydrophilic spots for 24 hours. Microscopy techniques for on-chip and non-destructive study of cell number and viability were successfully validated. In the same work, the on-chip chemical analysis of each spot with combinatorial formulations of biomaterials was also implemented.

The second experimental work carried out in this thesis – described in Chapter 6 – allowed introducing a novel concept in the field of high-throughput analysis of biomaterials: the on-chip assessment of cells-3D porous scaffolds interactions. Cell-laden hydrogels, used in Chapter 5, are currently the most common way of performing combinatorial studies of cells-biomaterials interactions in a 3D environment. However, some biomaterials are not amenable to be processed in the mild conditions that allow cell encapsulation. Moreover, modulation of porous scaffolds' porosity, pore size and degree of interconnectivity not only influence cell seeding efficiency and migration, but were also reported to influence cellular response. Although in a straightforward approach one would accept that the concept of high-throughput ideally relies in the maximum miniaturization of each individual unit in the arrays, due to the micrometric size of cells, biomaterials must have a representative size, allowing their encapsulation or seeding of cell suspensions. As such, the miniaturization of the samples in Chapter 6 took in consideration the minimum size required for a

successful design of porous scaffolds, i.e. a pore size that allows cells to be seeded and migrate. Such pores belong to a scaffold with a significant number of pores, i.e. with a significant size that allows the structure to be interconnected. Interestingly, arrays of dried porous scaffolds may be an interesting way of commercializing biomaterials sets in ready-to-use, off-the-shelf platforms for cell-biomaterials tests. Still in Chapter 6, DMA and μCT techniques were adapted and validated to study biomaterials on-chip, under dry conditions, in a high-throughput manner. In the case of DMA equipment, a specially designed piece was added to the original equipment, and a gutter was used to fix the samples and allow their 2D displacement.

In Chapter 7, the concept developed on Chapter 6 for in-situ on-chip DMA of biomaterials was expanded to be used in physiological-like conditions, i.e. with the biomaterials arrays immersed in PBS at 37°C. In this work, a concrete application of the biomaterials was set for bone tissue regeneration strategies. Chitosan was used as a polymeric matrix to form nanocomposites with bioactive glass nanoparticles. The combinatorial formulations were later chemically crosslinked on-chip using genipin in two distinct concentrations. A suspension of pre-osteoblasts MC3T3-E1 cells, considered as a reliable model for bone studies, was added to the arrays, so selective cellular adhesion to each spot was studied. Moreover, the proliferation and morphology of the cells growing in each biomaterial were evaluated by microscopy and image analysis techniques previously optimized in Chapters 5 and 6. As the amount of varying factors, respective number of levels of each factor and number of responses to be studied were higher in this work than in previous the previous chapters, factorial analysis using Surface Response Models was used. The use of design of experiments and factorial analysis software was later transposed to Chapter 8.

Another aim of this thesis was increasing the degree of biological complexity of the environment surrounding the arrays of biomaterials on the chips. One particular and complex aspect that is often neglected while testing biomaterials *in vitro* is the effect of inflammatory response caused by the biomaterial upon implantation. However, immunomodulation is determinant for biomaterials integration on the tissue and it actively intervenes in crucial aspects for biomaterials successful integration and performance. Moreover, conventional biomaterials implantation often requires the use of high numbers of animals. The implantation a high number of biomaterials in a single animal would be a major ethical breakthrough in the area of biomaterials development. In Chapter 8 polystyrene superhydrophobic patterned chips with 36 biomaterials were implanted subcutaneously in Wistar rats. Biomaterials were all constituted by chitosan crosslinked with genipin in the form of a porous sponge, where ionic hydrogels of alginate and carrageenans were added. The hypothesis was that the different inflammatory responses caused by distinct biomaterials combinatorial

formulations would be identified in each scaffold by analyzing the presence of inflammatory cells on-chip, such as T lymphocytes and activated macrophages. In fact, such results were able to generate conclusive and reproducible data after 24 hours and 7 days of implantation. The results were also in agreement with the scores attributed to the histological sections cut around the tissue where the chips were implanted. All results were validated by using chips in which biomaterials were randomly disposed, so effects of possible crosstalk between biomaterials spots were excluded. Hydrogels with conventional dimensions were also implanted individually as controls. Although the hypothesis of this work was proved, the control over biomaterials degradation and respective debris' migration in long term studies may be one of the main challenges of this approach. Despite such concerns, this approach opens the possibility of making combinatorial high-throughput studies for tissue regeneration in the complex *in vivo* environment considering important phenomena as immunomodulation and *in vivo* clearance conditions.

The successful application of a TE strategy is not always dependent solely on direct cells-biomaterials interactions. Some tissue defects require the prolonged exposure to bioactive molecules in order to fully regenerate. Moreover, in some cases there is also a need for delivery of drugs to the defect site in order to e.g., decrease inflammatory response or avoid infections. The correct administration of such agents is often dependent on a tailored delivery mechanism from polymeric matrices, whose role is usually to act simultaneously as a biomaterials sustaining cell growth. During the development of this thesis, to the best of our knowledge, methods for the high-throughput monitoring of bioactive agents delivery from biomaterials were nonexistent. In Chapter 9, a simplifying alternative to the conventional drug release profile assessment methods was suggested. Superhydrophobic biomimetic surfaces were imprinted with ring-shaped transparent spots with concentric superhydrophobic millimetric regions to be used as bioactive agents release study platforms. An array where polymeric precursors (sodium alginate) mixed with a growth-factor model protein (BSA) labeled with a fluorescent tag was designed, so such mixtures could be dispensed in the concentric highly repellent regions and crosslinked afterwards, generating a polymeric protein-loaded sphere. The ring-shaped region was then filled with PBS that covered the polymeric sphere. The acquisition of sequential images of each spot over time using fluorescence microscopy allowed monitoring the protein release by image-based fluorescence quantification. Future perspectives for this approach may include the adaptation of the system to mimic standardized organs dynamics in the spots and to be used in a wider range of bioactive agents release studies.

The last work developed in this thesis aimed at exploring another approach in biotechnology that does not use biomaterials, and where fully cellular microtissues function as *in vitro* disease models or as building blocks for organ printing strategies. Cell suspensions of two distinct cell lines were patterned in the wettable spots of the chips, which were later turned 180° for cell culture, generating a robust hanging-drop setup. The cellular spheroids generated in this approach were used as tumor-like disease models and their sensitivity for different concentrations of doxorubicin was tested on-chip. Image analysis was used to analyze cell death in the cellular models. By using a different treatment than the phase-separation one used from Chapter 5 to 9 to make polystyrene surfaces superhydrophobic, cell suspensions were amenable to be patterned in the wettable spots not only by manual pipetting, but also by dragging the cell suspension through the chip. Each patterning method allowed working with distinct throughputs and degrees of precision. The platforms were able to comprise static or dynamic environments in each droplet, opening the possibility to be used as mini-bioreactors for shear stress stimulation or for cellular exposure to dynamic molecular compositions overtime.

Several advantages are drawn from the use of superhydrophobic surfaces as chips for high-throughput analysis. They allow dispensing biomaterials in totally flat platforms, making their physicochemical characterization easier as compared to commercially available plates or other types of chips where samples are surrounded by walls. In superhydrophobic chips the samples are totally exposed to the environment and unconfined, allowing easy passage of irradiation through the biomaterials, easy reaching of probes to the miniaturized biomaterials and testing in unconfined conditions. Moreover, the total flatness of the surfaces allows their storage in a space-saving manner, allowing a configuration similar to a “deck of cards”. The cost of production of the superhydrophobic chips is low, and the technology is amenable to easily being scaled-up. One aspect that makes this technology versatile is the easy patterning of wettable spots with different shapes, sizes, disposition, contact angles and even anisotropy inside the spots. Moreover, the high contrast of wettability allows having biomaterials with different sizes simply by varying its volume to be dispensed in the wettable spot. Another useful aspect of this technology is that the chips may be prepared with specific sizes and shapes, or their size/shapes may be tailored after preparation, to meet the needs of existing imaging and analysis technology. The flexibility of the polystyrene film can also vary, in order to fullfil the requirements of specific applications, such as *in vivo* implantation, where the platform must adapt to the shape of the implantation site.

In conclusion, it can be stated that superhydrophobic platforms patterned with wettable spots used in this thesis proved to be compatible with the study of 3D biomaterials-cells *in vitro* interactions, as well as *in vivo* high-throughput biomaterials testing. They also opened the possibility of testing on-chip other important parameters in TE strategies, such as bioactive molecules delivery profiles and drug activity in 3D cellular microtissues, functioning as relevant tissue models. The knowledge gathered in this thesis improved the applications of high-throughput platforms for TE studies, and opened several perspectives that may be developed in future work, namely for the use of porous scaffolds in high-throughput strategies, the on-chip complete physicochemical characterization of biomaterials and their assessment in the *in vivo* complex environment.